



Terms and Conditions of Use of Digitised Theses from Trinity College Library Dublin

Copyright statement

All material supplied by Trinity College Library is protected by copyright (under the Copyright and Related Rights Act, 2000 as amended) and other relevant Intellectual Property Rights. By accessing and using a Digitised Thesis from Trinity College Library you acknowledge that all Intellectual Property Rights in any Works supplied are the sole and exclusive property of the copyright and/or other IPR holder. Specific copyright holders may not be explicitly identified. Use of materials from other sources within a thesis should not be construed as a claim over them.

A non-exclusive, non-transferable licence is hereby granted to those using or reproducing, in whole or in part, the material for valid purposes, providing the copyright owners are acknowledged using the normal conventions. Where specific permission to use material is required, this is identified and such permission must be sought from the copyright holder or agency cited.

Liability statement

By using a Digitised Thesis, I accept that Trinity College Dublin bears no legal responsibility for the accuracy, legality or comprehensiveness of materials contained within the thesis, and that Trinity College Dublin accepts no liability for indirect, consequential, or incidental, damages or losses arising from use of the thesis for whatever reason. Information located in a thesis may be subject to specific use constraints, details of which may not be explicitly described. It is the responsibility of potential and actual users to be aware of such constraints and to abide by them. By making use of material from a digitised thesis, you accept these copyright and disclaimer provisions. Where it is brought to the attention of Trinity College Library that there may be a breach of copyright or other restraint, it is the policy to withdraw or take down access to a thesis while the issue is being resolved.

Access Agreement

By using a Digitised Thesis from Trinity College Library you are bound by the following Terms & Conditions. Please read them carefully.

I have read and I understand the following statement: All material supplied via a Digitised Thesis from Trinity College Library is protected by copyright and other intellectual property rights, and duplication or sale of all or part of any of a thesis is not permitted, except that material may be duplicated by you for your research use or for educational purposes in electronic or print form providing the copyright owners are acknowledged using the normal conventions. You must obtain permission for any other use. Electronic or print copies may not be offered, whether for sale or otherwise to anyone. This copy has been supplied on the understanding that it is copyright material and that no quotation from the thesis may be published without proper acknowledgement.

Investigations of the solid-state, powder flow and tableability properties of comminuted active pharmaceutical ingredients

Presented by

Evelyn O' Shea, B.Sc.

being a thesis submitted for the degree of
Doctor of Philosophy in Pharmaceutics

at the

University of Dublin, Trinity College

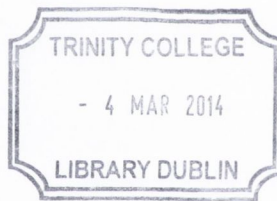
under the direction and supervision of

**Anne Marie Healy,
B.Sc. (Pharm.), Ph.D., M.P.S.I., F.T.C.D.**

**Lidia Tajber,
M.Sc. (Pharm), Dip. Stat. QI., Ph.D.**

**Professor Owen I. Corrigan,
B.Sc. (Pharm.) (N.U.I.), M.A., Ph.D. (N.U.I.), F.T.C.D., F.P.S.I.**

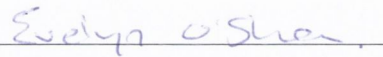
July 2013



Thesis 10268

DECLARATION

This thesis is submitted by the undersigned to the University of Dublin, Trinity College, for examination for the degree of Doctor of Philosophy. This thesis has not been submitted as an exercise for a degree at any other university. It is entirely the work of the undersigned author, except where duly acknowledged. This manuscript was completely written by the undersigned author, with the aid of editorial advice from Professor Anne Marie Healy, Dr. Lidia Tajber and Professor O.I. Corrigan. It is agreed that the library may lend or copy this thesis upon request.



Evelyn O' Shea

TABLE OF CONTENTS

Acknowledgements	<i>i</i>
Presentations associated with this thesis	<i>ii</i>
Abbreviations and Symbols	<i>iii</i>
Summary	<i>v</i>

INTRODUCTION

Origin and scope of this thesis	1
---------------------------------	---

Chapter 1 Introduction

1.1 Solid state properties of pharmaceutical materials	3
1.1.1 Crystalline state	3
1.1.2 Polymorphs	3
1.1.3 Pseudo - polymorphs (Solvates and Hydrates)	5
1.1.4 Salts	7
1.1.5 Amorphous state	7
1.2 Comminution	9
1.2.1 Ball milling	10
1.2.2 The effect of ball milling on the solid state properties	13
1.3 Powder flow	16
1.3.1 Factors influencing the flowability of powders	17
1.3.2 Flow characterisation	20
1.4 Tableting	22
1.4.1 Factors influencing the tabletability	24
1.5 Background to drugs used in current work	26
1.5.1 Sulfadimidine	26
1.5.2 Sulfadimidine sodium salt	27
1.5.3 Sulfathiazole	27
1.5.4 Sulfathiazole sodium salt	28

EXPERIMENTAL

Chapter 2 Materials and Methods

2.1 Materials	30
2.2 Methods	32

2.2.1	Ball Milling	32
2.2.2	Crystallisation of sulfadimidine	34
2.2.3	Production of sulfathiazole polymorph form I	34
2.2.4	Production of amorphous standards by melt quenching	34
2.2.5	Thermal analysis	35
2.2.5.1	Differential scanning calorimetry (DSC)	35
2.2.5.2	Modulated temperature differential scanning calorimetry	35
2.2.5.3	Thermogravimetic analysis	36
2.2.6	X-ray diffraction	36
2.2.6.1	Powder x-ray diffraction	36
2.2.6.1.1	Calculation of the crystallinity percentage by powder X-ray diffraction	36
2.2.6.1.2	Normalised Bragg peak intensity	37
2.2.6.1.3	Variable temperature X-ray diffraction	37
2.2.7	Microscopy	37
2.2.7.1	Scanning electron microscopy	37
2.2.7.2	Light microscopy	37
2.2.8	Dynamic vapour sorption	38
2.2.9	Particle size analysis	38
2.2.10	Specific surface area analysis by Brunauer, Emmett, Teller (BET) isotherm	38
2.2.11	Density measurements: Bulk (aerated) and Tap Density	39
2.2.12	Carr's Index	39
2.2.13	Tableting	39
2.2.13.1	Tablet geometry	39
2.2.13.2	Evaluation of tablet hardness test	40
2.2.14	Preparation of physical mixtures	40
2.2.14.1	Calibration curve (amorphous versus crystalline)	40
2.2.14.2	Polymorphic mixtures	41
2.2.15	Temperature and humidity readings	41
2.2.16	Calculation of the amorphous fraction by differential scanning calorimetry	41
2.2.17	Solid state stability study	42
2.2.18	Statistical analysis and data fitting	42

Results and Discussion

Chapter 3 Ball milling of sulfadimidine

3.0	Introduction	43
3.1	Sulfadimidine unmilled	44
3.1.1	Powder X-ray diffraction	44
3.1.2	Dynamic vapour sorption	45
3.1.3	Thermal analysis	46
3.1.3	Particle size analysis, surface area and morphology	47
3.2	Amorphous quantification	49
3.3	Influence of milling conditions on crystallinity of sulfadimidine	52
3.3.1	Ball milling at room temperature	52
3.3.1.1	Powder X-ray diffraction (PXRD)	52
3.3.1.2	Thermal analysis	56
3.3.1.3	Particle size, morphology and specific surface area	63
3.3.2	Ball milling at 4 °C	69
3.3.2.1	Powder X-ray diffraction	69
3.3.2.2	Thermal analysis	73
3.3.2.3	Particle size and morphology	79
3.4	PXRD peak area and DSC amorphous content changes at RT and 4 °C	83
3.5	Storage of ball milled SD	86
3.5.1	Powder X-ray diffraction	87
3.5.2	Thermal analysis	92
3.5.3	Crystallisation kinetics	98
3.6	Conclusions	104

Chapter 4 Ball milling of sulfadimidine sodium salt

4.0	Introduction	106
4.1	Sulfadimidine sodium salt unmilled (SDNa)	107
4.1.1	Powder X-ray diffraction	107
4.1.2	Thermal analysis	108
4.1.3	Particle size, surface area and microscopy	109
4.2	Ball milling of sulfadimidine sodium salt	111

4.2.1	Powder X-ray diffraction	111
4.2.2	Thermal analysis	114
4.2.3	Particle size, specific surface area and microscopy	118
4.3	Storage of SDNa	121
4.4	Conclusions	125

Chapter 5 Ball milling of sulfathiazole and sulfathiazole sodium salt

5.0	Introduction	126
5.1	Analysis of sulfathiazole starting materials	126
5.1.1	Powder X-ray diffraction (PXRD)	126
5.1.2	Thermal analysis	128
5.1.3	Morphology and particle size	130
5.1.4	Analysis of the polymorphic forms by NIR	132
5.2	Binary mixtures	132
5.2.1	Powder X-ray diffraction	133
5.2.2	Thermal analysis	134
5.3	Ball milling STZ III	136
5.3.1	Investigating the affect of the ball-to-powder weight ratio of 20:1	136
5.3.1.1	Powder X-ray Diffraction	136
5.3.1.2	Thermal analysis	140
5.3.1.3	Morphology and particle size	145
5.4	Investigating the affect of the ball-to-powder weight ratio of 40:1	149
5.4.1	Sulfathiazole Form III, batch Y	149
5.4.1.1	Analysis directly after milling	149
5.4.1.1.1	Powder X-ray Diffraction	149
5.4.1.1.2	Thermal analysis	151
5.4.1.1.3	Particle size by laser diffraction	156
5.4.1.1.4	Morphology and specific surface area	158
5.4.1.2	Storage of the ball milled STZ III-Y	159
5.4.1.2.1	Powder X-ray diffraction	159
5.4.1.2.2	Thermal analysis	162
5.5	Sulfathiazole Form I (STZ I)	167
5.5.1	Directly after milling	167
5.5.1.1	Powder X-ray diffraction	167

5.5.2	Thermal analysis	170
5.5.3	Particle size, surface area and morphology	173
5.5.2	Storage of the ball milled samples	176
5.5.2.1	Powder X-ray diffraction	176
5.5.2.2	Thermal analysis	178
5.6	Sulfathiazole sodium salt (STZNa)	179
5.6.1	Sulfathiazole sodium salt unmilled	180
5.6.1.1	Powder X-ray diffraction	180
5.6.1.2	Thermal analysis	181
5.6.1.3	Morphology	182
5.6.2	Sulfathiazole sodium salt ball milled	182
5.6.2.1	Powder X-ray diffraction	182
5.6.2.2	Thermal analysis	185
5.6.2.3	Particle size, specific surface area and morphology	188
5.7	Conclusions	191

Chapter 6 Powder flow and tableting

6.0	Introduction	193
6.1	Powder flow	194
6.1.1	Carr's compressibility index (CI)	194
6.2	Compaction	198
6.2.1	Determination of the critical formation pressure	198
6.2.1	Tableting properties of the unmilled materials	200
6.2.3	Tablet hardness	201
6.2.4	Tablet specific surface area	206
6.3	Correlations	208
6.3.1	Spearman correlation	208
6.3.2	Powder flow correlation study	210
6.3.3	Tablet hardness and surface area correlation study	215
6.4	Storage and tablet hardness	221
6.5	Conclusions	227

Chapter 7 General discussion

7.0	Introduction	229
-----	--------------	-----

7.1 Physicochemical changes incurred as a result of ball milling	230
7.1.1 Methods of evaluating change	230
7.1.2 The effect of the ball to powder weight ratio and temperature	232
7.1.3 The effect of ball milling time	235
7.1.4 Stability of the induced amorphous phase	240
7.2 A review of the morphology and particle size changes incurred as a result of ball milling	243
7.2.1 Morphology	243
7.2.2 Particle size	245
7.3 Powder flow and tablet hardness	247
7.3.1. Powder flow	247
7.4 The influence ball milling had on the tabletability	249
7.5 Conclusion	252
7.6 Main findings	253
7.7 Future work	254
References	255
Appendices	
Appendix I	273
Appendix II	278
Appendix III	280

Acknowledgements

I would like to thank my supervisor, Prof. Anne Marie Healy, Dr. Lidia Tajber and Prof. Owen Corrigan for the opportunity, their guidance, support, time and advice during the course of my research and preparing this thesis.

This work would not have been possible without the support from SFI and the SSPC cluster. The cluster brought great support and is a wonderful organisation which has contributed so much to the scientific community and I wish them the best with their future endeavours.

The postdocs, Vincent Caron, Youness Amhara and Krzysztof Paluch, thank you for the time and advice, you were a tremendous help. I am grateful to the academic, secretarial staff and technical staff and I would like to thank Neal from CMA for his help and advice with the microscope.

I would like to thank Stefano Bianco and Vincent Curtin for their company, support, discussions and their songs! It was a pleasure to work with you both. To Christine, Stephaney, Joanne, Clare, Ines, Johanna and Anita, thank you for the long conversations, nights out and of course our coffee breaks, it was all time well spent! To the 'guys upstairs', thank you for all the nights out and your help through out the past few years.

To my close friends, Imelda, Elaine, Catriona, Sarah and Yvonne, thank you so much for the chats, encouragement and the holidays, all of which helped me to keep going.

A special thank you to my parents and sisters for your love, support and encouragement. To my 'new' in-laws, The Pierses, thank you for being so welcoming and inviting, whether its a week of work or a relaxed weekend, you have always been there with open arms and I am very grateful.

I dedicate this to my husband, Declan, who has given me unending support, love, kindness and patience throughout my years of study. Thank you for everything, from the encouragement, to the cups of coffee in the morning and everything in between.

Presentations associated with this thesis

Poster presentation

‘The effect of mechanical activation of solid-state nature of commercially available sulfathiazole’ at the American Association of Pharmaceutical Scientists, Los Angeles, USA, November 2009. [O’ Shea E., Caron V., Tajber L., Corrigan O.I., Healy A.M.]

‘Investigation into the effects on tablet hardness as a result of changes to the solid state and micromeritic properties incurred on milling’ at the American Association of Pharmaceutical Scientists, Washington, USA, October 2011. [O’ Shea E., Caron V., Tajber L., Corrigan O.I., Healy A.M.]

‘Comminution of Sulfathiazole Polymorphs’ at the Crystal Growth of Organic Materials, Limerick, Ireland, June 2012. [E. O’ Shea, L. Tajber, O. I. Corrigan, A. M. Healy]

‘The effect of different comminution techniques on commercially available sulfadimidine’ at Academy of Pharmaceutical Sciences (APS) –Amorphous III conference, Nottingham UK, April 2010. [O’ Shea E., Caron V., Tajber L., Corrigan O.I., Healy A.M.]

‘The effect of varying milling conditions on the solid-state characteristics of sulfadimidine’ at the UK PharmSci conference, Nottingham UK, September 2010. [O’ Shea E., Caron V., Tajber L., Corrigan O.I., Healy A.M.]

Abbreviations and Symbols

Amor.	amorphous
ANOVA	analysis of variance
~	approximately
BET	Brunauer, Emmett and Teller
BTP	ball-to-power (weight ratio)
CCDC	Cambridge Crystallographic Data Centre
CI	Carr's Index
Ø	diameter
°C	degrees Celsius
DSC	differential scanning calorimetry
DVS	dynamic vapour sorption
df	Degrees of freedom
ΔH_{cr}	enthalpy of crystallisation
ΔH_m	enthalpy of melt
ΔH_{poly}	enthalpy of polymorphic transformation
g	grams
g/cm^2	grams per centimetre squared
hr	hour
Hz	Hertz (revolutions per second)
J/g	joules per gram
kPa	kilopascals
m^2/g	meters squared per gram
mg	milligrams
min	minutes
mm	millimeter
	modulated temperature differential scanning
MTDSC	calorimetry
mW	milliwatt
n	number of repeats, number of pairs
NPI	normalised peak intensity
NUIG	National University of Ireland, Galway
T_{cr}	onset temperature of crystallisation

T _m	onset temperature of melt
T _{poly}	onset temperature of polymorphic transformation
-	to
3D	Three dimensional representations
PA	peak area
%	percentage
PXRD	powder x-ray diffraction
rpm	revolutions per minutes
RT	room temperature
SD	sulfadimidine
SDNa	sulfadimidine sodium salt
SEM	scanning electron microscopy
SSA	specific surface area
STZ I	sulfathiazole form I
STZ III	sulfathiazole form III
STZ	sulfathiazole
STZNa	sulfathiazole sodium salt
TGA	Thermogravimetry analysis
UL	University of Limerick
µm	micrometers
vrs.	verses
VTXRD	variable temperature x-ray diffraction
w/v	weight in volume
w/w	weight in weight

Summary

An understanding of the effect of processing on the solid-state properties of active pharmaceutical ingredients (APIs) is essential for product manufacturing success. During product development it is possible to induce physical changes in the API, for example amorphisation (transformation from crystalline state to amorphous state) or polymorphic transformations. The rate and extent of such phase transitions within the API will depend on physicochemical characteristics of the API. The presence of even a small amount of amorphous component(s) in a crystalline product may have a considerable impact on the stability, processability and bioavailability of the material, and its performance during product manufacture and use. The main focus of this thesis was to determine the impact of a milling, or comminution, process on the physicochemical properties of a range of sulfonamide (sulfa) materials, and to evaluate how these changes affected the material's ability to flow as well as the impact of these changes on the properties of tablets produced using the comminuted powders.

Ball milling was used as the comminution technique and it was performed using a Retsch PM100 planetary mill (PM) ball mill. The sulfa materials milled included: sulfadimidine, sulfadimidine sodium salt, sulfathiazole (as two polymorphic forms: Form III and Form I) and sulfathiazole sodium salt. The various ball milling parameters investigated included time, temperature and the ball to powder (BTP) weight ratio. The characterisation techniques employed to investigate solid-state changes included: Powder X-ray Diffraction (PXRD), Differential Scanning Calorimetry (DSC), Modulated Differential Scanning Calorimetry (MDSC), particle size analysis by laser diffraction, specific surface area analysis (BET analysis) and Scanning Electron Microscopy (SEM). The powder flowability of the unmilled and ball milled samples was determined by the Carr's compressibility index (CI). The unprocessed and milled powders were also compressed and tablet hardness was determined. Ball milled samples were stored at 4 °C over phosphorous pentoxide and stability studies of the induced amorphous phase were also carried out. The stored ball milled sulfadimidine powders were also compressed and their tablet hardness was evaluated.

The results showed that a larger quantity of the crystalline material was converted to an amorphous phase as a result of ball milling using a BTP weight ratio of 40:1 at 4 °C when compared to ball milling with a lower BTP weight ratio of 20:1 at room temperature (Chapter 3 and 5). Evaluation of the crystallisation kinetics using a modified Avrami equation showed that the different levels of the induced amorphous phase crystallised at different rates (Chapter 3). Thermal analysis appeared to be a more suitable technique for quantifying the change of the amorphous phase that was induced by ball milling, as opposed to PXRD peak area analysis (Chapter 3). Sulfadimidine sodium salt was found to be more readily amorphised than sulfadimidine and the amorphous phase was more thermally stable when compared to the non-salt form, when stored at 4 °C over phosphorus pentoxide. This was attributed to the difference between the materials' glass transition temperatures (T_g), as the T_g of sulfadimidine was ~78 °C and sulfadimidine sodium salt had a T_g of ~156 °C. The molecular mobility is reduced when processing is carried out at temperatures significantly lower than the material's T_g (Chapter 3 and 4). The sulfa materials that were ball milled at room temperature with a BTP weight ratio of 40:1 had a reduced CI compared to their unmilled counterparts and the majority of the milled powders had either poor or very poor flow properties (Chapter 6). The hardness of tablets obtained from the compressed ball milled powders was greater than the hardness of tablets prepared from the unmilled compressed powders. The hardness of tablets made using the ball milled sulfadimidine powders that were first stored for different time periods prior to tableting was, as a result of storing the powders for prolonged periods (84 days), generally decreased for the majority of the samples, compared to when material was freshly milled. Changes to the powder flow properties and the tablet hardness were attributed to the induced changes which resulted from the ball milling process. These changes included the loss of crystallinity and the reduced particle size. Overall it was found that, as a result of ball milling, the powder flow and tablet hardness properties of the materials changed measurably, showing that the decreased particle size and the increased amorphous content induced by ball milling has a direct effect on the processability of the sulfa materials.

Origin and Scope

Milling is a process that is frequently used in the pharmaceutical industry to reduce the particle size of a material in order to improve solubility and bioavailability (Frenchini, 2007; Shekunov *et al.*, 2007). Ball milling has been shown to result in physical changes to the active pharmaceutical ingredient (API). Changes can include complete or partial amorphisation (Descamps *et al.*, 2007; Willart *et al.*, 2007; Wilfong *et al.*, 2006; Dudognon *et al.*, 2006) and/or polymorphic conversion (De Gusseme *et al.*, 2008; Brittain, 2002).

Amorphous solids have higher solubility, higher dissolution rate and sometimes better compression characteristics than corresponding crystals (Martin, 1993; Hancock 2007; Hancock *et al.*, 2002). There is significant interest in producing the amorphous phase of a material in order to benefit from the high solubility of this solid state. More often than not, processing via ball milling, would create an amorphous sample unintentionally (Hancock 2007, Grisedale *et al.*, 2010). The presence of low levels of amorphous phase in predominantly crystalline samples (and visa versa), can be the cause of unexpected processing or stability problems. There are numerous debates as to how the amorphous phase is induced during the milling process. However the wide variety of different ball milling parameters and the range of materials investigated results in gaps in the research, regarding how the different milling parameters affect the material's solid state nature.

Milling is but one of many processing steps involved in the manufacture of a drug product. After the milling process the material should, ideally, be able to flow from hoppers or silos and, if the powder is used for tablets, it should be easily compressed (Guerin *et al.*, 1999). Sebhatu and Alderborn (1999) found that an amorphous lactose sample produced a significantly higher tablet hardness than its crystalline counterpart and Maggi *et al.* (1998) demonstrated how an amorphous α -cyclodextrin hydrate had poorer flow properties when compared to the crystalline sample. However this research was limited to completely amorphous or completely crystalline systems. Lappalainen and Karppinen (2010) stated that the presence of even a tiny amount of amorphous component(s) in a crystalline product may have considerable impact on the stability, processability and bioavailability of the material and its performance

during product manufacture and use. The amorphous phase is known to be less physically stable than its crystalline counterpart and during the manufacturing process powders can be stored for a time before they are used, which can result in the induced amorphous phase recrystallising (Hancock *et al.*, 1995; Zhou *et al.*, 2003; Jouppila *et al.*, 1998). Therefore it is essential to understand the parameters that result in an induced amorphous phase, the stability of the amorphous phase and how the amorphous phase impacts on the material's ability to flow and its tabletability.

The scope of this thesis was:

- To investigate and characterise the influence of various ball milling parameters on several sulfonamide APIs in order to determine the best combination of parameters that may be used to either induce an amorphous phase or prevent it from being formed. These initial investigations would form the basis for further research on how the different levels of disorder would affect the powder flow and tabletability of the material.
- To study the physical stability (solid-state stability) of the induced amorphous phase and the polymorphic forms of the milled materials.
- To examine if the ball milling process affected the materials' flowability and tabletability.
- To investigate correlations between the physical changes incurred during the milling process and changes in flowability and tabletability, in order to determine if and to what degree different levels of induced amorphous phase affect these properties.
- To examine the changes, if any, to the materials' tabletability as a result of storing the ball milled powders that consisted of different levels of an amorphous content over a defined period of time.

Introduction

1.1 Solid state properties of pharmaceutical materials

Solid state properties can be divided into crystalline and amorphous states. Crystalline materials can then be further divided into three groups: non-polymorphic, polymorphic and pseudo-polymorphic (solvates and hydrates) structures. Another crystal structure of interest is the salt form of the active pharmaceutical ingredient (API).

1.1.1 Crystalline state

A crystalline material consists of regularly repeating unit cells which are indefinitely repeated in three dimensions in space. Each crystal can be classified as a member of one of seven possible crystal systems or crystal classes that are defined by the relationships between the individual dimensions, a , b and c , of the unit cell and between the individual angles α , β and γ of the unit cell (Callister, 1998). The majority of drugs are used in the crystalline solid state due to reasons of stability and ease of handling during various stages of drug development.

1.1.2 Polymorphs

Crystalline polymorphs are defined as having the same chemical composition but different internal crystal structure. This results in the polymorphs having different physicochemical properties. The different crystal structures in polymorphs arise when the drug substance crystallises in different conformations (Vippagunta *et al.*, 2001).

Polymorphs can exist as enantiotropic or monotropic structures depending on their thermodynamic properties. For an enantiotropic polymorphic system the stable polymorph is different above and below a transition temperature (Figure 1.1 a). In the case of enantiotropy the low melting form is the thermodynamic stable form below the transition point and above this point the high melting form is the thermodynamic stable form (Giron *et al.*, 2004). In contrast to this, for monotropic polymorphs only one polymorph is stable at all temperatures, while all other polymorphs remain unstable, regardless of temperature (Vippagunta *et al.*, 2001) (Figure 1.1 b). The thermodynamic relationship for both of these systems is outlined in Figure 1.1. Figure 1.1 illustrates the relationship of the solid phases for an enantiotropic system, where polymorph 'a' is stable below the transition temperature (T_1) due to the lower free energy (G_A) when compared to polymorph B. As a result of heating, the temperature

increases to beyond the T_t point. At this point polymorph B has a free energy (G_B) that is less than the free energy (G_A) of polymorph A which results in polymorph B becoming more stable than polymorph A. The transition is reversible at a particular transition temperature and this is observed where the free energy curves cross before the melting point is approached. Figure 1.1 b outlines a monotropic system and from the graph it can be observed that at no point the two Gibbs energy curves meet, this is in contrast to the enantiotropic system. In this system no reversible transition from the metastable to the stable polymorph can be observed below the melting point.

Thermal analysis by differential scanning calorimetry (DSC) is often used to characterise polymorphic forms. In the case of monotropy, the thermodynamic stable form is the higher melting enthalpy form (Giron *et al.*, 2004). Thermal analysis of a material will allow the detection of certain transition temperatures where one polymorphic form undergoes a solid state transition to another form (Willart *et al.*, 2005).

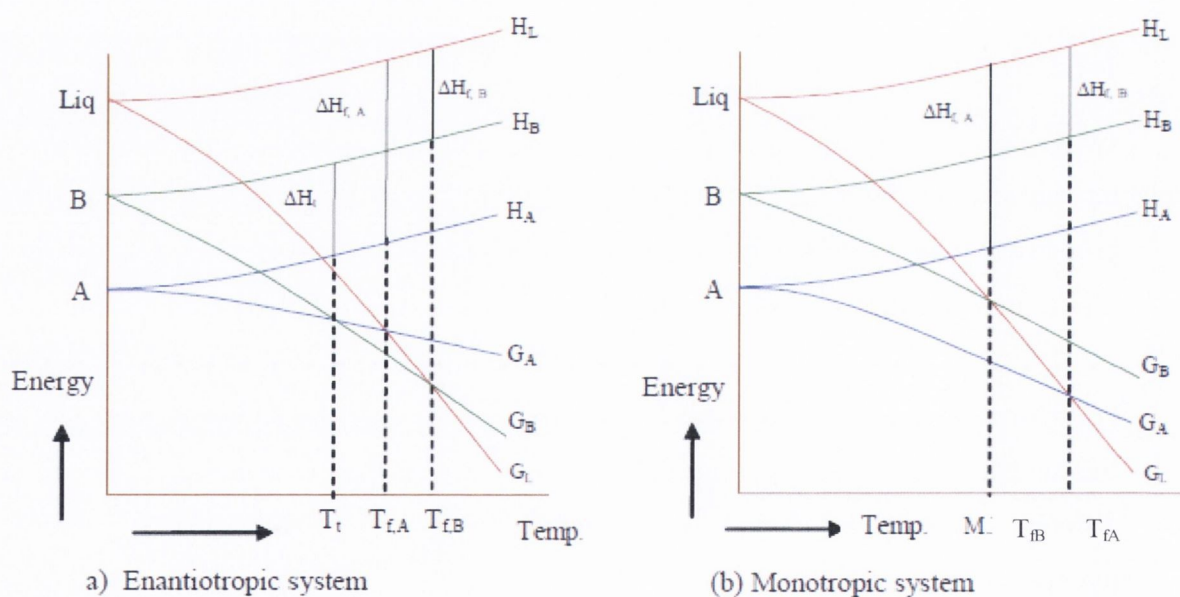


Figure 1.1: Variation of Energy with temperature for the solid and liquid phases (Liq) of a single compound, showing a) enantiotropy, and b) monotropy. Curves H_A , H_B and H_L are for enthalpy. Curves G_A , G_B and G_L are for Gibbs free energy. ΔH_{fA} and ΔH_{fB} represent enthalpy of fusion and ΔH_t represents enthalpy of transformation. T_t is for temperature of transition. T_{fB} and T_{fA} are the fusion temperatures of polymorphs A and B, respectively. (Giron, 2001)

Due to the different crystal packing and/or molecular conformations between crystalline polymorphs and solvates, there are usually significant differences in physical properties such

as density, hardness, tableability, refractive index, melting point, enthalpy of fusion, vapour pressure, solubility, dissolution rate, other thermodynamic and kinetic properties and even colour (Grant, 1999). Monitoring these changes during production is essential as changes to the physical properties may affect processing parameters such as powder flow and compressibility (Haleblian and M^cCrone, 1969) and the solubility of the drug, which can result in modified absorption rates (Martin, 1993).

Powder X-ray diffraction has been particularly suited to the quantitative identification of different polymorphic forms and the solvated and anhydrous form of a compound (Black and Lovering, 1977; Willart *et al.*, 2005). X-ray diffraction (XRD) is a non-destructive analytical technique used to investigate structural characteristics of a given material. XRD is a quantitative and qualitative technique which is used for the 'fingerprint' characterisation of crystalline materials and their crystal structures (Newman and Byrn, 2003). A crystalline material consists of a regular three dimensional distribution of atoms in space, which make up lattice planes. The separation of these planes varies from material to material and from polymorph to polymorph. The detection of certain characteristic peaks by PXRD allows the determination of the polymorphic form present within the material (Willart *et al.*, 2005).

1.1.3 Pseudo - polymorphs (Solvates and Hydrates)

The expression pseudo-polymorphism applies to hydrates and solvates (Giron *et al.*, 2004). Solvates may be formed when a pure organic solvent or a mixture of solvents are used as the solvent for crystallising the compound. Hydrates are formed when water is incorporated into the lattice structure, often in stoichiometric proportions. Depending on the conditions surrounding the sample, such as temperature and humidity, several different stoichiometric hydrate species may form (Tiwary, 2007). The water molecule, because of its small size, can easily fill structural voids and because of its multidirectional hydrogen bonding capabilities, it is ideal for linking a majority of drug molecules into stable crystal structures (Byrn *et al.*, 1999). Water is omnipresent in the atmosphere and as a result of high levels of relative humidity, water may be absorbed by the sample of interest resulting in a hydrated structure. Giron *et al.*, (2002) stated that water is often used in crystallisation steps and dehydration steps may occur in drying, milling and the tableting process. Between manufacturing and environmental conditions the sample may undergo unexpected hydration and dehydration

which results in the need to characterise hydrates as part of the study of the physical properties of the drug substance (Giron *et al.*, 2002).

Vippagunta *et al.* (2001) stated that hydrates can be classified into three categories. They describe these classes as follows: the first (class I) are the isolated site hydrates, where the water molecules are isolated from direct contact with other water molecules by intervening drug molecules. The second (class II) are known as channel hydrates. This is where water molecules included in the lattice lie next to other water molecules of adjoining unit cells along an axis of the lattice. These form channels through the crystal. The channel hydrates can be further divided into two subcategories. The first consists of expanded channels or nonstoichiometric hydrates. These can take up additional moisture in the channels, when exposed to high levels of humidity. This can result in the expansion or contraction of the crystal lattice as hydration or dehydration occurs. The second subcategory comprises of planar hydrates. These are channel hydrates in which water is localised in a two-dimensional order or plane. The third category of hydrates (class 3) are the ion-associated hydrates in which metal ions are coordinated with water.

The presence of water has been shown to impact on properties such as flow and compaction (Maggi *et al.*, 1998; Bolhuis *et al.*, 2009). Several hydrates of a substance may be possible and they may be stable at ambient conditions (Giron and Grant, 2002), while others can be influenced by environmental and processing conditions. Two methods that can be used to characterise the hydrate forms are dynamic vapour sorption (DVS) and thermogravimetric analysis (TGA). A DVS isotherm describes the equilibrium vapour uptake as a function of vapour partial pressure. If a material forms a stoichiometric hydrate species at distinct vapour pressures, then the corresponding equilibrium uptake and resulting isotherm can be used to calculate the stoichiometry of the hydrated species. To illustrate, consider an anhydrous material, Sample A with molecular weight, (MW). If Sample A forms a hydrated species at a particular vapour partial pressure, then the percentage weight gain at that partial pressure can be used to calculate the stoichiometry of the hydrate. Similar analysis could be applied for solvate stoichiometries. Thermal analysis can be used by evaluating the mass loss as a function of temperature and the quantity of mass loss may be associated with the hydrate/solvate formed.

1.1.4 Salts

Key aspects to consider during the drug development and manufacturing process include solubility and chemical stability (Huang and Tong, 2004). Solubility is often improved by particle size reduction and/or salt formation. The formation of a salt involves the addition of a counterion to an electrolyte drug which modifies the lattice structure. Changes to the lattice structure may result in physiochemical property changes such as improved solubility, density, melting point etc. (Huang and Tong, 2004). A salt formation occurs from the reaction of an acid with a base, which involves either a proton transfer or a neutralising reaction. Salt formation may be used to alter the physiochemical, biopharmaceutical and processing properties of a drug substance without modifying its fundamental chemical structure. In general, the salts of a drug rarely change its pharmacology, however the bioavailability of the product may be improved (Corrigan, 2007). Common salt formers include hydrochlorides and chlorides of basic drugs and sodium salts of acidic drugs (Pfannkuch *et al.*, 2011). According to Stahl and Wermuth (2008) almost 90% of the pharmaceutical salts formed are with sodium, calcium, potassium, magnesium, meglumine or ammonia and over 55% are produced with sodium cations.

1.1.5 Amorphous state

Unlike the crystalline phases where three-dimensional long range order exists, amorphous materials have no distinguishable crystal lattice and may be regarded as super-cooled liquids (Zhang *et al.*, 2004). Hancock and Zografi's (1997) schematic diagram of enthalpy or specific volume of a solid substance as a function of temperature, illustrates how glass and crystal systems differ (Figure 1.2).

A small increase in enthalpy (H) and volume (V) occurs as temperature is increased for a crystalline material. There is a discontinuity in both H and V at the melting temperature (T_m) indicating the first-order phase transition to the liquid state (Hancock and Zografi, 1997). Rapid cooling of the melt results in H and V following the equilibrium line for the liquid, in advance of the melting temperature. This follows on to the super cooled liquid region and further cooling then results in a change in slope at the glass transition temperature (T_g) (Hancock and Zografi, 1997). The glass transition temperature (T_g) is a characteristic property of the amorphous phase which signifies the temperature where the liquid state of the melt

becomes thermodynamically frozen and results in a disordered solid structure (Shah *et al.*, 2006). The Kauzmann temperature (T_k) is known as the point where the enthalpy of a liquid phase below this temperature would be lower than the enthalpy of the solid and this is thermodynamically impossible. Therefore, at the T_k the system has an entropy of zero and the structure is thought to be ‘frozen’ (i.e. low molecular mobility).

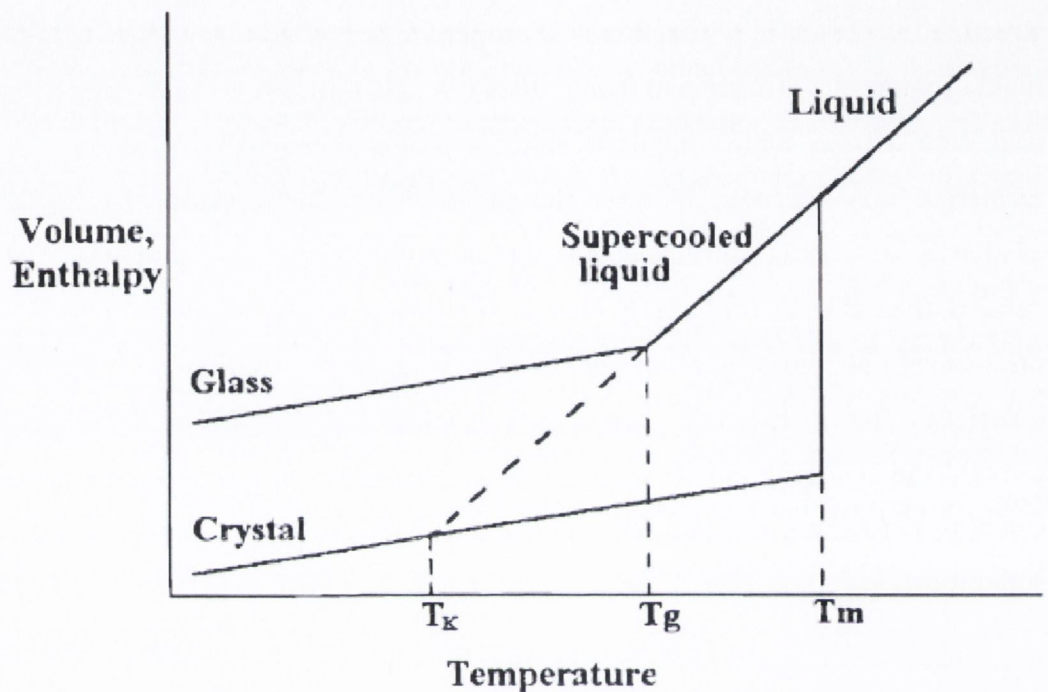


Figure 1.2: Schematic diagram of the variation of enthalpy (or volume) with temperature (Hancock and Zografi, 1997).

Amorphous solids have higher solubility, higher dissolution rate and sometimes better compression characteristics than corresponding crystals (Hancock 2007; Hancock *et al.*, 2002). The true or absolute density of the amorphous phase is 5-20% less than that of the crystalline phase. This is due to the less efficient packing of molecules that are randomly orientated relative to each other (Hancock, 2007). Amorphous materials will absorb significant amounts of water vapour from their surroundings, relative to their crystalline counter parts. Although amorphous materials may have advantages such as higher bioavailability they are generally less stable physically and chemically than corresponding crystals (Yu, 2001; Mallick *et al.*, 2008).

Characterisation of the amorphous form has been achieved by PXRD and thermal analysis such as differential scanning calorimetry. The lack of crystal order is reflected by a diffractogram that has no distinct peaks and is referred to as an amorphous halo. Thermal analysis of an amorphous material may consist of an inflection in the thermogram which is characterised as the T_g and a recrystallisation exotherm may be present.

Overall, it is very important to control the crystal form of the drug during various stages of drug development because any phase change due to polymorph interconversions, desolvations of solvates, formation of hydrates and changes in the degree of crystallinity can alter the bioavailability of the drug. When going through phase transition, a drug may undergo a change in its thermodynamic properties, with consequent changes in its dissolution and bioavailability characteristics (Nerurkar *et al.*, 2000).

1.2 Comminution

Comminution is the reduction of material particle size to a smaller size and it is achieved by several different processes such as grinding and crushing. Control of the particle shape, size and polymorphic form may be achieved by altering crystallisation conditions. However, it is often difficult to obtain the desired size distribution through crystallisation alone and therefore comminution is commonly used for this purpose (Chikhalia *et al.*, 2006). Obtaining a desired particle size is essential to all solid dosage form manufacturing steps, such as tableting and tablet die filling and this will adversely affect the drug delivery process. To ensure manufacturing runs smoothly particles are produced with a known size distribution. Tablet die filling is achieved when a known volume is released from the silo (i.e. storage tank) and compressed. Changes to the particle size and shape could affect the quantity of powder released from the silo, the flowability of the powder and the properties of the compressed tablet (Luukkonen *et al.*, 1999; Kaerger *et al.*, 2004). The particle size of a material has also been shown to influence the material's bioavailability where a decreased particle size results in an increased surface area which leads to an increase in the rate of dissolution (Frenchini, 2007; Shekunov *et al.*, 2007).

Milling is a mechanical process regularly used in the pharmaceutical industry for the reduction of particle size. Particle fracture and changes in the crystal structure of the material occurs when sufficient strain is generated in the solid particles by the high levels of mechanical energy applied (Buckton *et al*, 1988). There are several different types of mills available for particle size reduction such as the ball mill, fluid energy mill, cutter mill, hammer mill, pin mill, vibration mill, etc. The fluid energy mill and the ball mill are the only two systems that can typically reduce the particle size to less than 5 μm by dry milling (Parrott, 1974).

There are advantages and limitations to both mill types. Micronisation is achieved in the fluid energy mill as a result of particle-particle and particle-wall collisions. Gas is used to force the material into and around the milling chamber and as there are no moving parts there is minimal product contamination caused by wear. Operation of the fluid energy mill requires knowledge and experience as to how the different gas pressure may affect the micronisation process (Vastaraj *et al.*, 2003). While, the fluid energy mill requires constant attention the ball mill can be programmed and allowed to run for long periods of time.

1.2.1 Ball milling

The ball mill of interest is the planetary ball mill which owes its name to the planet-like movement of its jars/milling chambers. These are arranged on a rotating support disk and a special drive mechanism causes them to rotate around their own axes. The centrifugal force produced by the jars rotating around their own axes and the force produced by the rotating support disk both act on the milling jar contents which consists of the material to be ground and the grinding balls. These forces cause the grinding balls to run down the inside wall of the jar, which creates the friction effect, followed by the material being ground and grinding balls lifting off and travelling freely through the inner chamber of the jar and colliding against the opposing inside wall, which results in the impact effect (Figure 1.2) (Suryanarayana, 2001).

Several parameters can be varied and should be considered as they have been shown to affect the solid state nature of the material milled. These include parameters such as milling container (size and material); milling speed; milling time; size and size distribution of the balls used; ball-to-powder weight ratio (BTP); milling atmosphere and temperature of milling

(Suryanarayana, 2001, Rubinstein and Gould, 1987). All these process variables are not completely independent. For example, the optimum milling time depends on the type of mill, size of the grinding medium, temperature of milling, ball-to-powder ratio, etc.

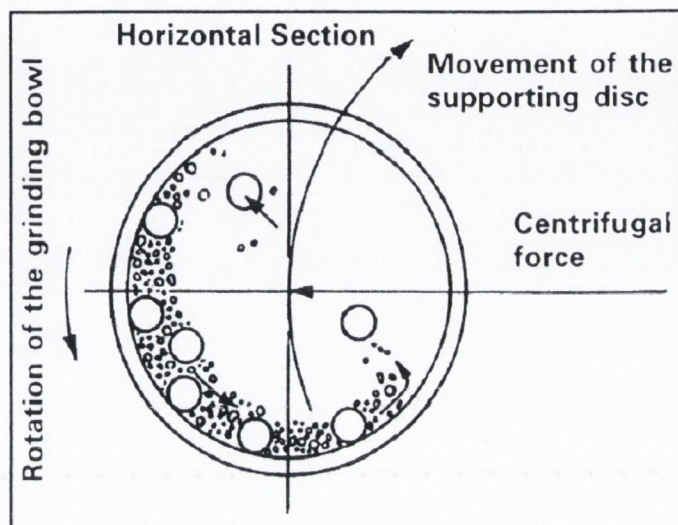


Figure 1.2: Schematic depicting the ball motion inside the ball mill. (Suryanarayana, 2001)

Milling container: The material used for the container is important as ball impact may cause wear and in turn contamination. The powder is seen to act as a protective layer for the inner wall but any wear should be noted.

Grinding medium: It is essential to ensure that the density of the grinding medium is sufficient to create a high impact force on the powder, so that the particle size reduction is achieved (Suryanarayana, 2001). Several different materials have been used for the milling jar and the balls, such as hardened steel, tool steel, tempered steel and zirconia. A study by Talekar *et al.*, (2005), found that by using an oscillatory ball mill containing two 9 mm diameter stainless steel balls, form 1 ranitidine hydrochloride converted to form 2 after 10 hours of milling. When the same conditions were used except for the size of the stainless steel milling balls were changed to 12 mm in diameter, the same polymorphic conversion was achieved in 3 hours. It was suggested that the larger balls used resulted in a faster conversion due to the higher impact energy (Chieng *et al.*, 2006).

Milling speed: It is naturally assumed that the higher the speed the higher is the energy input and as a result this may affect the crystallinity of the material by converting it to a partial or completely amorphous phase. It may also be presumed that greater particle size reduction is

obtained at higher milling speeds. However, this is not always the case. With high speeds the balls will be pinned to the inner walls of the container and do not fall down to exert any impact force. It is important to run the mill below this critical speed to ensure maximum collision. With high speeds the temperature of the jars increases. Suryanarayana, (2001) stated that high temperatures within the milling jar can result in unwanted solid state transformations such as polymorphic conversion and/or amorphisation and the high temperatures may result in decomposition during the milling process.

Milling time: The time required to achieve a particular particle size reduction is dependent on, the milling intensity, ball-powder weight ratio and the temperature. If milling time is too short the desired results might not be reached but if milling time is too long unwanted states and degradation could occur. Rubenstein and Gould (1987) found that initial ball milling results showed a decrease in particle size but continuous milling did not always result in further particle size reduction.

Temperature: During milling the temperature increases and for a planetary mill it is possible to reach high temperatures (Retsch, 2009). This high temperature may degrade or induce phase changes within the material. The increase in temperature is due to ball-to-ball, ball-to-powder and ball-to-wall collisions and friction. The temperature difference between the wall of the jar and the milling ball may create an uneven distribution of heat. By stopping the mill for a period of time the heat becomes more evenly distributed. Kwon *et al.* (2002) noted that about 80 % of the energy generated in the mill is consumed to heat the balls. It was also seen that, as the powders coated the balls, the temperature within the jar decreased (Kwon *et al.*, 2002). The increased temperature within the milling jars may cause crystallisation of an already induced amorphous phase (Abdelloui and Gaffet, 1996). Depending on the powder's thermal properties, solid-state transformations or/and degradation is possible. By storing the mill in a cold room, flushing it with gas or by introducing a pause into the milling cycle the temperature remains low (Milhailenko *et al.*, 2007; Kwon *et al.*, 2002). Zhang *et al.*, (2002) used a fan to cool the mill and with every 15 minutes of milling a pause of 15 minutes followed.

Ball-to-Powder weight ratio (BTP): The ball-to-powder weight ratio (BTP) will affect the movement of the balls within the jar and the number of collisions endured. A higher BTP weight ratio should result in a higher number of collisions which will result in more energy being transferred to the powder particles (Suryanarayana, 2001). As noted above, the number

of collisions affects the temperature, which can influence the solid-state of the material. An investigation by Rubinstein and Gould (1987) of how the ball milling variables affected particle size, showed that the sample loading was not an essential factor to consider, as doubling sample size results in doubling the milling time.

1.2.2 The effect of ball milling on the solid state properties

Milling is a key process for the preparation of many solid dosage forms, particularly in the last processing step in the production of bulk substance, in order to reduce particle size. It is often accompanied by a decrease in crystallinity due to the creation of lattice defects, beginning at the surface of the powder (Ward and Schultz, 1995; Erizal *et al.*, 2008). The mechanism by which the disordering of the crystalline phase is induced during milling is still under debate. Shakhshneider and Boldyrev (1999) stated that the amorphous phase is induced by a melt/quench process. They described this hypothesis, where at elevated temperatures, local 'hot spots' were induced as a result of the number of collision incurred by the milling balls. These 'hot spots' were thought to exceed the melting temperature of the material. The temperature of the material should return to room temperature at the end of the milling process and this rapid change in temperature acts as a quench mechanism, resulting in amorphisation of the sample.

Fecht (1992) argues that disordering is achieved by the accumulation of defects. Boldyrev and Tkáčová, (2000) attributed this event to the continuous collisions that are encountered during the milling process which can result in the shearing of particles and the accumulation of defects during the milling process, resulting in an amorphous phase. The thermal properties of the material are thought to influence the possibility of inducing an amorphous phase.

Studies by Willart *et al.*, (2001 & 2006) and Caron *et al.*, (2007) noted the significance of a material's glass transition temperature when attempting to produce an amorphous material via ball milling. The formation of the amorphous phase as a result of ball milling below the T_g has been reported for several materials such as trehalose, lactose, sucrose, glucose, budesonide (Descamps *et al.*, 2007; Willart *et al.*, 2007; Wilfong *et al.*, 2006; Dudognon *et al.*, 2006). Changes to the polymorphic form as a result of milling has been reported as a result of

milling at temperatures above the material's glass transition temperature (T_g) and this has been reported for fananserine (De Gusseme *et al.*, 2008; Brittain, 2002). In the case of fananserine where the T_g was reported to be at 19 °C and two of its polymorphs (III and IV) were milled at RT (25 °C) in a controlled chamber at 0 °C, the results showed that ball milling at RT resulted in a polymorphic conversion to the metastable form I (regardless of the initial polymorph milled) and ball milling at 0 °C resulted in a glassy amorphous state or a partial transformation (De Gusseme *et al.*, 2008). They suggested that below the T_g the molecular mobility is slow and the induced level of disorder remains, while above the T_g of the material's Gibbs energy is sufficient enough to allow the reorganisation of its crystal structure, illustrating the importance of the materials T_g and the ball milling temperature used.

The position of the T_g has been shown to influence the formation of the amorphous phase and its stability. To investigate the relationship between a material's T_g and its ability to amorphise, Caron *et al.* (2007) ball milled, for 12 hours via a planetary ball mill, several physical mixtures of different molar fractions of crystalline trehalose ($T_g = 120$ °C) and crystalline mannitol ($T_g = 10.6$ °C). The purpose was to 'finely tune' the T_g in order to observe when the material amorphised, as the T_g of the corresponding alloy crossed the milling temperature zone (room temperature). From the results generated, Caron *et al.* (2007) concluded that if milling was performed above the T_g of the material, the lifetime of the amorphised fraction would be short and rapid recrystallisation would occur. However, if milling was performed below the T_g an amorphous phase would be induced which would be reluctant to crystallise.

Patterson *et al.* (2005) ball milled several compounds with different T_g s above room temperature for 120 minutes. These included dipyridamol ($T_g = 40$ °C), glibenclamide ($T_g = 73$ °C) and indomethacin ($T_g = 45$ °C). Amorphisation as a result of milling occurred for the three materials and this was characterised by the detection of an amorphous halo by PXRD and the detection of a glass transition by DSC. The ball milled amorphous samples were stored under different conditions (25 °C/<10% RH, 25 °C/75% RH and 40 °C/<10% RH) and tested one week after they were milled. The stability of the induced amorphous phase was different for each sample, all of the dipyridamol crystallised after 1 week regardless of the storage conditions. Glibenclamide was reported to remain predominantly amorphous, but the

recrystallisation exotherms of the samples stored at 25 °C/75% RH and 40 °C/10%RH were significantly smaller than that observed for the sample stored at 25 °C/10% RH, suggesting that the amorphous sample was more stable when stored at a lower temperature and RH. The indomethacin sample stored for 1 week at 25 °C/<10% RH was only partially amorphous while the milled samples stored under the other conditions recrystallised to the γ form. Overall the results showed that storage at a lower temperature and RH resulted in the induced amorphous phase to remain or to be partially recrystallised while storage at the higher temperature and RH resulted in the conversion of the disordered amorphous phase to an ordered crystalline phase. Hancock and Zografi, (1997) stated that the amorphous systems show some tendency to spontaneously crystallise, possibly at different rates above and below the T_g . Therefore it is important to evaluate if an amorphous phase has been induced and the stability of this phase, as it may result in the formation of a metastable polymorphic form.

In the case of indomethacin the amorphous phase is converted to the stable polymorphic form γ (Patterson *et al.*, 2005). Ball milling of indomethacin by Desprez and Descamps (2006) resulted in the formation of the metastable form α as a result of ball milling for 5 hours. This metastable phase is more often an undesirable phase due to its instability. Comparing both studies shows that the use of different parameters and machines can result in different phases induced and this can also be observed for the level of amorphous content induced during the milling process. The lack of consistency between the milling conditions used from one study to the next makes it difficult to determine key parameters that influence property changes that are induced as a result of ball milling.

The introduction of a polymorphic species and/or amorphisation during milling is not an uncommon event. Some polymorphic conversions can take several hours to occur (Zhang *et al.*, 2002; Talekar *et al.*, 2005), while others can occur in minutes (Prittimaki *et al.*, 1993). The time required for the conversion from crystalline to amorphous has also been shown to depend on ball milling time (Desprez and Descamps 2006; De Gusseme *et al.*, 2008), but other factors such as temperature are shown to affect the material. Dujardin *et al.* (2008) investigated the effect of ball milling on the α and β forms of glucose ($T_g = 38$ °C), both at room temperature (RT) and at -15 °C and for 14 hours. They showed that at the lower temperature both polymorphic forms were converted to an amorphous phase, while no change

was evident, (neither amorphisation nor polymorphic transformation occurred), as a result of ball milling at RT (Dujardin *et al.*, 2008). They stated that as a result of ball milling at 25 °C both polymorphic forms undergo amorphisation but this was not detected as the induced amorphous phase readily recrystallised which prevented it from being detected. They attribute the fact that it was possible to induce an amorphous phase at lower temperatures to this environment resulting in a low molecular mobility which prevents the recrystallisation from counterbalancing the mechanical disordering which results in a fully amorphous state.

Complete amorphisation and polymorphic transformation allow better understanding as to how a material behaves but more often than not a partial transformation occurs. This was observed by Shakhtshneider (1997), as a result of ball milling sulfathiazole form III. The results showed that a partial amorphous phase was detected and a polymorphic conversion occurred. As the ball milling process is often only one step in a number of processing steps it is essential to understand the effect the different milling parameters have on the solid state nature of the material of interest and whether a partial or complete conversion occurred as a result of the ball milling process. Overall the different ball milling parameters used in the reported studies, such as time and temperature, make it difficult to indicate what factors have more impact in changing the solid state nature of a material. It is essential to bridge this gap by controlling the ball milling parameters and testing several materials which have different T_g in order to observe a trend between which factors are essential in reducing the particle size (without inducing an amorphous phase or polymorphic transformation) and what ball milling parameters will aid the formation of an amorphous phase.

1.3 Powder flow

Manufacturing of pharmaceutical solid dosage forms involves several processing steps that include flow through hoppers, sieving, pouring, blending, die-filling and compaction (Guerin *et al.*, 1999). The ability of the powder to flow is critical to manufacturing and understanding the factors that affect powder flow is essential to the process. Powder flow is not an inherent material property but is a result of a combination of a material's physical properties. Properties that have been shown to influence a powder's ability to flow include particle size (Luukkonen *et al.*, 1999; Mullarnet *et al.*, 2003), morphology (Liu *et al.*, 2008; Kaerger *et al.*, 2004), formation of agglomerates (Nokhodchi *et al.*, 2007; Geldart *et al.*, 2009), surface area

(Kaerger *et al.*, 2004; Luukkonen *et al.*, 1999) and cohesiveness (Peleg, 1983; Rodes 1998). Varying these material properties can have a positive impact on the process, resulting in good flow, or they can hinder powder flow. The phrase “good flow” behaviour usually means that bulk solid flows easily, i.e., it does not consolidate much and the powders flow out of a silo or a hopper due to the force of gravity alone and no flow promoting devices are required. Products are “poorly flowing” if they experience flow obstructions or consolidate during storage or transport (Schulze, 2011).

1.3.1 Factors influencing the flowability of powders

Flow behaviour is multidimensional in nature and it depends on the materials physical characteristics (Ganesan *et al.* 2008). Prescott and Barnum (2000) stated that flowability is a consequence of the combination of a material’s physical properties that influence as well as the environmental conditions, the equipment used for handling, storing and processing these materials. It is essential that a material has the ability to flow during the manufacturing of a drug product. Bad flow properties result in stoppage due to the inability of a material to flow out of a silo. This, in turn, results in stoppage which inadvertently resulting in material loss and profit loss. An example of this would include the die filling process for the tablet press. This process is volume controlled where the silo will open for a known period of time to allow a certain volume to flow out of it and into the die where a known mass is compressed, producing a tablet. If the flow was affected in any way the incorrect powder volume would be released resulting in a product that has either too much or too little mass. As the pharmaceutical industry is highly regulated it is essential that the flow properties of the material are not adversely affected in order to obtain the desired product. Factors that can affect powder flow can include parameters such as particle size and size distribution, shape, surface texture and roughness, moisture content, solid state nature and surface energy.

Particle size and size distribution

Several studies investigating the influence of particle size on the flowability of materials have been undertaken in order to gain an insight into the complex relationship which exists between particle size and powder flow. Powder flow is improved if the particles are larger in size. Staniforth (2002) noted that particles larger than 250 μm are usually free-flowing and as

the particles size falls below 100 μm powders become cohesive and flow problems are likely to occur. If the particle size is reduced to below 10 μm the powders are extremely cohesive and resist flow under gravity. Larger particle size was shown to have improved flowability properties for several materials, such as ibuprofen, where the median particle size ranged from 390 to 67.3 μm (Liu *et al.*, 2008). Ball milling is used to reduce the particle size of a material. Kaerger *et al.* (2004) found that micronised particle of paracetamol were between 2 and 6 μm and were unevenly shaped and had worse flow properties when compared to their untreated paracetamol particles which were 40 μm needle shaped particles. They suggested that as a result of the micronised uneven morphology and higher surface area, flow was inhibited due to the increased number of interparticle interactions at both macroscopic (mechanical) and microscopic (van der Waals) levels (Kaerger *et al.*, 2004).

Particle shape and size

Mullarney *et al.* (2003) stated that smaller particle sizes have a larger contact area between the particles which can contribute to an increase in the friction coefficient and decrease flowability of the material. Mullarney *et al.* (2003) studied the flow behaviour of 4 different sweetening materials; sucrose, acesulfame potassium, saccharin sodium and aspartame, which had a median particle size of 629, 294, 11 and 6 μm , respectively. They examined the morphology of the powder and found that sucrose consisted of square particles, acesulfame potassium had round particles, saccharin sodium was made up of square particles with smaller irregular shaped particles dispersed throughout and aspartame had needle shaped particles. Carr's Index analysis of the samples showed that the larger particles flowed better than the smaller particles which was previously stated but shows how these parameters are dependent on one another. Mullarney *et al.* stated that the bad flow was a result of the elongated particle shape and small particle size which was observed for the aspartame samples and that processing with powders that had bad flow may result in a high tablet weight variation, unacceptable blend uniformity and difficulty in filling containers and dies.

These studies suggest that if the particle size of the ball milled material is reduced to less than 10 μm and if the shape of the particle is needle-like, the powder flow properties may be hindered. The morphology of the particles is also critical as it is easier to move spherical balls than elongated rods from one container to another. Liu *et al.*, (2008) suggested that the

particle shape may also affect the flow properties as the ‘sphericity’ of the particles decreases with increasing particle size and the larger needle like particles will have greater contact area with other particles and these will need to dilate more in order to flow. This was found to occur by Liu *et al.*, (2008) for the powder flow properties of different ibuprofen powders.

Powders that have a reduced particle size or size distribution are known to be cohesive in nature. Cohesive powders are fine grained powders that have poor flow due to inter-particle forces between particles (e.g. flour) (Peleg, 1983). The term cohesion is used to indicate powders stickiness and is an indication of poor flow and agglomeration. Geldart *et al.*, (2009) stated that if fine powder cohesion is caused by interparticle forces such as van der Waals forces, other factors such as mechanical interlocking may also play a role, particularly in coarser materials if they are non-spherical.

Powder surface properties

The surface area of a powder can be increased if the particle size is decreased or if the particles are porous in nature. The previous studies have shown that the powder flow is hindered by small particle size and an increased surface area as a result of the cohesive nature of the powders. Several studies have shown that modification of the powders surface properties such as dry coating, may improve powder flow properties. Yang *et al.*, (2005) and Ramlakhan *et al.*, (2000) both showed that dry coating the powder with nano-particles, which coat the surface of the main particles creates a nano-scale roughness which reduces the cohesive force among dry coated particles. Yang *et al.*, (2005) and Ramlakhan *et al.*, (2000) investigated this by using different size fractions of silica to cover cornstarch particles.

Han *et al.*, (2011) noted the effect different surface properties could have on the flowability of a material and noted that polymer coatings improved flow properties. They explored the effect of micronising PVP with ibuprofen but did so with such small quantities that an amorphous phase would not be induced. They added small quantities of PVP in order to preserve the crystallinity of the material. They noted that they were only interested in the crystalline material as it was the more desired form due to its long term stability. They found that the

surface coating of PVP improved flowability. They attributed this to the decrease in the surface charge which resulted in a less cohesive powder.

Ball milling has been shown to induce a partially amorphous form which is often accidentally induced (Caron *et al.*, 2007) and this amorphous phase has been shown to result in an increased surface energy (Buckton *et al.*, 1999). Hancock and Zografi (1997) stated that the induced amorphous phase on the surface of a material will result in unwanted changes in the physical and chemical properties of the system. These changes should have an impact on a material's flow properties. Different milling parameters affect the powders differently, changes such as particle size reduction, agglomeration, surface area, morphology, amorphisation, changes to the crystallite size etc., and how these different changes impact the powder flow properties has not been reported previously.

1.3.2 Flow characterisation

Carr's compressibility index or Carr's Index (CI) evaluates flowability of a powder by comparing the tapped density (ρ_a) and the bulk density (ρ_b) of a powder, (Carr, 1965). CI is calculated by using equation 1.4. Overall it measures a powder's ability to consolidate. Once calculated it can be interpreted by using the classifications given in table 1.1. The greater the compressibility of a bulk solid, the poorer its flow properties. In general, the borderline between free flowing and non-free flowing is approximately 20–21% compressibility (Carr, 1965). Amidon *et al.*, (2009) states that free flowing powder interparticle interactions, which lead to consolidation are generally less important and that bulk and tap densities will be close in value. However, the tapped and bulk densities are essential, as loss of air between the powder particles during storage may lead to consolidated powder resulting in a bad flow properties.

$$CI = \frac{\rho_b - \rho_a}{\rho_b} \times 100$$

Equation 1.4

Table 1.1: Carr's Index table (Carr, 1965)

Carr's Index (%)	Type of flow
5-15	Excellent
12-16	Good
18-21	Fair to passable
23-35	Poor
33-38	Very poor
>40	Extremely poor

Tapped and bulk density are two of the most important properties that determine the ease with which pharmaceutical powders can be stored, handled and processed and they have been used to characterise powders into cohesive and non cohesive categories (Mullarney *et al.*, 2011). Guerin *et al.*, (1999) looked at seven different materials. They stated that three of the powders were known to display free flowing behaviour (Di calcium phosphate Di-tab®, extra fine lactose and free flowing lactose). Lactose fine was known as a powder that had intermediate flow and the three other powders were known for their poor flow properties (ketoprofen, acebutol chlorohydrate and celiprolol chorohydrate). These powders were used to validate test procedures, which were performed to evaluate powder flow. They found that tap testing to determine the Carr Index was a quick way to evaluate flow properties of powders by measuring particle behaviour under gravitational packing. A similar conclusion was drawn by Ghoroi *et al.*, (2012) as a result of comparing several different test methods such as the FT4 powder rheometer, angle of repose and the bulk and tapped densities.

The affect of a particle's size and shape and how this affects the CI was outlined by Nokodchi *et al.*, (2007) as they investigated the flowability of agglomerated carbamazepine powders, naproxen powders and lactose powders with their non-agglomerated counterpart by Carr's Index. They found that the CI for the agglomerates had better flow properties compared to the original powders. They attributed this improvement to the large spherical shape of the agglomerated particles that were obtained through crystallisation methods. They stated that the fine particles had a high surface to mass ratio which resulted in a more cohesive nature compared to the coarser particles and these were more influenced by gravitational force. They commented on how the shape of the particles affect the powder flow and stated that the

flowability of powders decreases as the shapes of the particles become more irregular. Nokodchi *et al.*, (2007) reported that powders with similar particles sizes but different shapes can have different flow properties due to the differences in interparticle contact areas. They credited these reasons to the improved flow properties of the agglomerated powders (Nokodchi *et al.*, 2007).

1.4 Tableting

Armstrong (2007a) stated that for tablets to be produced with satisfactory quality the formulation must have three essential attributes; the first requirement is that the powder must flow into the die space of the tablet press sufficiently rapidly and in a reproducible manner; the second condition is that the particles must form a solid compact when subjected to compression and that compact must remain intact after the compressive force is removed; the third requirement is that the tablet can be removed from the press without damage to the tablet or the press. This process is straightforward enough when the sample that is processed fulfils all the right conditions, but Armstrong (2007a) stated that very few APIs possess all three essential requirements while some possess none. This may impact high dosage forms only as the addition of other excipients may compensate for the API's deficiencies. Several material characteristics have been found to affect these requirements such as particle size, surface area, polymorphic form, morphology, moisture content and the crystallinity or lack of crystallinity within the material (Riepma *et al.*, 1992; Sun, 2008; Masteau and Thomas, 1999; Busignies *et al.*, 2011; Sun and Grant 2001; Picker-Freyer *et al.*, 2007; Maggi *et al.*, 1998; Sebhatu and Alderborn 1999; Kaerger *et al.*, 2004).

The characteristics that affect the production of tablets are evaluated by producing tablets under a known compressive pressure and assessing the tablet hardness or tensile strength of that tablet. An understanding of the events that occur as a result of the applied pressure and the terminology that is associated with tableting is essential to understanding the factors that impact on a material's tabletability.

Sun and Grant (2001) defined tabletability as the capacity of a powdered material to be transformed into a tablet of specified strength under the effect of compaction pressure. They

stated that the tableability describes the effectiveness of the applied pressure in increasing the tensile strength of the tablet and demonstrates the relationship between the cause, compaction pressure and the effect, the strength of the compact. The term compression is often used to describe the process of volume reduction (Bogda, 2007) and the term compaction is used to describe the whole process, including the subsequent establishment of bonds (Armstrong, 2007b). The mechanical strength of pharmaceutical tablets is frequently assessed as part of process control during manufacturing and as a means of understanding the compaction behaviour of a material (Davies and Newton, 1996). The physical strength of a tablet is dependent on the extent and strength of interparticulate bonds and these, in turn, are related to the compressive force which is applied (Armstrong, 2007b). The strength is usually assessed as the force required to fracture a tablet. This is generally referred to as the 'hardness' of the tablet but it is an expression of the physical strength or mechanical strength of the tablet. Hardness or crushing strength is measured in Newtons (N) or kilograms (kg), obtained by using a tablet hardness press which uses compressive forces with the aim to fracture the tablet. This technique is used to compare tablets of the same size and shape, such as an in-process control. The physical strength of tablets is dependent on the dimensions of the tablet.

The strength of a tablet composed of a certain material can be used to measure the compactibility of that material. (Mattsson, 2000) Compression of powders involves four stages: slippage and rearrangement of particles, elastic deformation of particles, plastic deformation or brittle fracture of particles and compression of the solid crystal lattice (Doelker 1994).

When the powder is compressed the particles rearrange under the low compaction pressure to form a closer packing structure. Particles with a regular shape appear to undergo rearrangement more easily than those of an irregular shape (York, 1978). Deberg and Nyström (1986) studied the volume reduction behaviour of materials during compaction. The applied pressure has been shown to reach a maximum level where, at this applied pressure, additional rearrangement of the compressed particles is prevented and subsequent volume reduction is achieved by plastic or elastic deformation and/or fragmentation of the tablet particles (Deberg and Nyström, 1986). This plastic and elastic deformation will depend on the material's brittle or ductile nature. Brittle particles are likely to undergo fragmentation into

smaller units. Brittle materials which undergo extensive fragmentation generally result in tablets of relative high porosity due to the large number of bonding points created during compression, which prevent further volume reduction. Unlike brittle materials, ductile materials often result in tablets of low porosity due to the high degree of plastic deformation that occurs upon compression, which enables particles to move close to one another (Mattsson, 2000). Capping and lamination are problems encountered by materials that undergo elastic deformation. These can be reduced or eliminated by slowing the compression process, lowering the rate of force applied (larger compression roller diameter) or increasing the time of compression (multistage compression) (Bogda, 2007). Consolidation or bonding is influenced by the material's chemical nature, surface area of the contact point and interparticle distance.

1.4.1 Factors influencing the tableability

Particle size, shape and morphology

Smaller particles provide a larger total area for bonding than larger particles thus resulting in higher forces required to fracture (Sun and Grant, 2001). Comminution has been shown to influence the properties that impact tableability of materials such as particle size reduction, increased specific surface area and polymorphic transformation. The comminution process has also been shown to induce a complete or partially amorphous phase and more often than not this change is not desired. If the level of disorder is 'small' it is often overlooked but this 'small' change can impact on other processing steps further down the line, therefore it is essential to understand the impact of these 'small' changes. Asolfsson *et al.*, (1998) stated that the change in surface properties by milling will probably affect the interaction between particles under compaction and they evaluated the extent that the induced disordered phase, which was caused by the milling process, affected the interparticulate bonding mechanism of sodium chloride particles. They 'milled' the material using a pestle and mortar for approximately 5 minutes. While they determined the change in particle size by dry sieving, they failed to quantify the induced amorphous phase. They found that the tensile strength of the compacts prepared from the milled sodium chloride was greater than that of compacts prepared from the unmilled material. They noted that the increased surface area and decreased particle size contributed to the increased tensile strength but they believed that these changes did not explain the large increase in tensile strength. They attributed the increased tensile

strength to the increased mobility of the surface structure which may have facilitated the development of bonds over a large surface area. The limited understanding as to how the changes induced by milling affected the tensile strength of the tablets may be attributed to the lack of characterisation of the changes to the solid state nature of the material after the milling process.

The details of the materials used and experiments carried out by Kaerger *et al.* (2004) are described in section 1.3.1 (powder flow). In addition to their analysis of the flowability, micronised paracetamol was tableted. Kaerger *et al.* characterised the micronised powders by thermal analysis and stated that the absence of an exothermic recrystallisation event, at 76 °C, indicated the absence of amorphous material. They found that the micronised paracetamol material had a higher tensile strength than the unmilled sample. They suggested that the particle processing and shape determine the apparent mechanical properties such as compressibility and compactibility and stated that the inherent properties of the micronised drug have a strong influence on the compaction.

The morphology of the material has been shown to affect the tableting properties of material. Sun and Grant (2001) investigated the tableting properties of sulfamerazine polymorphs in order to understand the influence of the polymorphic structure on the tablet properties. Two polymorphs of sulfamerazine were compacted and their tensile strength was obtained from compressive tests. The starting materials both had a particle size range between 10 and 40 µm but there was a difference between the morphology of the samples with form I consisting of rectangular shaped crystals while form II had hexagonal-like crystal shape. The tensile strength compacts made from form I was higher than those of form II. Sun and Grant attributed this to the fact that polymorph I had a greater plasticity which resulted in a larger interparticular bonding area and therefore a greater compressibility and tableability over II (Sun and Grant, 2011). Evaluation of the tableability of three sulfathiazole polymorphs (I, II and III) was carried out by Picker-Freyer *et al.*, (2007). The compaction properties of flat faced tablets of sulfathiazole were evaluated in order to compare the affect of the microstructural differences between the polymorphic forms and how this factor impacted on the compaction properties. Picker-Freyer *et al.*, (2007) showed that the powder with the greater hardness value was Form III in comparison to the tablets produced using the Form I and II powders. They attributed this increased tablet hardness to the hexagonal plates which

are characteristic of STZ III and they stated that they compact more efficiently compared to the needle shaped Form I crystals. These studies suggest that even if the particle size is similar, the morphology of the samples still has an impact on the tablet strength.

Solid-state nature

Sebhatu and Alderson (1999) noted that the tensile strength of amorphous lactose resulted in tablets with higher tensile strength than crystalline lactose. They found that the moisture content of the amorphous lactose had a significant effect on the tablet strength. Overall the tablet strength increased with reduced particle size for both amorphous and crystalline lactose forms. They stated that the possible difference between the amorphous and crystalline materials could be due to the possible deformability differences between the particles.

The importance of these changes was expressed previously at the end of the powder flow section but the impact of the material properties have been shown to influence the tableability of the material, hence the importance of investigating how small or largely changes is reiterated.

1.5 Background to drugs used in current work

The sulfonamides are organic sulphurous compounds that contain the sulfonamide functional group, $-S(=O_2)-NH_2$, a sulfone group connected to an amine group (Adsmund and Grant 2001). Sulfonamides exhibit interesting solid-state properties, among which is the ability of many of these drugs to exist in two or more polymorphic forms (Adsmund and Grant, 2001). The sulfa drugs used for this study include sulfadimidine (SD), sulfadimidine sodium salt (SDNa), sulfathiazole; form I (STZ I) and III (STZ III) and sulfathiazole sodium salt (STZNa).

1.5.1 Sulfadimidine

CAS registration number 57-68-1, chemical formula $C_{12}H_{14}N_4O_2S$, chemical name 4- N1-(4,6-Dimethyl-2-pyrimidinyl) sulfanilamide, molecular weight 278.33 g/mol. Sulfadimidine has a monoclinic structure crystal structure (Tiwari, 1984). The chemical structure is outlined

in figure 1.10. It is a white or almost white powder or crystals, very slightly soluble in water but soluble in acetone (British Pharmacopeia, 2009).

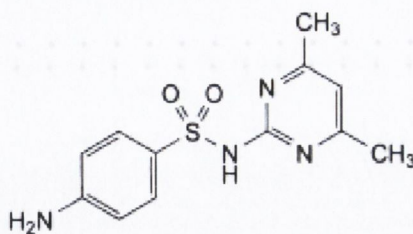


Figure 1.10: Chemical structure of sulfadimidine.

1.5.2 Sulfadimidine sodium salt

CAS registration number 1981-58-4, chemical formula $C_{12}H_{13}N_4NaO_2S$, chemical name 4-amino-n-(4,6-dimethyl-2-pyrimidinyl)-benzenesulfonamide monosodium salt, molecular weight 300.31 g/mol. It is white or milk white crystalline powder, odourless or almost odorless; easily soluble in water, slightly soluble in ethanol (Wujiang Bolin Industry, 2007). The structure of sulfadimidine sodium salt is shown in figure 1.11. The crystals are held in a triclinic formation and a single dehydrate form has been reported (Patel, 1995).

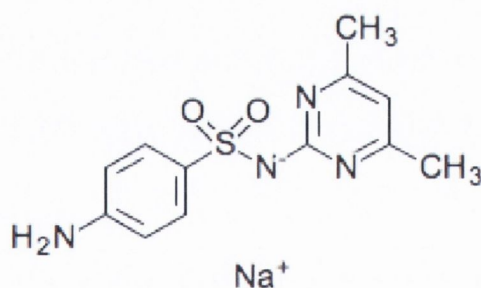


Figure 1.11: Chemical structure of sulfadimidine sodium salt.

1.5.3 Sulfathiazole

CAS registration number 72-14-0, chemical formula $C_9H_9N_3O_2S_2$, chemical name 4-amino-N-(1,3-thiazol-2-yl)benzenesulfonamide, molecular weight 255.32 g/mol. Sulfathiazole has five known polymorphic structures. The Cambridge crystallography data centre (CCDC) reference codes of the 5 characterised crystalline phases are suthaz01 (form I), suthaz (form II), suthaz02 (form III), suthaz04 (form IV) and suthaz05 (form V). The main differences

between the polymorphs of sulfathiazole is attributed to the hydrogen bonding and its effects on the arrangement of the molecules in the crystal lattice (Blagden *et al.*, 1998). Table 1.2 outlines the main properties of each polymorphic form and Figure 1.4 illustrates the chemical structure of sulfathiazole.

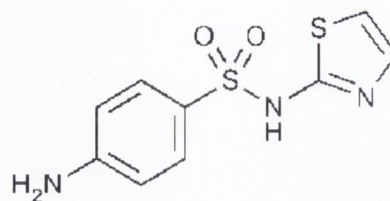


Figure 1.12: Chemical structure of sulfathiazole

Table 1.2: Summary of sulfathiazole polymorph characteristics

<i>Characteristic</i>	<i>Form I</i>	<i>Form II</i>	<i>Form III</i>	<i>Form IV</i>	<i>Form V</i>	Reference
Melting or transition temperature (°C)	201	Between 130-170	173.6	Between 130-170	196	Lagas and Lerk (1981), Zeitler <i>et al.</i> , (2006); Munroe <i>et al.</i> , 2012
Morphology	Neddle	cuboid	hexagon	hexagonal structure	Plate like	Blagden <i>et al.</i> , 1998
X-ray angle 2θ/ degrees	peak at 17.7° 2θ	major peak at 21.6° 2θ, peak at 25.18° 2θ, triplet at 15° 2θ	major peak triplet at 21.7° 2θ, peak at 22.9° 2θ, doublet at 20-20.4° 2θ	major peak at 22.22° 2θ peak at 25.57° 2θ	peak at 23.3° 2θ doublet at 15.9-16.2° 2θ	Munroe <i>et al.</i> , 2012

1.5.4 Sulfathiazole sodium salt

CAS registration number 144-74-1, chemical formula $C_9H_8N_3NaO_2S_2$, chemical name 4-Amino-N-(2-thiazolyl)benzenesulfonamide sodium salt, molecular weight 277.30 g/mol. It is a white or yellowish white crystalline powder or granules and is freely soluble in water (B.P., 2009). Sulfathiazole sodium is also known to be highly (pseudo) polymorphic and, a

monohydrate, a sesquihydrate, a 4.6.H₂O hydrate and an exahydrate have been reported in the literature (Crusellas, 1943; Rubino, 1989). The structure of sulfathiazole sodium salt is shown in figure 1.13.

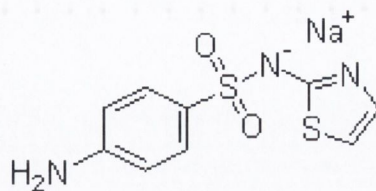


Figure 1.13: Chemical structure of sulfathiazole sodium salt

Experimental

2.1 Materials

Material	Supplier
Sulfadimidine (Sulfamethazine) (C ₁₂ H ₁₄ N ₄ O ₂ S)	Sigma, Ireland
Sulfadimidine sodium salt (Sulfamethazine sodium salt) (C ₁₂ H ₁₃ N ₄ NaO ₂ S)	Sigma, Ireland
Sulfathiazole (C ₉ H ₉ N ₃ O ₂ S ₂)	Sigma, Ireland
Sulfathiazole sodium salt (C ₉ H ₈ N ₃ NaO ₂ S ₂)	Sigma, Ireland
Ethanol	Cooley distillery, Ireland
Acetonitrile (HPLC grade)	Fisher Scientific, UK
Magnesium stearate	Aldrich
Nitrogen gas (high purity, oxygen free)	BOC Gases, Ireland
Water deionised (H ₂ O)	Purite Prestige Analyst HP, Millipore Elix 3 (UK)

2.2 Methods

2.2.1 Ball Milling

Ball milling was carried out with a Retsch PM 100 Planetary Mill (Retsch, UK) (Figure 2.1) at room temperature (RT) (23 ± 1.5 °C) and $4^{\circ}\text{C} \pm 0.33^{\circ}\text{C}$. Stainless steel milling jars of 50 cm^3 with three balls ($\text{Ø} = 20\text{ mm}$) of the same material were used. The quantities milled included 5g, 3.3g, 2.8g and 2.4g corresponding to a ball-to-powder weight ratio (BTP) of 20:1, 30:1, 35:1 and 40:1, respectively. Samples were milled for 5, 30, 60, 120 minutes and 5, 10, 15 and 20 hours. To avoid overheating, every 30 minutes of milling was followed by a 10 minute rest period and reverse rotation was implemented after each 30 minute milling period. Milling speed was set at 400 rpm, which corresponds to 6.7 Hz. Table 2.1 outlines the experimental parameters used for each material.



Figure 2.1: Retsch PM 100 Planetary mill

Table 2.1: Ball milling parameters used for each material

Material	Temperature	Ball-to-powder weight ratio	Time (minutes)
Sulfadimidine	Room temperature	40:1	5, 30, 60, 120, 300, 600, 900, 1200
		20:1	5, 30, 60, 120, 300, 600, 900, 1200
	4 °C	40:1	5, 30, 60, 120, 300, 600, 900, 1200
		35:1	5, 30, 60, 120, 300
		30:1	5, 30, 60, 120, 300
		20:1	5, 30, 60, 120, 300, 600, 900, 1200
Sulfadimidine sodium salt	Room temperature	40:1	5, 30, 60, 120, 300, 600
		20:1	5, 30, 60, 120, 300, 600, 900
	4 °C	40:1	5, 30, 60, 120, 300, 600
		20:1	5, 30, 60, 120, 300, 600, 900
Sulfathiazole Form III	Room temperature	40:1 (batch Y)	5, 30, 60, 120, 300, 600, 900, 1200
		20:1 (batch X)	5, 30, 60, 120, 300, 600, 900, 1200
	4 °C	20:1 (batch X)	5, 30, 60, 120, 300, 600, 900, 1200
Sulfathiazole Form I	Room temperature	40:1	5, 30, 60, 120, 300, 600, 900, 1200
Sulfathiazole sodium salt	Room temperature	40:1	5, 30, 60, 120, 300

2.2.2 Crystallisation of sulfadimidine

Sulfadimidine was crystallised from a saturated solution in acetonitrile (Tiwari *et al.*, 1984). Acetonitrile (50 ml) was placed in a beaker with a teflon-coated magnetic stirrer and heated to below its boiling temperature (82 °C) on a hot plate (Stuart, Staffordshire, UK, SD162, $\pm 0.5^\circ\text{C}$). Excess solid, i.e. 1g of sulfadimidine was added to the beaker to create a saturated solution. This was agitated at 250 rpm and allowed to equilibrate for 30 minutes. After equilibration, agitation was stopped and the solids were allowed to settle. Samples of the clear saturated solution (10 ml) were transferred from the beaker to dry weighed vials, and these were covered with parafilm, which was pierced with three holes. To determine the best conditions for solvent evaporation and crystal growth, vials were stored at 25 °C, 45 °C and RT and monitored daily. A sample of the un-dissolved solute was examined by PXRD to ensure that the original phase had not transformed. The sulfadimidine crystal growth from the saturated solution was analysed by powder X-ray diffraction (PXRD), differential scanning calorimetry (DSC) and light microscopy (Olympus, CKX41). The positions of the PXRD Bragg peaks for the crystallised SD were compared to the peak positions from the diffractogram obtained from the Cambridge Crystallographic Data Centre (CCDC). The enthalpy of melt obtained for the crystallised sample and that obtained for the commercially available sample were compared.

2.2.3 Production of sulfathiazole polymorph form I

Sulfathiazole (Sigma, Ireland) (10g) was placed on aluminium plates (Fisher Scientific, 57 mm Ø, Catalogue No.: 08732101). The sample was heated in an oven (Memmert, Germany) to $\sim 175^\circ\text{C}$ for 6 hours. Above 170°C the polymorphs convert to Form I (Chan *et al.*, 1999). The samples were analysed by PXRD and compared to the CCDC diffractogram to ensure characteristic peaks of form I were detected and thermal analysis (DSC) was carried out to ensure the thermogram was characteristic of the pure Form I. Once the sample was confirmed to be Form I it was used for further analysis.

2.2.4 Production of amorphous standards by melt quenching

Amorphisation of sulfadimidine and sulfathiazole was achieved by placing approximately 5 g of the material obtained from Sigma on a aluminium plate (57 mm Ø) (Catalogue No.: 08732101) and heating on a hot plate (Stuart, UK, SD162, $\pm 0.5^\circ\text{C}$) until all the powder reached its liquid state. The liquid state was reached at $\sim 200^\circ\text{C}$ for both materials. Once the liquid state was reached, a tongs was used to immerse the aluminium pan into liquid nitrogen. The glassy material was removed from the aluminium pan and ground with a pestle and mortar until a powder consistency was reached. Samples were characterised by PXRD and used for heat capacity measurements, which was carried out by modulated temperature differential scanning calorimetry (MTDSC). Melt quench amorphous samples were used to construct calibration curves described in section 2.2.14.1.

2.2.5 Thermal analysis

2.2.5.1 Differential scanning calorimetry (DSC)

Differential scanning calorimetry (DSC) analysis was carried out using a Mettler Toledo DSC 821^e (Switzerland) combined with a refrigerated cooling system (LabPlant RP-100). The purge gas for each test was nitrogen. Once the sample was placed in the aluminium pan and the mass noted, they were hermetically sealed and three vent holes were then placed in the lid. Sample weights varied from 5 mg to 10 mg. A heating/cooling rate of $10^\circ\text{C}/\text{min}$ was used, unless stated otherwise. Mettler Toledo STAR^e software (version 6.10) was used to control and analyse the DSC scans and results. The unit was calibrated with indium and zinc regularly. All samples were run at least in duplicate.

2.2.5.2 Modulated temperature differential scanning calorimetry

Modulated temperature differential scanning calorimetry (MTDSC) was performed using a DSC Q200 from TA instruments (UK) combined with a DSC TA refrigerated cooling system (RCS90 (120v/60Hz), (UK)). Nitrogen was used as the purge gas. Prior to sample testing a calibration run was carried out under the same heating rate conditions as the sample with indium used as the calibration standard. Measuring the heat capacity required the use of sapphire as the calibration standard. The sample was weighed in a TA hermetic pan and one vent hole was placed in the lid. Sample weight varied from 4 mg to 6 mg. To measure the heat

capacity of a sample the following conditions were used: equilibrate at 2 °C; modulate at 1.00 °C every 200 s; isothermal for 5.00 minutes; ramp 1.00 °C/min to above the melt temperature of the material. To evaluate events such as crystallisation and melt, samples were heated from 25 °C to above the melt temperature of the material with a ramp of 10 °C/min. TA Q series software was used to set up analysis and TA universal analysis software was used to analyse the results. All samples were run at least in duplicate.

2.2.5.3 Thermogravimetric analysis

A Mettler TG 50 (Switzerland) module linked to a Mettler MT5 balance was used to analyse the mass loss by thermogravimetric analysis (TGA). The sample was placed in an open aluminium pan and placed in the heating chamber. Sample weights varied from 3 mg to 6 mg. Nitrogen gas was used to purge the chamber. The heating rate of 10 °C/min was employed for all measurements. Mettler Toledo STAR^c software (version 6.10) was used to control and analyse the TGA system and results. All samples were run at least in duplicate.

2.2.6 X-ray diffraction

2.2.6.1 Powder X-ray diffraction

Powder X-ray diffraction analysis was carried out with a Rigaku MiniFlex II (Japan) with a combined Haskris cooling system. Analysis of each sample was carried out using a Cu K_α radiation ($\lambda = 1.54 \text{ \AA}$) for an angle range of 5–40° (2θ), with a step size of 0.05° (2θ) per second. Silicon mounts were used as sample holders. PowDLL converter software was used to convert the raw data to Excel and cpi format for analysis. Microsoft Excel and Traces software was used for further investigation. All samples were run at least in duplicate.

2.2.6.1.1 Calculation of the crystallinity percentage by powder X-ray diffraction

Quantification of the crystallinity of each sample is based on the integration of the total peak area of the PXRD diffraction pattern of the processed material and the unmilled material. The unmilled samples were taken to be 100% crystalline in nature unless otherwise stated. The percentage of crystalline material present in the sample was calculated from:

$$\text{Crystallinity \%} = (T_{\text{MILL}}/T_{\text{RAW}}) * (100) \quad (\text{Equation 2.1})$$

where, T_{MILL} and T_{RAW} are the areas under the peaks of the ball milled sample and the unprocessed/raw material crystalline sample, respectively. The areas of the diffraction patterns are expressed as a percentage of the total peak area (peak and halo) (British Pharmacopeia, 2010).

2.2.6.1.2 Normalised Bragg peak intensity

For comparison purposes in certain cases, the intensity of the Bragg peaks were 'normalised'. This was calculated for each Bragg peak:

$$\text{NPI} = (P_o / P_{\text{max}}) * (100) \quad (\text{Equation 2.2})$$

Where NPI is equal to the normalised peak intensity, P_o is the original peak intensity and P_{max} refers to the max peak intensity that was measured for the diffractogram of interest. The diffractograms that were normalised are noted in the results chapters.

2.2.6.2 Variable temperature x-ray diffraction

Variable temperature XRD was carried out with a Phillips PANalytical X'Pert PRO MPD (Multi purpose diffractometer) diffractometer equipped with an Anton Paar HTK 1200 furnace (UK). The angle range of 5–40° (2θ) and a Cu K α radiation at 1.542 Å was used. A heating rate of 10 °C/min was used with a step size and scan speed of 0.01° (2θ) and 0.02 °/s, respectively. The powder samples were placed on an aluminium oxide sample holder and heated to the temperature of interest and scanned. All samples were run at least in duplicate.

2.2.7 Microscopy

2.2.7.1 Scanning electron microscopy

SEM was carried out with a MiraTescan XMU (Czech Republic) scanning electron microscope. Powdered samples were stuck to the aluminium sample stubs and sputter-coated with gold prior to analysis. All samples were run at least in duplicate.

2.2.7.2 Light microscopy

Light microscopy was carried out using an inverted microscope, Olympus CKX41 (UK). Images were magnified to x40. The imaging software was Cell^A/analysis SIS.

2.2.8 Dynamic vapour sorption

Samples were analysed using a Dynamic Vapour Sorption Advantage apparatus (DVS Surface Measurement Systems, UK) in order to detect if an amorphous phase was present in the unmilled materials received from Sigma. A mass weight of 4-6 mg was loaded into a steel net sample holder and positioned in a microbalance located inside a temperature and relative humidity controlled cabinet. The temperature was maintained constant at 25 ± 0.1 °C. The DVS system measures the uptake and loss of water vapour gravimetrically with a mass resolution of ± 0.1 μ m. The relative humidity was increased by 10 %-step changes from 0 to 90 % and back to 0 %. Deionised water was used to achieve the programmed humidity. Each sample was subjected to a two sorption-desorption cycle (or otherwise stated). Samples were run in duplicate.

2.2.9 Particle size analysis

Particle size was determined with the use of a laser diffraction particle sizer - Mastersizer 2000 (Malvern Instrument, UK). Dry powders were dispersed using a Scirocco dry powder feeder attachment, using 2.5 bar pressure setting and vibrational feed rate of 70 % (or as otherwise stated). A refractive index of 1.57 and absorption index of 0.01 were used for all sulfa compounds (Tajber, 2005). Samples were run in triplicate.

2.2.10 Specific surface area analysis by Brunauer, Emmett, Teller (BET) isotherm

BET analysis was used to determine the surface area of samples. The samples were first dried with a Gemini Smart Prep (USA) under nitrogen and the temperature was set to 30 °C over night to remove any residual water from the surface. A Micromeritics Gemini VI was used to determine surface area. Saturation pressure (P_0) was determined prior to each sample analysis. The samples were exposed to six relative pressures (P/P_0) ranging from 0.05 to 0.3 with an equilibrium time of 10 s. The free space was determined separately for each sample using helium gas. Samples were run at least in duplicate.

2.2.11 Density measurements: Bulk (aerated) and Tap Density

Bulk density (bp) was obtained by measuring the weight of the powder required to occupy a 1 ml volume in a graduated glass syringe poured under gravity. Tapped density (tp) was determined by vertically tapping the sample onto a level bench-top surface from a height of 5 cm x 100 times. The tapped density was calculated as the ratio of the mass to the tapped volume of the sample. Measurements were performed in triplicate unless otherwise indicated, and are expressed as an average +/- standard deviation.

2.2.12 Carr's Index

Carr's Index (CI) is related to powder flowability, for which smaller values indicate better flowability (Wu *et al*, 2001). Equation 2.3 shows how Carr's Index (Carr, 1965) was calculated using bulk and tap densities. Samples were run in at least duplicate.

$$\text{Carr's Index (CI) \%} = [(tp-bp)/tp] \times 100 \quad (\text{Equation 2.3})$$

where, tp and bp are equal to the tapped and bulk density, respectively.

2.2.13 Tableting

Compaction of 0.85 g flat faced tablets with a diameter of 13 mm was carried out with a Cavier C hydraulic press (Germany). The die was prelubricated with magnesium stearate and loaded manually. Compression was carried out in a range from 73 MPa to 292 MPa. Pressure was released immediately after reaching the required compression force. Tablets were removed by pushing them out of the die using the upper punch. Samples were run at least in triplicate.

2.2.13.1 Tablet geometry

Tablet height (h) and diameter (d) were determined with an electronic outside micrometer IP 54 form RS (0.25 mm \pm 0.001 mm) equipped with ABS –anti crushing system (Fowler, China).

2.2.13.2 Evaluation of tablet hardness test and tensile strength

Tablet hardness was determined with a Schleuniger 6D tablet tester (Dr Schleuniger Production AG, Switzerland). Fracture load (shear strength under compressive load) (P) [N] was recorded for each tablet (n=3). The tensile strength (σ_t) was then calculated for each sample using equation 2.4, introduced by Rudnick, Hunter and Holden (1963) and Fell and Newton (1970).

$$\sigma_t = 2P / \pi h d \quad (\text{Equation 2.4})$$

2.2.14 Preparation of physical mixtures

2.2.14.1 Calibration curve (amorphous versus crystalline)

To construct a calibration curve to test the limit of detection (LOD) and limit of quantification (LOQ) of the amorphous phase by PXRD and DSC, physical mixtures of crystalline and amorphous sulfadimidine samples were prepared. The total weight for each test sample was 500 mg. The samples tested contained 100, 98, 96, 90, 85, 80, 70, 60, 50, 40, 30, 20, 10, 6, 4, 2 and 0 % crystalline material supplied from Sigma (Ireland) and the remainder was made up with the amorphous sulfadimidine prepared by melt quench sample. The powders were mixed in a mortar with a spatula for 2 minutes and a new sample was mixed for each test. (n=3).

Limit of detection and limit of quantification was calculated from the linear regression line constructed in Microsoft Excel (as per Eqs. 2.5 and 2.6) from the data collected from the DSC and PXRD analysis. The DSC data was used to calculate the amorphous content (2.2.2.16) and the PXRD total peak area was determined for each sample. These were graphed against the experimental quantities. The experimental quantities and the tested sample quantities were graphs against one another for both the DSC amorphous content and the PXRD peak area.

$$\text{LOD} = 3.3 * (\text{SD} / \text{S}) \quad (\text{Equation 2.5})$$

$$\text{LOQ} = 10 * (\text{SD} / \text{S}) \quad (\text{Equation 2.6})$$

Where SD is equal to the standard deviation of the response and S is equal to the slope of the line.

2.2.14.2 Polymorphic mixtures

Physical mixtures of sulfathiazole Form I (prepared as per the method described in section 2.2.3) and Form III obtained from Sigma (Ireland) were prepared by mixing the powders in a mortar with a spatula. The total weight of each mixture was 500 mg. The weight ratios of Form III to Form I used were: 9.7:0.3, 9.5:0.5, 9:1 and 1:1. Immediately after mixing the samples were tested by DSC and PXRD. A new sample was mixed for each analysis and all analysis were performed at least in duplicate.

2.2.15 Temperature and humidity readings

Temperature and humidity of the milling room and cold room were monitored by a Testo 175 H1, 2 channel temperature and humidity data logger, (Germany). The temperature measuring range of this monitor is -10°C to $+50^{\circ}\text{C}$ with an accuracy of 3%. The temperature of the milling jars was monitored with an ETI RayTempTM 8, laser thermometer (Electronic Temperature Instruments, UK). The temperature measurement range of the thermometer is -60 to 500°C and the accuracy is $\pm 2^{\circ}\text{C}$. At least two temperature readings were taken from the powder immediately after milling.

2.2.16 Calculation of the amorphous fraction by differential scanning calorimetry

The amorphous content was determined with the following formulae (Lefort *et al.*, 2004). This method was used because the induced amorphous phase does not always fully crystallise upon heating during the crystallisation event. If it does not fully crystallise it remains in the sample until it melts and the enthalpy of melt can be compromised. Therefore the following equations corrects for this event and the equations allow for the calculation of the induced amorphous phase more precisely.

Equation 2.7 was used first to calculate the enthalpy of melt for the pure crystalline state ($\Delta H_{cr}(T_{cr})$). To calculate the fraction of material that did not crystallise upon heating (α) with equation 2.8. The total amorphous fraction (τ_{DSC}) by DSC is obtained using equation 2.9.

$$\Delta H_{cr}(T_{cr}) = \Delta H^a_m(T_m) - (T_m - T_{cr}) * \Delta C_p = \Delta H^a_m(T_{cr}) \quad (\text{Equation 2.7})$$

$$1 - \alpha = (\Delta H_m(T_m)) / (\Delta H^a_m(T_m)) \quad (\text{Equation 2.8})$$

$$\tau_{DSC} = (\Delta H_{cr}(T_{cr}) / \Delta H^a_m(T_{cr})) * (1 / (1 - \alpha)) \quad (\text{Equation 2.9})$$

Where (ΔH^a_m) is equal to the enthalpy of melt of the pure crystalline material, T_m is the melting temperature, T_{cr} is the temperature of crystallisation, ΔC_p is the heat capacity, α is the fraction of material that does not crystallise upon heating and τ_{DSC} is the DSC amorphous content.

2.2.17 Solid state stability study

Ball milled samples were subjected to stability studies in desiccated conditions over phosphorus pentoxide at 4 °C. Humidity and temperature were monitored using a data logger (section 2.2.15). Samples were characterised after 1, 2, 3, 4, 8 and 12 weeks of storage using PXRD and DSC.

2.2.18 Statistical analysis and data fitting

Statistical analysis was carried out using the following software:

- Origin[®] Software, version 7.5, Aston Scientific Ltd.
- Microsoft[®] Excel, Office package, version 2003.
- GraphPad Prism Software, version 5, 2007.

Data fitting was accomplished using Origin Software (Version 7.5, Aston Scientific Ltd) to determine the Avrami k value. Statistical analysis such as ANOVA and Tukeys paired t-tests and the Spearman correlations were preformed using GraphPad Prism software (Version 5).

Results and discussion

Ball milling of sulfadimidine

3.0 Introduction

Ball milling can result in changes of a materials physiochemical and micomeritic properties such as decreased crystallinity, increased amorphous content, polymorphic transformations, reduction in particle size, increased surface area and changes to the morphology. These changes may be influenced by the materials thermal and solid-state nature (Dubinskaya, 1999) and/or by one or more of the several ball milling parameters (Suryanarayana, 2001; Rubinstein and Gould, 1987) such as time, temperature, rotational speed and the quantity of material used in relation to the weight of the milling balls.

This chapter first examines the characterisation of the unmilled API material received from Sigma, Ireland. The model API was sulfadimidine (SD). The effects of different ball milling parameters were investigated. The ball-to-powder (BTP) weight ratios of 40:1 and 20:1 were used to investigate the influence they had on the crystal structure of SD when milled at room temperature (RT) and 4 °C for 5, 30, 60, 120 minutes and 5, 10, 15 and 20 hours at a rotational speed of 400 rpm. Further analysis of how different BTP weight ratios influenced changes to the crystal structure was investigated by milling SD at 4 °C with BTP weight ratios of 30:1 and 35:1 for 5, 30, 60 and 120 minutes and 5 hours. The study was preformed by varying one factor at a time. Changes induced by milling which evaluated the loss of crystallinity by powder X-ray diffraction (PXRD), quantification of amorphous content by thermal analysis, changes to the particle size distribution by laser diffraction and surface area measurements by BET. Statistical analysis by Tukey's multiple comparison test and ANOVA was used to investigate statistical differences between the unmilled and milled samples. The results obtained from this study may indicate if significant changes to the material's solid state incurred as a result of milling for short milling times (after 5 or 30 minutes) or whether the changes were due to prolonged milling (up to 20 hours). To evaluate thermal changes within the jar the temperature of the sample was recorded. Changes to the induced amorphous phase characterised by DSC analysis, upon storage of the milled SD samples were evaluated and the Avrami equation was used to investigate the crystallisation kinetics.

3.1 Sulfadimidine unmilled

3.1.1 Powder X-ray diffraction

Figure 3.1 illustrates the diffractograms for sulfadimidine (SD) obtained from Sigma (Ireland), the Cambridge Crystallographic Data Centre (CCDC) referenced from Tiwari *et al.*, (1984) and sulfadimidine crystallised from solution, following the procedure described by Tiwari *et al.*, (1984). The diffractogram obtained from CCDC was simulated from single crystal XRD analysis. Each XRD pattern displays distinct Bragg peaks characteristic of a crystalline material. The angular diffraction peak positions for all three materials were the same, confirming that the material obtained from Sigma Ireland was SD. The intensity of the peaks were different but this was due to a contribution of preferential orientation, instrumental effects and the fact that CCDC data is simulated from single crystal XRD analysis.

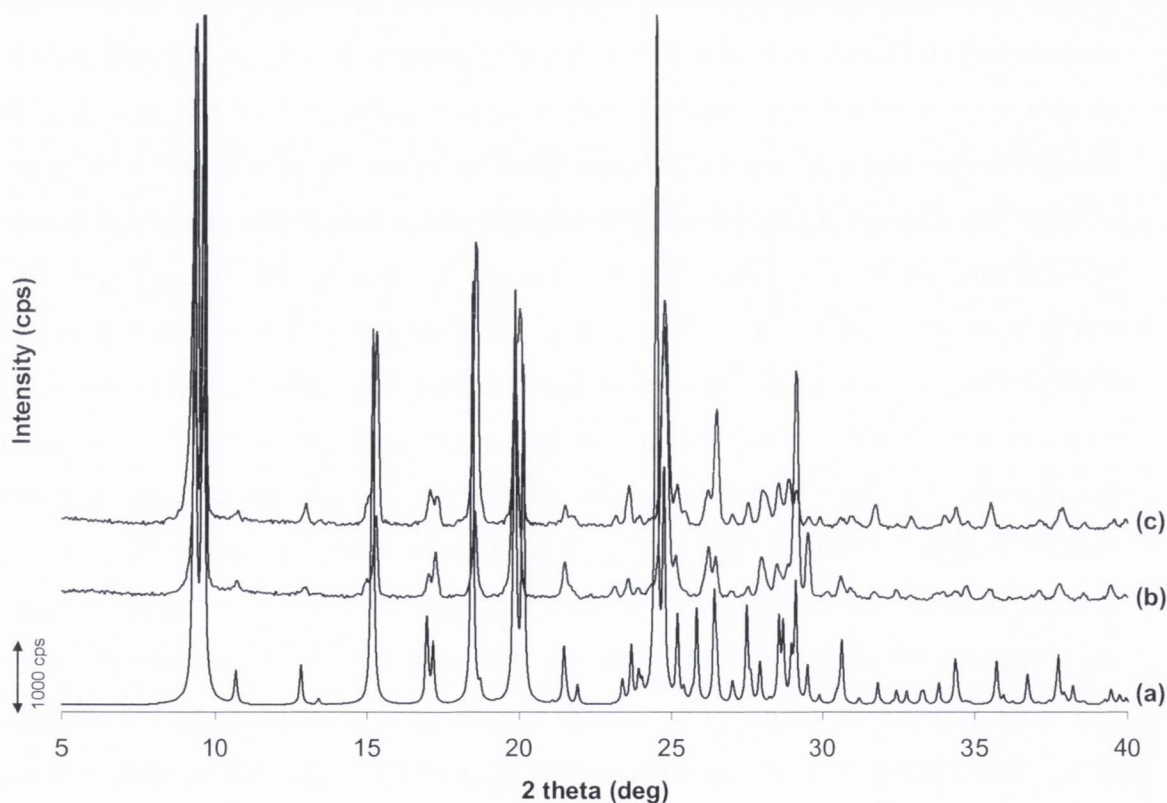


Figure 3.1: Powder XRD of SD (a) diffractogram obtained from CCDC; (b) SD crystallised from solution; (c) SD from Sigma unmilled sample.

3.1.2 Dynamic vapour sorption

Dynamic vapour sorption (DVS) analysis has been used to determine the presence of an amorphous phase within crystalline materials, containing as little as 0.05 %w/w amorphous content (Buckton and Darcy, 1995). Amorphous solids uptake relatively large amounts of water vapour compared to their crystalline counterparts. The sorbed water can act as a plasticising agent, lowering the glass transition temperature to below the storage temperature which results in a phase transition. Mackin *et al.*, (2002) has illustrated the crystallisation of amorphous xemilofiban as a result of exposing the material to increasing relative humidity (RH). They found that, at 60 % RH, a sharp decrease in weight was observed and attributed this to the expulsion of water indicating the phase transition. A sharp decrease in mass indicates a water-induced crystallisation event, as water acts as a plasticising agent, thus lowering the glass transition temperature and inducing spontaneous crystallisation.

Analysis of the unmilled SD material by DVS is shown in Figure 3.2. Relative humidity was increased from 0-90 %RH to ensure the unmilled material from Sigma was crystalline in nature and contained no residual amorphous phase. The steady increase in water vapour with no sudden mass loss steps confirmed the crystalline nature of the material. The presence of a decrease in the mass uptake sorption cycle, described by Buckton and Darcy (1995) and Mackin *et al.*, (2002) indicates an amorphous phase but the lack of this decrease would suggest no amorphous phase present within the material. Fast and small uptake levels indicate surface water adsorption on the sample (Gregg and Sing, 1982). The low water uptake observed as RH was increased from 0% RH to 80% RH may indicate that the water was sorbed onto the surface. The large uptake observed as RH was increased from 80 to 90 %RH may indicate saturation of the sample.

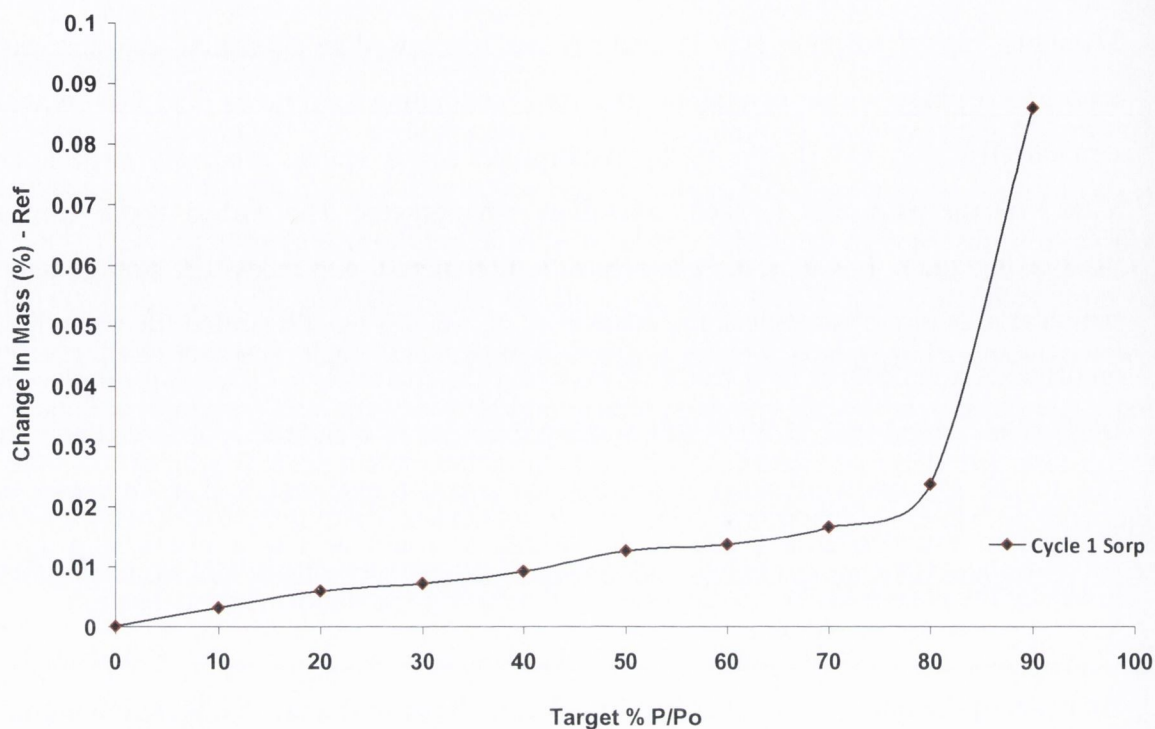


Figure 3.2: Water sorption isotherm for unmilled sulfadimidine (Sigma, Ireland) at 25 °C.

3.1.3 Thermal analysis

Thermal analysis by differential scanning calorimetry (DSC) of SD received from Sigma and SD crystallised from solution, shows one thermal event onset at 197 °C representing a melt (Figure 3.3a and b). This corresponds to the reported literature value of 197 °C and the enthalpy change for the observed peak for both samples corresponds to the reported enthalpy of fusion as reported by Nolan (2008) of ~120 J/g. This one thermal event suggests a crystalline state. Thermogravimetric analysis shows a mass loss of ~1.38 % when heated from 25 to 200 °C. Modulated temperature DSC analysis of the unmilled SD material shows that the crystalline material has a heat capacity of ~0.015 J/g^oC.

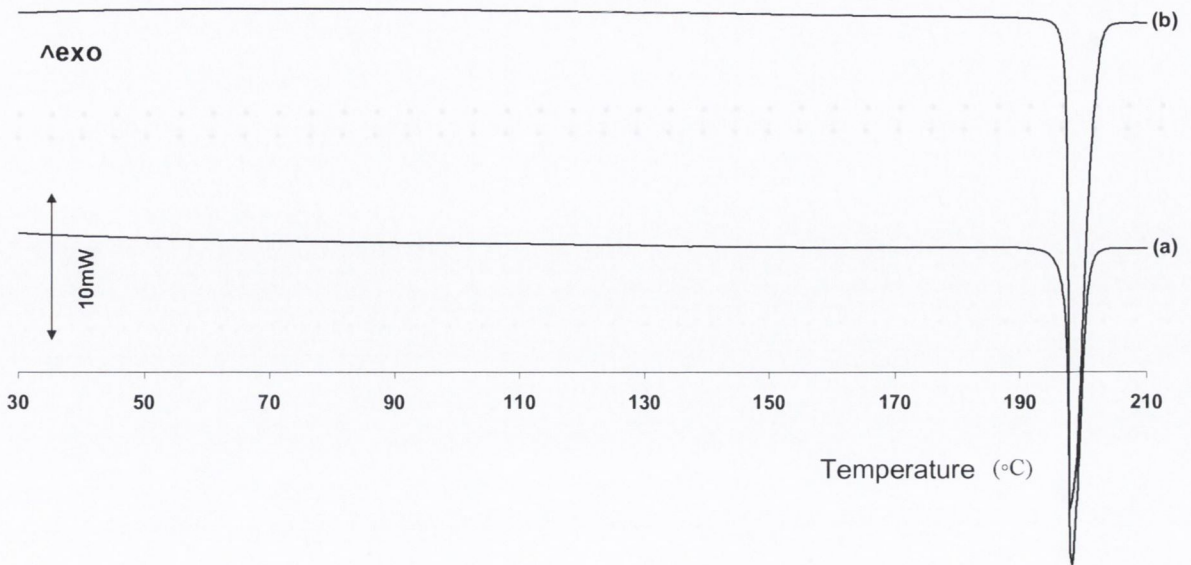


Figure 3.3: DSC scan of (a) unmilled SD received from Sigma, (Ireland) and (b) crystallised from solution.

3.1.3 Particle size analysis, surface area and morphology

Table 3.1 shows the particle size as analysed by laser diffraction and the specific surface area (SSA) as analysed by BET for SD unmilled (Sigma). The particle size distribution was monomodal in shape (Figure 3.4) and the median particle size was $7.69 \pm 0.12 \mu\text{m}$. The specific surface area for crystalline SD was $0.99 \pm 0.30 \text{ m}^2/\text{g}$.

Table 3.1: The particle size and specific surface area of SD unmilled Sigma (Ireland).

Particle size (μm)			SSA
d10	d50	d90	(m^2/g)
3.23 (0.12)	7.69 (0.12)	17.72 (3.66)	0.99 (0.30)

Standard deviation in parentheses. $n = 3$

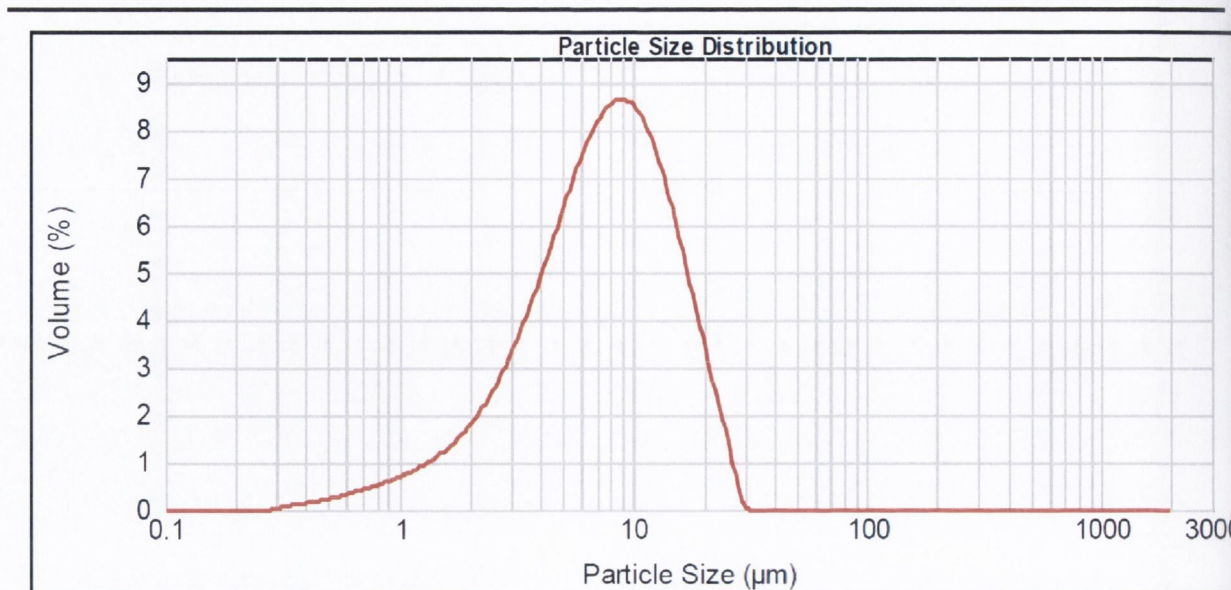


Figure 3.4: Particle size distribution profile of sulfadimidine unmilled determined by Malvern laser diffraction.

SEM micrographs (Figure 3.5 a and b) revealed that sulfadimidine received from Sigma consisted of crystalline particles that have irregular shape and size. The size range determined by laser diffraction analysis is reflected in the micrographs, with particles ranging from less than 5 μm to greater than 10 μm . The material received from Sigma was a fine white powder. Optical micrographs of SD crystallised from acetonitrile show a mix of needle like particles (Figure 3.5 c) and plates (Figure 3.5 d). The crystals prepared using the method by Tiwari *et al.*, 1984 were clear and small but upon grinding with a pestle and mortar the sample resembled the white powder obtained from Sigma.

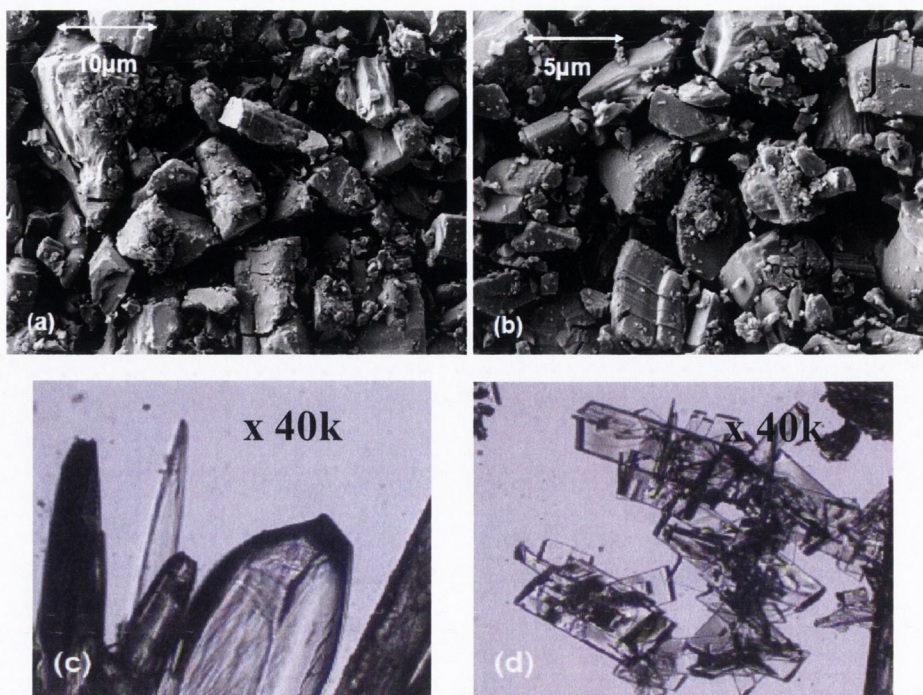


Figure 3.5: (a) and (b) SEM morphology of sulfadimidine (Sigma, Ireland), (c) and (d) Optical micrographs of SD crystallised from acetonitrile x40k.

3.2 Amorphous quantification

Quantification of the amorphous content was evaluated by PXRD and thermal analysis using methods described in chapter 2, sections 2.2.16. By preparing mixtures of known amorphous/crystal compositions, calibration curves were generated. The accuracy of each method was then evaluated. The crystallinity of unmilled SD was assumed to be 100 %. The British Pharmacopoeia (2010) method for quantification of the crystallinity by PXRD, quantifies phases of a mixture based on the integration of peak intensities. In brief, the areas of the diffraction peaks are expressed as a percentage of the total peak area (peaks and halo). Figures 3.6 a and b shows a linear correlation between the total peak area (%) obtained from the PXRD diffractograms and the calculated percentage DSC amorphous content measured for each mixture, respectively. The x-axis in figure 3.5a represents the theoretical crystal quantity of the SD mixtures. The peak area of the unmilled SD was taken to be 100 %. Figure 3.6a illustrates a good fit with $R^2 = 0.9995$ and shows that the method was capable of measuring low levels of crystal content. The limit of detection (LOD) for an amorphous phase by XRD is suggested to be 5-10% (Giron *et al.*, 1997). The LOD and LOQ (limit of quantification) in this study were calculated to be 2 % and 5 %, respectively.

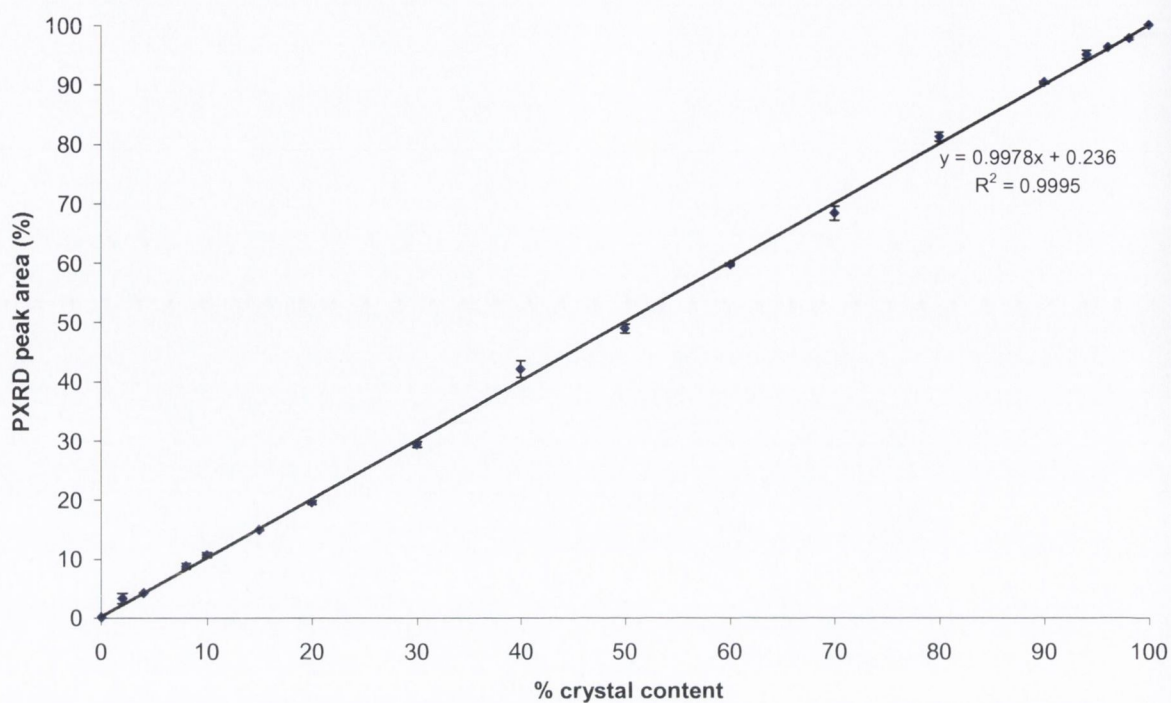


Figure 3.6a: The total peak area of amorphous and crystalline SD mixtures determined by PXR D, plotted against the known crystal content weight fraction. Samples were measured in at least duplicate.

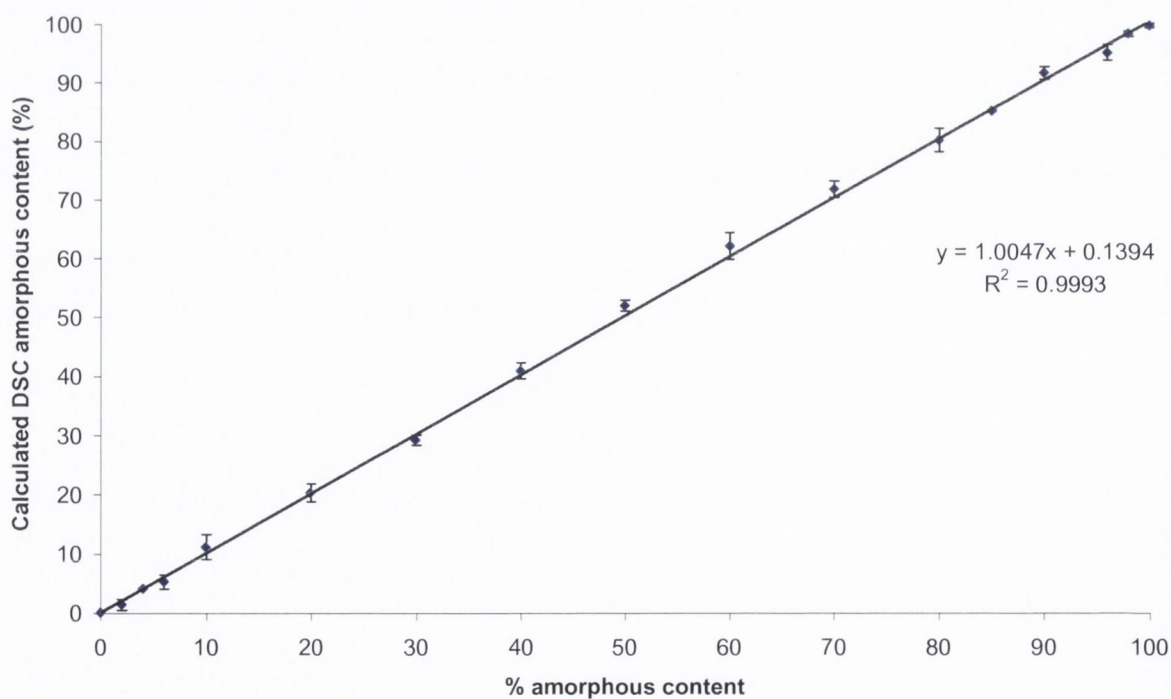


Figure 3.6b: The calculated DSC amorphous content of the mixed SD crystalline and amorphous samples, plotted against the known amorphous content weight fraction. Samples were measured in at least duplicate.

Figure 3.6b compares the calculated DSC amorphous content calculated from the thermograms with the percentage for the amorphous content mixed in each of the SD amorphous/crystal mixtures. A good fit was achieved with an R^2 value of 0.9993 obtained. The DSC amorphous content was calculated using equations described by Lefort *et al.*, (2004). The LOD and LOQ determined from the calibration curved are 3 % and 7 %, respectively. Lefort *et al.*, (2004) used this method to quantify the amorphous fraction induced by ball milling trehalose at a rotational speed of 400 rpm. Their results obtained showed a 3% difference between the calculated amorphous percentage and the expected amorphous fraction when physically mixing amorphous/crystal known compositions. Table 3.2 outlines the theoretical amorphous and crystalline weight fraction for each of the mixtures compared with the calculated DSC amorphous content and the total PXRD peak area for each mixture.

Table 3.2: Comparison of the amorphous fraction measured by weight and determined by powder XRD and DSC.

Theoretical amorphous content (%)	DSC amorphous content (%)	Peak area (%) (PXRD crystalline content)	Theoretical crystalline content (%)
10	11.06 (2.14)	90.30 (0.21)	90
20	20.20 (1.51)	81.15 (0.81)	80
30	29.16 (0.86)	68.28 (1.22)	70
40	40.87 (1.36)	59.65 (0.25)	60
50	51.93 (0.89)	48.90 (0.78)	50
60	62.05 (2.27)	41.99 (1.41)	40
70	71.73 (1.37)	29.31 (0.48)	30
80	80.09 (2.02)	19.50 (0.35)	20
90	91.59 (1.10)	10.60 (0.42)	10
100	99.72 (0.40)	0	0

Standard deviation is in parentheses. n=3

3.3 Influence of milling conditions on crystallinity of sulfadimidine

Ball milling was performed with a Retsch PM100 Planetary mill. Ball milling of sulfadimidine was carried out at room temperature (RT) and 4 °C, with varied ball to powder (BTP) weight ratio of 20:1, 30:1, 35:1 and 40:1, with a milling speed of 400 rpm (6.7 Hz) and milling times of 5, 30, 60 and 120 minutes and 5, 10, 15 and 20 hours. Table 3.3 outlines the combinations of parameters evaluated. Lefort *et al.*, (2004) used similar parameters to induce an amorphous phase when ball milling trehalose. They carried out ball milling with a planetary mill (Pulverisette 7-Fritsch) at RT with a rotational speed of 400 rpm for different periods of time (5 and 15 minutes and 1, 2 and 20 hours).

Table 3.3: Processing parameters for ball milled sulfadimidine

Temperature	Ball to powder weight ratio	Time
Room temperature	40:1	5, 30, 60, 120 minutes & 5, 10, 15 and 20 hours
	20:1	5, 30, 60, 120 minutes & 5, 10, 15 and 20 hours
4 °C	40:1	5, 30, 60, 120 minutes & 5, 10, 15 and 20 hours
	35:1	5, 30, 60, 120 minutes & 5 hours
	30:1	5, 30, 60, 120 minutes & 5 hours
	20:1	5, 30, 60, 120 minutes & 5, 10, 15 and 20 hours

3.3.1 Ball milling at room temperature

3.3.1.1 Powder X-ray diffraction (PXRD)

Figure 3.7 a and b compares the PXRD of sulfadimidine unmilled and ball milled at RT from 5 minutes to 20 hours. Figure 3.7a displays the results obtained as a result of ball milling SD with a ball to powder weight ratio (BTP) of 40:1 and Figure 3.7b displays the diffractograms obtained when SD was milled with a BTP weight ratio of 20:1. Characteristic Bragg peaks observed for SD unmilled indicate a crystalline material. The intensity of the Bragg peaks

decreased as milling time was increased from 5 minutes to 20 hours (Figure 3.7a). Table 3.4 outlines the decrease of the total peak area as milling time is increased. The total peak area was obtained by Traces software and these results represent the percentage crystallinity. The total area of the diffracted peaks of the milled material was used and is expressed as a percentage of the total area of the diffracted peaks of the unmilled SD (Grisedale *et al.*, 2011). As there was only water uptake observed by DVS analysis and the Bragg peaks are in the same positions as those the CCDC simulated pattern and the sample prepared from the method outlined by Tiwari *et al.*, (1984), the crystallinity of the unmilled SD material obtained from Sigma was taken to be 100%.

De Gusseme *et al.*, (2008) reported that as a result of ball milling fananserine that the increased broadness of the Bragg peaks is likely due to the small crystallite sizes and lattice distortions of the crystal as a result of milling. Caron *et al.*, (2011) reported that the crystalline defects induced by the milling process results in a static disorder which is not expected to contribute to a change in the heat capacity at the glass transition temperature. The decrease of crystallites as a result of ball milling can be reflected as a broadening of the diffraction peaks. This may be confirmed by the decrease of the melting temperature according to the Gibbs-Thomas law. Therefore the initial peak area decrease may be attributed to a decrease in crystallite size.

The structural evolution of SD, as milling time was increased, is observed in Figure 3.7a, Bragg peaks give way to a predominantly amorphous halo as milling time reaches 20 hours. Peaks detected at $9.7\ 2\theta$ and $24.95\ 2\theta$ degrees for the 20 hour milled samples, indicated that a certain level of crystal order remained within the structure. Figure 3.5b showed that ball milling SD with a decreased BTP weight ratio to 20:1 resulted in distinct Bragg peaks detected regardless of the milling times investigated, indicating that the structure is still predominantly crystalline.

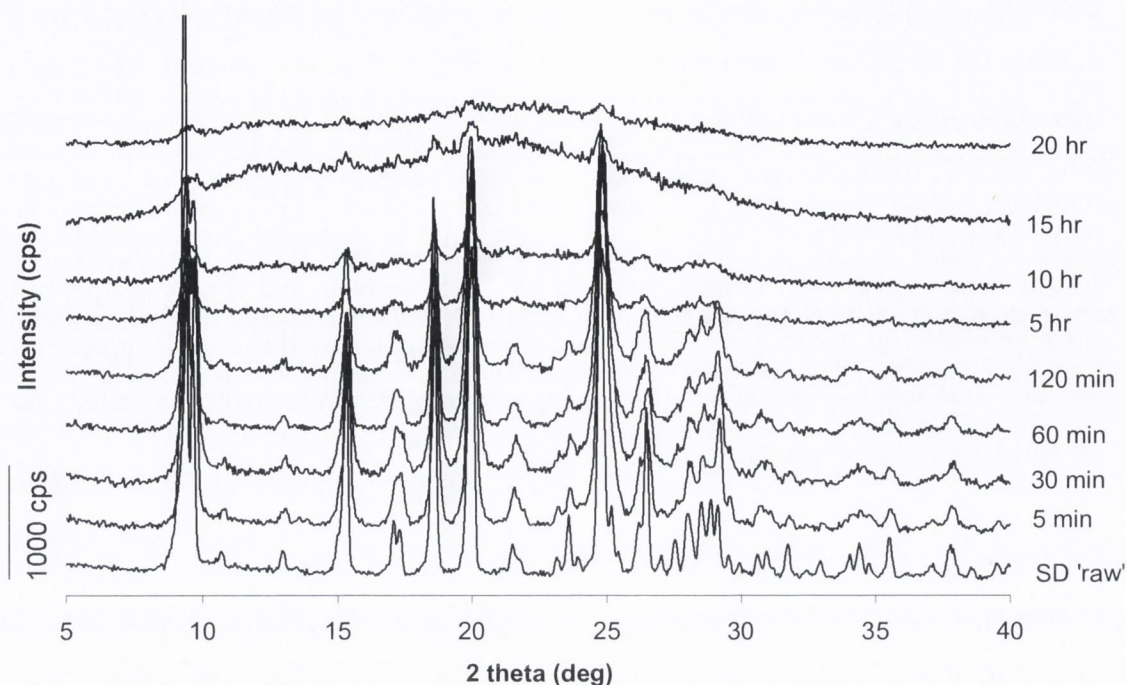


Figure 3.7a: PXRD of SD unmilled ('raw') and milled at RT with a rotational speed of 400 rpm and a BTP weight ratio of 40:1 from 5 minutes to 20 hours.

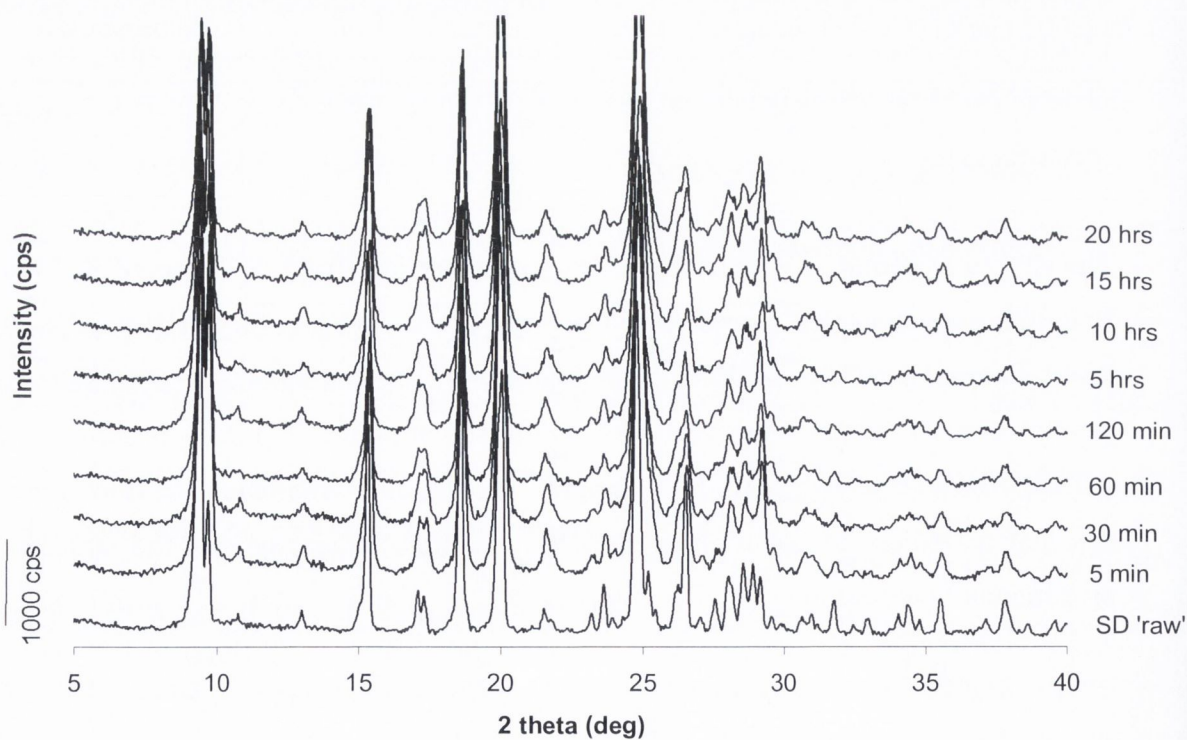


Figure 3.7b: PXRD of SD unmilled ('raw') and milled at RT with a rotational speed of 400 rpm and a BTP weight ratio of 20:1 from 5 minutes to 20 hours.

Initial milling of 5 minutes showed that changes to the crystallinity was less than 1 % for both BTP weight ratios investigated (Table 3.4). Ball milling for 30 minutes resulted in drop in crystallinity to $91.83\pm 0.93\%$ and $98.89\pm 0.14\%$ for BTP weight ratios of 20:1 and 40:1, respectively. Statistical analysis between the samples milled for 30 minutes at both 20:1 and 40:1 BTP weight ratio showed a statistical difference between the samples ($p < 0.0001$). No statistically significant difference was observed between the SD milled samples (5 minutes up to 20 hours) when using a BTP ratio of 20:1 when compared using ANOVA ($p = 0.1376$). Figure 3.8 illustrates the change of PXRD crystallinity of SD unmilled and SD milled from 5 minutes to 20 hours at RT for both BTP weight ratios investigated. This graph was generated from the data shown in Table 3.4 which was generated from the change in total peak areas of the diffractograms in Figures 3.7 a and b.

Prolonged ball milling with a BTP weight ratio of 40:1 resulted in a decrease in crystallinity (Table 3.4). Ball milling for 20 hours resulted in the total peak area to drop to $5.31\pm 0.01\%$ of the unmilled material. Statistically comparing all of the SD samples milled with a BTP weight ratio of 40:1 with ANOVA indicated a difference between the samples. Further analysis using Tukey's multiple comparison test showed a significant difference between the majority of the samples but did suggest that there was no difference between the SD milled samples for 60 and 120 minutes and SD milled for 15 and 20 hours.

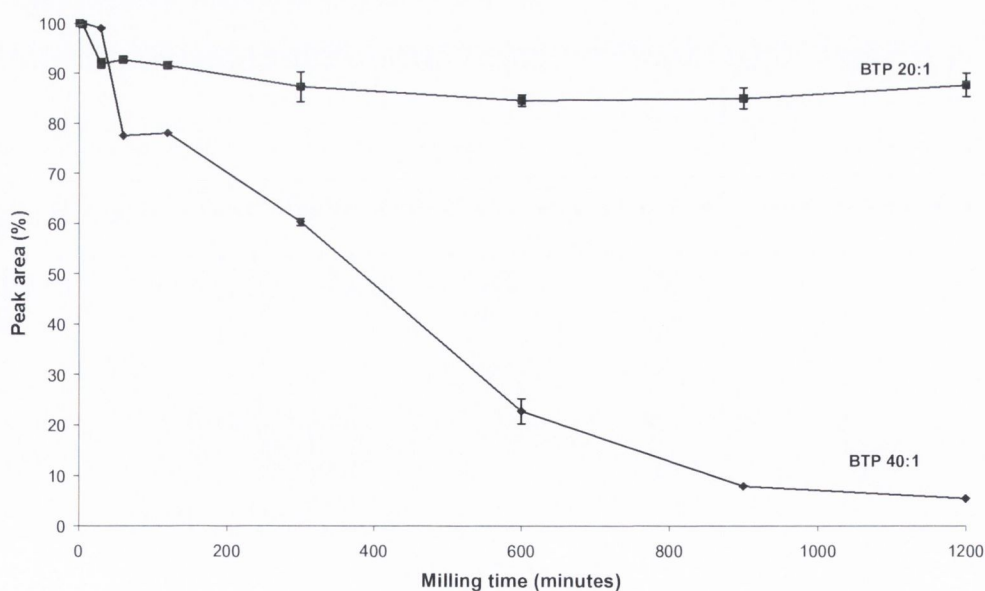


Figure 3.8: Total PXRD peak area for SD unmilled and SD milled from 5 minutes to 20 hours at RT with a BTP weight ratio of 40:1 and 20:1.

Table 3.4: Total peak area for SD unmilled and the percentage of the total peak area remaining as compared to the unmilled SD, as SD was milled at RT with a BTP weight ratio of 40:1 and 20:1 calculated from the PXRD data.

Time (minutes)	BTP 20:1 Peak area (%)	BTP 40:1 Peak area (%)
Unmilled	100	100
5	99.69 (0.49)	99.99 (0.04)
30	91.83 (0.93)	98.89 (0.14)
60	92.62 (0.45)	77.40 (0.01)
120	91.44 (0.71)	77.93 (0.01)
300	87.18 (2.98)	60.21 (0.71)
600	84.42 (1.10)	22.59 (2.46)
900	84.83 (2.10)	7.74 (0.11)
1200	87.53 (2.41)	5.31 (0.01)

Standard deviation in parentheses. n=3

Determining the crystallite size is possible by using the Scherrer equation (Scherrer, 1918) if no tailing at the end of the Bragg peaks is present and the peaks analysed are detected for each sample. These requirements were not met during this study which prevented the crystallite size and the change in the crystallite size to be determined.

3.3.1.2 Thermal analysis

Figure 3.9 shows the thermal analysis by DSC of SD unmilled and milled with a BTP weight ratio of 40:1 at RT. As discussed above the unmilled material was crystalline with a single melt endotherm with an onset at 197 °C. Ball milling for 5 minutes resulted in a thermogram which displayed a single melt endotherm characteristic of a crystalline material. SD samples milled for longer periods (30 min to 20 hours) exhibited two thermal events. For samples milled from 30 to 120 minutes a closer look was required to observe the first exothermic event detected around 80 °C, which is characteristic of a crystallisation event. The

crystallisation exotherm for SD milled for 60 minutes is shown in Figure 3.9. The crystallisation exothermic event observed for samples milled for longer periods (5 to 20 hours) and the second thermal event was attributed to the crystalline melt. The intensity of the crystallisation event increased with milling time as enthalpy (ΔH) of the crystallisation after 5 hours of milling was ~ 26 J/g and the enthalpy increased to ~ 43 J/g after SD was milled for 20 hours (Table 3.5). The onset temperature for crystallisation shifts to higher temperatures with milling time. Ball milling for 30 minutes resulted in a crystallisation onset detected at ~ 53 °C, after 60 minutes of milling the crystallisation onset temperature of ~ 65 °C is measured and as milling time is increased to 20 hours crystallisation is detected at ~ 88 °C. Melting of the unmilled crystal material was detected at ~ 198 °C with an enthalpy of ~ 129 J/g. SD milled samples (5 minutes to 20 hours) have an onset melt temperature detected between 196 and 199 °C and the melt enthalpy was between 127 and 129 J/g.

Chieng *et al.*, (2006) and Brodka–Pfeiffer *et al.*, (2003) observed a similar change in crystallisation and melt temperatures and corresponding enthalpies as a result of ball milling samples for different time periods. Chieng *et al.*, (2006) stated that the difference in thermal behaviours is related to the amount of amorphous drug present. The crystallisation exotherms detected for the milled samples spanned over a 17 degree range, while the melt endotherms temperature ranged within 5 degrees from one another (Chieng *et al.*, 2006). Brodka–Pfeiffer *et al.*, (2003) attributed the difference in the recrystallisation temperature to the fact that the material with the highest amorphous content required more energy to revert back to its thermodynamically stable state. Descamps *et al.*, (2007) reported that ball milling sorbitol for 10 hours at RT resulted in a decrease in the crystallite sizes which was confirmed by the decrease of the melting temperature. The correlation was accredited to the Gibbs Thomas effect which predicts a depression of the melt temperature as a result of the crystallite size change. The decrease in the melt temperature in this study may be as a result of a reduction in the crystallite size induced during the ball milling process. This suggests that the decrease in the total peak area could also be accredited to the change in crystallite size more so than an induced amorphous phase. A decrease in the melt temperature can be observed from Table 3.10. The sample ball milled with a BTP weight ratio were more affected than those ball milled with a ratio of 20:1, as no change was observed. Comparing the melt temperature of the milled SD samples with a ball milled with a ratio of 40:1 showed that a temperature drop was evident after 5 minutes from 197 to 196 °C. A further drop to 195 °C was observed for

samples milled for 30, 60 and 120 minutes. As the DSC amorphous content increased to above 50% the melt temperature increased to 196 °C after 5 and 10 hours and 199 °C for SD samples milled for 15 and 20 hours. This increase may have resulted in a residual amorphous phase that did not crystallise during the recrystallisation event that took place at the lower temperatures.

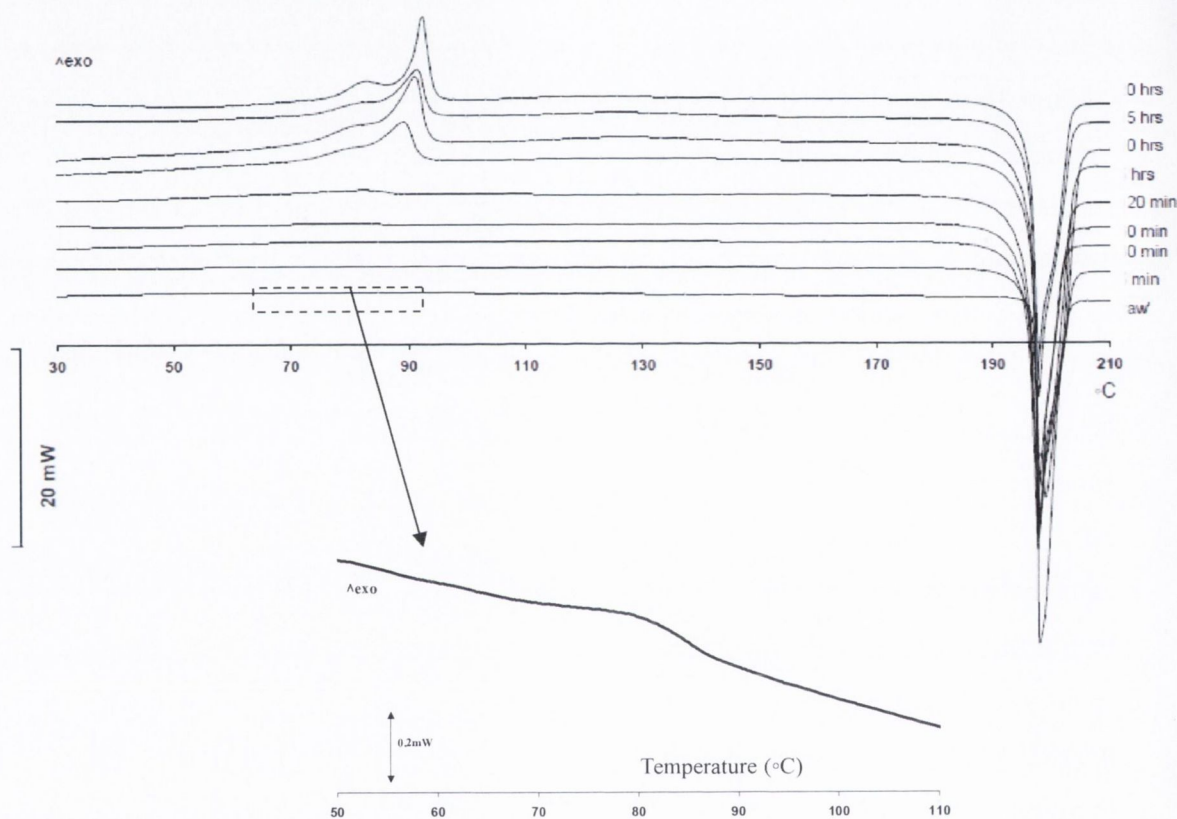


Figure 3.9: DSC scans of sulfadimidine unmilled and milled at RT with a rotational speed of 400 rpm and a BTP weight ratio of 40:1. Magnified area is of crystallisation exotherm detected for SD milled for 60 minutes.

A double crystallisation exotherm peak profile for SD milled for 5, 10, 15 and 20 hours was observed in Figure 3.9. Trasi *et al.*, (2010) observed a double exothermic peak for ball milled griseofulvin and suggested that it was due to a non-uniform distribution of energy within the sample. The rate of crystallisation of surface amorphous material was higher than the bulk of a material (Zhu *et al.*, 2008). Boldyrev and Tkáčová (2000) stated that as a result of milling, energy can accumulate at the surface, then the volume of the bulk, which resulted in an

amorphous material. Trasi *et al.*, (2010) stated that the difference in the rate of crystallisation can be explained by the difference in molecular mobility between the surface and the bulk, and the activation energy required for nucleation and/or growth. The molecules at the surface are in a less confined arrangement than the bulk which led the authors to conclude, that the first exotherm represented crystallisation, which was related to the surface of the amorphous particles and the second exotherm, corresponded to 3D nucleation and growth of the bulk material (Trasi *et al.*, 2010). These changes may have occurred as a result of ball milling sulfadimidine which resulted in the formation of a double exothermic peak.

Detection of a glass transition temperature (T_g) was not possible using conventional DSC techniques as the broad crystallisation peak prevented its detection. Factors contributing to a broad crystallisation peak include a large number of defects, voids and strain (Khatirkar and Murty, 2010). Shah *et al.*, (2006) also suggested that difficulties in observing the T_g could be due to the low levels of amorphous material within the sample. Evaluation of the melt quenched SD samples, by modulated temperature differential scanning calorimetry (MTDSC) to determine the heat capacity at T_g found that the T_g of the amorphous phase induced by melt quench, was ~ 78 °C and heat capacity of 1.37 J/g/°C (data not shown). This corresponds to the reported T_g of ~ 75 °C reported by Caron *et al.*, (2011).

Figure 3.10 illustrates the thermograms for SD unmilled and SD milled at RT with a rotational speed of 400 rpm and a BTP weight ratio of 20:1. Samples milled for 5, 30 and 60 minutes have one thermal event detected at ~ 197 °C, attributed to the melt. Ball milling for 120 minutes, 5, 10, 15 and 20 hours resulted in two thermal events. The crystallisation event detected between 65 and 70 °C is only observed upon magnification. This is followed by a melt endotherm at ~ 197 °C. No statistical difference was observed when comparing the crystallisation enthalpies measured for SD milled for 5, 10, 15 and 20 hours ($p=0.1573$). The melt onset temperature of ~ 197 °C measured for all SD milled materials with a BTP weight ratio of 20:1 from 5 minutes to 20 hours was the same as the unmilled SD material. The melt enthalpy for the milled samples was measured between ~ 128 and ~ 130 J/g (Table 3.5).

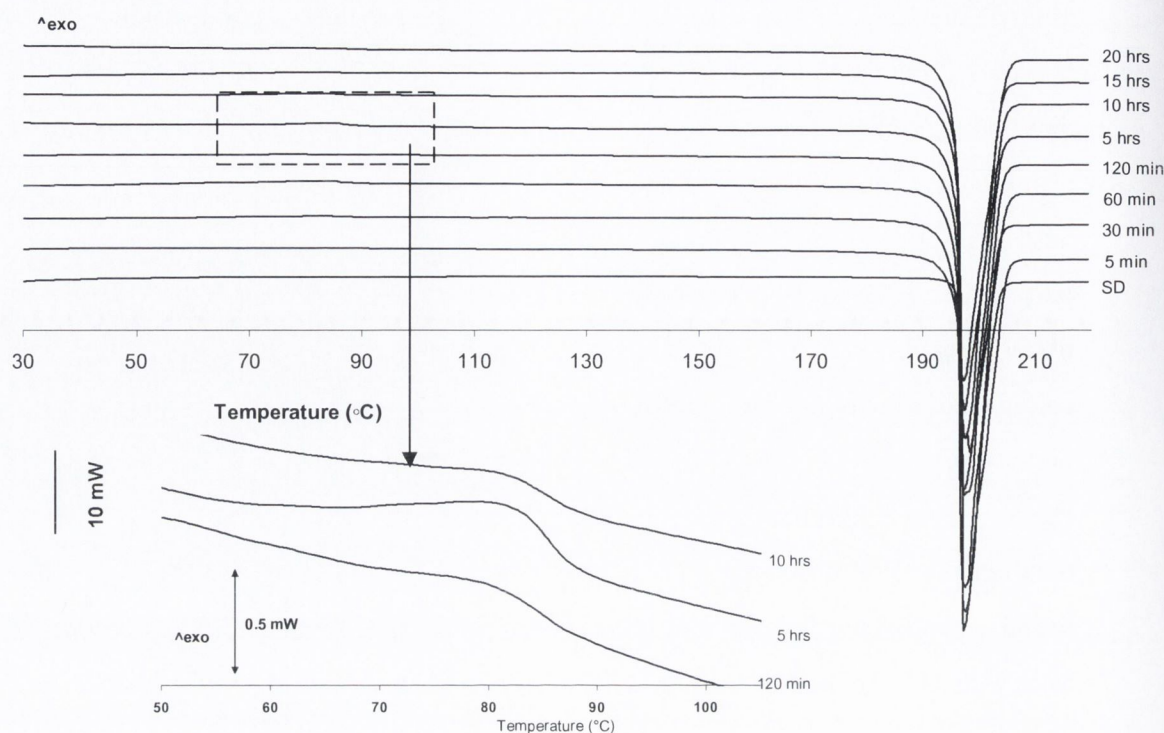


Figure 3.10: DSC scans of sulfadimidine unmilled and milled at RT with a rotational speed of 400 rpm and a BTP weight ratio of 20:1. Magnified section of crystallisation exotherm detected for SD milled for 120 minutes and 5 and 10 hours.

Table 3.5 outlines the crystallisation (ΔH_c) and melting enthalpy (ΔH_m), crystallisation (T_{cr}) and melt (T_m) onset temperatures and the amorphous content calculated using the method described in section 2.2.16, for samples milled with a BTP weight ratio of 40:1 and 20:1. These data were derived from the DSC scans given in Figure 3.9 and 3.10. Thermal analysis showed that ball milling with a BTP weight ratio of 40:1 resulted in a larger level of disorder induced compared to ball milling with a BTP weight ratio of 20:1 for corresponding times. Ball milling with a BTP weight ratio of 40:1 resulted in an increased level of disorder induced with increasing time, as 79.73 ± 0.35 % DSC amorphous content was calculated after 20 hours. DSC amorphous content of 0.65 ± 0.22 % was measured for SD milled for 120 minutes with a BTP weight ratio of 20:1. The highest level of DSC amorphous content obtained when milled with a BTP weight ratio of 20:1 was after 10 hours, calculated at 1.55 ± 1.15 %. No statistically significant difference was observed on comparing the DSC amorphous content induced when comparing the samples ball milled from 5 hours to 20 hours with a BTP weight ratio of 20:1

($p=0.966$). Figure 3.11 illustrates the increased of DSC amorphous content with milling time for both BTP weight ratios investigated.

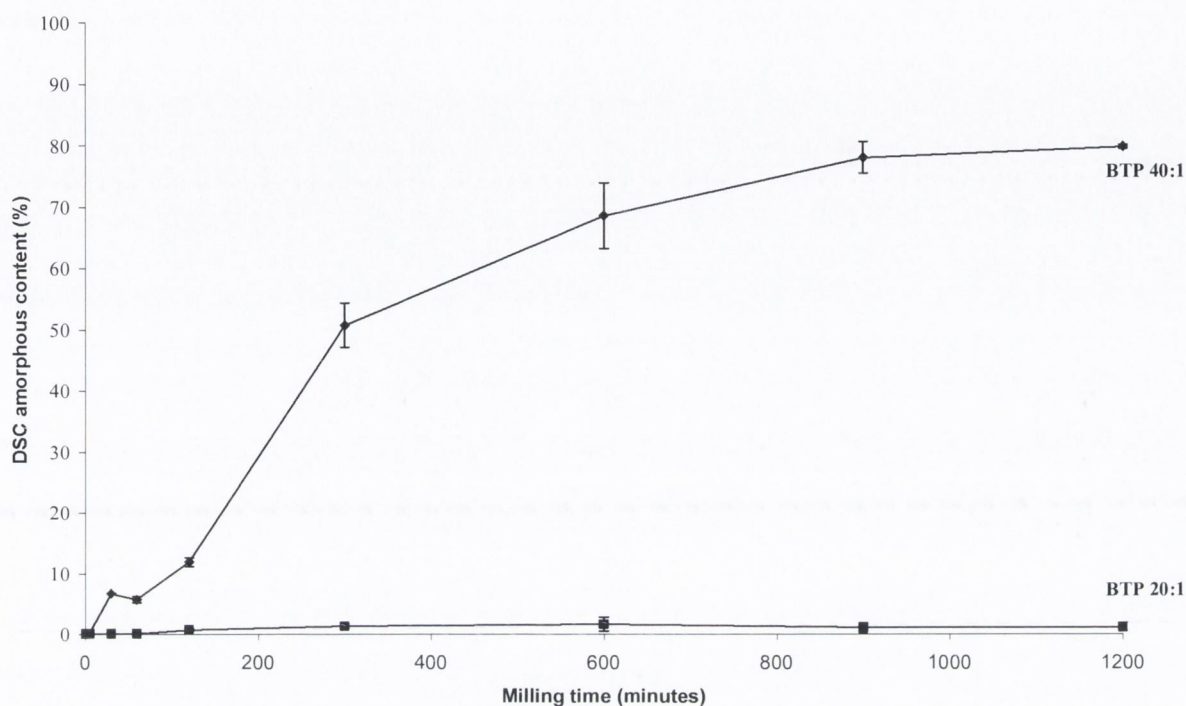


Figure 3.11: DSC amorphous content calculated for SD milled from 5 minutes to 20 hours at RT with a BTP weight ratio of 40:1 and 20:1.

Peak area analysis of PXRD diffractograms showed that ball milling for 20 hours with a BTP weight ratio of 40:1, resulted in a reduction of crystallinity to $\sim 5\%$ (Table 3.4) but DSC analysis of the same sample resulted in a calculated DSC amorphous phase of $\sim 79\%$ (Table 3.5). The crystallisation exotherm event displayed by a DSC thermogram indicated the energy involved in changing the amorphous content to a more thermodynamically stable state and in the case of SD ball milled with a BTP weight ratio of 40:1 at RT this is ~ 40 J/g. PXRD analysis of the powdered samples can include both the disordered and ordered phases. These phases could include crystallites of a variety of sizes, lattice defects, an amorphous halo etc. The peak intensity is related to the formation of atoms, (i.e. crystal structure) as X-ray diffraction intensity corresponds to the number of atoms present at their relevant positions within the crystal motif. Brittain (2002) stated that the milling process causes a variety of deformations and fractures in a solid. Changes to the structure may occur as a result of processing, these changes could be attributed to lattice strain, voids and/or defects but this

does not affect the peak position but does affect the peak intensity. In this study it is possible that as a result of milling the change to the total PXRD peak area of SD milled could be attributed to minor deformation such as strain; voids etc. and to the amorphous phase induced. As mentioned previously the change in the Bragg peak area has also been attributed to the change in the crystallite size (Descamps *et al.*, 2007).

Caron *et al.*, (2011) reported similar problems when evaluating the level of disorder induced as a result of ball milling alpha lactose. Analysis was carried out by PXRD, NMR and DSC. Caron *et al.*, (2011) stated that these techniques can easily distinguish pure crystalline matter from pure amorphous matter but as a result of ball milling the differentiation between the mix of definite crystalline and amorphous phases could not be distinguished.

Table 3.5 outlines the weight loss by TGA for the unmilled and ball milled SD samples occurring between ~25 and 220 °C. The samples ball milled with a BTP weight ratio of 40:1 resulted in a higher mass loss in comparison to those milled with a BTP weight ratio of 20:1. A study by Buckton and Darcy (1996) on water mobility in amorphous lactose below and close to the glass transition temperature noted that the presence of even small amounts of water (as little as 1% of the total weight) may have a significant impact on the physico-chemical nature of the material. They explained that the presence of water can lower the T_g as it acts as a plasticiser until eventually the material has the ability to crystallise. Water trapped in a collapsed amorphous structure may well give rise to problems of instability. The high weight loss by TGA may be attributed to the loss of moisture and this moisture content may affect the stability of the induced amorphous phase.

Table 3.5: Thermal characteristics of SD unmilled and milled at RT

	BTP 40:1						BTP 20:1					
	ΔH_c (J/g)	ΔH_m (J/g)	T_c (°C)	T_m (°C)	DSC amor. content (%)	TGA (%)	ΔH_c (J/g)	ΔH_m (J/g)	T_c (°C)	T_m (°C)	DSC amor. content (%)	TGA (%)
unmilled	-	129.26 (0.24)	-	196.79 (0.89)	0 (0.00)	1.38 (0.02)	-	129.26 (0.24)	-	196.79 (0.89)	0 (0.00)	1.38 (0.02)
5 min	-	128.53 (1.45)	-	196.12 (0.67)	0.00 (0.00)	1.36 (0.03)	-	129.62 (0.21)	-	197.22 (0.07)	0.00 (0.00)	1.54 (0.16)
30 min	2.45 (0.21)	127.05 (0.07)	57.66 (0.60)	195.37 (0.16)	6.61 (0.05)	1.89 (0.23)	-	130.04 (0.09)	-	197.63 (0.71)	0.00 (0.00)	1.51 (0.12)
60 min	2.54 (0.45)	127.66 (0.48)	64.97 (0.91)	195.29 (0.29)	5.62 (0.54)	1.92 (0.11)	-	128.01 (0.47)	-	197.29 (0.06)	0.00 (0.00)	1.43 (0.02)
120 min	5.01 (0.03)	127.43 (0.04)	61.82 (0.02)	195.00 (0.07)	11.85 (0.72)	2.32 (0.32)	0.54 (0.02)	129.21 (0.34)	70.10 (1.09)	197.01 (0.01)	0.65 (0.22)	1.31 (0.03)
5 hrs	26.09 (2.5)	127.50 (1.12)	84.27 (0.35)	195.66 (0.56)	50.64 (3.59)	4.36 (0.25)	1.67 (0.10)	128.11 (0.66)	65.3 (3.54)	197.78 (0.05)	1.23 (0.36)	2.14 (0.03)
10 hrs	34.25 (0.09)	127.83 (1.81)	83.29 (0.43)	195.91 (0.56)	68.53 (5.36)	4.31 (0.39)	0.93 (0.13)	127.68 (0.67)	66.94 (0.01)	197.88 (0.04)	1.55 (1.15)	1.64 (0.21)
15 hrs	39.65 (0.14)	127.75 (0.45)	83.35 (0.40)	198.97 (0.01)	77.98 (2.53)	5.44 (0.52)	0.71 (0.16)	138.92 (0.57)	67.21 (0.81)	197.57 (0.04)	1.02 (0.80)	1.49 (0.07)
20 hrs	43.32 (0.09)	127.20 (0.85)	87.83 (1.76)	197.81 (0.21)	79.73 (0.35)	5.26 (0.46)	0.62 (0.18)	126.25 (0.21)	66.26 (0.89)	197.30 (0.08)	1.08 (0.70)	1.29 (0.18)

Standard deviation in parentheses. n=3, (DSC amor. = DSC amorphous content)

3.3.1.3 Particle size, morphology and specific surface area

Table 3.6 outlines the particle size measurement results for SD unmilled and milled with both BTP weight ratios (20:1 and 40:1) at RT measured by laser diffraction. Figure 3.12 a and b shows the histograms obtained from Malvern laser diffraction analysis for SD milled with a BTP weight ratio of 40:1 and 20:1, respectively. The median particle size for SD unmilled was $7.69 \pm 0.12 \mu\text{m}$. The particle size distribution for SD unmilled consists of a number of small and larger particles which contribute to the shoulders observed on either side of the major peak (Figure 3.12 – unmilled). The change to the particle size distributions as milling time was increased with both BTP weight ratios is outlined in Figure 3.12. Ball milling of SD with both BTP weight ratios at RT resulted in a bi-modal distribution for all samples. Staniforth and Aulton (2007) states that as a result of milling a bi-modal population occurs.

Considering the d10 and d50 measurements, a reduction of particle size was obtained after 5 minutes for both BTP weight ratios. ANOVA was used to compare the unmilled and milled samples of both BTP weight ratios investigated and shows a statistical difference between the SD unmilled and milled ($p \leq 0.0001$). Statistically comparing the d10 measurements for both 20:1 and 40:1 showed that no change was observed until the samples were milled for 5 hours or longer. Ball milling for 5 minutes resulted in a decrease of the median particle size for both BTP weight ratios investigated. As milling time was increased the median particle size increased and a statistically significant difference was detected when comparing the median particle size of sample milled for 5 minutes, 120 minutes, 5 hours and 20 hours, indicating increased milling time resulted in an increased median particle size for the samples that were ball milled with a BTP weight ratio of 20:1.

Particle size analysis of d90 measurements showed that as a result of milling, even for 5 minutes increased the d90, compared to the unmilled sample for both BTP weight ratios investigated. SD milled with a BTP weight ratio of 40:1 resulted in statistical significant differences for d90 measurements between samples milled for 60 minutes vs. 10 hours and 5 hours vs. 10 hours. All other d90 measurements for SD milled with a BTP weight ratio of 40:1 at RT were statistically equal. No statistical difference was present for the d90 measurements for SD milled with a BTP weight ratio of 20:1. This particle size increase was also observed by Brodka-Pfeiffer *et al.*, (2003) when ball milling salbutamol sulphate at RT

from 5 minutes to 5 hours. They found that with increased milling time the portion of coarse particles increased. They suggested that a possible explanation for this phenomenon could be the simultaneous recrystallisation of the amorphous material and therefore particle growth (Brodka-Pfeiffer *et al*, 2003). Staniforth and Aulton (2007) stated that with particle diameters below approximately 5 μm , interactive cohesive forces between the particles generally dominate over comminution stresses as the comminution forces are distributed over increasing surface areas. This eventually will result in particle agglomeration as opposed to particle fracture and size reduction stops.

Table 3.6: Particle size measurements for SD unmilled and SD milled at RT. ANOVA statistical analysis was used to compare the milled materials to the unmilled SD samples.

		d10 (μm)	d50 (μm)	d90 (μm)
	0	3.23 (0.12)	7.69 (0.12)	17.72 (3.66)
BTP 40:1	5 min	1.94 (0.21)	5.94 (0.56)	57.15 (4.23)
	30 min	1.14 (0.04)	5.92 (0.42)	55.03 (3.42)
	60 min	1.20 (0.04)	5.29 (0.30)	49.32 (0.25)
	120 min	1.19 (0.03)	5.30 (0.18)	67.82 (7.19)
	5 hrs	1.28 (0.11)	5.14 (0.03)	50.67 (5.66)
	10 hrs	1.63 (0.19)	6.59 (1.07)	71.92 (7.19)
	15 hrs	1.57 (0.12)	6.25 (0.03)	59.86 (0.71)
	20 hrs	1.72 (0.21)	6.49 (0.43)	61.25 (0.73)
	BTP 20:1	5 min	0.89 (0.09)	3.81 (0.77)
30 min		0.96 (0.08)	5.04 (1.18)	60.17 (7.10)
60 min		0.96 (0.01)	5.02 (0.20)	60.30 (5.43)
120min		0.95 (0.07)	4.86 (0.62)	60.95 (2.58)
5 hrs		1.03 (0.04)	4.95 (0.27)	51.73 (5.48)
10 hrs		1.01 (0.08)	5.36 (0.45)	66.02 (2.55)
15 hrs		1.02 (0.03)	5.54 (0.64)	67.92 (12.41)
20 hrs		1.27 (0.08)	5.53 (0.83)	69.13 (15.74)

Standard deviation in parentheses. n = 3.

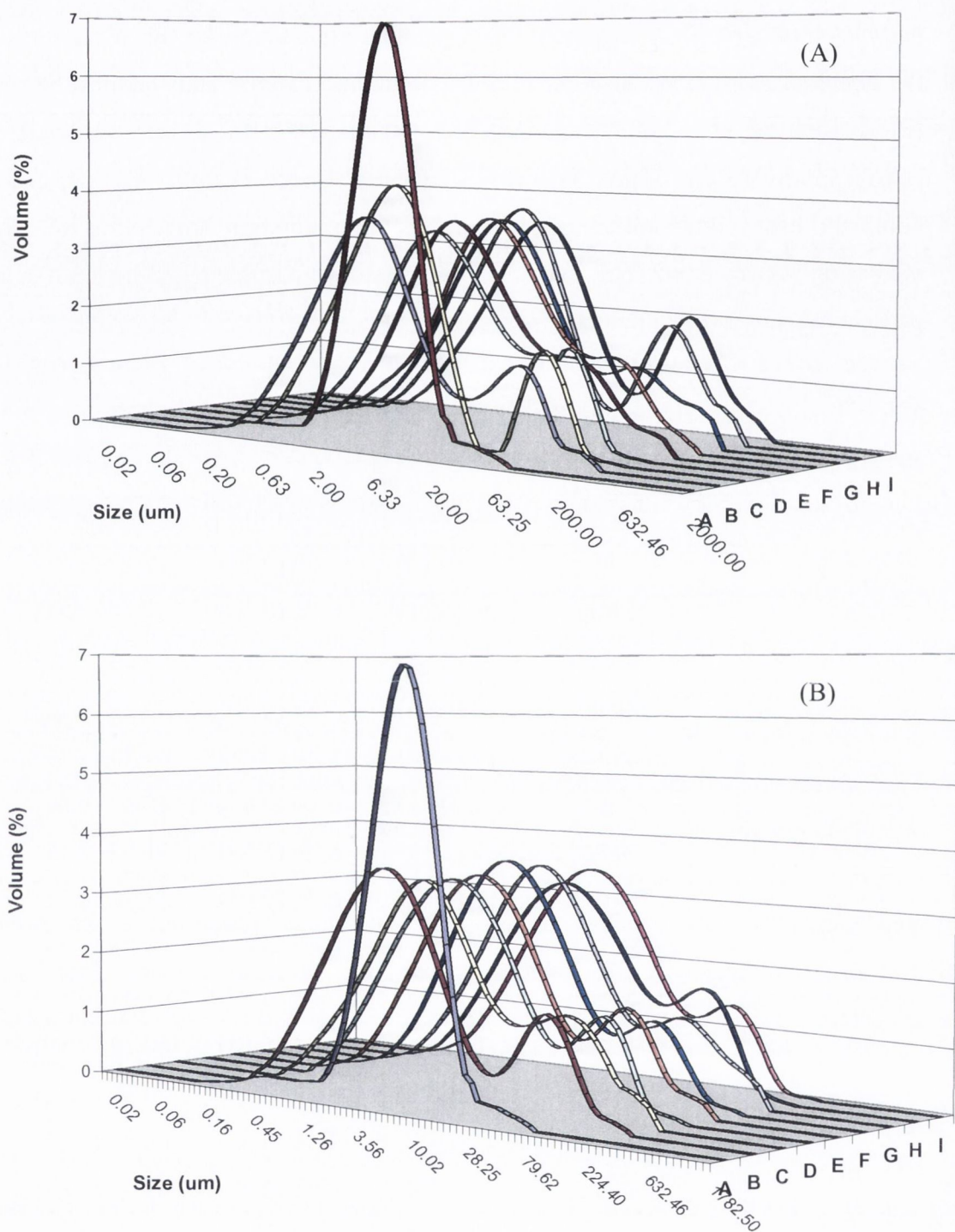


Figure 3.12: Laser diffraction particle size distribution profiles (obtained by the Malvern Mastersizer 2000) for SD unground and milled at RT with a BTP weight ratio of (a) 40:1 (b) 20:1. The letters refer to the length of time the samples were milled for; A = unground SD, B= 5, C=30, D= 60, E= 120 minutes, F=5, G=10, H =15 and I =20 hours.

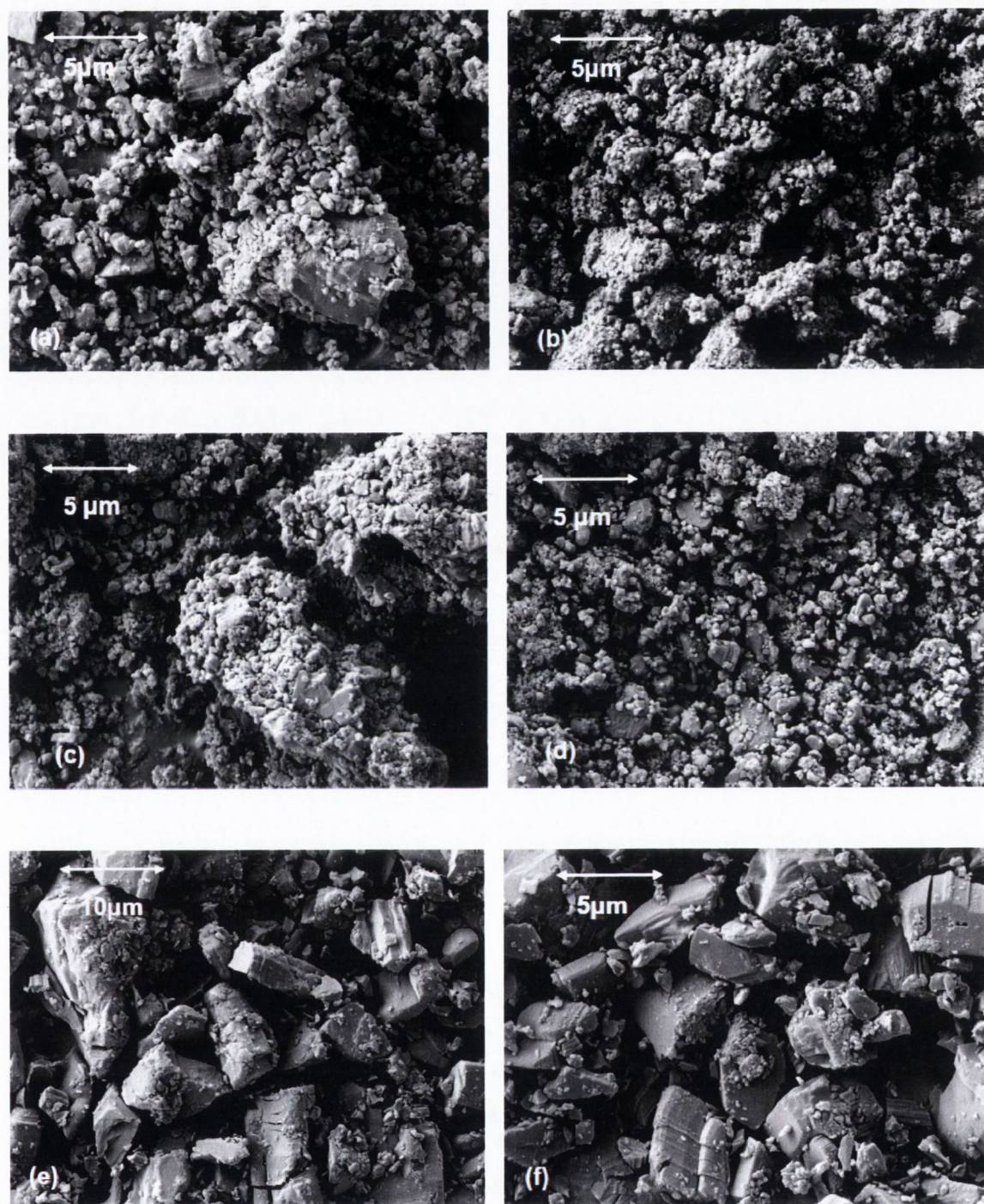


Figure 3.13: SEM micrographs of SD milled at RT (a) BTP 20:1 for 5 minutes; (b) BTP 20:1 for 20 hours; (c) BTP 40:1 for 5 minutes and (d) BTP 40:1 for 20 hours (e and f) SD unmilled.

SEM micrographs (Figure 3.13 a to d) illustrate the particle size reduction and agglomeration of the fine particles for both BTP weight ratios. For comparison purposes the micrographs obtained for the unmilled SD material is also presented here (Figure 3.13 e and f). This phenomenon was observed as a result of long (20 hours) and short (5 minutes) milling times. A similar agglomeration of ball milled salbutamol sulphate particles was observed for Brodka-Pfeiffer *et al.*, (2003). The bimodal distribution obtained by particle size analysis (Figure 3.12) for milled SD can be attributed to agglomeration of the smaller particles, evident in Figure 3.13.

Table 3.7 outlines the changes incurred to the specific surface area measured by BET as a result of increased milling time at RT with a BTP weight ratio of 40:1. The specific surface area for the SD unmilled received from Sigma was measured to be 0.99 ± 0.03 m²/g. Upon milling for 5 minutes the surface area increased to 3.72 ± 0.56 m²/g. The increase in specific surface area is not dependent on milling time. For example, SD milled for 15 hours resulted in a specific surface area of 15.15 ± 0.41 m²/g while a drop to 5.10 ± 0.38 m²/g was achieved after 20 hours of milling. The change in surface area can be affected by the change in particle size, as the particle size decreases the surface area increases. ANOVA statistical analysis of the results showed that there is a significant difference between the unmilled and SD milled at RT with a BTP weight ratio of 40:1.

Table 3.7: Specific surface area analysis by BET of SD unmilled and milled at RT and BTP weight ratio of 40:1.

Sample	BET specific surface area (m ² /g)
Unmilled	0.99 (0.30)
5 min	3.72 (0.56)
30 min	5.63 (2.16)
60 min	14.71 (0.75)
120 min	17.79 (3.18)
5 hrs	10.48 (4.02)
10 hrs	14.14 (3.85)
15 hrs	15.15 (0.41)
20 hrs	5.10 (0.38)

Standard deviation in parentheses. n=3

3.3.2 Ball milling at 4 °C

Ball milling of sulfadimidine at 4 °C was carried out with BTP weight ratios of 40:1, 35:1, 30:1 and 20:1. The ball milling times investigated are outlined in Table 3.3.

3.3.2.1 Powder X-ray diffraction

Figure 3.14 (a, b, c and d) shows the PXRD patterns for SD unmilled and milled at 4 °C with the varied BTP weight ratios (40:1, 35:1, 30:1 and 20:1, respectively). The diffractograms of SD milled with a BTP weight ratio of 40:1 milled for 5, 30, 60, 120 minutes and 5, 10, 15 and 20 hours and the unmilled SD are shown in Figure 3.14 a. The distinct Bragg peaks for SD milled for 5, 30, 60 and 120 minutes indicate a crystalline material. Further milling for 5, 10, and 15 hours resulted in a significant peak area decrease with only minor Bragg peaks detected (Figure 3.14 a). Increasing ball milling time to 20 hours with a BTP weight ratio of 40:1 at 4 °C produced a halo indicating a complete disordered phase. Peak area analysis of SD milled with a BTP weight ratio of 40:1 at 4 °C showed that as milling time was increased total peak area of the diffractogram decreased (Table 3.8) to 85.75±6.21% after 5 minutes and 4.76±0.73 % measured after 20 hours in comparison to the unmilled SD material where the total peak area was taken to be 100%.

Figure 3.14 b, c and d illustrates the effects of milling with a BTP weight ratio of 35:1, 30:1 and 20:1, respectively. The presence of Bragg peaks for all SD milled samples indicates the crystalline nature of the samples. Ball milling for 5 hours with a BTP weight ratio of 35:1 and 30:1 resulted in a decrease and broadening of the crystalline peaks and the presence of an amorphous halo. Peak area analysis for the milled samples is outlined in Table 3.8. No statistical significant difference occurred when comparing the peak area for SD ball milled for 5 minutes with a BTP weight ratios of 35:1 and 30:1 as the peak area of 95.72±1.82 % and 95.81±1.44 %, were obtained for the samples respectively ($p = 0.999$). Ball milling for 5 hours resulted in peak area drop to 20.86±2.75 % and 23.18±2.02 % for samples milled with a BTP weight ratio of 35:1 and 30:1, respectively. No statistical difference was observed between these two samples with a p value of 0.2381. For both of these BTP weight ratios (35:1 and 30:1), as milling time was increased the crystallinity decreased, indicated from the total peak area analysis (Table 3.8). Evaluation of the difference between the two BTP weight ratios (30:1 and 35:1) where no statistical difference was observed when comparing both the 5

minutes milled powders and the powders obtained after milling for 30 minutes, a significant statistical difference was observed when comparing the set of powders obtained from the different ratios as a result of ball milling for 30, 60 and 120 minutes, with p values for 0.0811, 0.0841 and 0.0016, obtained by ANOVA, respectively.

Distinct Bragg peaks were detected for all SD samples milled with a BTP weight ratio of 20:1 (Figure 3.14 d). Peak area analysis outlined in Table 3.8 of the milled samples showed that there was no statistical difference between the samples milled at a BTP weight ratio of 20:1 when compared using ANOVA ($P=0.5697$).

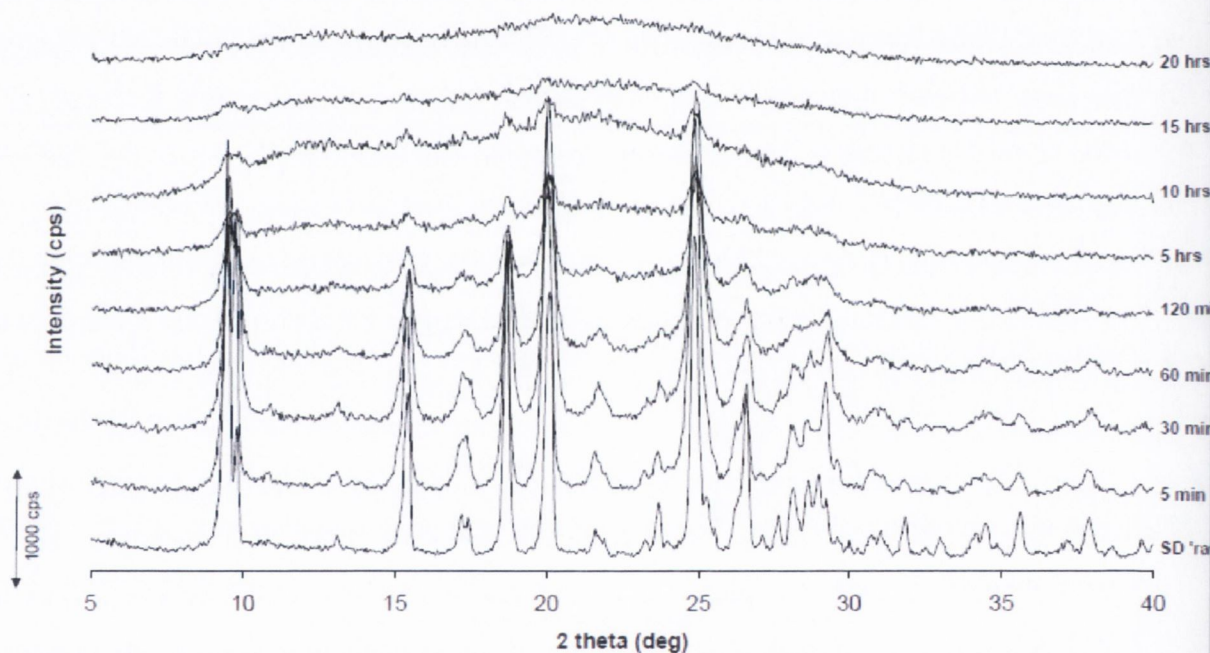


Figure 3.14 (a): XRD of sulfadimidine unmilled ('raw') and milled at 4 °C with a rotational speed of 400 rpm and a BTP weight ratio of 40:1 from 5 minutes to 20 hours.

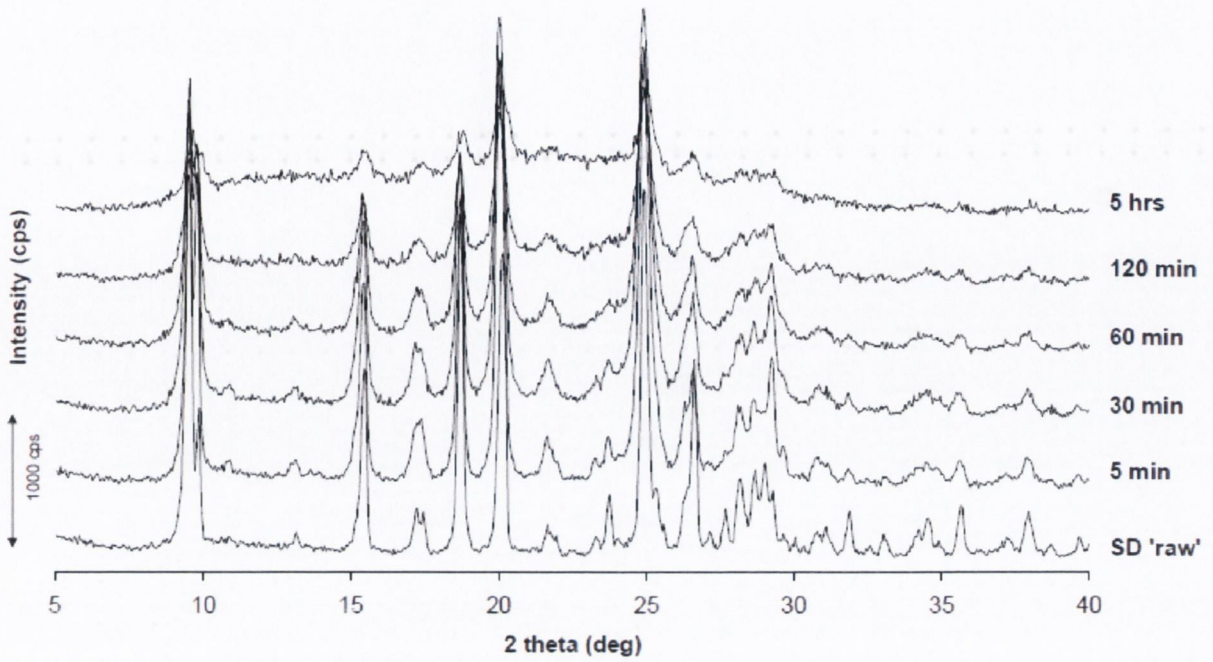


Figure 3.14 (b): PXRD of sulfadimidine unmilled ('raw') and milled at 4 °C with a rotational speed of 400 rpm and a BTP weight ratio of 35:1 from 5 minutes to 20 hours.

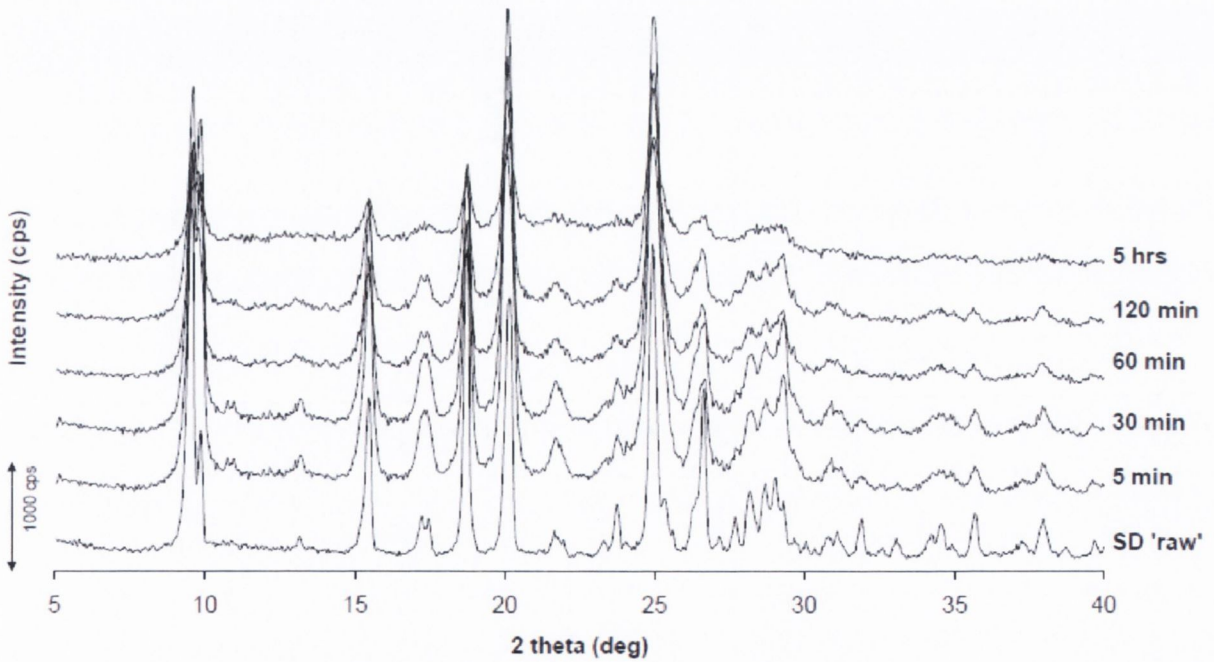


Figure 3.14 (c): PXRD of sulfadimidine unmilled ('raw') and milled at 4 °C with a rotational speed of 400 rpm and a BTP weight ratio of 30:1 from 5 minutes to 20 hours.

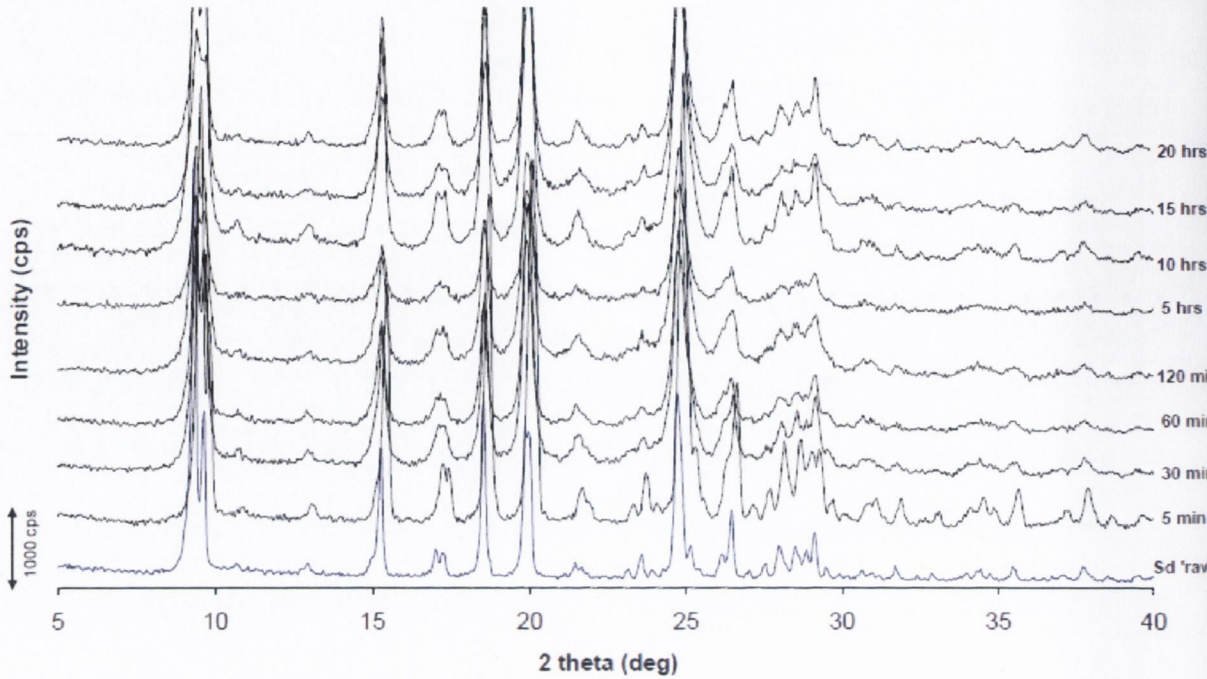


Figure 3.14 (d): PXR D of sulfadimidine unmilled ('raw') and milled at 4 °C with a rotational speed of 400 rpm and a BTP weight ratio of 20:1 from 5 minutes to 20 hours.

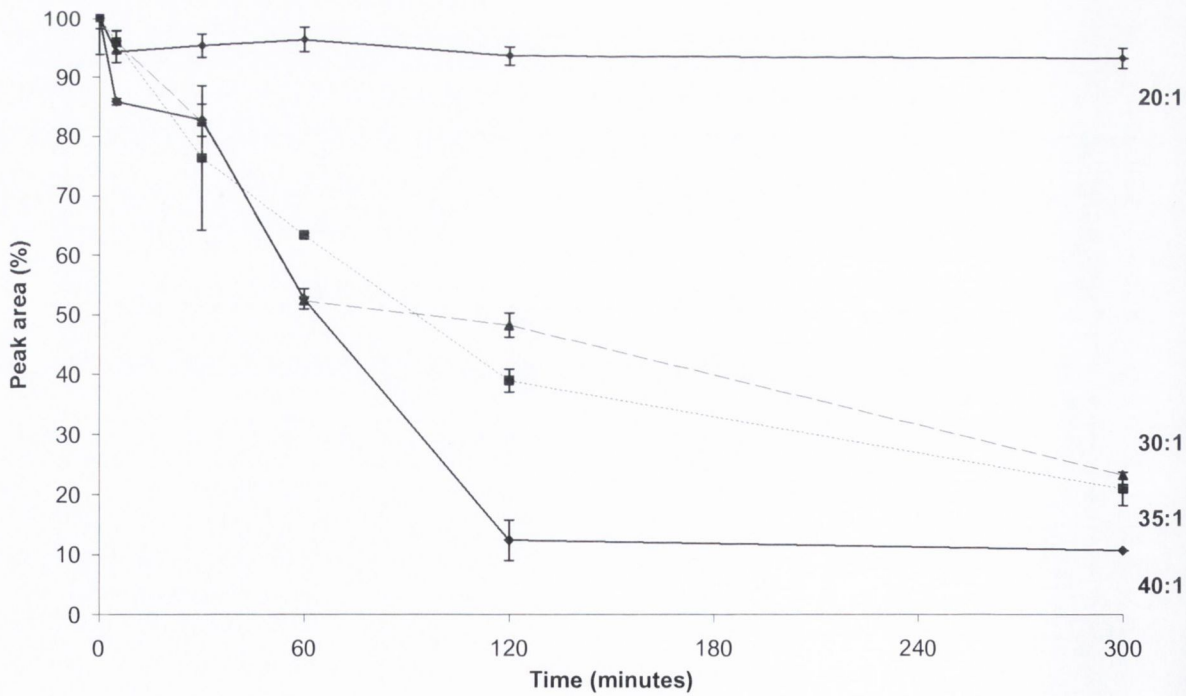


Figure 3.15: Total PXR D peak area change for SD milled at 4 °C for 5, 30, 60, 120 and 300 minutes with BTP weight ratio of 20:1, 30:1, 35:1 and 40:1.

Figure 3.15 illustrates the change of the PXRD peak area for the SD samples milled with the different BTP weight ratios as milling time was increased. Overall the results showed that as milling time increased the total peak area decreased in comparison to the unmilled SD samples what was taken to be 100 %.

Table 3.8: The total PXRD peak area of the SD unmilled and the percentage peak area remaining after the SD samples were ball milled at 4 °C with a ball BTP weight ratio of 40:1, 35:1, 30:1 and 20:1.

Time (minutes)	BTP 40:1 (%)	BTP 35:1 (%)	BTP 30:1 (%)	BTP 20:1 (%)
0	100.00 (0.00)	100.00 (0.00)	100.00 (0.00)	100.00 (0.00)
5	85.75 (6.21)	95.72 (1.82)	95.81 (1.44)	94.15 (1.91)
30	82.61 (0.53)	76.22 (2.19)	82.32 (1.97)	95.19 (1.82)
60	52.57 (2.74)	63.25 (0.03)	52.25 (0.25)	96.23 (1.97)
120	12.29 (1.73)	38.92 (1.19)	48.14 (0.67)	93.52 (2.13)
300	10.57 (3.38)	20.86 (2.75)	23.18 (2.02)	93.08 (1.56)
600	6.33 (0.02)	-	-	89.48 (1.74)
900	4.76 (0.73)	-	-	92.09 (3.38)
1200	0	-	-	91.66 (2.30)

Standard deviation is in parentheses, n = 3

3.3.2.2 Thermal analysis

Figures 16 a and d shows the DSC thermograms of SD unmilled and milled at 4 °C with varied BTP weight ratios (40:1 and 20:1) from 5 minutes to 20 hours. Figures 3.16 b and c illustrate DSC scans of SD unmilled and milled with BTP weight ratios of 35:1 and 30:1, respectively, at 4 °C from 5 minutes to 5 hours. The average and standard deviations obtained from the thermograms for the unmilled and ball milled SD samples for the crystallisation and melt onset temperature and enthalpies are outlined in Table 3.9. The two main thermal events detected as a result of ball milling SD were attributed to a crystallisation exotherm which

occurred between 60 °C and 90 °C and the second was consistent with a melt endotherm at 197 °C. SD ball milled for 10, 15 and 20 hours with a BTP weight ratio of 40:1 had a double crystallisation exotherm. This was similar to the thermal event documented for SD milled at RT for 40:1 for 20 hours. Both thermal events were evident for samples milled with the BTP weight ratios of 40:1, 35:1 and 30:1 milled for 30 minutes or longer. A crystallisation event was detected for SD milled for 5 minutes with a BTP weight ratio of 40:1, while no crystallisation peak was detected for samples milled for 5 minutes for all other BTP weight ratios. Crystallisation enthalpy (ΔH_{cr}) intensity for the milled samples depended on time and BTP weight ratio used. The higher crystallisation enthalpies were obtained after ball milling with a BTP weight ratio of 40:1. In contrast the lowest crystallisation enthalpies were a result of milling with a BTP weight ratio of 20:1. This may suggest that, with less powder in the milling jar the powders particles were exposed to a higher number of ball-to-powder impacts, which could have increased the number of shear stresses induced which could contribute to induced amorphous phase.

Quantification of the amorphous phase shows that ball milling with a BTP weight ratio of 40:1 produced the highest disordered phase of the investigated BTP weight ratios. A high level of DSC amorphous content was achieved for samples milled with a BTP weight ratio of 35:1 and 30:1, with corresponding levels of 74.50 ± 0.74 % and 56.85 ± 2.48 %, obtained after 5 hours. Ball milling with a BTP weight ratio of 20:1 resulted in a DSC amorphous content level of 2.01 ± 0.84 %, induced after 20 hours. Higher levels of disorder were achieved with higher BTP weight ratios. As the BTP weight ratios were decreased the level of disorder induced decreased. An example of this was that a 6.73 ± 3.09 % DSC amorphous content was induced after 5 hours with a BTP weight ratio of 20:1, compared to 98.89 ± 8.59 % achieved when using a BTP weight ratio of 40:1. As milling time was increased and the level of DSC amorphous content increased the crystallisation temperature (T_{cr}) shifted to the higher temperature. Ball milling for 5 and 30 minutes with BTP weight ratios 20:1, 30:1 and 35:1 resulted in a T_{cr} detected at ~ 60 °C, but as the amorphous content increased the T_{cr} was detected at higher temperatures. This was observed in Figure 3.16 a, b and c and Table 3.9. A similar shift of the crystallisation exotherm to higher temperatures as a result of increased milling time was also observed by Dujardin *et al.*, (2008) as a result of ball milling glucose at -15 °C. The authors suggested that this behaviour was as a result of an increased stability of the amorphous state. Detection of a T_g was not possible as the broad crystallisation exotherm

overlapped the area in which it was expected. The increased level of disorder with increased milling time and BTP weight ratios was also observed by PXRD analysis in the form of an amorphous halo and evaluation of the total peak areas, as discussed above.

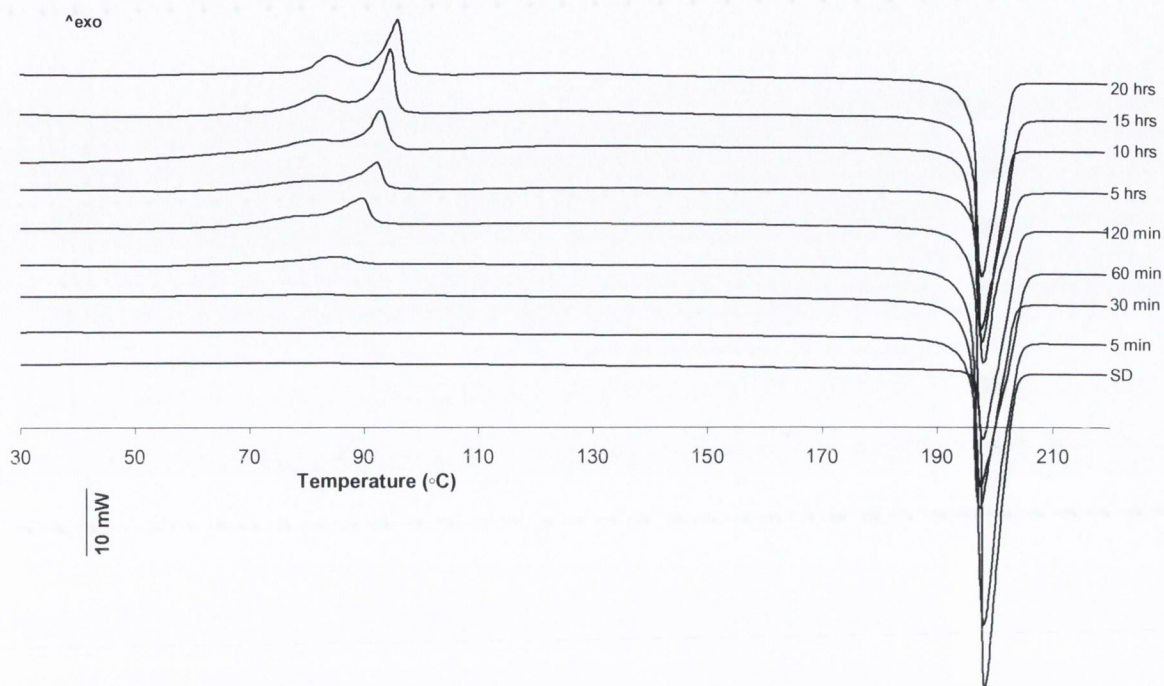


Figure 3.16 (a): DSC thermograms SD unground and milled at 4 °C with a BTP weight ratio of 40:1 at a rotational speed of 400 rpm from 5 minutes to 20 hours.

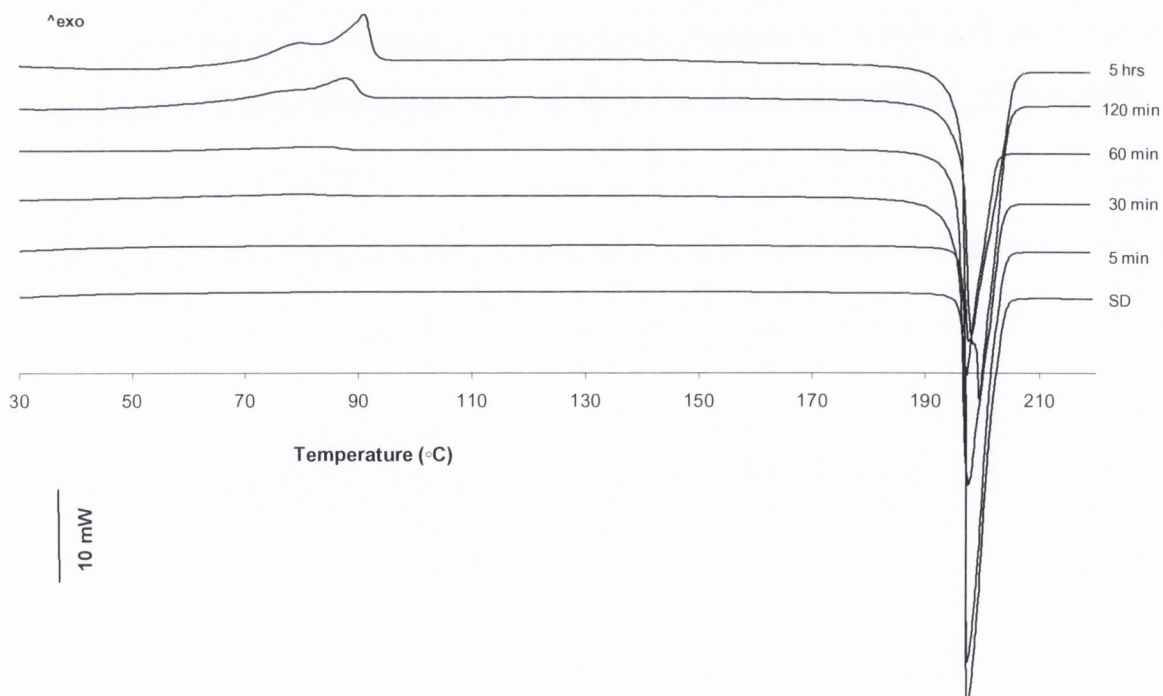


Figure 3.16 (b): DSC thermograms SD unground and milled at 4 °C with a BTP weight ratio of 35:1 at a rotational speed of 400 rpm from 5 minutes to 5 hours.

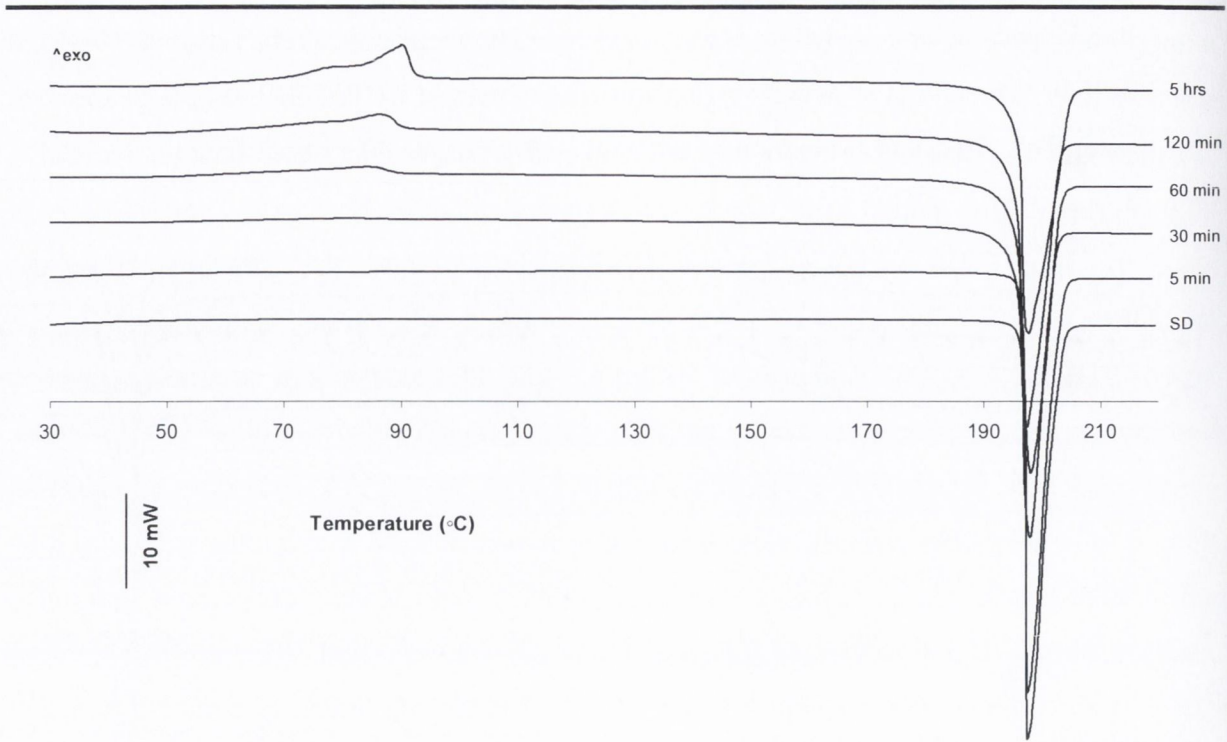


Figure 3.16 (c): DSC thermograms SD unmilled and milled at 4 °C with a BTP weight ratio of 30:1 at a rotational speed of 400 rpm from 5 minutes to 5 hours.

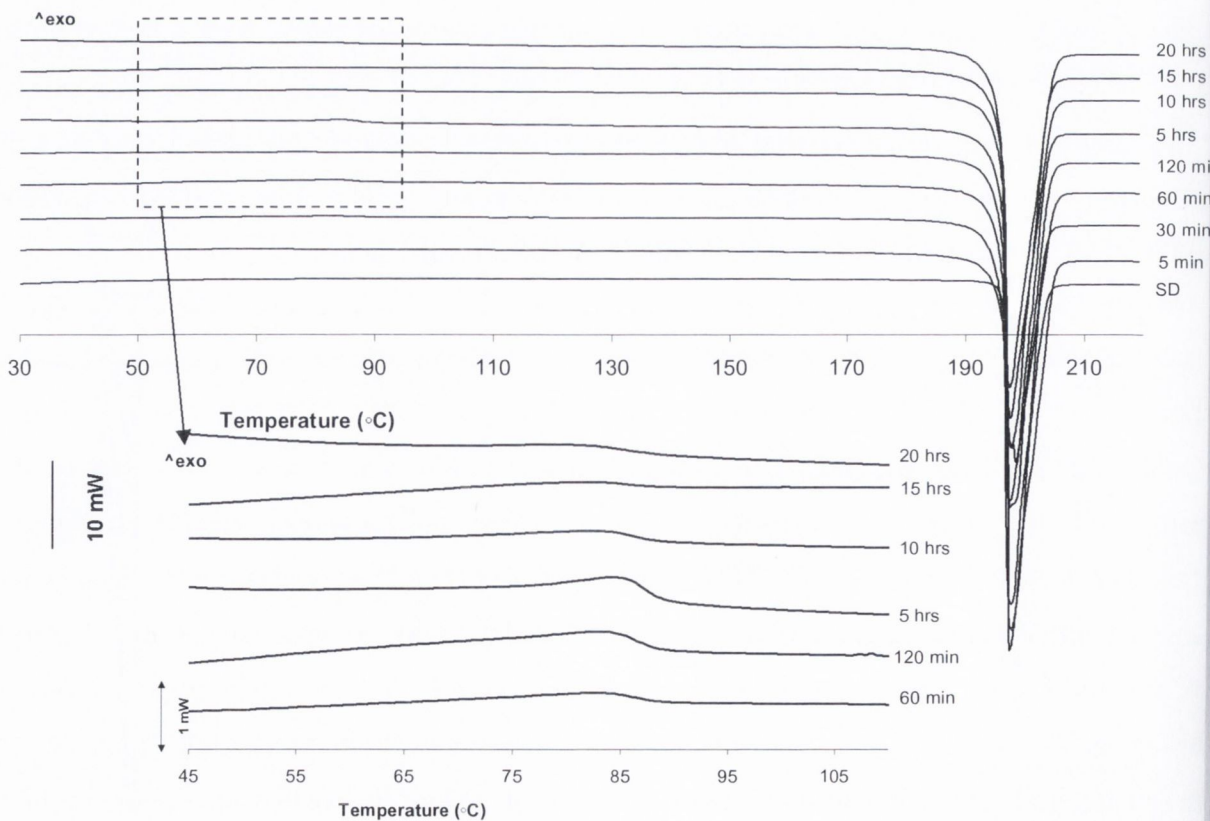


Figure 3.16 (d): DSC thermograms SD unmilled and milled at 4 °C with a BTP weight ratio of 20:1 at a rotational speed of 400 rpm from 5 minutes to 20 hours.

Table 3.9: Thermal characteristics of SD unmilled and milled at 4 °C.

		ΔH_{cr} (J/g)	ΔH_m (J/g)	T_{cr} (°C)	T_m (°C)	DSC amorphous content (%)
	0	-	129.26 (0.24)	-	196.79 (0.89)	0 (0.00)
BTP 40:1	5 min	1.74 (0.12)	122.26 (2.72)	65.82 (0.43)	196.24 (0.18)	4.78 (0.16)
	30 min	4.16 (0.41)	124.22 (0.18)	60.34 (1.21)	195.31 (0.24)	8.22 (1.16)
	60 min	11.38 (0.08)	124.02 (0.89)	74.03 (1.94)	195.58 (0.09)	24.53 (1.79)
	120 min	28.87 (0.18)	123.14 (0.40)	78.01 (1.32)	195.63 (0.04)	57.55 (2.23)
	5 hrs	36.69 (0.16)	117.92 (0.55)	87.00 (0.37)	196.44 (0.12)	79.80 (2.07)
	10 hrs	47.50 (0.16)	123.59 (0.95)	89.08 (1.72)	195.78 (0.08)	84.03 (5.77)
	15 hrs	45.38 (0.17)	122.58 (0.15)	91.02 (4.63)	195.84 (0.05)	81.54 (4.37)
	20 hrs	45.64 (0.23)	123.90 (0.25)	92.22 (1.23)	195.78 (0.05)	98.89 (8.59)
BTP 35:1	5 min	-	125.32 (0.16)	-	196.78 (0.07)	0.00 (0.00)
	30 min	3.78 (0.14)	124.13 (0.15)	53.97 (1.15)	195.73 (0.04)	8.56 (0.18)
	60 min	9.56 (0.21)	122.95 (0.23)	61.05 (0.64)	195.55 (0.04)	18.22 (3.98)
	120 min	22.31 (0.01)	122.44 (1.27)	76.51 (3.14)	195.54 (0.06)	46.73 (3.50)
	5hrs	36.58 (0.09)	120.39 (0.91)	83.67 (2.48)	195.87 (0.04)	74.50 (0.74)
BTP 30:1	5 min	-	125.02 (0.19)	-	196.25 (0.07)	0.00 (0.00)
	30 min	4.20 (0.07)	123.46 (0.17)	59.08 (0.42)	195.80 (0.03)	9.75 (0.53)
	60 min	9.47 (0.12)	124.67 (0.34)	67.95 (0.05)	195.57 (0.05)	19.62 (0.02)
	120 min	14.87 (1.06)	123.06 (1.02)	75.39 (0.42)	195.47 (0.04)	30.94 (0.48)
	5hrs	30.02 (0.31)	123.13 (1.14)	79.71 (0.34)	195.65 (0.04)	56.85 (2.48)
BTP 20:1	5 min	-	125.95 (1.21)	-	196.22 (1.04)	0.00 (0.00)
	30 min	2.13 (0.24)	126.06 (0.11)	68.72 (0.38)	195.83 (0.16)	1.44 (0.91)
	60 min	1.53 (0.14)	125.62 (0.05)	66.58 (0.37)	195.82 (0.04)	2.38 (0.14)
	120 min	1.74 (0.09)	125.36 (1.16)	64.25 (0.42)	195.90 (0.05)	3.67 (2.05)
	5 hrs	3.36 (0.05)	125.14 (0.45)	73.37 (0.39)	195.86 (0.01)	6.73 (3.09)
	10 hrs	2.52 (0.09)	125.81 (0.86)	72.87 (1.64)	195.78 (0.21)	5.05 (1.95)
	15 hrs	1.32 (0.16)	125.91 (0.12)	62.34 (1.48)	195.86 (0.03)	2.76 (0.22)
	20 hrs	0.99 (0.47)	126.73 (1.11)	66.44 (0.53)	195.64 (0.04)	2.01 (0.84)

Standard deviation in parentheses, n=3

Figure 3.17 outlines the DSC amorphous content induced with different BTP weight ratios when milled for 5, 30, 60, 120 minutes and 5 hours. Evaluating SD milled for 30 minutes by Tukey's multiple comparison test showed that there was a difference between samples milled with a ratio of 20:1 to all other ratios investigated, while no difference was detected between 30:1, 35:1 and 40:1. Statistical analysis by ANOVA showed there was no statistical difference between the DSC amorphous content induced for SD samples milled for 60 minutes with BTP weight ratios of 40:1, 35:1 and 30:1 ($p = 0.1679$). Comparing the DSC amorphous content induced after 5 hours for the different BTP weight ratios by Tukey's multiple comparison test showed that a statistical difference occurred between all samples with the exception of SD milled with a BTP weight ratio of 40:1 and 35:1.

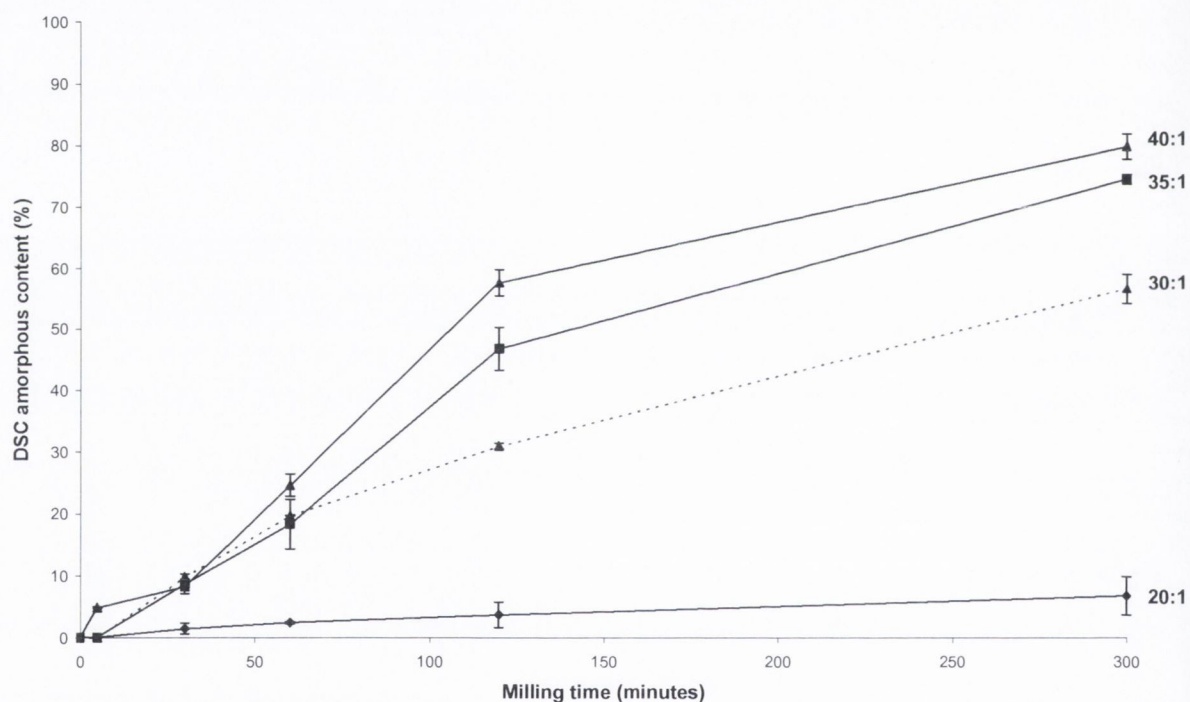


Figure 3.17: Illustrates the DSC amorphous content induced when milling with different ball to powder weight ratios. This graph represents the DSC amorphous content.

3.3.2.3 Particle size and morphology

Table 3.10 outlines the particle size measured by laser diffraction for SD milled at 4 °C with the different BTP weight ratios after 5, 30, 60, and 120 minutes and 5 hours. The distributions of the milled materials have a bimodal distribution, very similar to the distributions shown in Figure 3.12. The d10 measurement for SD unmilled of ~3.23 µm was reduced by ~1 µm for all milled samples with these conditions (Table 3.10). Comparing all d10 measurements obtained from the milled samples with the unmilled material by ANOVA shows a significant difference, was observed ($p < 0.0001$). The median particle size for SD unmilled is 7.69 ± 0.12 µm. Statistical analysis by Tukey's multiple comparison test of the median particle size showed that samples milled with a BTP weight ratio 20:1 and milled for 5, 30, 60 and 120 minutes and SD milled with a BTP weight ratio of 40:1 for 60 minutes were different to the unmilled SD material. All other milled samples at 4 °C are not significantly different to the unmilled material.

The median particle size for SD milled with a BTP weight ratio of 20:1 was lower compared to the median particle size measurements obtained for SD milled with ratios of 40:1, 35:1 and 30:1 (Table 3.10). The samples that illustrate a statistically significant difference with the samples ball milled with a BTP weight ratio of 20:1 are outlined in Table 3.11. Overall the median particle size ranged from 4.74 ± 0.94 µm obtained after ball milling for 5 minutes with a BTP weight ratio of 20:1 to 7.69 ± 1.13 µm after ball milling with a BTP weight ratio of 35:1 for 120 minutes. Analysis of the d90 measurements resulted in an increase from 17.72 ± 3.66 µm for SD unmilled to 107.72 ± 15.95 µm obtained after 5 minutes with a BTP weight ratio of 40:1. The d90 measurements for all SD milled samples at 4 °C ranged between ~61 µm to 107 µm as outlined in Table 3.10.

Table 3.10: Particle size measurements for SD unmilled and SD milled at 4 °C.

		d10 (µm)	d50 (µm)	d90 (µm)
	0	3.23 (0.12)	7.69 (0.12)	17.72 (3.66)
BTP 40:1	5 min	1.13 (0.06)	6.53 (0.85)	107.99 (15.95)
	30 min	1.16 (0.06)	6.35 (0.68)	86.58 (29.59)
	60 min	1.20 (0.01)	5.31 (0.24)	68.34 (8.76)
	120 min	1.51 (0.04)	5.99 (0.18)	65.34 (7.56)
	5 hrs	1.72 (0.06)	6.72 (0.67)	72.24 (28.24)
BTP 35:1	5 min	1.92 (0.59)	6.51 (0.87)	76.51 (2.18)
	30 min	1.12 (0.01)	6.11 (0.18)	77.77 (13.17)
	60 min	1.31 (0.05)	7.51 (0.60)	94.81 (21.83)
	120 min	1.42 (0.21)	6.60 (2.04)	74.00 (15.75)
	5 hrs	1.59 (0.10)	6.50 (0.54)	77.52 (14.33)
BTP 35:1	5 min	1.00 (0.11)	5.51 (0.33)	86.92 (7.98)
	30 min	1.13 (0.04)	5.74 (0.73)	61.16 (10.80)
	60 min	1.22 (0.02)	5.97 (0.12)	73.56 (8.85)
	120 min	1.43 (0.05)	7.69 (1.13)	86.68 (1.56)
	5 hrs	1.62 (0.05)	7.36 (0.13)	77.41 (5.27)
BTP 20:1	5 min	0.96 (0.07)	4.74 (0.94)	84.18 (15.58)
	30 min	0.98 (0.02)	5.00 (0.37)	87.56 (15.13)
	60 min	1.00 (0.03)	5.13 (0.26)	79.03 (16.39)
	120min	1.04 (0.09)	5.62 (0.84)	89.32(15.82)
	5 hrs	1.05 (0.05)	5.70 (0.91)	97.52 (33.1)

Standard deviation in parentheses. n=3

Table 3.11: SD milled samples at 4°C that have a statistical difference between their median particle sizes.

Sample		Time	BTP weight ratio
	vs.	5 hrs	40:1
SD BTP 20:1 milled for 5 minutes	vs.	5 hrs	30:1
	vs.	120 min	30:1
	vs.	60 min	35:1
	vs.	60 min	35:1
SD BTP 20:1 milled for 30 minutes	vs.	120 min	30:1
	vs.	5 hrs	30:1
	vs.	60 min	35:1
SD BTP 20:1 milled for 60 minutes	vs.	120 min	30:1
	vs.	5 hrs	30:1
SD BTP 20:1 milled for 120 minutes	vs.	120 min	30:1

SEM analysis of the ball milled samples compared to the unmilled SD materials showed that a reduction in particles was evident and agglomerates were formed (Figure 3.18 a, b, and d). A similar morphology was observed for all milled samples regardless of time and BTP weight ratio. Ball milling of SD produced a morphology that consisted of irregular shaped and sized particles. Large particles were detected after 5 minutes (Figure 3.18 a) while prolonged milling resulted in clusters of agglomerated particles. This behaviour was observed for both BTP weight ratios. The agglomerated particles contribute to the increase in d90 particle size measurements by laser diffraction.

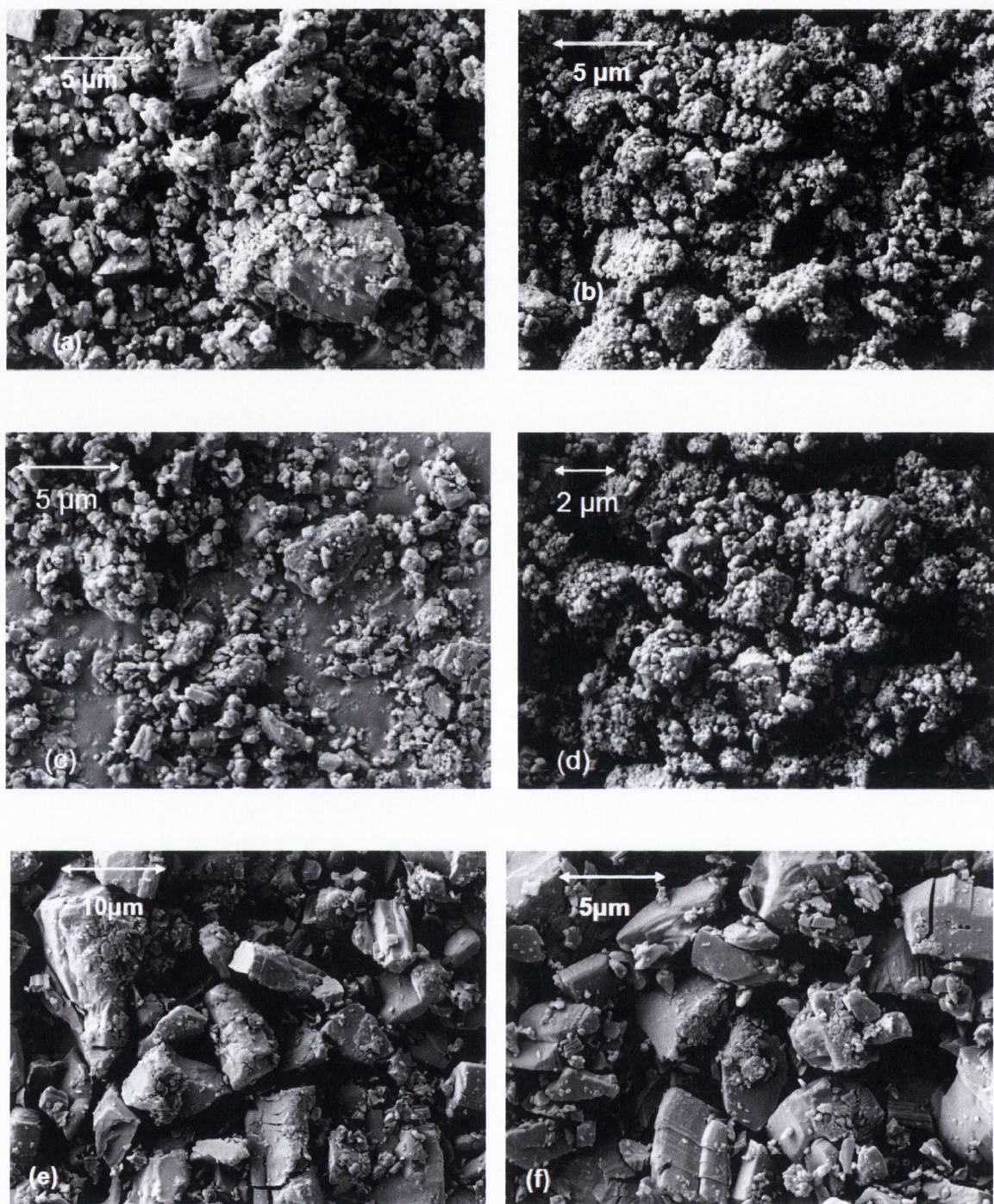


Figure 3.18: SEM micrographs of SD milled at 4 °C with a rotational speed of 400 rpm (a) BTP weight ratio 20:1 for 5 minutes; (b) BTP weight ratio 20:1 for 20 hours; (c) ball BTP weight ratio 40:1 for 5 minutes; (d) BTP weight ratio 40:1 for 20 hours; (e and f) sulfadimidine unmilled.

3.4 PXRD peak area and DSC amorphous content changes at RT and 4 °C

The change to the PXRD total peak area of SD milled with a BTP weight ratio of 40:1 at RT and 4 °C is shown in Figure 3.19. These data were generated with the data given in Tables 3.4 and 3.8. The decrease of the total peak area for SD milled at RT was more gradual compared to SD milled samples at 4 °C. Comparing the PXRD peak area obtained from SD ball milled for 20 hours at RT and 4°C by Tukey's multiple comparison test suggested that there was no significant statistical difference between these samples. This was also observed for the samples ball milled at RT and 4 °C for 15 hours. In contrast to the similarities observed between these samples there was statistically significant difference when comparing the PXRD peak area analysis for all other milled SD samples at RT and 4 °C, such as 5 minutes versus 5 minutes, 30 minutes versus 30 minutes etc.

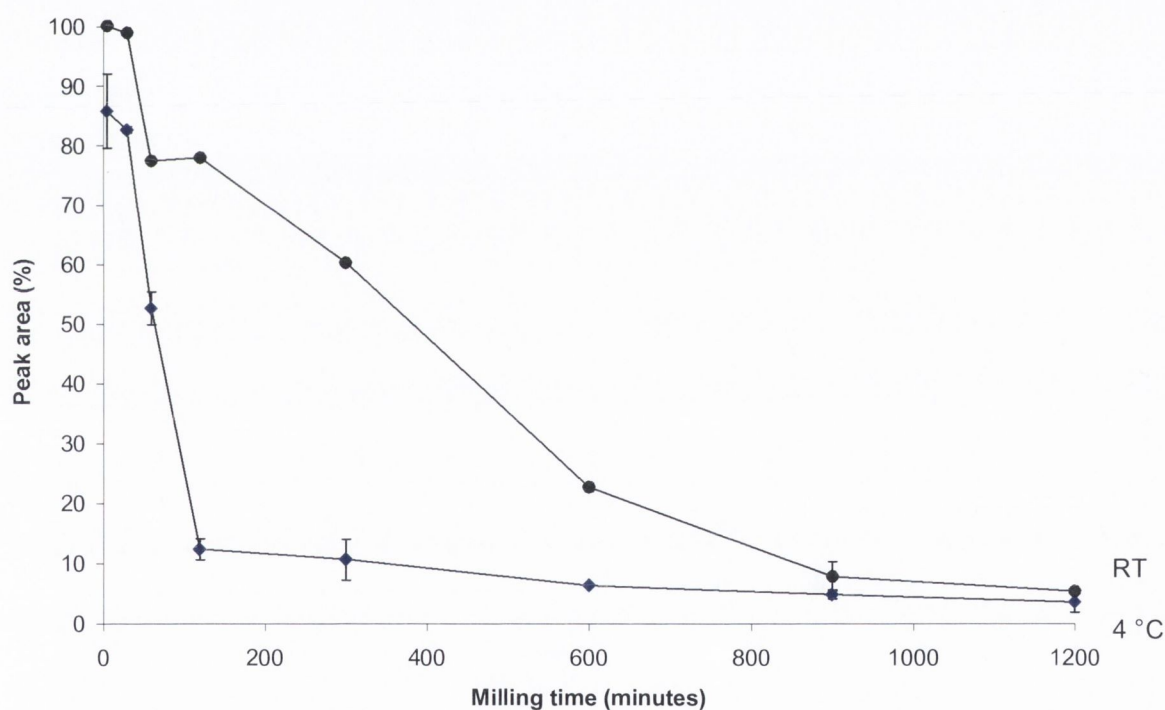


Figure 3.19: PXRD total peak area of SD milled at RT and 4 °C with a BTP weight ratio of 40:1.

Figure 3.20 shows the DSC amorphous content for SD milled at RT and 4 °C with a BTP weight ratio of 40:1. This graph was generated with data shown in Table 3.5 and 3.9. As discussed before the DSC amorphous content increased as a function of time. No statistical difference was observed between the two SD milled samples for 5 minutes at RT and 4 °C.

This is also the case for samples milled for 30 minutes. Comparing the samples milled at RT and 4 °C for 60 minutes by Tukey's multiple comparison test indicated that there was a statistically significant difference. A similar difference was observed between the two samples milled for 120 minutes, the samples milled for 5 hours and the samples milled for 10 hours. The samples milled at RT and 4 °C for 15 hours and 20 hours showed no statistical significant difference. Several studies have investigated the affect of processing temperatures on the materials solid state nature. De Gusseme *et al.*, (2008) reported an increased amorphous phase as a result of ball milling fananserine at -15 °C as opposed to ball milling at 25 °C. Similar reports have been documented in literature to indicate that amorphisation occurs more readily at lower temperatures as opposed to ball milling samples at RT or higher (Dujardin *et al.*, 2008).

Dubnskaya (1999) notes that during mechanical treatment several transformations occur, these include firstly; rupture and formation of valence bonds and deformation of bond angles and secondly; both destruction and generation of weaker intermolecular interactions (disordering, amorphisation of the crystal structure, conformational transitions and polymorphic transformations). Caron *et al.*, (2007) reported that the level of amorphous phase induced into the material structure as a result of ball milling was due to the position of the materials T_g . The T_g of lactose and mannitol mixtures was varied by varying the ratios. Samples that had a higher T_g compared to the T_{mill} resulted in an amorphous phase while samples with a T_g close to the T_{mill} remained crystalline.

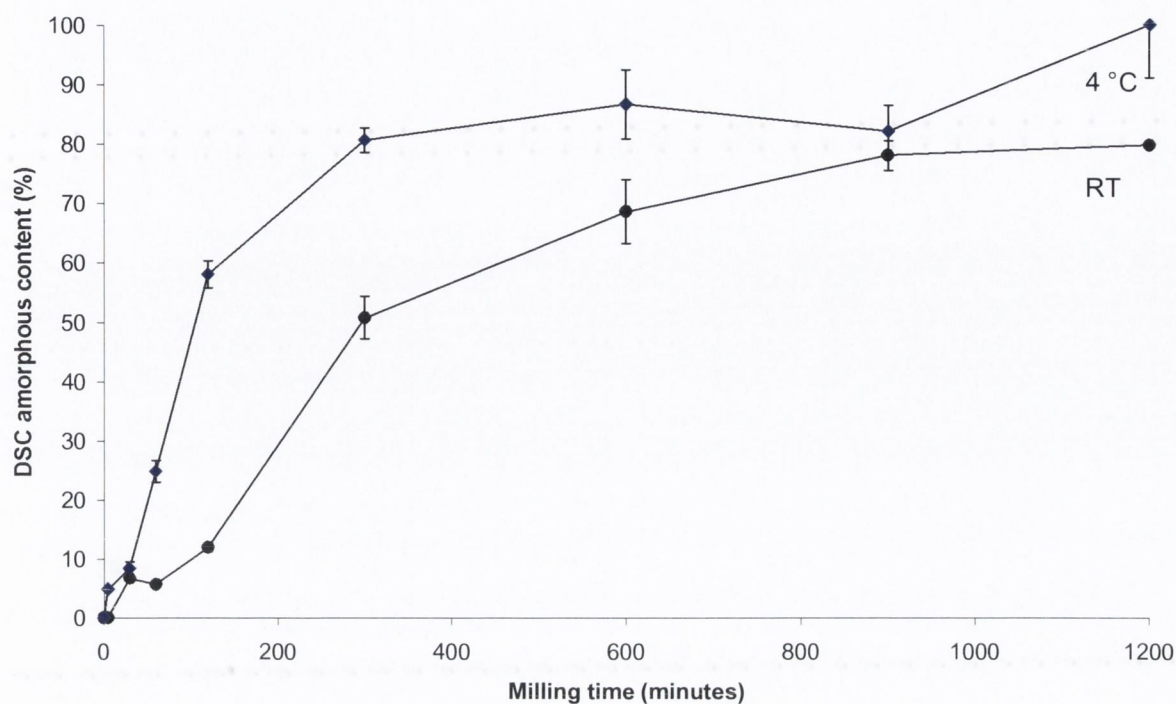


Figure 3.20: DSC amorphous content for SD milled at RT and 4 °C with a BTP weight ratio of 40:1.

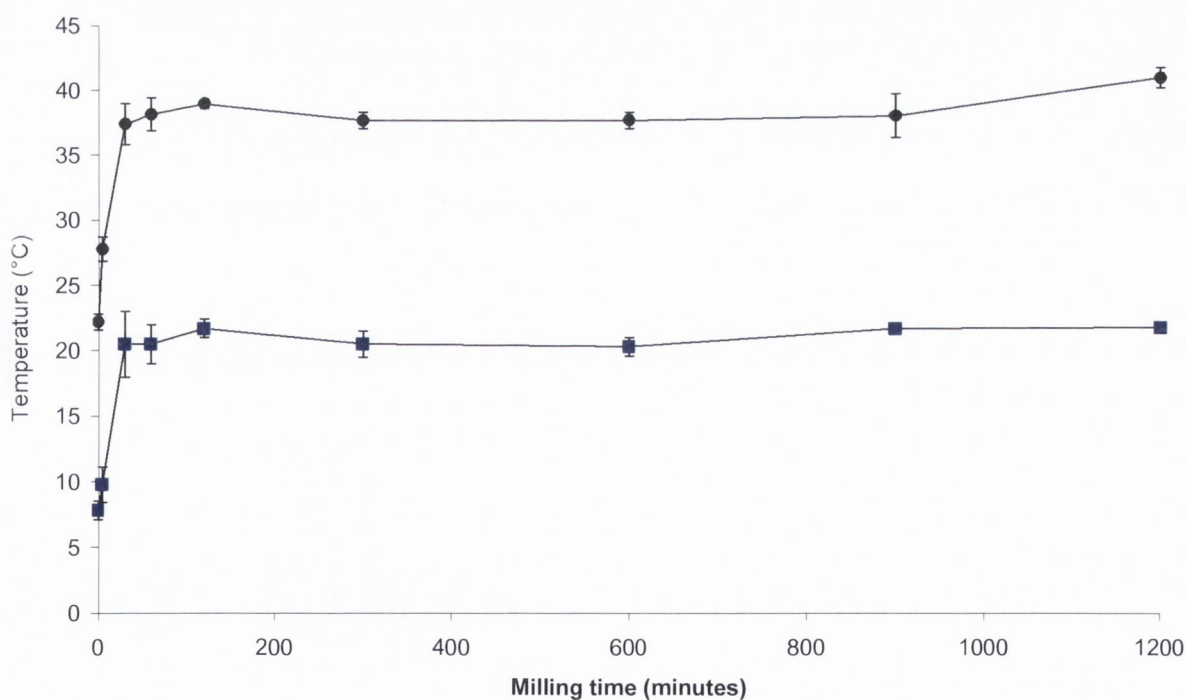


Figure 3.21: Temperature inside the milling jars determined by laser thermometer, measured immediately after milling. Samples analysed included SD milled with a BTP weight ratio of 40:1 at RT (circle) and 4 °C (square) for 5, 30, 60 and 120 minutes and 5, 10, 15 and 20 hours.

Figure 3.20 illustrates the average temperature inside the milling jar immediately after milling for SD milled at RT and 4 °C with a BTP weight ratio of 40:1 for 5, 30, 60, 120 minutes and 5, 10, 15 and 20 hours. For both conditions the temperature of the powder was found to increase dramatically after 30 minutes of milling. There was little variation in temperature for samples milled for 60 minutes and over the different time periods up to 20 hours. This trend was observed for both milling temperatures investigated. The maximum temperature recorded was 40.93 ± 0.80 °C after 20 hours at RT while a temperature of 21.72 ± 0.42 °C was reached when milling at 4 °C for 20 hours.

Kwon *et al.*, (2002) investigated the change in temperature in the milling jar and how it changed as the ball size used was increased. They stated that the temperature rise during milling was mainly attributed to ball-to-ball, ball-to-power, ball-to-wall collisions. They found that the temperature increased as the ball size increased. A change in the ball diameter was not an aspect of this study but the change in temperature in relation to the temperature at which the ball milling is shown. The results showed that as a result of prolonged milling (60 minutes or longer) the temperature within the milling chamber increased by ~20 degrees. The temperature jump may have contributed to the difficulties in producing a completely amorphous phase at RT with SD after and this change in temperature should be taken into consideration if the material of interest had a low T_g .

3.5 Storage of ball milled SD

Ball milling at RT resulted in a gradual change over the time periods investigated in terms of PXRD total peak area changes and DSC amorphous content. Analysis of the rate of the induced disordered phase by PXRD peak area analysis and DSC amorphous content was carried out on the SD ball milled samples at RT with a BTP weight ratio of 40:1 to observe changes to the induced level of disorder over an 84 day period. The samples were stored at 4°C over phosphorous pentoxide. This combination of storage conditions were chosen so the influence of temperature and relative humidity would be minimised as best as possible so that they would not encourage the crystallisation process.

3.5.1 Powder X-ray diffraction

The diffractograms obtained from the PXRD analysis of SD milled for 5, 10, 15 and 20 hours at RT with a BTP weight ratio of 40:1 are shown in Figure 3.23 a, b, c and d, respectively. These graphs show the diffractograms obtained directly after milling and stored over 84 days and are compared to the unmilled SD material. The samples were stored directly after milling which reduced their exposure to lab environmental conditions; the RT of 23 ± 2 °C and RH of 41 ± 7 % and the samples were tested after different storage periods. A new sample was milled for each set of analysis to ensure the results would truly reflect the length of storage time investigated. Storage conditions were monitored over 45 days and are outlined in Figure 3.22. This showed that the storage temperature never exceeded 5.4 °C and the relative humidity was kept below 4.5 %. Analysis was carried out after 7, 14, 21, 28, 56 and 84 days. Figure 3.23a illustrates the diffractograms for SD milled for 5 hours. As discussed previously in section 3.3.1.1, the samples consisted of a disordered phase as the PXRD peak area of the milled materials had decreased in comparison to the unmilled material (c in Figure 3.23 a). However, by one week later, an increase in total peak area was detected, indicating a re-ordered crystal structure to its more crystalline stable form. Storage after 84 days resulted in a crystalline material for all of the milled samples but the total peak area never reverted back to the original intensity measured for SD unmilled, regardless of the sample tested. The difference between the peak area of the stored milled samples and the unmilled sample may have been due to a residual amorphous phase present within the samples but it could also be attributed to a change in the sample's crystallite size. Over the storage period, the samples may not have had sufficient time to revert back to their original size. Figure 3.23 b and c illustrates the PXRD for SD milled for 10 and 15 hours, respectively. Analysis after 7 days of storage of the SD sample that was ball milled for 10 hours, resulted in a predominantly amorphous halo (c Figure 3.23 b). After 14 days Bragg peaks were detected (d Figure 3.23 b). After 21 days of storage the Bragg peaks were distinct and an obvious increase in the total peak area was apparent. This trend was also apparent for the samples milled for 15 hours and stored (b and c Figure 3.23 b) Figure 3.23d illustrates the diffractograms for SD milled for 20 hours and stored. After 7 days the sample remains largely disordered. Storage for 14 and 21 days resulted in an increase of the peak intensity. No further change was apparent after 28 days of storage when compared to the 14 and 21 day samples and the diffractograms appeared unchanged for the remainder of the storage times investigated (28, 56 and 84 days). The diffractograms for SD milled for 30, 60 and 120 minutes, stored and tested over the different

time periods is shown in Appendix I. The results indicated that no obvious change was observed over the storage period for each of the milled samples. The peak area analysis of the samples is shown in Table 3.12 and Figure 3.24 illustrates the changes to each sample over the period of storage.

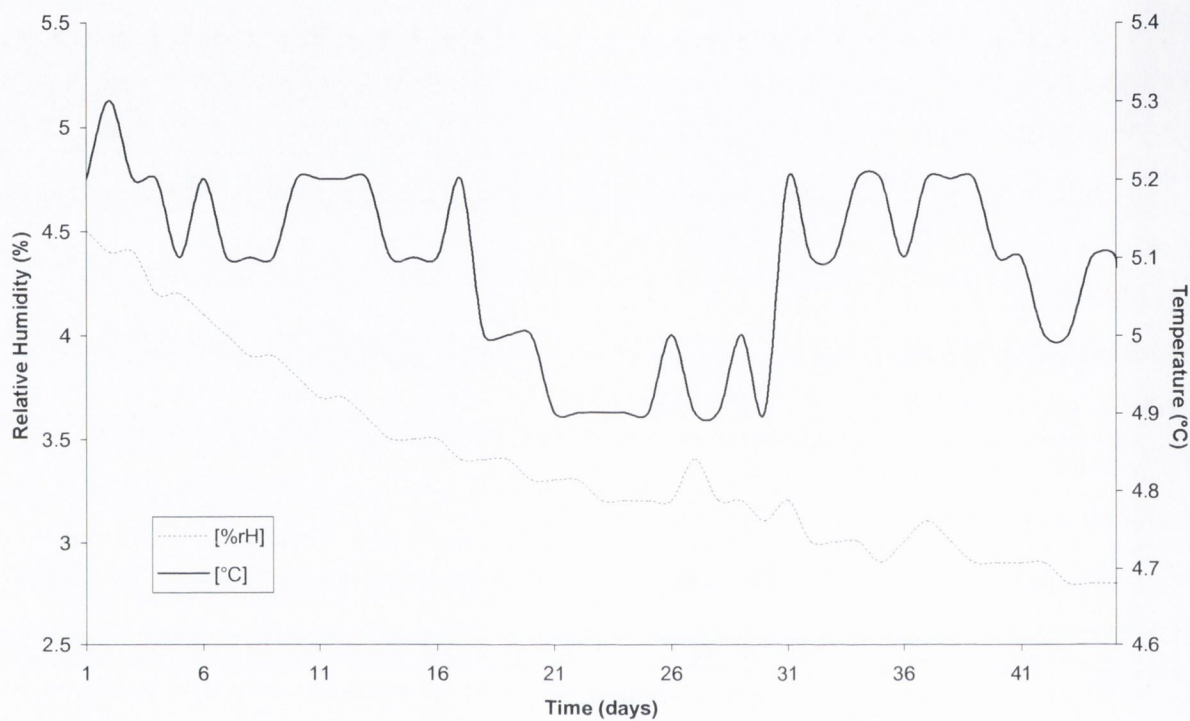


Figure 3.22: Monitored storage conditions of the desiccant condition where the ball milled SD samples were stored, monitoring time was over 45 days.

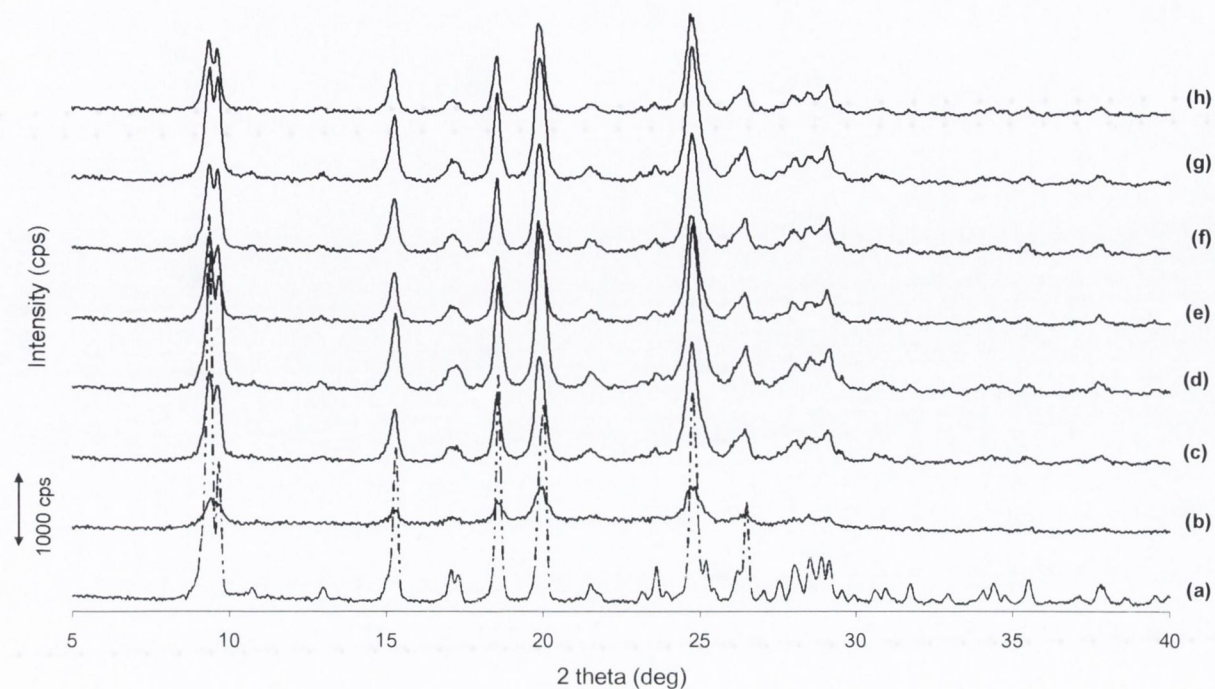


Figure 3.23a: PXR D of (a) SD unground (b) SD milled for 5 hours and tested directly after milling and SD milled for 5 hours (c) stored for 7 days, (d) stored for 14 days, (e) stored for 21 days, (f) stored for 28 days, (g) stored for 56 days and (h) stored for 84 days.

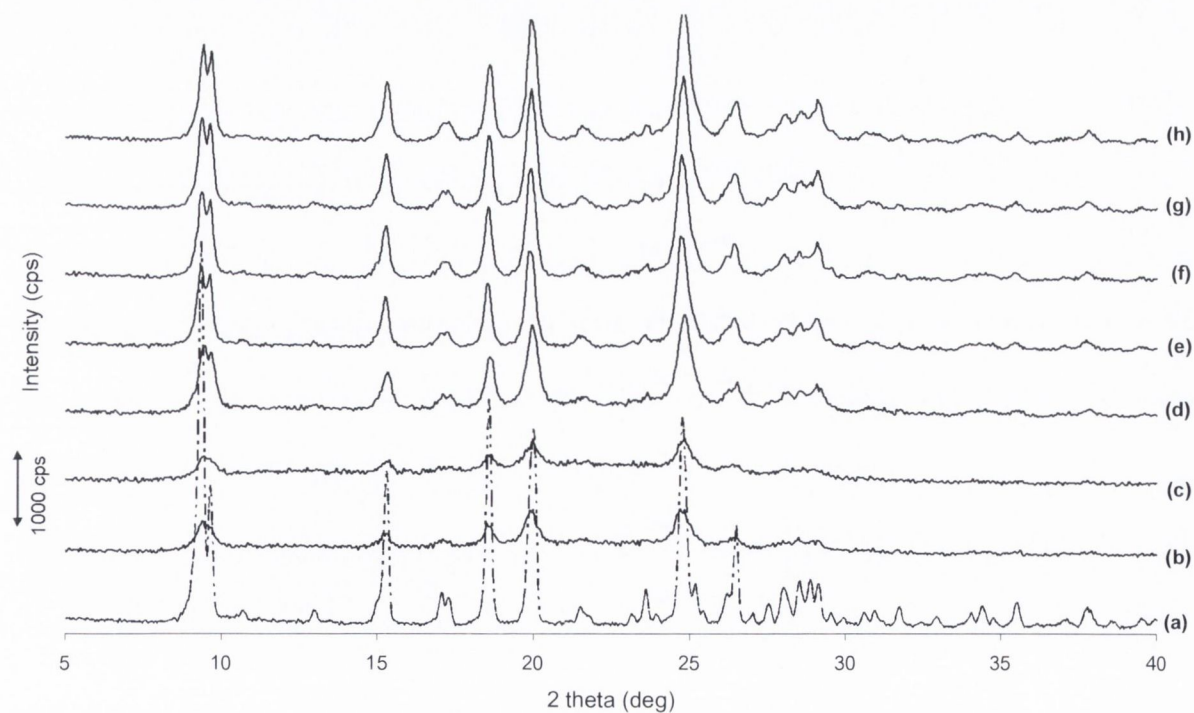


Figure 3.23b: PXR D of (a) SD unground, (b) SD milled for 10 hours and tested directly after milling and SD milled for 10 hours (c) stored for 7 days, (d) stored for 14 days, (e) stored for 21 days, (f) stored for 28 days, (g) stored for 56 days and (h) stored for 84 days.

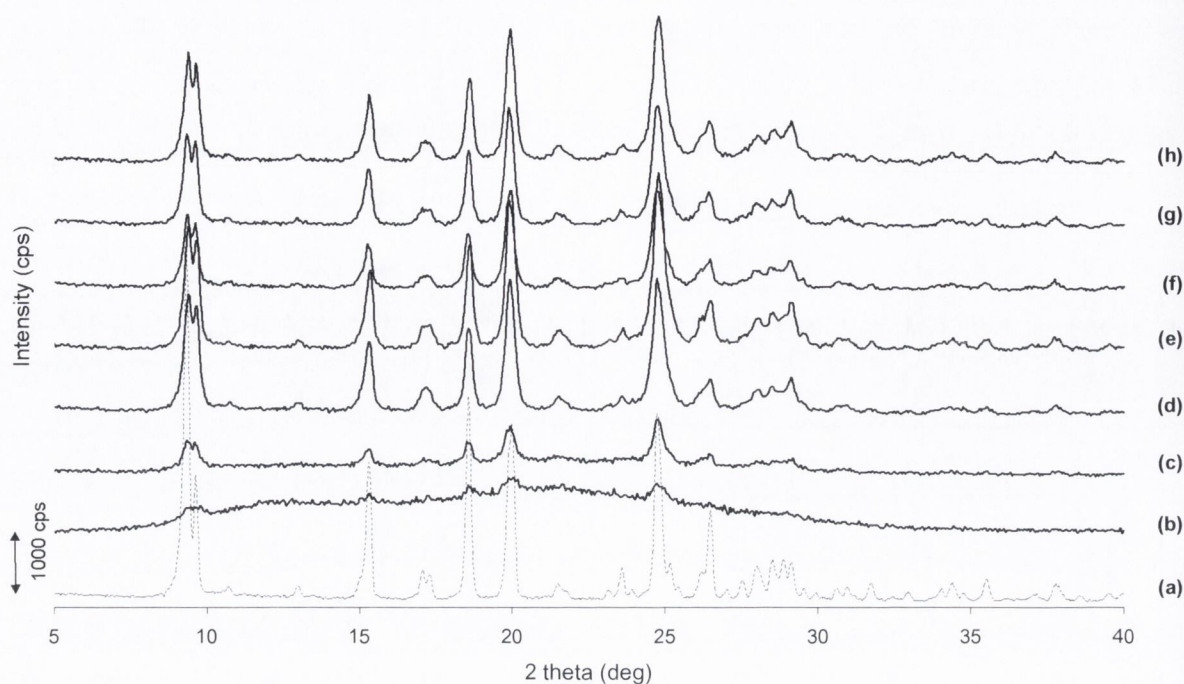


Figure 3.23c: PXR of (a) SD unmilled (b) SD milled for 15 hours and tested directly after milling and SD milled for 15 hours (c) stored for 7 days, (d) stored for 14 days, (e) stored for 21 days, (f) stored for 28 days, (g) stored for 56 days and (h) stored for 84 days.

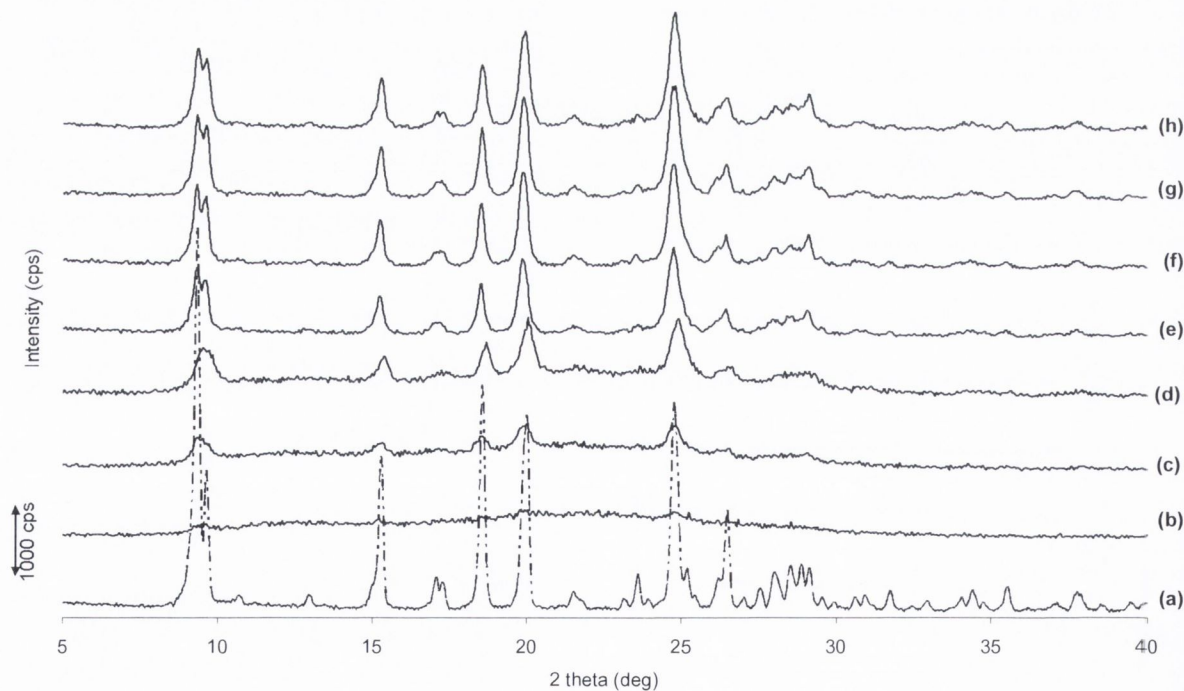


Figure 3.23d: PXR of (a) SD unmilled (b) SD milled for 20 hours and tested directly after milling and SD milled for 20 hours (c) stored for 7 days, (d) stored for 14 days, (e) stored for 21 days, (f) stored for 28 days, (g) stored for 56 days and (h) stored for 84 days.

Table 3.12: PXRD total peak area analysis of the unmilled SD and for the SD milled samples analysed directly after milling and stored over 12 weeks at 4 °C over phosphorus pentoxide. T₀, T₇, T₁₄, T₂₁, T₂₈, T₅₆ and T₈₄ represent the total peak area measured directly after mill, after 7, 14, 21, 28, 56 and 84 days respectively.

Ball milling time (minutes)	T ₀	T ₇	T ₁₄	T ₂₁	T ₂₈	T ₅₆	T ₈₄
0	100.00 (0.00)	100.00 (0.00)	100.00 (0.00)	100.00 (0.00)	100.00 (0.00)	100.00 (0.00)	100.00 (0.00)
30	98.89 (0.14)	98.99 (0.03)	100.00 (0.09)	100.00 (0.58)	100.00 (0.44)	100.00 (0.51)	100.00 (0.00)
60	77.40 (0.01)	76.19 (6.99)	78.87 (7.53)	88.21 (7.05)	91.51 (1.51)	90.71 (1.93)	92.83 (2.12)
120	77.93 (0.01)	80.73 (8.36)	80.98 (0.47)	89.38 (6.06)	91.98 (5.65)	91.11 (7.72)	97.00 (3.06)
300	60.21 (0.71)	66.38 (11.99)	66.12 (9.34)	68.06 (4.71)	69.15 (2.04)	74.22 (2.36)	72.23 (0.14)
600	22.59 (2.46)	55.26 (3.66)	54.56 (8.85)	56.31 (2.64)	56.84 (5.44)	78.85 (1.90)	80.92 (6.36)
900	7.74 (0.11)	26.73 (3.25)	25.62 (3.27)	62.94 (4.50)	64.16 (7.80)	64.04 (8.35)	69.69 (1.98)
1200	5.31 (0.01)	24.08 (12.09)	32.63 (4.61)	53.70 (6.77)	62.46 (0.57)	63.67 (0.62)	81.03 (3.60)

Standard deviation in parentheses. n=3

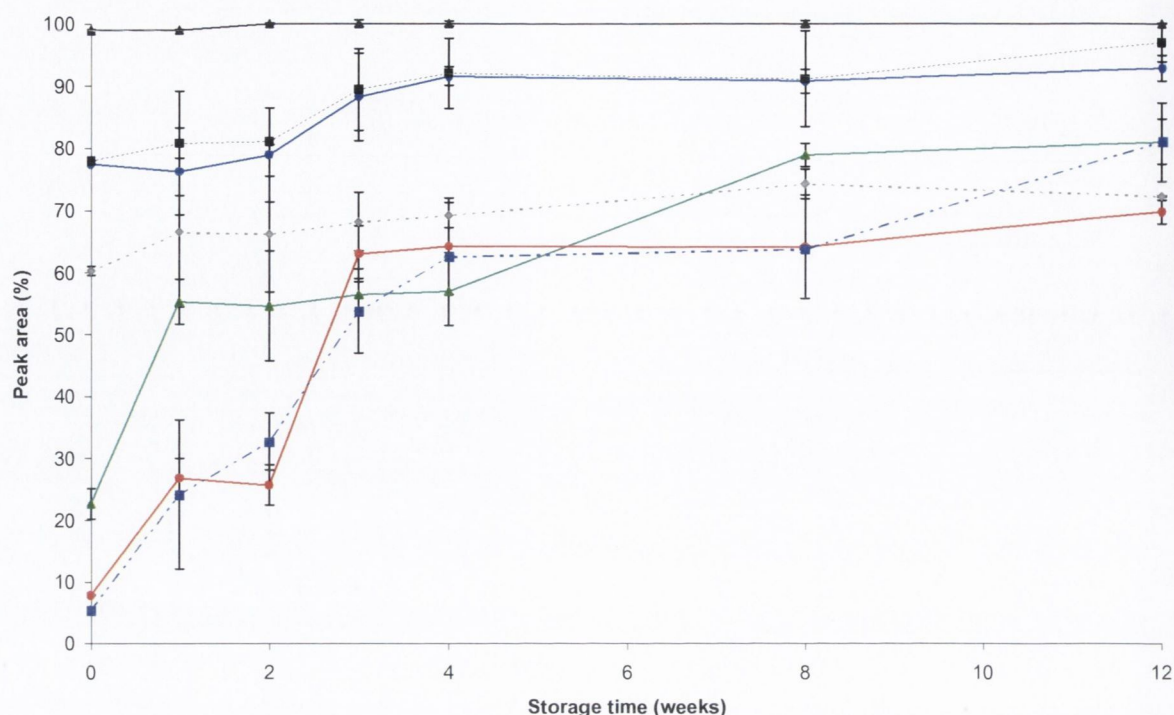


Figure 3.24: PXR D total peak area changes for SD milled for 30 (black solid line, triangle), 60 (blue solid line, circle) and 120 minutes (dashed black line, square) and 5 hour (grey dashed line, diamond), 10 hour (green solid line, triangle), 15 hours (red solid line, circle) and 20 hours (blue dashed line, square), tested directly after milling and after storage at 4 °C over phosphorus pentoxide.

3.5.2 Thermal analysis

Figure 3.25 a, b, c, d illustrates the thermograms obtained for SD samples milled for 5, 10, 15 and 20 hours at RT with a BTP weight ratio of 40:1, respectively. The thermograms were acquired directly after milling and after each storage period of interest (7, 14, 21, 28, 56 and 84 days). The thermal events detected for the unmilled and milled samples when analysed directly after milling, were previously discussed in sections 3.1.3 and 3.3.1.2, respectively. For the majority of the thermograms obtained for the ball milled samples, two thermal events were detected. The first was attributed to a crystallisation exotherm and the second endotherm was due to the melting of the material. The broad crystallisation peak prevented the detection of a glass transition temperature of the milled samples. The onset temperature of the crystallisation exotherm was detected at ~ 70 °C and the melt endotherm was detected at ~ 196 °C. The peak intensity change in the crystallisation exotherm indicated a change in the

amorphous phase present. The amorphous phase of each sample was calculated using the equation described by Lefort *et al.*, (2004).

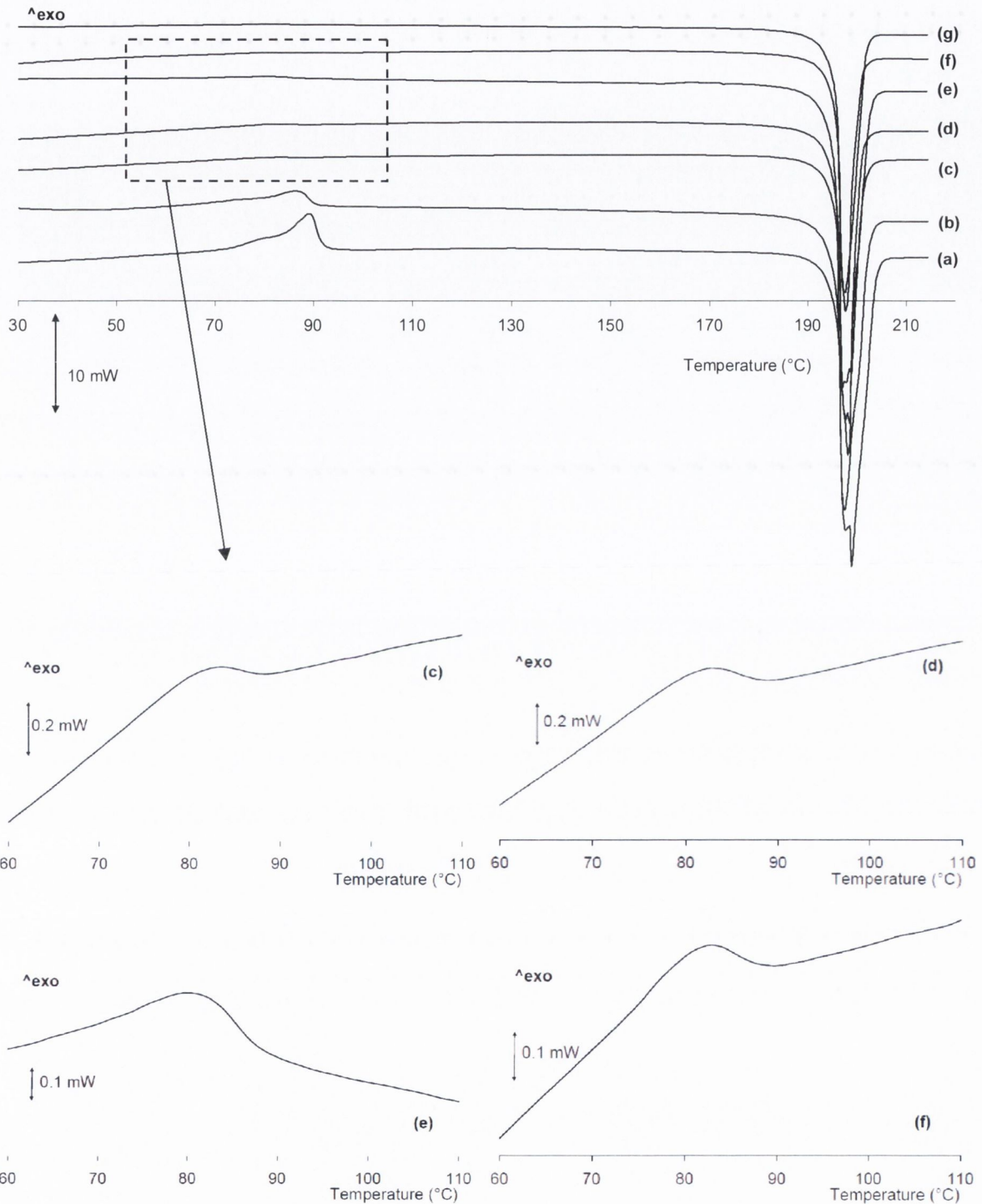


Figure 3.25a: DSC thermograms for (a) SD milled for 5 hours and tested directly after milling and SD milled for 5 hours and stored at 4 °C, for (b) 7 days (c) 14 day, (d) 21 days, (e) 28 days, (f) 56 days and (g) 84 days. Magnified crystallisation exotherms are shown (c) 14, (d) 21, (e) 28 and (f) 56 days.

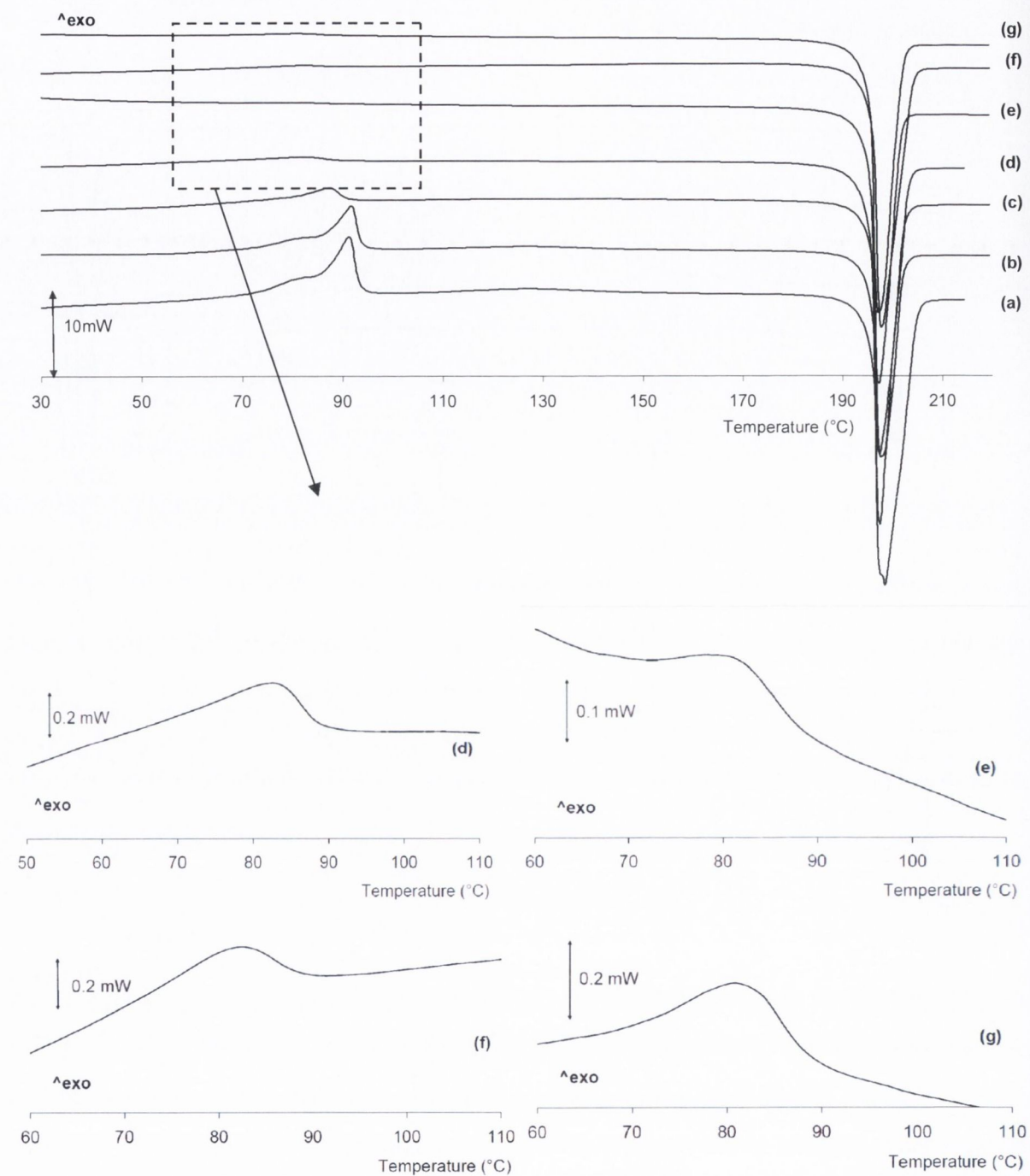


Figure 3.25b: DSC thermograms for (a) SD milled for 10 hours and tested directly after milling and SD milled for 10 hours and stored at 4 °C, for (b) 7 days (c) 14 day, (d) 21 days, (e) 28 days, (f) 56 days and (g) 84 days. Magnified crystallisation exotherms are shown (d) 21, (e) 28 (f) 56 and (g) 84 days.

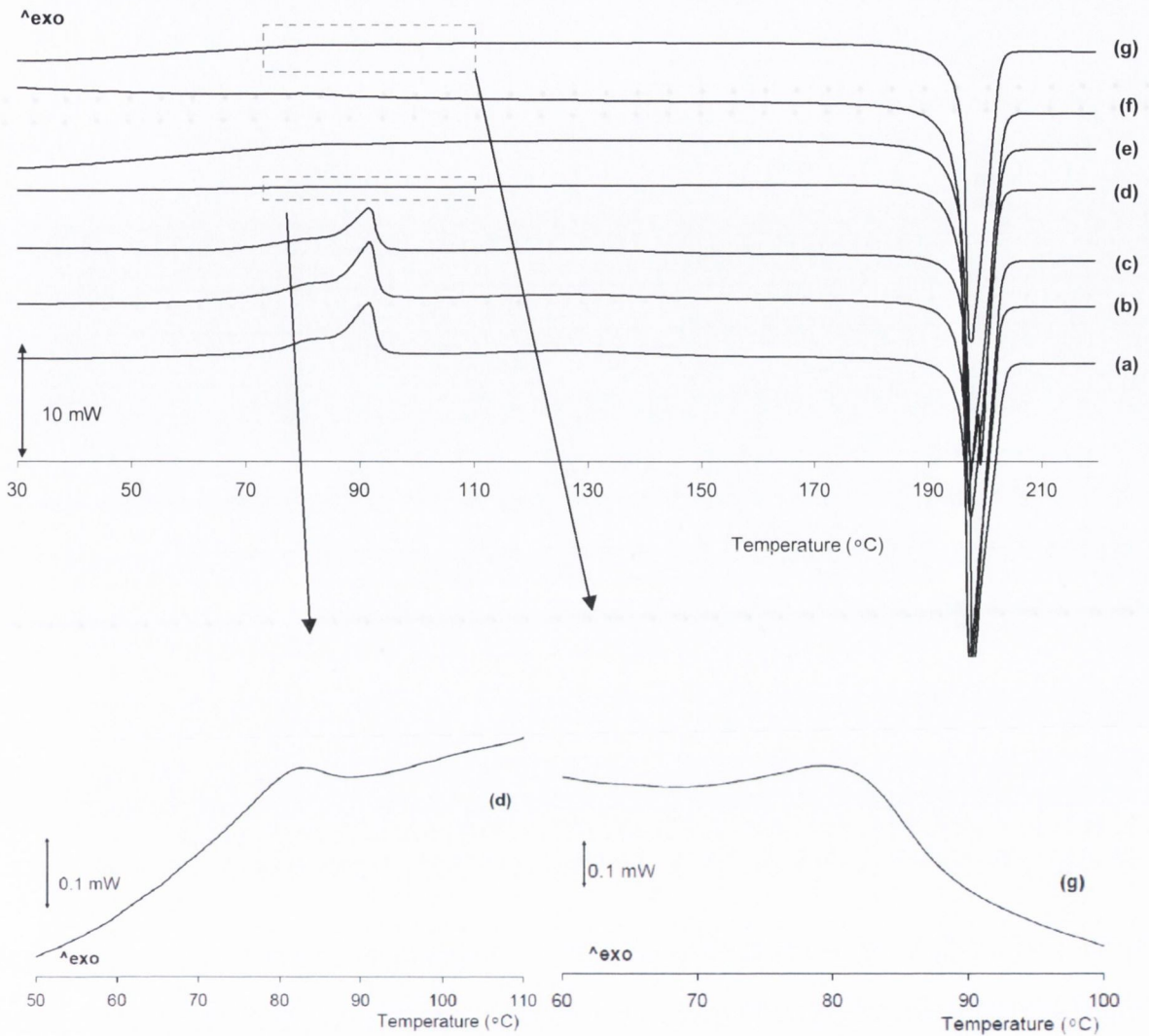


Figure 3.25c: DSC thermograms for (a) SD milled for 15 hours and tested directly after milling and SD milled for 15 hours and stored at 4 °C, for (b) 7 days (c) 14 day, (d) 21 days, (e) 28 days, (f) 56 days and (g) 84 days. Magnified crystallisation exotherms are shown (d) 21 and (g) 84 days.

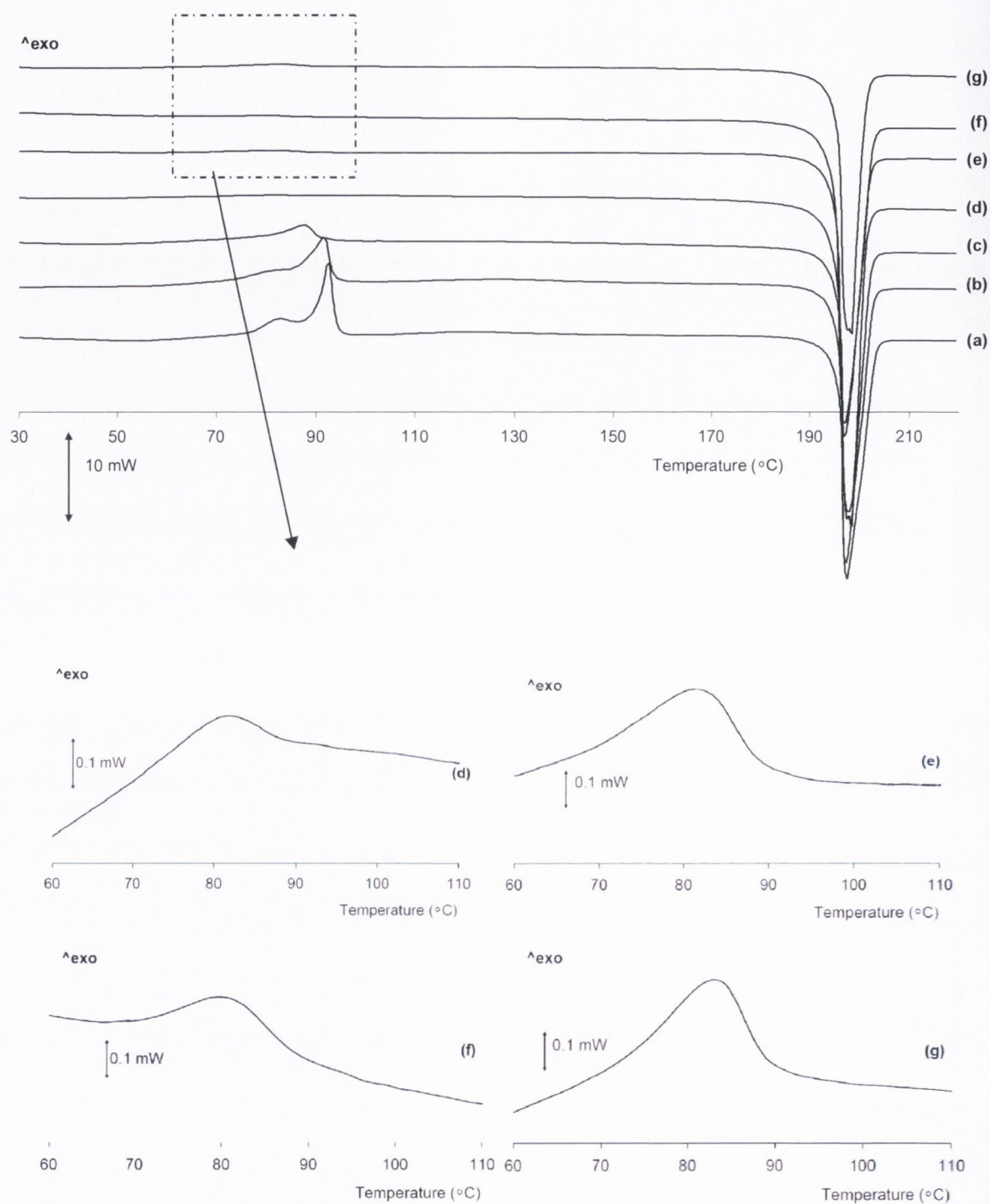


Figure 3.25d: DSC thermograms for (a) SD milled for 20 hours and tested directly after milling and SD milled for 20 hours and stored at 4 °C, for (b) 7 days (c) 14 day, (d) 21 days, (e) 28 days, (f) 56 days and (g) 84 days. Magnified crystallisation exotherms are shown (d) 21, (e) 28 (f) 56 and (g) 84 days.

Quantification of the DSC amorphous content for each sample milled and stored is given in Table 3.13. DSC amorphous content at isothermal storage conditions for each sample is shown in Figure 3.26. SD milled for 30 minutes resulted in the DSC amorphous content of ~3 % after 7 days and analysis after 28 days suggested complete crystallisation. Ball milling for 60 and 120 minutes resulted in a DSC amorphous content of ~6 and ~12 %, respectively. A decrease was observed for both samples after 7 days and prolonged storage of 84 days resulted in a DSC amorphous content of less than 2 %. Ball milling for 5 and 10 hours resulted in a DSC amorphous content that was reduced by about 5 % after 7 days of storage. Ball milling for 15 and 20 hours appeared to have slower crystallisation trend with the DSC amorphous content detected above 50 % after 14 days. Figure 3.26 shows a decline in DSC amorphous content. For samples milled for 5, 10, 15 and 20 hours less than 5 % of the DSC amorphous phase was detected after 28 days of storage. With the exception of SD milled for 30 minutes, all other samples milled and stored for 84 days still had a residual amorphous phase.

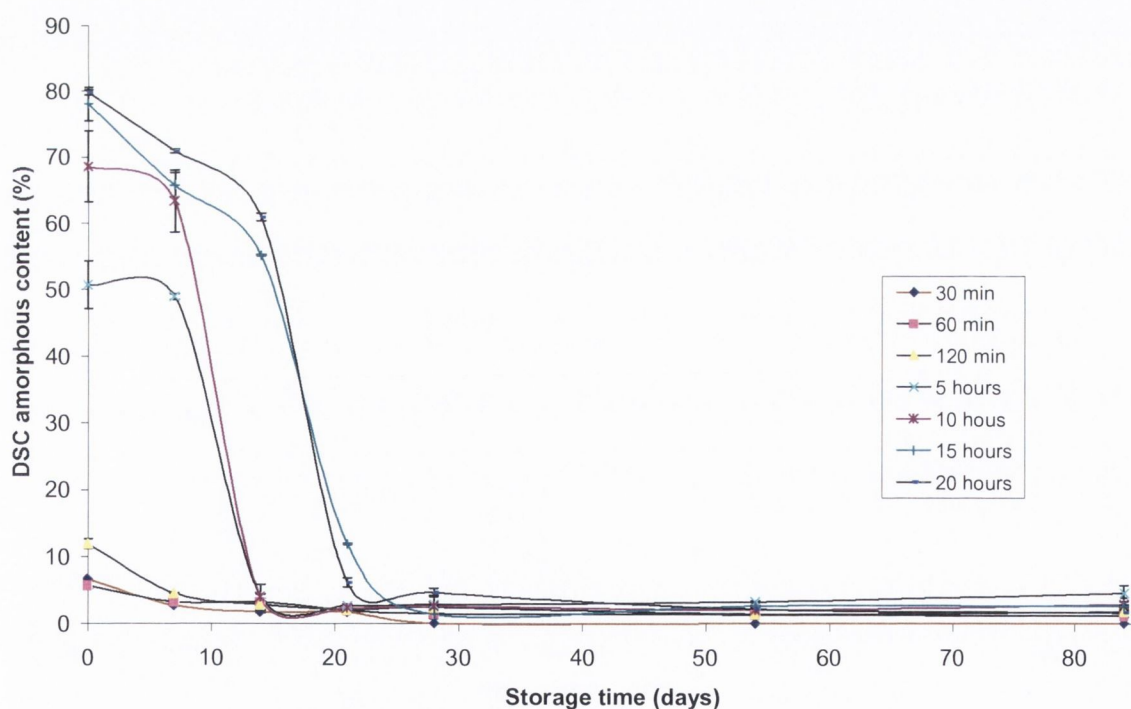


Figure 3.26: Changes to the induced DSC amorphous content for SD milled for 30, 60 and 120 minutes and 5, 10, 15 and 20 hours, measured directly after milling and after storage at 4 °C over phosphorus pentoxide.

Table 3.13: DSC amorphous content of SD directly after milling and stored over 12 weeks at 4°C over phosphorus pentoxide. T₀, T₇, T₁₄, T₂₁, T₂₈, T₅₆ and T₈₄ represent the total peak area measured directly after mill, after 7, 14, 21, 28, 56 and 84 days respectively.

Ball milling time (minutes)	T ₀	T ₇	T ₁₄	T ₂₁	T ₂₈	T ₅₆	T ₈₄
0	0.00 (0.00)	0.00 (0.00)	0.00 (0.00)	0.00 (0.00)	0.00 (0.00)	0.00 (0.00)	0.00 (0.00)
30	6.61 (0.05)	2.68 (0.15)	1.72 (0.13)	1.66 (0.09)	0.00 (0.00)	0.00 (0.00)	0.00 (0.00)
60	5.62 (0.54)	3.19 (0.27)	3.07 (0.10)	1.92 (0.01)	1.46 (0.09)	1.34 (0.02)	1.16 (0.05)
120	11.85 (0.72)	4.50 (0.06)	2.81 (0.19)	2.05 (0.44)	2.39 (0.12)	1.43 (0.06)	1.77 (0.26)
300	50.64 (3.59)	48.86 (0.45)	4.03 (0.36)	2.62 (0.22)	2.8 (1.33)	3.26 (0.16)	4.52 (1.18)
600	68.53 (5.36)	63.29 (4.71)	3.92 (1.85)	2.29 (0.16)	2.55 (0.21)	2.05 (0.64)	2.83 (1.01)
900	77.98 (2.53)	65.70 (1.90)	55.11 (0.10)	11.81 (0.10)	1.37 (0.64)	2.62 (0.12)	2.60 (0.24)
1200	79.73 (0.35)	70.84 (0.31)	60.86 (0.57)	6.06 (0.69)	4.59 (0.59)	2.12 (0.18)	1.63 (0.75)

Standard deviation in parentheses. n=3

3.5.3 Crystallisation kinetics

To understand the mechanism of the transformations, the crystallisation kinetics for the SD samples which were milled at RT with a BTP weight ratio of 40:1 were evaluated by using a modified version of the Avrami equation described by Yang *et al.* (2010). The samples were stored at 4 °C over phosphorous pentoxide. The Avrami equation, equation 3.1 (Avrami, 1939) was developed to model crystallisation from amorphous solids, where $\alpha(t)$ is related to the crystallisation time, k is the crystallisation rate constant and n is the Avrami exponent. The Avrami equation assumes that the nucleation rate is constant throughout the recrystallisation process which over-predicts the relative crystallinity and under-predicts the

time for complete recrystallisation. Yang *et al.*, (2010) explains that the driving force for nucleation is the energy difference between amorphous state and crystalline state and as this remains constant at isothermal conditions. As crystallisation continues, the nucleation rate tends to decrease with respect to time. This is due to the fact that the available nucleation sites are consumed throughout the recrystallisation process.

$$\alpha(t) = 1 - \exp(-kt_n) \quad \text{Equation 3.1}$$

Yang *et al.* (2010) reported a new kinetic model that accounts for the change in the nucleation rate over time. The equation given by Yang *et al.* (2010) is outlined below (Equation 3.2), where Y is the crystallinity, k is the crystallisation rate constant, n is the Avrami exponent which depends on the nucleation mechanism and the number of dimensions in which growth is occurring and t is time.

$$Y = (k * (t^n)) / (1 + (k * (t^n))) \quad \text{Equation 3.2}$$

By fitting the data presented in 3.12 and 3.13 the best fit Avrami exponent (n) was determined. The value of n depends on the nucleation mechanism and the number of dimensions in which growth occurred. The crystallisation rate constants (k) were also determined. The calculated (k) rate constants for each of the milled and stored samples analysed by both DSC and PXRD are given in Table 3.14. Evaluation of the data showed that the best fit curves for the models were obtained when n=3. The nucleation value, n was thought to indicate three-dimensional crystal growth (Schmitte *et al.*, 1999; Avrami 1939). When calculating the rate of crystallisation the highest level of crystallised material (i.e. in this study, the total crystallised after 84 days) is taken to equal 1 (or 100%) as the amorphous phase that has crystallised during the storage period was of interest. Figure 3.27 represents the crystallisation kinetics obtained from the PXRD peak area, from data obtained over the 84 day storage period. A characteristic 'S' shaped curve was detected for all of the milled and stored samples. Yang *et al.*, (2010) stated that the 'S' shaped curve of recrystallisation is due to the small number of nuclei at the very beginning, followed by a rapid recrystallisation and, due to the consumption of the nucleation sites, a decline in the recrystallisation rate towards the end of the recrystallisation process. The rate at which each sample crystallised was different, with k ranging from 0.0006 day^{-1} (± 0.000071), $R_2 = 0.7806$ for SD milled for 60 minutes and

stored, to 0.00023 day^{-1} (± 0.000018), $R^2 = 0.8996$ obtained for SD ball milled for 20 hours and stored. The crystallisation rate is higher for the samples milled for the shorter time due to the higher number of seed crystals available as the majority of the sample was crystalline in nature. From the results shown the model was best fitted to the data collected from the samples milled for 120 minutes and 20 hours with R^2 values of 0.8733 and 0.8996 obtained, respectively.

Figure 3.28 (A to F) represents the crystallisation kinetics obtained from the DSC amorphous content and there is more of a distinct difference between the results compared to those observed for the PXRD peak area analysis. All the graphs show an 'S' shaped profile. The fastest crystallisation rate was detected for the SD 60 minute milled powder with $k = 0.082 \text{ days}^{-1}$ (± 0.0003), $R^2 = 0.8139$. In contrast to this the slowest crystallisation rate was obtained for SD ball milled for 20 hours, which resulted in the highest level of DSC amorphous content for the samples investigated, $k = 0.0005 \text{ days}^{-1}$ (± 0.000039), $R^2 = 0.8174$. This difference was observed for the PXRD data and it was suggested that the crystallisation of the induced amorphous phase occurred faster due to the larger number of nucleation crystals, which was a result of the majority of the material existing in its crystalline state.

Table 3.14: Crystallisation kinetic values for k (day^{-1}) analysed for SD milled and stored samples, characterised by DSC and PXRD. Note the Avrami exponent $n=3$ for all samples

Time (minutes)	k (day^{-1}) PXRD analysis	R^2	k (day^{-1}) DSC analysis	R^2
60	6.0×10^{-4} (7.1×10^{-5})	0.7806	8.2×10^{-2} (3.0×10^{-4})	0.8139
120	1.2×10^{-4} (4.02×10^{-5})	0.8733	7.3×10^{-3} (7.2×10^{-5})	0.8993
300	3.8×10^{-4} (4.31×10^{-5})	0.7936	1.1×10^{-3} (2.4×10^{-5})	0.8471
600	3.0×10^{-4} (1.2×10^{-5})	0.6960	1.2×10^{-3} (4.8×10^{-5})	0.8416
900	3.3×10^{-4} (1.5×10^{-5})	0.7245	3.3×10^{-3} (4.3×10^{-5})	0.8714
1200	2.3×10^{-4} (1.8×10^{-5})	0.8996	5.0×10^{-4} (3.9×10^{-5})	0.8174

Standard deviation in parentheses, $n = 3$

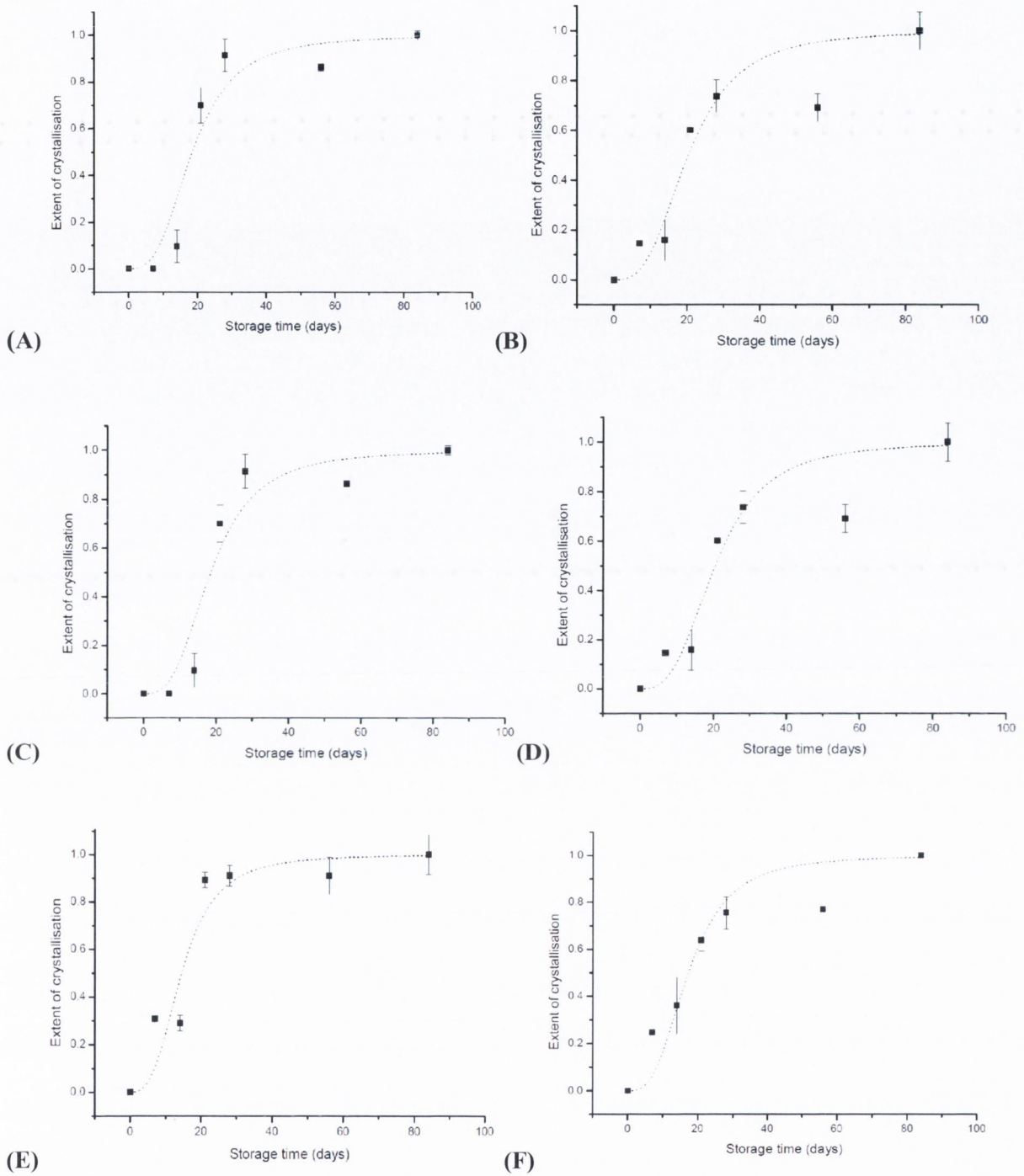


Figure 3.27: The extent of crystallisation of the PXRD total peak area for SD ball milled samples. The samples were milled for (A) 60 minutes, (B) 120 minutes, (C) 5 hours, (D) 10 hours, (E) 15 hours and (F) 20 hours, they were stored and monitored over an 84 day storage period.

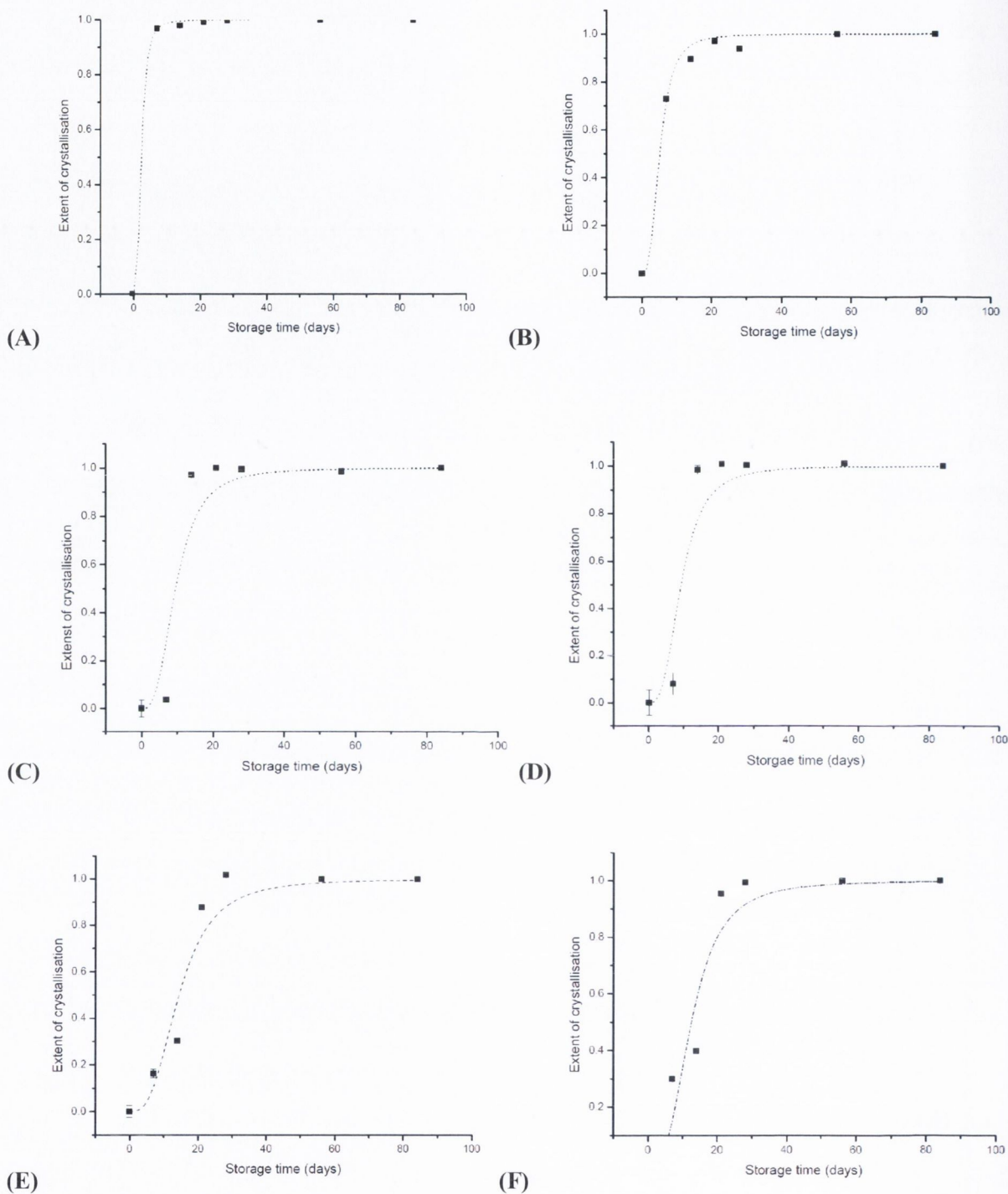


Figure 3.28: Extent of crystallisation of the induced DSC amorphous phase of SD ball milled samples. The samples were milled for (A) 60 minutes, (B) 120 minutes, (C) 5 hours, (D) 10 hours, (E) 15 hours and (F) 20 hours, they were stored and monitored over an 84 day storage period.

The PXRD peak area measures changes to the material's crystal structure. Such changes include decreased crystallite size, stress and strain to the lattice structure and the loss of crystallinity. The Avrami equation measures the rate of crystallisation of an induced amorphous phase. For this study the change in the PXRD peak area was used to describe the change in the induced amorphous phase but as there is significant difference between the PXRD peak area and the DSC amorphous content crystallisation kinetics it is possible that the changes observed to the PXRD peak area may not be exclusively attributed by the change in amorphous content. Changes to the peak area over the storage time may be attributed to the relaxation of the stress and strain induced into the crystal structure as a result of milling. This suggests that the analysis of the crystallisation kinetics that was induced by ball milling should be carried out using DSC analysis as opposed the PXRD peak area analysis.

Several factors may have contributed to the crystallisation of the amorphous SD phase. The presence of a crystalline material within an amorphous phase will act as a driving force, encouraging recrystallisation of the less stable state to a more thermodynamically stable state. Zhou *et al.* (2008) describes two different types of nucleation mechanism. The first is continuous nucleation, where nuclei are formed continuously during the crystallisation process. The second type of nucleation process involves a fixed number of nuclei and the number of nuclei does not change with changes in the experimental conditions. This is due to the fact that the rate of nucleation is much smaller than the rate of crystal growth. They note that this process occurs when the sample is intentionally seeded. Once nuclei are formed, crystal growth occurs quickly until the amorphous phase has completely crystallised. Further nucleation during growth is negligible because of the slow nucleation rates. A different level of disorder was induced for each ball milling time period investigated and none of the samples were completely amorphous. This would suggest that the different quantities of crystalline nuclei present with each sample contributed to the different k values obtained. The results indicate that the rate of crystallisation was dependent of the level of disorder induced into the material and confirms that a high level of disorder results in a lower rate of crystallisation.

It was suggested to store amorphous materials 50 °C below their T_g to reduce molecular mobility (Wilford *et al.*, 2006). The T_g of amorphous SD material has been reported by Caron *et al.*, (2011) to be ~78 °C and the storage temperature was 4 °C, suggesting that the molecular mobility of the SD material was reduced. Trasi *et al.*, (2010) found that small

amounts of crystalline material after milling affected the crystallisation behaviour of the remaining amorphous phase by acting as seeds for nucleation. In the case of SD, it is possible that the crystalline material that was present in each sample enabled crystallisation.

3.6 Conclusions

Ball milling at 4 °C with a BTP weight ratio 40:1 for 20 hours resulted in the highest level of disorder, quantified by PXRD peak area and DSC analysis compared to all other SD milled samples tested in this study. Comparing the samples milled at 4 °C and RT, a higher DSC amorphous content and a more significant PXRD peak area decrease was observed as a result of milling at the lower temperature. The increase of the DSC amorphous content and the decrease PXRD peak area for SD was found to be dependent on ball milling time, as a result of ball milling with a BTP weight ratio of 40:1 (at RT and 4 °C), 35:1 and 30:1 when milled at 4 °C. Ball milling with a BTP weight ratio of 20:1 at RT and 4 °C for up to 20 hours resulted in a Bragg peak intensity decrease to ~90 % and DSC amorphous content never exceeded 7%. Therefore induced amorphous content levels were not always seen to be dependent on milling time. Further milling may have achieved a higher disordered phase but compared to the other parameters in this study ball milling with a BTP weight ratio of 20:1 resulted in minor changes to the solid state nature of SD. The mechanism of amorphisation during milling is not completely understood. Caron *et al.*, (2007) reported that the level of amorphous phase induced into the material structure as a result of ball milling was due to the position of the material's T_g . They found that processing at a lower temperature in relation to the materials T_g reduces molecular mobility and prevents recrystallisation of the induced amorphous phase.

Increasing the BTP weight ratio resulted in an increase in disorder to the SD crystal structure, as observed when milling at 4 °C with ratio of 20:1, 30:1, 35:1 and 40:1. Large quantities of powder in a milling jar are thought to create a cushioning effect which results in reduction in the level of disruptions incurred by the crystalline structure (Suryanarayana, 2001). A smaller quantity of powder in the milling jar allows the number of ball-to-powder and powder-to-powder and powder-to-wall collision to increase.

A decrease in particle size was observed for all samples. The mono-modal distribution observed for the unmilled SD material was transformed to a bimodal distribution after 5 minutes of milling regardless of BTP weight ratio and temperature. Ball milling is often carried out to achieve a reduction in particle size and as a consequence of the process disorder may be induced. The parameters investigated in this study show that ball milling with a BTP weight ratio of 20:1 at RT for 5 minutes resulted in a particle size reduction with little change to the solid state nature of the material. Prolonged milling with increased BTP weight ratios resulted in a similar reduction to the particle size distribution but an increased level of disruption to the crystalline structure. Therefore, the results suggest that if a particle size reduction is required but no disruption to the solid state is preferred a low ball to powder ratio should be used.

Storage of SD milled at RT with a BTP weight ratio of 40:1 showed that the partial amorphous phase induced as a result of milling almost completely crystallised within 21 days. The higher the amorphous content induced the longer it took to crystallise, as indicated by the Avrami kinetics. Analysis of the crystallisation kinetics of amorphous phase that was induced as a result of ball milling should be determined by DSC analysis.

Ball milling of sulfadimidine
sodium salt

4.0 Introduction

Modification of the drug molecule by salt formation is common practice in the pharmaceutical industry to achieve desired biopharmaceutical properties. The formation of a salt involves the addition of a counterion to an electrolyte drug which modifies the lattice structure. Changes to the lattice structure may result in physicochemical property changes such as solubility, density, melting points etc., (Huang and Tong, 2004). Significant differences between physicochemical properties of sulfadimidine and sulfadimidine sodium salt include their molecular weight, glass transition temperature and melting point. Studies by Willart *et al.*, (2001 & 2006) and Caron *et al.*, (2007) noted the significance of a material's glass transition temperature when attempting to produce an amorphous material via ball milling. Studies showed amorphisation was easier to induce if processing, such as ball milling, was carried below the glass transition temperature (T_g) of the material. (Willart *et al.*, 2001; Shakhtshneider, 1997; Willart *et al.*, 2004 and Caron *et al.*, 2007). Willart *et al.* (2004) amorphised pure trehalose ($T_g = 120\text{ }^\circ\text{C}$) by milling at room temperature.

To investigate the relationship between a material's T_g and its ability to amorphise, Caron *et al.* (2007) ball milled, for 12 hours via a planetary ball mill, several physical mixtures of different molar fractions of crystalline trehalose ($T_g = 120\text{ }^\circ\text{C}$) and crystalline mannitol ($T_g = 10.6\text{ }^\circ\text{C}$). The purpose was to 'finely tune' the T_g in order to observe when the material amorphised, as the T_g of the corresponding alloy was systematically changed across the milling temperature zone (room temperature). From the results generated, Caron *et al.* (2007) concluded that if milling was performed above the T_g , the life time of the amorphised fraction would be short and rapid recrystallisation would occur. Although if milling was performed below T_g the induced amorphous phase would be induced which would not crystallise readily.

As previously observed in chapter 3, varying ball milling conditions had a significant effect on the level of disorder induced into the crystalline sulfadimidine material. Therefore the impact of ball milling on the sodium salt form of sulfadimidine was also explored. The ball milling parameters investigated in this study included ball to powder weight ratio and time, in order to study the feasibility of producing an amorphous phase. The storage stability of the amorphous phase induced as a result of milling was explored by PXRD and the crystallisation as a result of exposure to high relative humidity was examined.

4.1 Sulfadimidine sodium salt unmilled (SDNa)

Two batches of SDNa were obtained from Sigma, Ireland. The first batch (BT1) (no. 074K0599) was used when ball milling with a BTP weight ratio of 20:1 and the second batch (BT2) (no. BCCB6419) was milled with a BTP weight ratio of 40:1. Both the unmilled batches were evaluated by PXRD, DSC, TGA and DVS before milling to determine if any batch to batch variation occurred and to ensure the samples were completely crystalline.

4.1.1 Powder X-ray diffraction (PXRD)

Figure 4.1 illustrates the PXRD for both batches of sulfadimidine sodium salt (SDNa) unmilled and the diffractogram obtained from CCDC (Cambridge Crystallography Data Centre). The diffractogram obtained from CCDC was normalised (i.e. the largest peak intensity was taken to be 100%) and for comparison purposes both the diffractograms obtained for BT1 and BT2 were also normalised. Normalising the patterns allow for peak position comparisons to be made easier and to compare peak heights from the different patterns relative to one another. The distinct Bragg peaks for both batches indicate that both materials were crystalline in nature. The difference in peak intensity and peak width could be attributed to preferential orientation and/or the degree of crystallinity within the structure. Morris *et al.* (2000) proposed that the relative intensities of the peaks in a PXRD pattern correlate to preferential orientation exhibited by the crystallites, while a broadening of the peaks suggests smaller crystallites (Descamps *et al.*, 2007). The affect of preferential orientation and the size of the crystallites results in minor differences in the total PXRD peak area and the difference between the samples' crystallites which may have occurred during processing or even during PXRD sample preparation.

Analysis by DVS (data not shown) found that no crystallisation events were detected for the unmilled SDNa sample when exposed to a sorption-desorption cycle (0%RH up to 90%RH and back to 0%RH) confirming the results observed by PXRD, that the unmilled material was crystalline.

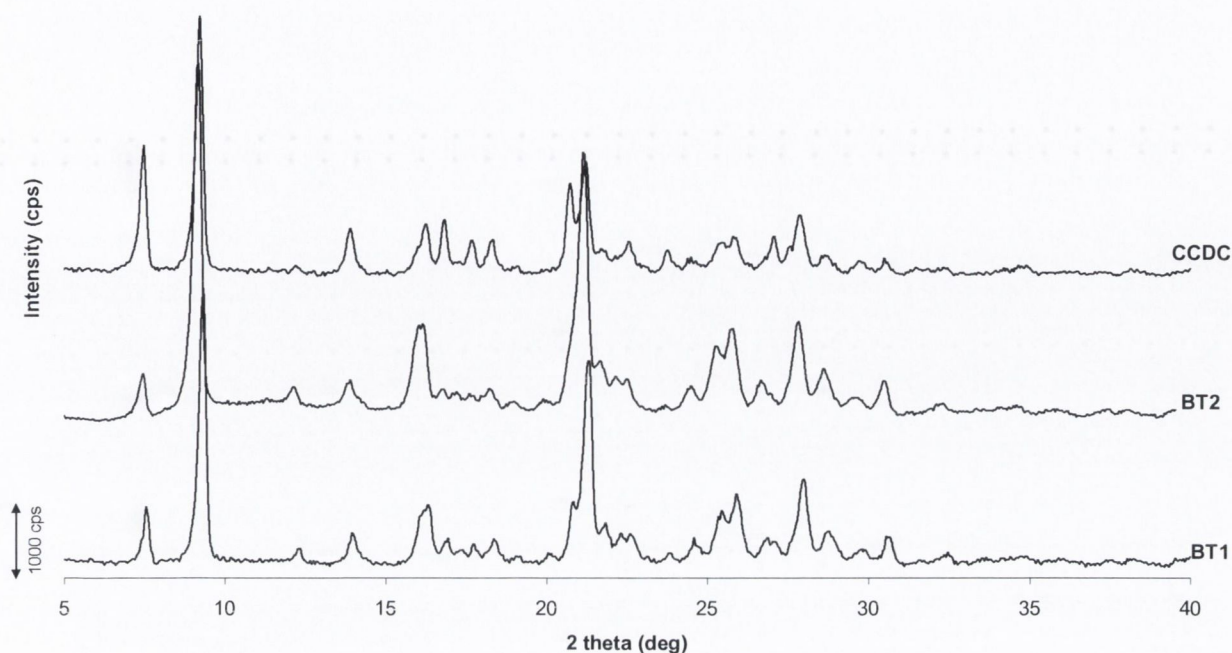


Figure 4.1: Powder X-ray diffraction pattern for both batches of SDNa received from Sigma, Ireland and the diffractogram obtained from Cambridge Crystallography Data Centre (CCDC).

4.1.2 Thermal analysis

Thermal analysis by DSC and TGA is shown in Figure 4.2 for both BT1 and BT2. Figure 4.2 a and b illustrate the DSC analysis where two thermal events were detected; the first endotherm below 100 °C was attributed to the loss of moisture from the structure and the second endothermic onset was the melt, detected at 303 °C. The corresponding TGA thermograms (Figure 4.2 c and d) showed that ~1 % (w/w) mass loss was detected from 25-100 °C. The low mass loss detected by TGA is consistent with moisture loss that may be present of the surface of the material of moisture that was loosely bound.

The melt enthalpy and onset temperature for BT1 was 121.04 J.g⁻¹ and 308.99 °C, respectively. Analysis of BT2 sulfadimidine sodium sample showed the melt enthalpy was 125.98 J.g⁻¹ and an onset of 305.90 °C was detected. This may suggest that a difference between the crystallite sizes was present between the two samples; this was first indicated by the different PXRD peak intensities and widths. This behavior is known as the Gibbs Thomas effect (Jackson and McKenna, 1990) which predicts that a depression of the melt point is

indirect proof of the crystallite size reduction. This suggests that the BT2 sample consisted of smaller crystallites in comparison to the BT1 sample.

Similar behavior was reported by Descamps *et al.* (2007) for sorbitol and attributed to a decrease of the sample's crystallite size when a decrease of the melting temperature and a broadening of the diffraction peaks were observed after sorbitol was milled for less than an hour.

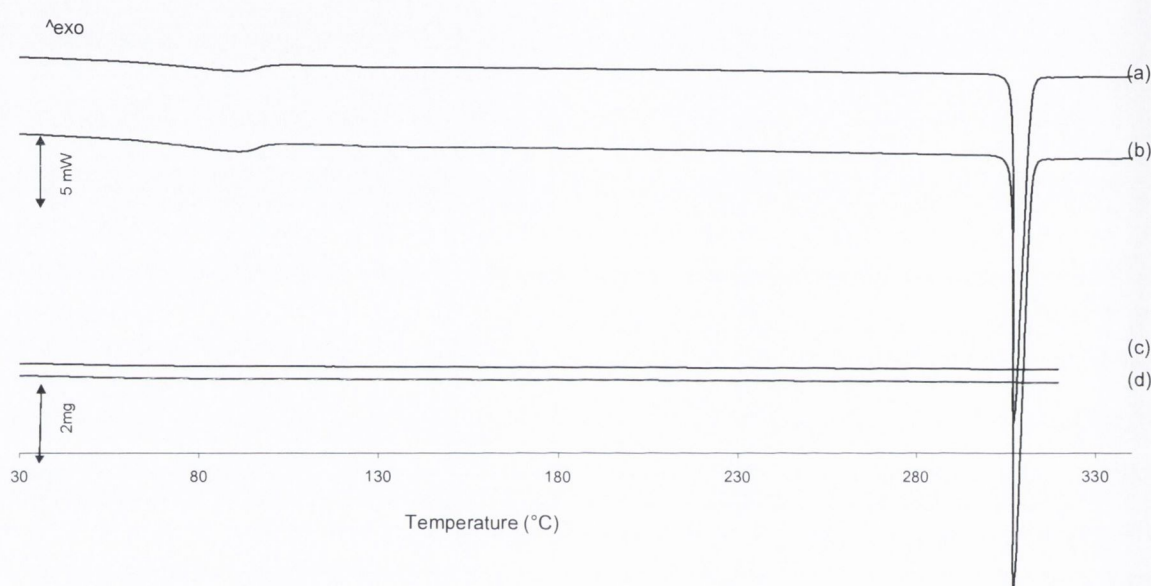


Figure 4.2: Thermal analysis of two batches of SDNa raw material: batch 1 (a) DSC, (c) TGA, and batch 2 (b) DSC and (d) TGA.

4.1.3 Particle size, surface area and microscopy

The particle size analysed by Malvern laser diffraction for BT1 and BT2 of SDNa unmilled is outlined in Table 4.1. Both batches have a mono-modal distribution and no statistically significant difference was observed between batches. The specific surface area determined by BET analysis for BT2 is also given in Table 4.1.

Table 4.1: Summary of the particle size data collected from the analysis of SDNa obtained from Sigma, Ireland.

	Particle size (μm)			SSA (m^2/g)
	d10	d50	d90	
Batch 1	1.83 (0.01)	6.62 (0.14)	16.88 (0.52)	NM
Batch 2	1.82 (0.21)	6.45 (0.07)	16.23 (0.91)	1.17 (0.24)

Standard deviation in parenthesis. n=3, NM = not measured

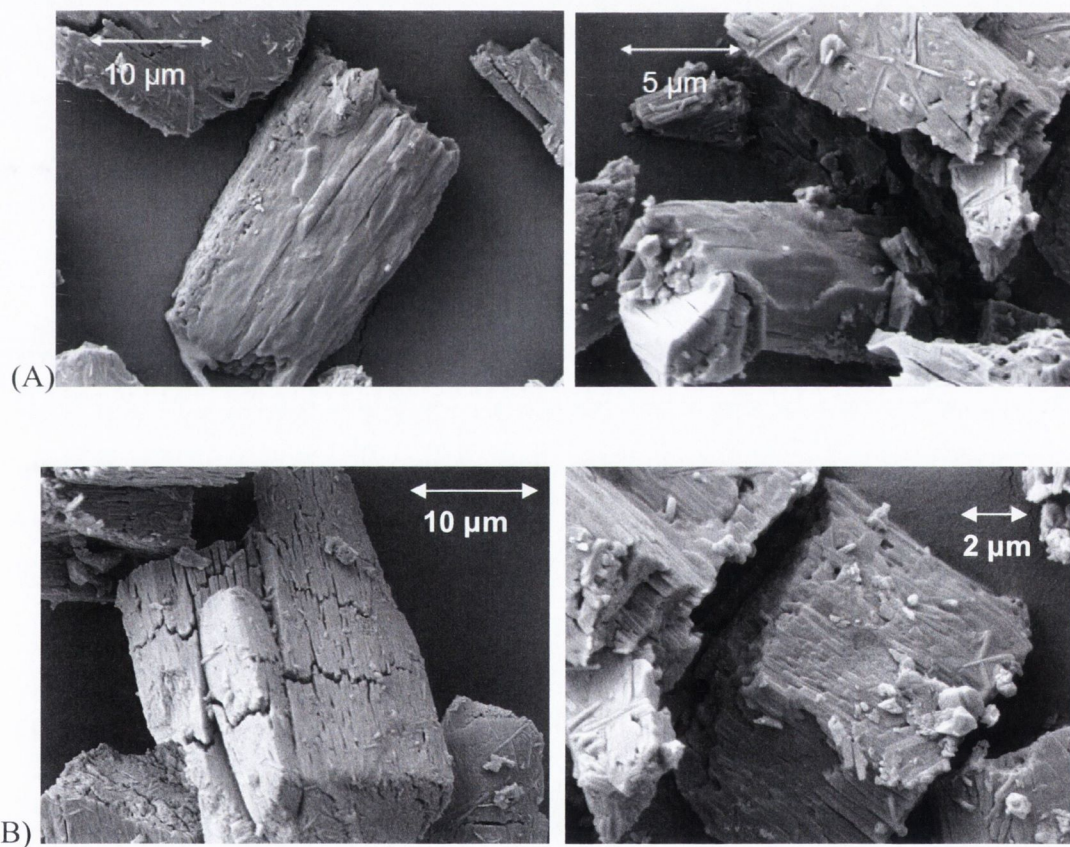


Figure 4.4: SEM morphology of sulfadimidine sodium salt unmilled (A) BT 1 and (B) BT 2. (Sigma, Ireland)

Figure 4.4 illustrates the micrographs of the SDNa received samples obtained by SEM analysis. Both batches have irregularly shaped particles. The size range observed by laser diffraction analysis is evident in the micrographs, with particles ranging from less than $5 \mu\text{m}$ to much greater than $10 \mu\text{m}$.

4.2 Ball milling of sulfadimidine sodium salt

The ball milling parameters that were tested for milling sulfadimidine sodium salt include BTP weight ratio and time. The combination of variables is outlined in Table 4.2. All ball milling was carried out at a rotational speed of 400 rpm (6.7 Hz). The aim was to establish process conditions that would induce an amorphous phase into the material.

Table 4.2: Processing parameters of ball milled sulfadimidine

Temperature	Ball to powder weight ratio	Time (min)
Room	40:1	5, 30, 60, 120, 300, 600
temperature	20:1	5, 30, 60, 120, 300, 600, 900

4.2.1 Powder X-ray diffraction

Figure 4.5 a and b illustrate the PXRD pattern of SDNa unmilled and milled at RT with a BTP weight ratio of 20:1 and 40:1, respectively. The PXRD patterns of the crystalline SDNa unmilled materials obtained from Sigma (Ireland), which were discussed in section 4.2.1, are shown in Figure 4.5a (BT1) and b (BT2) and are indicated by the label 'SDNa raw'. SDNa milled at both BTP weight ratios for 5 and 30 minutes showed crystalline Bragg peaks. Ball milling with a BTP weight ratio of 20:1 and 40:1 for 60 minutes resulted in the reduction of peak area and elimination of several crystalline peaks and an amorphous halo was observed. The crystal structure was completely destroyed after 120 minutes and an amorphous halo was detected as a result of milling with a BTP weight ratio of 40:1. An amorphous halo was detected for SDNa milled for 5 and 10 hours using a BTP weight ratio of 40:1. In contrast, ball milling for 120 minutes with a BTP weight ratio of 20:1 resulted in several crystalline peaks being detected at 9.55, 16.65 and 21.55 2θ degrees. Further milling for 5 hours resulted in total induced disorder and the amorphous phase, represented by the presence of a halo in the PXRD pattern, was detected after ball milling for 10 and 15 hours.

Peak area analysis in Table 4.3 shows the changes to SDNa milled from 5 to 120 minutes. Ball milling with a BTP weight ratio of 20:1 reduced the peak area by ~15 % after 5 minutes and the total peak area was reduced by ~19 % as a result of ball milling for the same period, but with a BTP weight ratio of 40:1. Increased milling time resulted in a decreased peak area

for both BTP weight ratios. Peak area analysis for SDNa milled with a BTP weight ratio of 40:1 showed that the reduction of crystallinity was faster compared to milling with a BTP weight ratio of 20:1. Ball milling for 60 minutes with a BTP weight ratio of 40:1 resulted in a peak area of less than 10 % and no crystalline peaks were detected after 120 minutes. Zografí and Tong (1999) reported the amorphisation of indomethacin sodium salt induced by ball milling, characterised by PXRD analysis. They showed that, as milling time increased, peak area decreased until an amorphous halo was detected (Zografí and Tong, 1999).

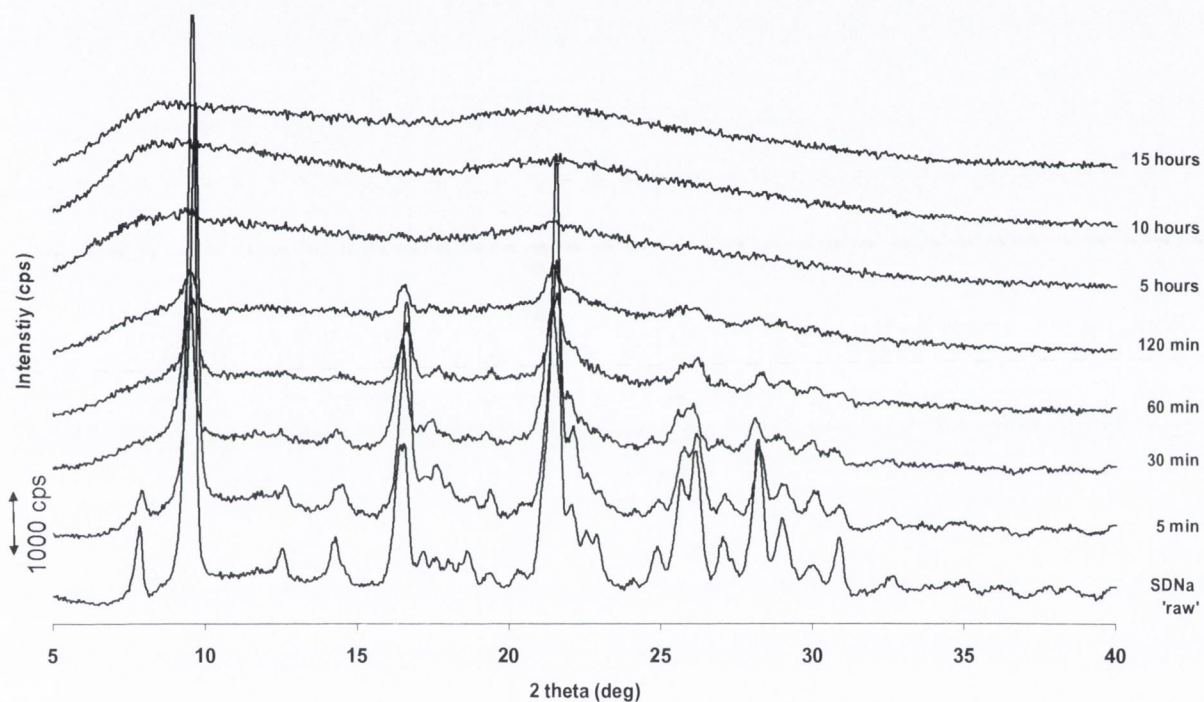


Figure 4.5 a: PXRD of SDNa unmilled (BT1) and milled at RT with a BTP weight ratio of 20:1 at a rotational speed of 400 rpm from 5 minutes to 15 hours.

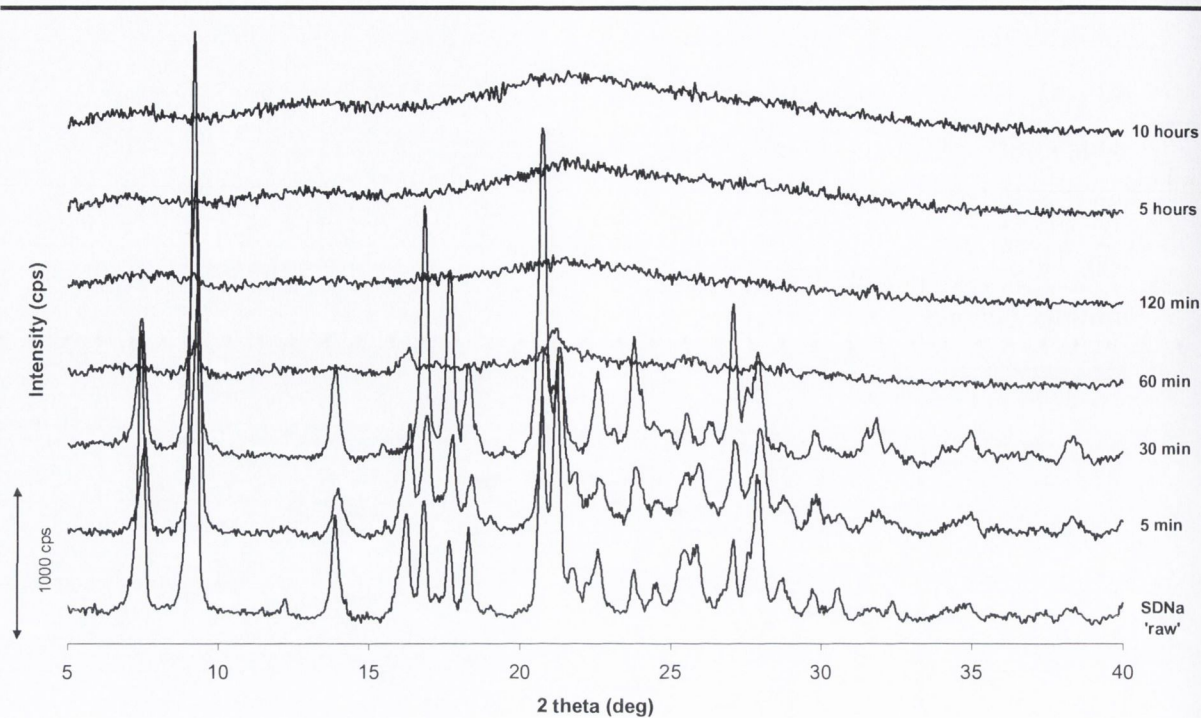


Figure 4.5 b: PXRD of SDNa unmilled (BT2) and milled at RT with a BTP weight ratio of 40:1 at a rotational speed of 400 rpm from 5 minutes to 10 hours.

Table 4.3: The total PXRD peak area obtained after the ball milling of SDNa at RT with a BTP weight ratio of 20:1 and 40:1 .

Time (minutes)	BTP 20:1 PXRD peak area	BTP 40:1 PXRD peak area
Unmilled	100	100
5	86.24 (3.42)	81.19 (3.45)
30	60.83 (2.14)	8.26 (6.31)
60	27.87 (2.95)	7.96 (2.84)
120	16.37 (5.31)	0.00 (0.00)
300	0.00 (0.00)	0.00 (0.00)
600	0.00 (0.00)	0.00 (0.00)

Standard deviation in parentheses. n=3

4.2.2 Thermal analysis

Figure 4.2 a and b presents the DSC thermograms of SDNa unmilled and milled with a BTP weight ratio of 40:1 and 20:1, respectively. Ball milling SDNa at RT resulted in three thermal events being detected for all milled samples. The first endothermic event corresponds to the loss of moisture which was observed below 100 °C, the second was attributed to a crystallisation exotherm, detected above 150 °C, and the third was a melt endotherm with an onset at ~309 °C. The magnitude and position of the second thermal event appears to be dependent on milling time.

With increased milling time the crystallisation exotherm peak becomes increasingly larger and shifts towards higher temperatures. These events were detected as a result of milling with both BTP weight ratios. A similar phenomenon was observed by Caron *et al.* (2001) when the ball milling of lactose resulted in complete amorphisation after one hour but further milling showed that the crystallisation exothermic peak shifted more than 20 °C to higher temperatures after 50 hours of milling. They stated that the shift reveals an increase of the thermal stability of the amorphous material (Caron *et al.*, 2001). They reported that the change in the peak shift could be attributed to the disappearance of the very last remaining crystalline nuclei which evaded the milling during the shorter milling times. The shift could also be attributed to an evolution of the local order in the amorphous material and this may change as a result of the nucleation and growth mechanism, driving the recrystallisation process (Caron *et al.*, 2001).

The data derived from the DSC thermograms is given in Table 4.4 for samples milled with a BTP weight ratio of 20:1 and 40:1. A glass transition temperature (T_g) at ~156 °C was detected for samples milled for 5 and 10 hours for both BTP weight ratios and for SDNa milled for 15 hours with a BTP weight ratio of 20:1. The broad crystallisation peak present in the thermograms of SDNa milled for periods of less than 5 hours prevented the detection of the T_g . The peak onset temperatures and enthalpies for both the melt and crystallisation events changed as a result of milling. Chieng *et al.*, (2006) stated that the difference in thermal behaviours was related to the amount of amorphous drug present and this was found as a result of ball milling ranitidine hydrochloride From 1. A DSC amorphous phase was induced after 5 minutes with a BTP weight ratio of 40:1 while no crystallisation exotherm was detected as a result of milling with a ratio of 20:1 for 5 minutes. Increased milling resulted in

an increased DSC amorphous content detected, for both BTP weight ratios. Ball milling for 120 minutes achieved a completely disordered phase with a ratio of 40:1, while a 90 % DSC amorphous content was obtained with a ratio of 20:1 for the same time. Ball milling for 5 hours with a ratio of 20:1 produced an amorphous SDNa material. The amorphous phase induced as milling time was increased for both ratios is shown in Figure 4.7. The results showed that an amorphous phase was possible using both BTP weight ratios but the lower ratio required more time. Tong and Zografi (1999) reported that the amorphous phase induced into the indomethacin sodium salt was also dependent on time of milling. This may be attributed to the fact that more material was enclosed in the milling container for the lower BTP weight ratio. With more material in the milling jars a cushioning effect was created, protecting particles from the ball-to-particle collisions. (Boldyrev and Tkáčová, 2000). Ball milling with a BTP weight ratio of 40:1 resulted in a higher amorphous content after 10 hours when compared to the 10 hours ball milled sample, using a BTP weight ratio of 20:1. This suggests that the less powder milled the higher the level of disorder induced.

Mass loss was determined by thermogravimetric analysis (Table 4.4). The loss of mass detected before 100 °C is attributed to the loss of water. Longer milling time (10 and 15 hours) resulted in a higher mass loss percent. Lefort *et al.* (2004) found that the adsorption of water during extensive milling was unavoidable. Relative to the corresponding crystalline state, molecules in an amorphous phase are capable of absorbing large quantities of water vapour into the solid bulk in addition to surface adsorption (Crowley and Zografi, 2002).

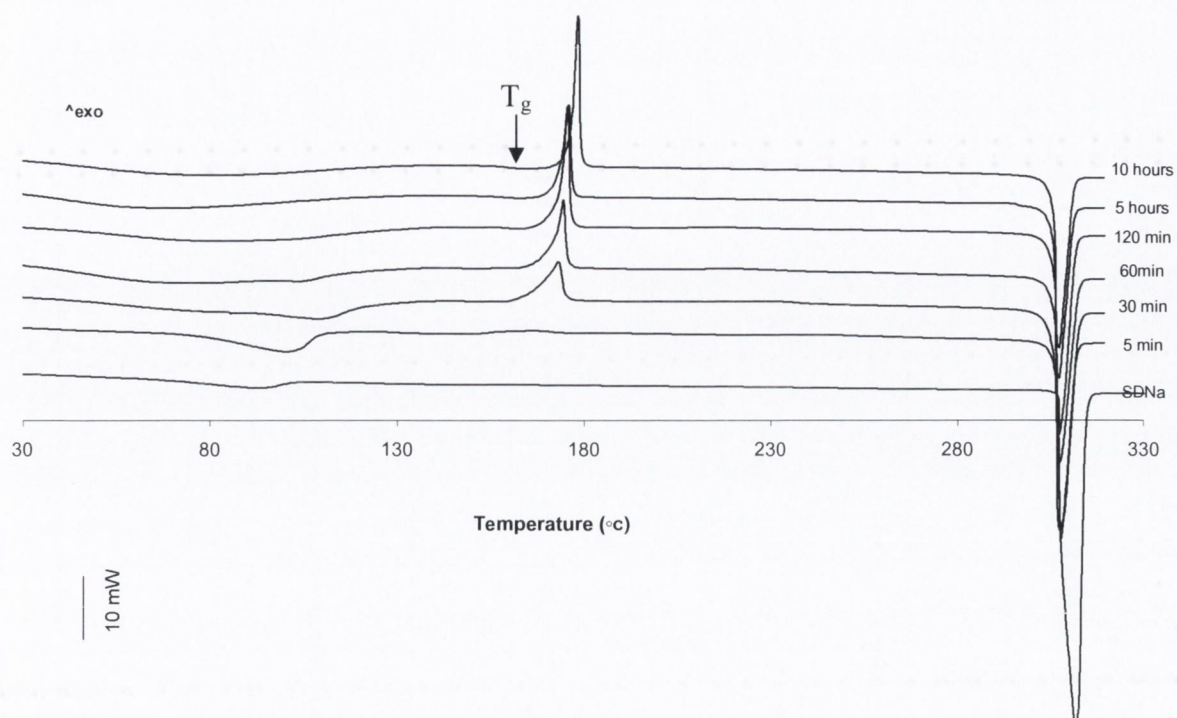


Figure 4.6a: Thermogram of SDNa unground (BT2) and milled at RT with a BTP weight ratio of 40:1 from 5 minutes to 10 hours.

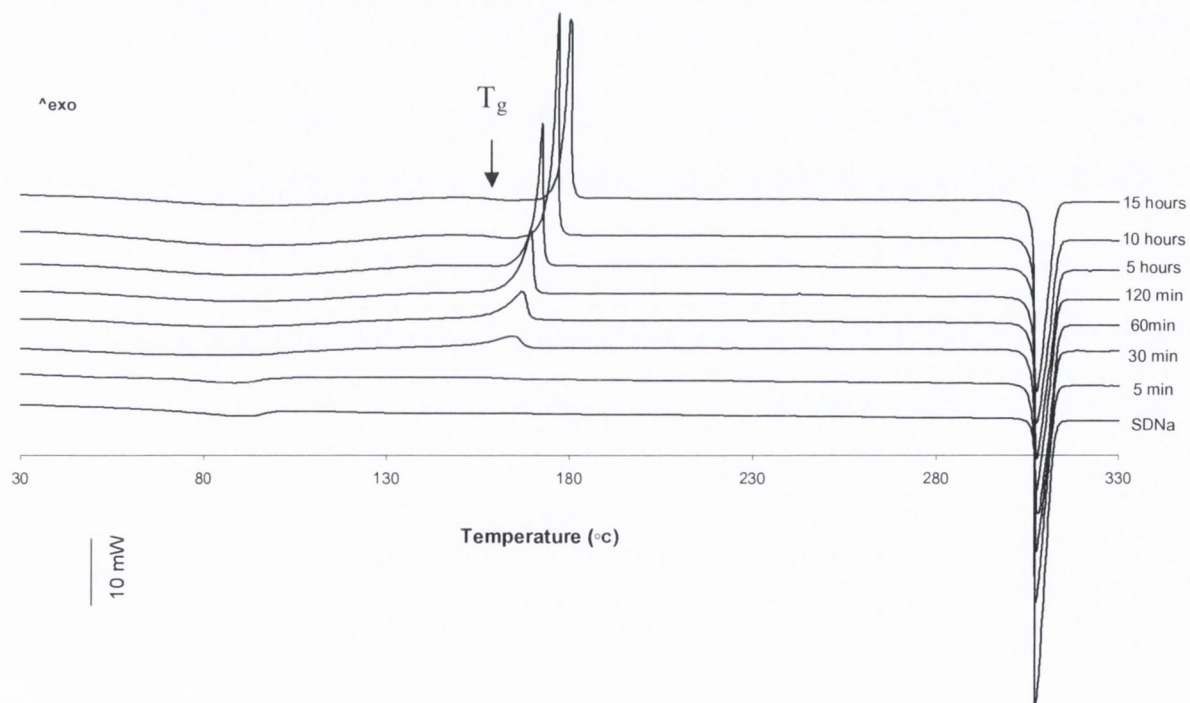


Figure 4.6 b: Themogram of SDNa unground (BT1) and milled at RT with a BTP weight ratio of 20:1 from 5 minutes to 15 hours.

Table 4.4: Thermal characteristics of SDNa unmilled and milled at RT. ND = not detected

	Milling time	T _g	ΔH _c (J/g)	ΔH _m (J/g)	T _c (°C)	T _m (°C)	Mass loss (%) 25°C to ~100°C	Mass loss (%) ~100 to 300°C	DSC amorphous content (%)
BT2	0			125.98 (0.49)		305.90 (0.57)	0.88 (0.09)	0.71 (0.04)	0 (0.00)
BTP 40:1	5 min	ND	5.68 (0.28)	117.47 (0.66)	153.77 (0.33)	306.85 (0.38)	1.50 (0.06)	0.93 (0.01)	15.20 (0.45)
	30 min	ND	28.27 (0.24)	117.91 (0.13)	172.66 (0.93)	305.99 (0.01)	2.89 (0.05)	1.68 (0.06)	65.09 (1.31)
	60 min	ND	37.99 (0.02)	116.18 (0.25)	173.33 (0.87)	306.02 (0.03)	3.73 (0.01)	2.33 (0.04)	88.64 (2.27)
	120min	ND	49.85 (0.25)	115.98 (0.03)	174.99 (1.39)	305.90 (0.14)	3.12 (0.09)	1.67 (0.01)	100 (0.00)
	5 hrs	157	62.83 (0.30)	117.32 (0.45)	174.26 (0.20)	305.86 (0.21)	4.22 (0.04)	2.52 (0.06)	100 (0.00)
	10 hrs	157	67.07 (0.33)	115.80 (0.28)	180.19 (0.27)	305.82 (0.25)	5.66 (0.16)	3.34 (0.66)	100 (0.00)
BT1	0			121.04 (0.38)		308.99 (0.62)	0.79 (0.06)	0.72 (0.07)	0
BTP 20:1	5 min			117.10 (0.29)			1.97 (0.04)	1.79 (0.04)	0
	30 min	ND	23.37 (0.57)	116.98 (1.41)	152.63 (1.05)	305.67 (0.31)	1.30 (0.04)	1.24 (0.03)	50.37 (7.13)
	60 min	ND	25.30 (0.61)	117.29 (1.03)	158.51 (0.47)	305.85 (0.13)	2.26 (0.03)	1.76 (0.01)	64.11 (2.17)
	120min	ND	33.45 (0.58)	113.48 (0.76)	163.33 (0.30)	305.19 (0.17)	1.93 (0.05)	1.61 (0.03)	90.64 (0.77)
	5 hrs	156	48.56 (0.80)	113.19 (0.81)	169.03 (0.08)	305.11 (0.10)	2.01 (0.01)	1.13 (0.04)	100 (0.00)
	10 hrs	156	58.70 (0.89)	112.46 (0.23)	172.14 (0.14)	304.86 (0.16)	2.45 (0.03)	2.56 (0.01)	100 (0.00)
	15 hrs	156	64.06 (0.18)	111.18 (0.88)	175.17 (0.15)	304.84 (0.17)	4.80 (0.01)	3.22 (0.01)	100 (0.00)

T_{poly} = onset temperature of solid state transition, ΔH_{poly} = enthalpy of solid state transition, T_{cr} = onset temperature of crystallisation, ΔH_{cr} = enthalpy of crystallisation, T_m = onset temperature of melt, ΔH_m = enthalpy of melt. DSC amor. = DSC amorphous content. Standard deviation in parenthesis, n=3.

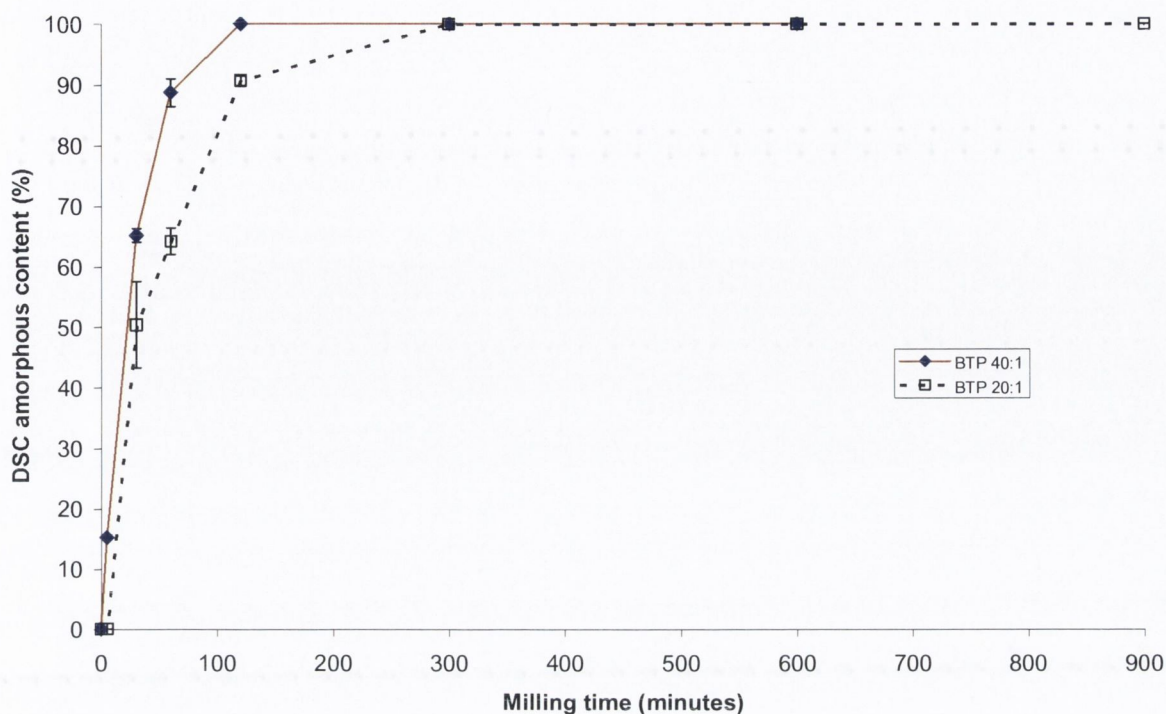


Figure 4.7: Comparison between the induced amorphous phases determined from the DSC thermograms for SDNa milled at RT with a BTP weight ratio of 20:1 and 40:1.

4.2.3 Particle size, specific surface area and microscopy

Particle size analysis by laser diffraction was carried out on a selection of samples to investigate the changes to the particle size of SDNa as a result of increased milling time and BTP weight ratios. Table 4.5 outlines the changes to the particle size parameters: d_{10} , d_{50} and d_{90} , as a result of ball milling for 30 and 60 minutes and 10 hours at RT with BTP weight ratios of 40:1 and 20:1. Particle sizing results show that for the 20:1 BTP weight ratio, as milling time was increased the d_{10} and d_{50} decreased (Table 4.5). The d_{90} measurement appeared to have increased after 30 minutes of milling but as time was increased this continued to decrease. The d_{10} measurements for SDNa ball milled with a BTP weight ratio of 40:1 for 30 minutes indicate a particle size reduction. A further size reduction was also observed after 60 minutes of milling. However, ball milling for 10 hours indicated an increase, as the d_{10} results increased to $2.69 \pm 1.47 \mu\text{m}$. The median particle size measurements (d_{50}) of SDNa ball milled with a BTP weight ratio of 40:1 indicated an initial increase, observed after 30 minutes of milling followed by an effective reduction, as a result of ball milling for 60 minutes and 10 hours. The d_{90} values indicated that as milling time was increased the particle sizes grew or they formed agglomerates (Table 4.5). The previous work

of Brodka–Pfeiffer *et al.*, (2003) on the subject of ball milling salbutamol sulphate also illustrated that with increased ball milling times the portion of coarse particles increased. They purposed that a possible explanation for this phenomenon may be the simultaneous recrystallisation of the amorphous material and therefore particle growth (Brodka–Pfeiffer *et al.*, 2003). Adi *et al.*, (2007) characterised the particles of ball milled lactose and indicated that the particulate interactive forces (e.g. electrostatic, intermolecular forces etc.) cause the adhesion of micronised fractions of fine powders (less than 15 μm) to the surface of larger particles and these agglomerated units will be measured as one large particle. Comparing the d90 measurements of particle sizes showed that by increasing the milling time as well as the BTP weight ratio the particle size increased. Charkhi *et al.*, (2010) reported a similar outcome from the experimental design study carried out to determine the optimum parameters required to produce nano zeolite powder by ball milling. No explanation was given as to why a size increase was obtained but as a result of prolonged milling they produced an amorphous phase characterised by XRD analysis. These results suggest that SDNa was not the only material subjected to a particle size increase as a result of milling and that a material may be subject to a particle size increase as a consequence of an induced amorphous phase. The increase particle size may also be attributed to the increased number of agglomerated particles.

Table 4.5: Particle size by laser diffraction for SDNa unmilled and milled at RT with a BTP weight ratio of 40:1 and 20:1 from 30 minutes up to 10 hours.

		d10 (μm)	d50 (μm)	d90 (μm)
SDNa	BT2	1.82 (0.21)	6.45 (0.07)	16.23 (0.91)
BTP 40:1	30 min	1.66 (0.25)	8.16 (2.40)	65.02 (9.02)
	60 min	1.22 (0.05)	6.17 (0.38)	56.62 (9.29)
	10 hrs	2.69 (1.47)	6.84 (1.00)	81.10 (22.90)
SDNa	BT1	1.83 (0.01)	6.62 (0.14)	16.88 (0.52)
BTP 20:1	30 min	1.19 (0.12)	6.79 (0.95)	62.93 (14.88)
	60 min	1.16 (0.08)	6.17 (0.68)	61.80 (8.63)
	10 hrs	1.07 (0.11)	5.13 (0.89)	45.11 (5.61)

Standard deviation in parentheses, n=3.

To study changes to the morphology as a result of ball milling and to confirm the particle size analysis results, samples were subjected to analysis by SEM. The SEM morphology of SDNa milled with a BTP weight ratio of 40:1 for 30, 60 minutes and 10 hours is shown in Figure 4.8. SEM images indicated that, as a result of ball milling for 30 and 60 minutes the particles lost their initial shape and were converted into agglomerated fine particles (Figure 4.8 a). These fine particles were also observed throughout the 10 hour milled samples but among the fine particle were larger irregularly shaped larger particles (Figure 4.8 c). The interactive forces described by Adi *et al.* (2007) may explain the formation of the agglomerated fine particle. The larger particles could be a result of the induced amorphous phase previously confirmed by DSC and PXRD analysis and described by Brodka–Pfeiffer *et al.* (2003). The increased surface energy that is caused by the increased amorphous phase results in a cohesive material which may easily form agglomerates.

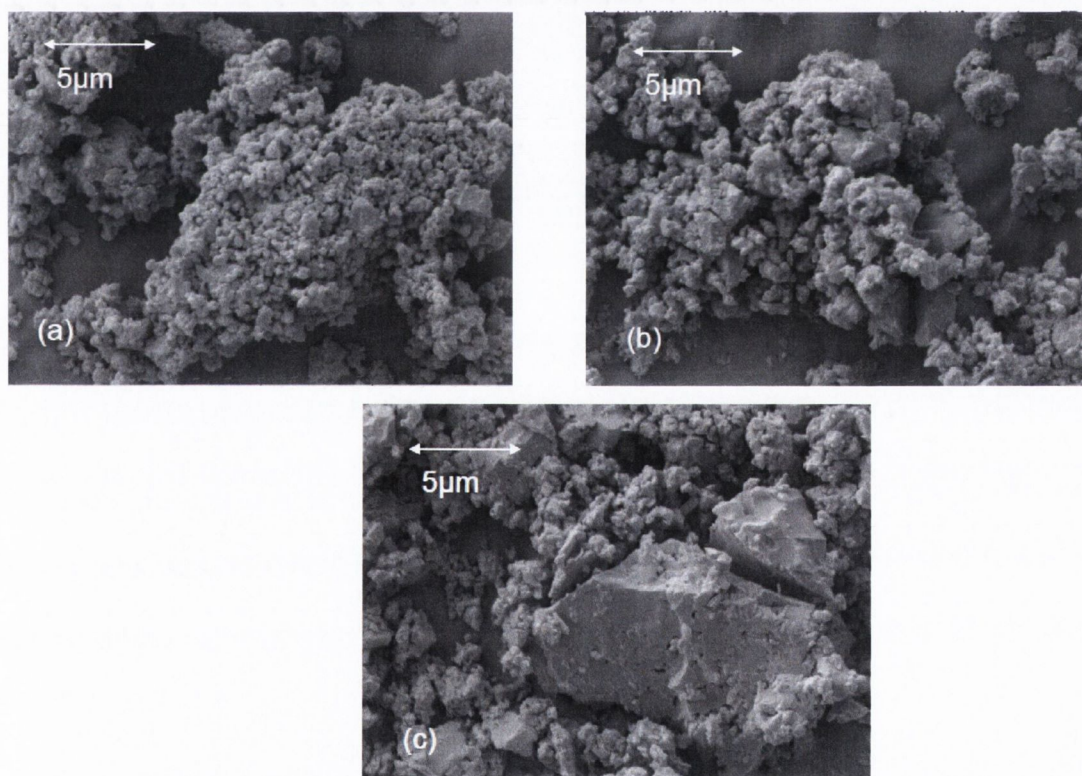


Figure 4.8: SEM morphology of SDNa milled at RT with a BTP weight ratio of 40:1 for (a) 30 minutes, (b) 60 minutes and (c) 10 hours.

The specific surface area (SSA) determined by BET for SDNa BT2 unmilled material and SDNa ball milled at RT with a BTP weight ratio of 40:1 is outlined in Table 4.6. Results indicate that after 5 minutes the SSA increased from $1.17 \pm 0.24 \text{ m}^2/\text{g}$ for the unmilled BT2

sample to $6.63 \pm 0.38 \text{ m}^2/\text{g}$. Analysis of the samples obtained from the subsequent milling times showed that their SSA were all calculated to be $\sim 6 \text{ m}^2/\text{g}$ (Table 4.6). These results suggest that the reduced particle size observed by laser diffraction and SEM analysis was reflected by an increased SSA.

Table 4.6: Specific surface area analysis by BET of SDNa BT2 unmilled and SDNa milled at RT and a BTP weight ratio of 40:1.

Sample	BET specific surface area (m^2/g)
Unmilled	1.17 (0.24)
5 min	6.63 (0.38)
30 min	6.02 (0.32)
60 min	6.54 (0.57)
120 min	6.61 (1.49)
5 hrs	6.40 (0.61)
10 hrs	6.63 (0.43)

Standard deviation in parenthesis. $n=3$.

4.3 Storage of SDNa

Stability of an amorphous phase is essential to product development. SDNa ball milled for 10 hours at RT with a BTP weight ratio of 40:1 were tested by PXRD directly after milling and after 7, 14, 21, 28, 56 and 84 days. The samples were stored at $4 \text{ }^\circ\text{C}$ which is $\sim 150 \text{ }^\circ\text{C}$ lower than the detected T_g of the milled amorphous samples. Storage at $50 \text{ }^\circ\text{C}$ below the T_g is expected to reduce the molecular motions and hinder structural reorganisation (Hancock *et al.*, 2002; Gusseme *et al.*, 2008). Evaluation of the relative humidity and the temperature over the storage period was reviewed in chapter 3, section 3.4.1.

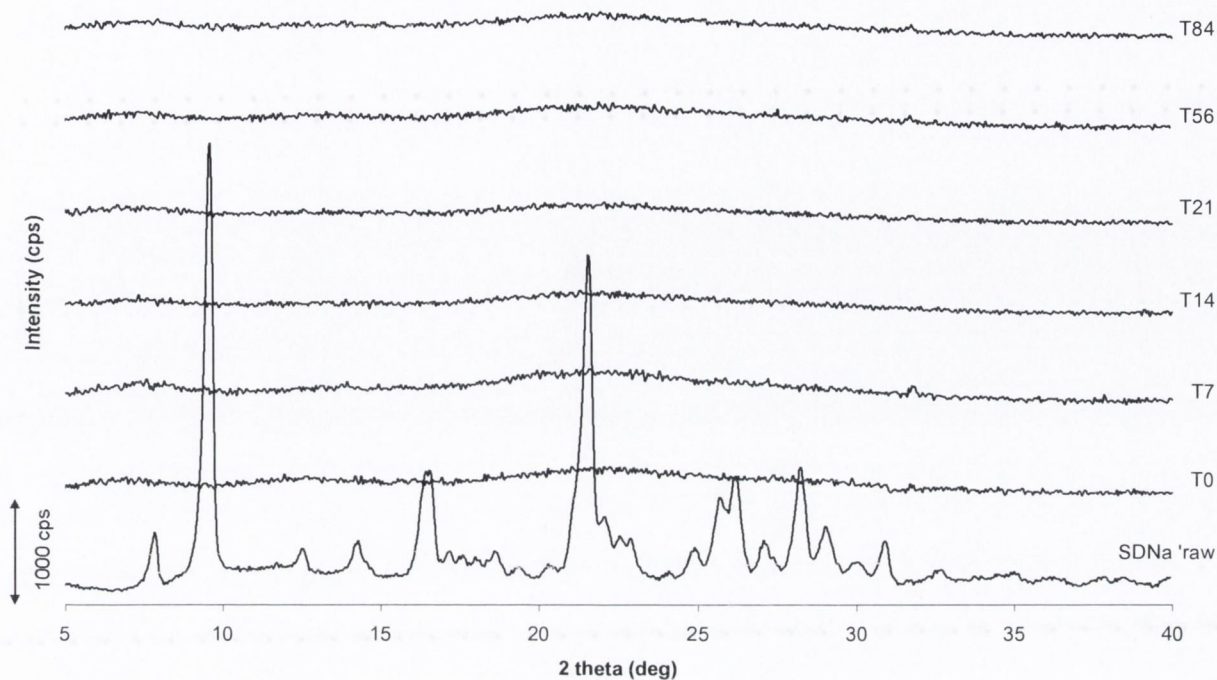


Figure 4.9: PXRD illustrates the diffractograms of SDNa BT2 ('raw') unmilled and SDNa milled for 10 hours at RT with a BTP weight ratio of 40:1 and tested directly after milling (T0), after 7 days (T7), after 14 days (T14), after 21 days (T21), after 56 days (T56) and after 84 days (T84).

Figure 4.9 shows the diffractogram for SDNa unmilled and milled for 10 hours. The crystalline Bragg peaks detected for the unmilled SDNa material were replaced after 10 hours of milling with an amorphous halo. Storage of the milled samples showed that an amorphous phase was still detected after 84 days of storage. To further evaluate the parameters required to induce crystallisation, the milled sample was exposed to different levels of relative humidity by dynamic vapour sorption analysis. The sample was exposed to relative humidity of 0 to 90 %, in incremental steps of 10% RH. This was followed by a desorption profile, achieved by decreasing the RH from 90% RH in steps of 10% RH. The moisture sorption-desorption isotherm is shown in Figure 4.10. The solid line corresponds to the sorption phase and the dashed line indicates the de-sorption cycle. A hysteresis was evident, which could indicate the formation of a hydrate. Increasing the relative humidity to 50 % resulted in an increase in water vapour uptake by the amorphous sample. The kinetics shown in Figure 4.11 show that as the sample was exposed to 60 % RH atmosphere an initial uptake of vapour was observed followed by a mass loss. Continued exposure to higher RH (70 to 90 % RH) resulted

in a further mass uptake of $\sim 3\%$. The absorbed water acted as a plasticising agent which forced the T_g of the amorphous phase to be reduced to the experimental temperature, consequently destabilising the amorphous phase and inducing crystallisation (Crowley and Zografi, 2002 and Fiebich and Mutz, 1999). Buckton and Darcy (1995) reported a mass loss after exposing partially amorphous lactose samples to high humidity environments. They explained that as humidity was increased the amorphous regions absorbed the water until crystallisation was induced; resulting in the water to be expelled from the material which was recorded as a mass loss. During the desorption phase from 90 % to 10% RH a $\sim 3\%$ mass loss was measured while a significant mass drop was observed from 10 % to 0%, where the mass returned to its initial dry state.

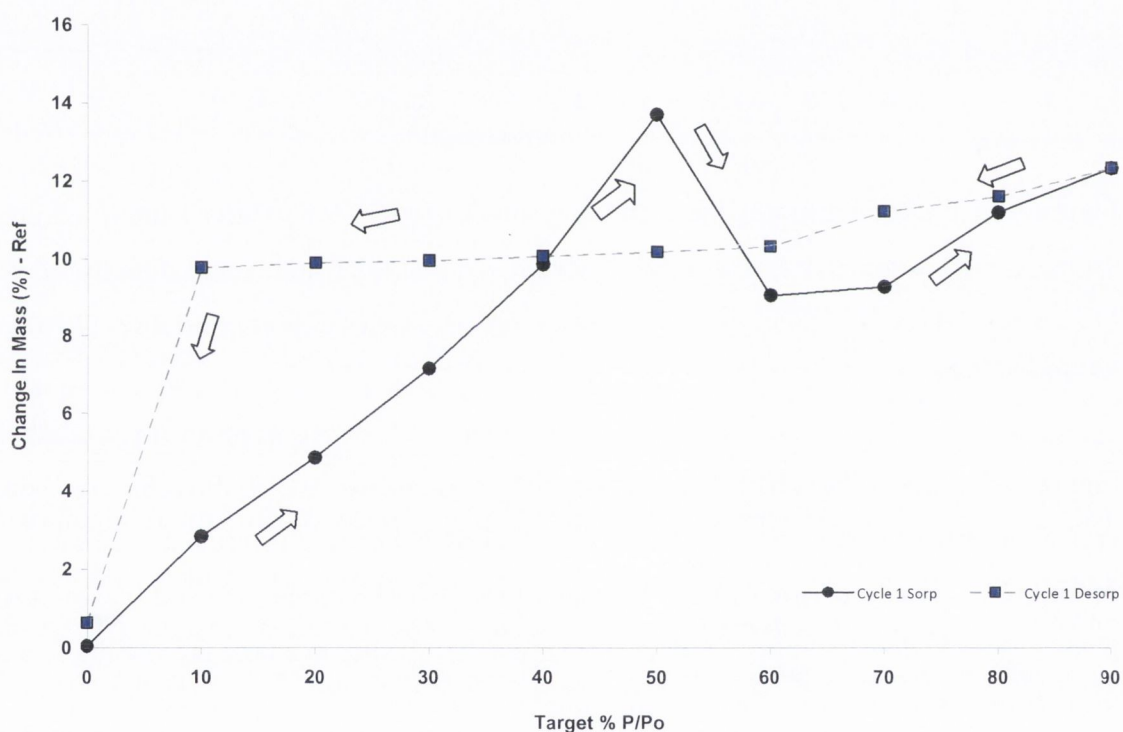


Figure 4.10: DVS isotherm for SDNa milled for 10 hours with a BTP weight ratio of 40:1

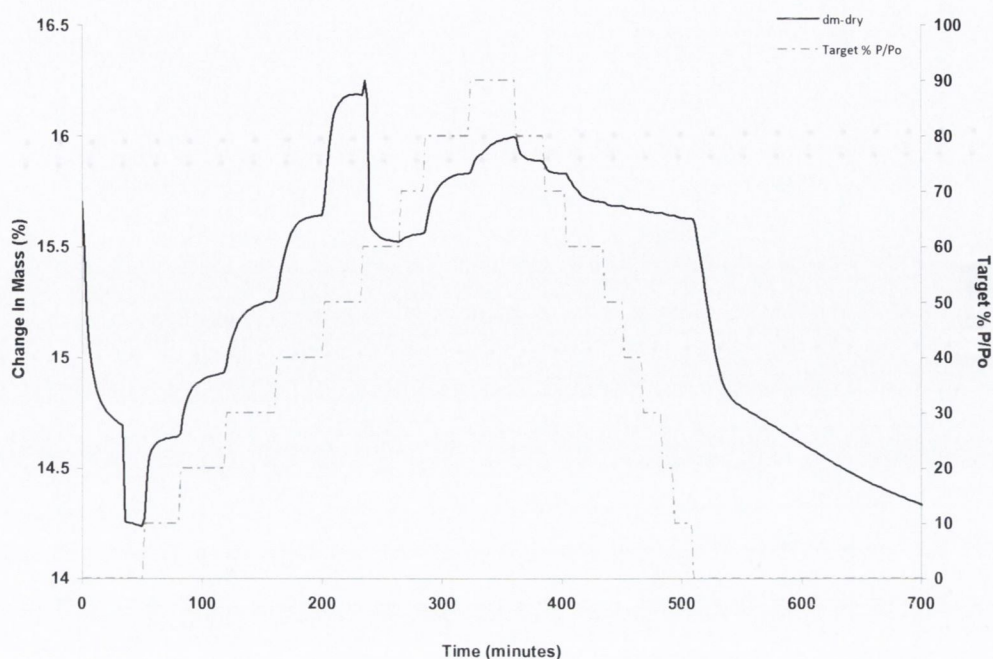


Figure 4.11: DVS kinetic plot for SDNa milled for 10 hours with a BTP weight ratio of 40:1 at RT.

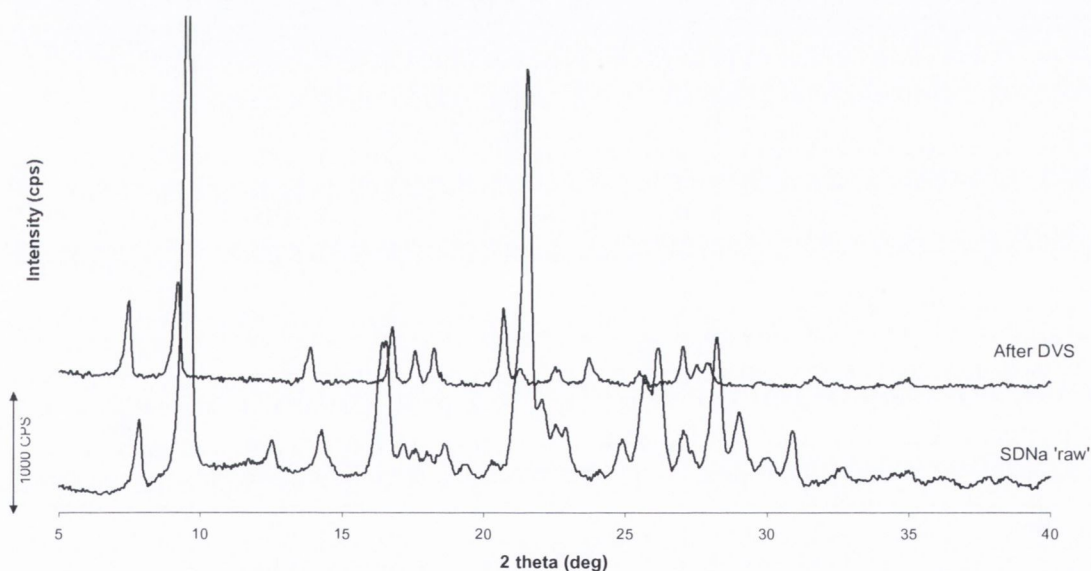


Figure 4.12: PXRD for SDNa BT2 unmilled and SDNa milled for 10 hours with a BTP weight ratio of 40:1 at RT after DVS analysis.

Figure 4.12 shows the PXRD of the sample collected after DVS analysis. The diffractogram obtained after the 10 hours SDNa milled sample was exposed to DVS shows that the material is in crystalline in nature but has several different peaks in comparison to the unmilled sample. The small sample size collected from DVS only allowed for PXRD analysis to be

carried out. The formation of the new peaks may be attributed to the formation of a structure that consists of a partially or complete hydrated form. Analysis by DVS showed, that environments higher than 50 % RH may result in the crystallisation of an amorphous phase induced by milling. This would suggest why the amorphous phase that was induced as a result of milling was stable over the storage period.

4.5 Conclusions

Ball milling of sulfadimidine sodium salt showed that the physicochemical state changed from a crystalline structure to a disordered amorphous phase. The induced amorphous phase was time dependent and the change occurred with less time as a result of ball milling with a BTP weight ratio of 40:1 compared to the BTP weight ratio of 20:1. For both BTP weight ratios a complete amorphous phase was induced after 5 hours and prolonged milling for 10 and 15 hours resulted in an amorphous phase. A change to the morphology was evident by SEM analysis. Large particles observed after ball milling for 10 hours suggested that these larger particles may be produced via recrystallisation as a result of amorphisation during ball milling or as a result of agglomeration of the fine particles. Imaging of the particles showed that the smaller particles formed agglomerated structures.

Storage of the completely amorphous phase at 4 °C showed that the induced amorphous phase was stable over 84 days. Crystallisation of the amorphous phase was only achieved upon exposure to relative humidity conditions of 50% RH or above and PXRD analysis indicated that this produced a different phase than the starting material.

Overall, these changes showed that, as a result of ball milling for as short as 5 minutes significant changes were induced to the crystallinity and morphology of the material. The effect of these changes to the compressibility, tablet hardness and powder flow properties will be evaluated.

Ball milling of sulfathiazole &
sulfathiazole sodium salt

5.0 Introduction

Sulfathiazole has five known polymorphic forms and is also available as a sodium salt. Previously it has been shown that ball milling of sulfathiazole can result in partial amorphisation and polymorphic transformations (Shakhtshneider and Boldyrev 1993; Shakhtshneider, 1997 and Caron *et al.*, 2011). Shakhtshneider (1997) ball milled form III (STZ III) with a BTP weight ratio of 20:1. The milling jars were cooled with water during the process and milling time did not exceed 40 minutes. Caron *et al.*, (2011) used zirconium oxide jars with a BTP weight ratio of 32:1 at RT. For every 20 minutes of milling a 10 minute rest interval followed which resulted in a total of 10 hours milling (15 hours including rest periods). These two studies also investigated the behaviour of ball milling sulfathiazole and PVP mixtures. Shakhtshneider and Boldyrev (1993) milled form III and I using a BTP weight ratio of 20:1. STZ III was milled for 1, 5, 40 90 and 300 minutes while form I (STZ I) was milled for different periods up to 120 minutes. Shakhtshneider and Boldyrev (1993) results showed that milling induced polymorphic transformation for both forms (III→I and I→III) although at the date of this publication only three polymorphic forms were acknowledged.

The purpose of the work presented in this chapter was to evaluate the effect of milling two different sulfathiazole polymorphs (Form I and III) and to compare how these behaved in comparison to the salt form. The effect of temperature, time and BTP weight ratio were investigated. The effect of varied milling parameters is limited for sulfathiazole, as varying time is the main parameter explored and in certain cases this is constant. Previous ball milling studies using sulfathiazole include Caron *et al.*, (2011). They varied the quantity of PVP in a binary mixture with sulfathiazole and milled for 15 hours, with a ball to powder weight ratio of 35:1. Shakhtshneider and Boldyrev (1993) and Shakhtshneider (1997) varied time while the BTP weight ratio was kept at 20:1.

5.1 Analysis of sulfathiazole starting materials

5.1.1 Powder X-ray diffraction (PXRD)

Two batches of sulfathiazole (Sigma, Ireland) were analysed by PXRD (Figure 5.1). Batch 108K1757 and batch 109K1442 are referred to as batch X and Y, respectively. Comparing

batch X and Y with the CCDC (Cambridge Crystallography Data Centre) theoretical patterns the materials were found to be form III. The CCDC patterns were generated from single crystal X-ray data. The Characteristic peaks of form III were found at 22.9 and 21.7 2θ degrees (Munroe *et al.*, 2012). There is a slight shift in peak position between the theoretical and experimental patterns. Munroe *et al.*, (2012) experienced a similar peak shift which they attributed to the change in lattice spacing and in the context of Bragg's equation; an increase in d value corresponds to a shift to lower 2θ value. Generation of single crystal X-ray data involves an increase in temperature which may adversely effect the positions of the Bragg peaks. To obtain a powder patterns that is identical to the theoretical patterns is very difficult because of low intensity peaks and preferred crystal orientation effects (Patel *et al.*, 2001; Anwar *et al.*, 1989).

Form I was made by heating Batch Y above 170 °C and it was allowed to cool at RT, as described in section 2.2.3. To confirm the material was Form I it was compared to the CCDC theoretical pattern as shown in Figure 5.1 (STZ I). The material made in the lab consisted of characteristic peaks at 17.7 and 20.9 2θ degrees (Munroe *et al.*, 2012) indicating a Form I structure.

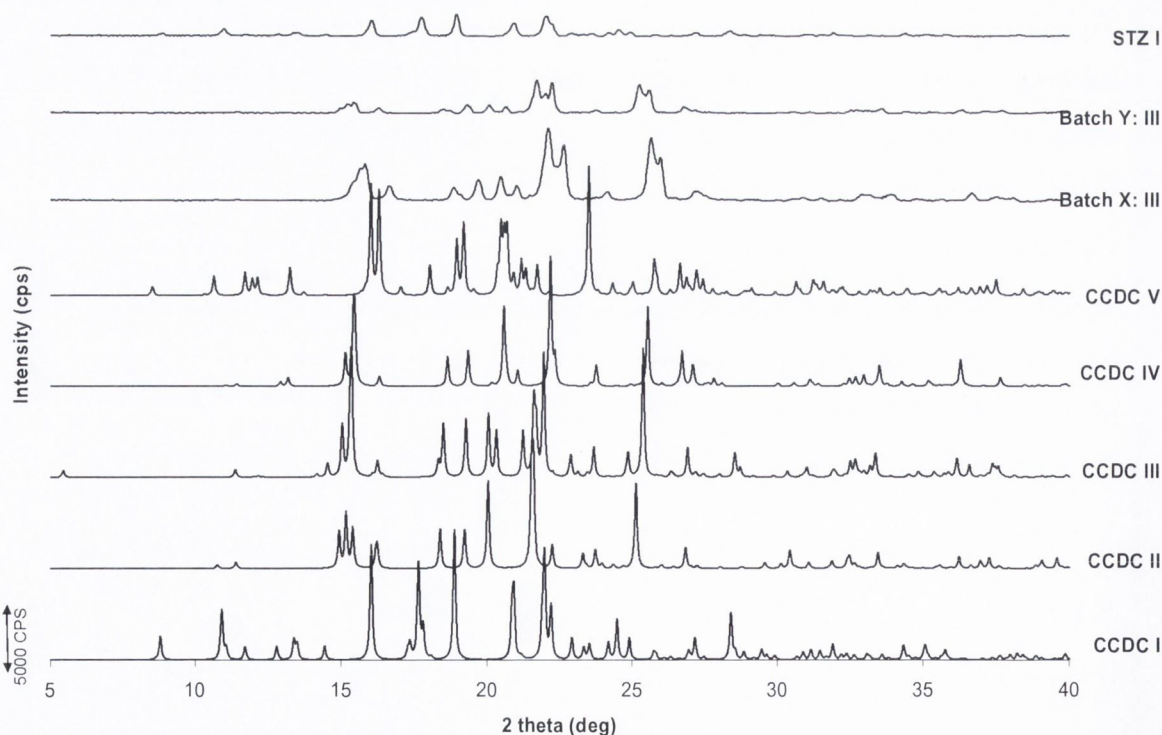


Figure 5.1: PXR D patterns simulated from the CCDC single crystal X-ray data Form I, II, III, IV and V, the PXR D of STZ III batch X and Y from Sigma, (Ireland) and STZ I.

5.1.2 Thermal analysis

Figure 5.2 shows the DSC scans of sulfathiazole unmilled materials and none of these scans show crystallisation exothermic events characteristic of an amorphous material. STZ I thermogram consists of one thermal event attributed to a melt with an onset at ~ 201 °C, which is characteristic of form I (Anwar *et al.*, 1989). Batch X and Y thermograms consist of two thermal events, the first being attributed to a polymorphic transformation to the form I. This endothermic event had an onset temperature at ~ 163 °C for batch X and ~ 150 °C for batch Y. The enthalpy for the polymorphic conversion detected for batch Y was ~ 29 J/g and it was ~ 28 J/g for batch X. The polymorphic conversion observed in the batch Y thermogram may be a result of more than one polymorphic form present in the material. The solid state transformation was followed by a second thermal event detected attributed to the melting of form I at ~ 201 °C. The enthalpy of melting (~ 110 J/g) of Form I estimated from the sharp endotherm is comparable with values reported previously (Zeitler *et al.*, 2006).

The solid state transformation of Form II, III and IV should occur between 115 and 180 °C (Lagas and Lerk, 1981; Zeitler *et al.*, 2006; Caron *et al.*, 2011 and Munroe *et al.*, 2012). Figure 5.3 outlines the DSC thermograms reported by Munroe *et al.*, (2012). Table 5.1 gives the thermal properties reported by Zeitler *et al.*, (2006). These studies show that the polymorphic transitions may occur over a broad temperature range and different transition temperatures have been reported. This difference may be a result of the solvent used to obtain the polymorphic forms, the sample quantity tested, the test method etc. PXRD analysis indicated that the unmilled materials (batch X and Y) were form III but the difference of onset temperatures indicated that this may not be the case, but they could be a mix of two or more polymorphic forms. The transition temperature of form IV occurs at a similar temperature range to Form III, which may explain the second peak observed in the thermogram of Batch Y. Changes to the solid state transition temperature, could be attributed to there being more than one polymorphic form present. Therefore batch X was thought to be form III due to the transition temperature of 177 °C reported by Zeitler *et al.*, (2006) and characteristic form III Bragg peaks observed by PXRD analysis. While batch Y was thought to be predominantly form III with residual amounts for form IV and/or form I. From this point on batch X and Y will be referred to as STZ III-X and STZ III-Y, respectively.

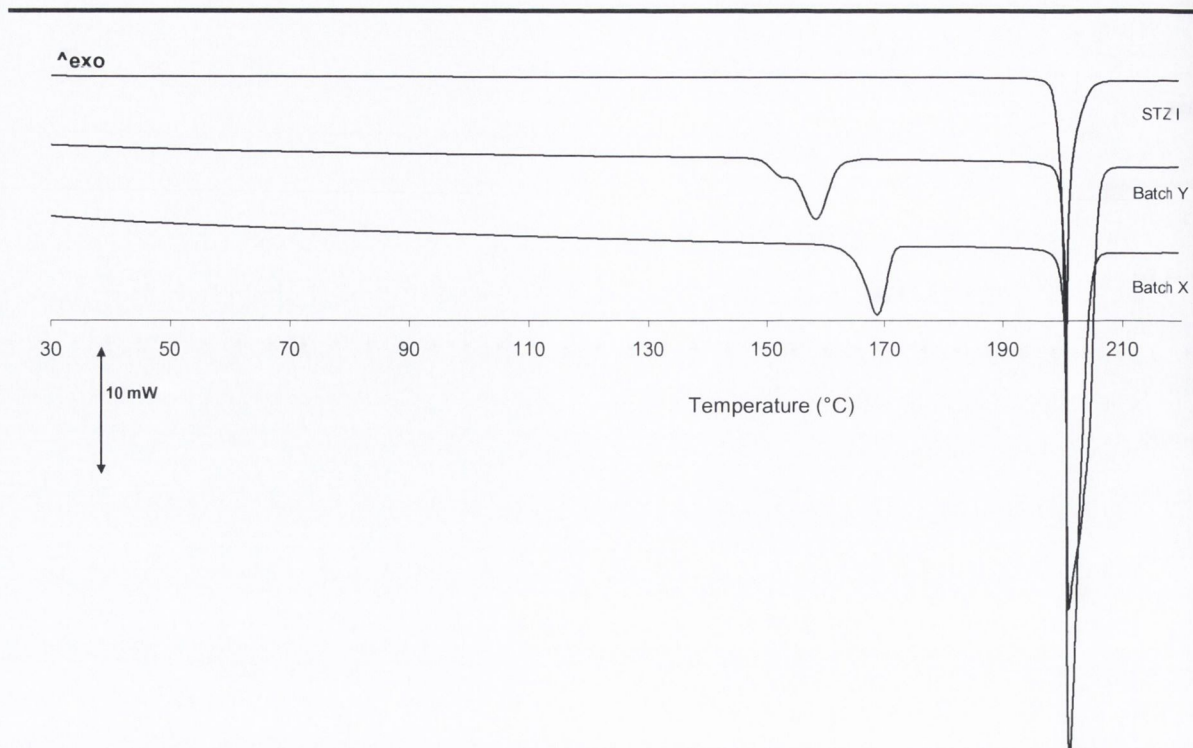


Figure 5.2: DSC thermograms of sulfathiazole batch X (STZ III-X) and Y (STZ III-Y) from Sigma, (Ireland) and STZ I.

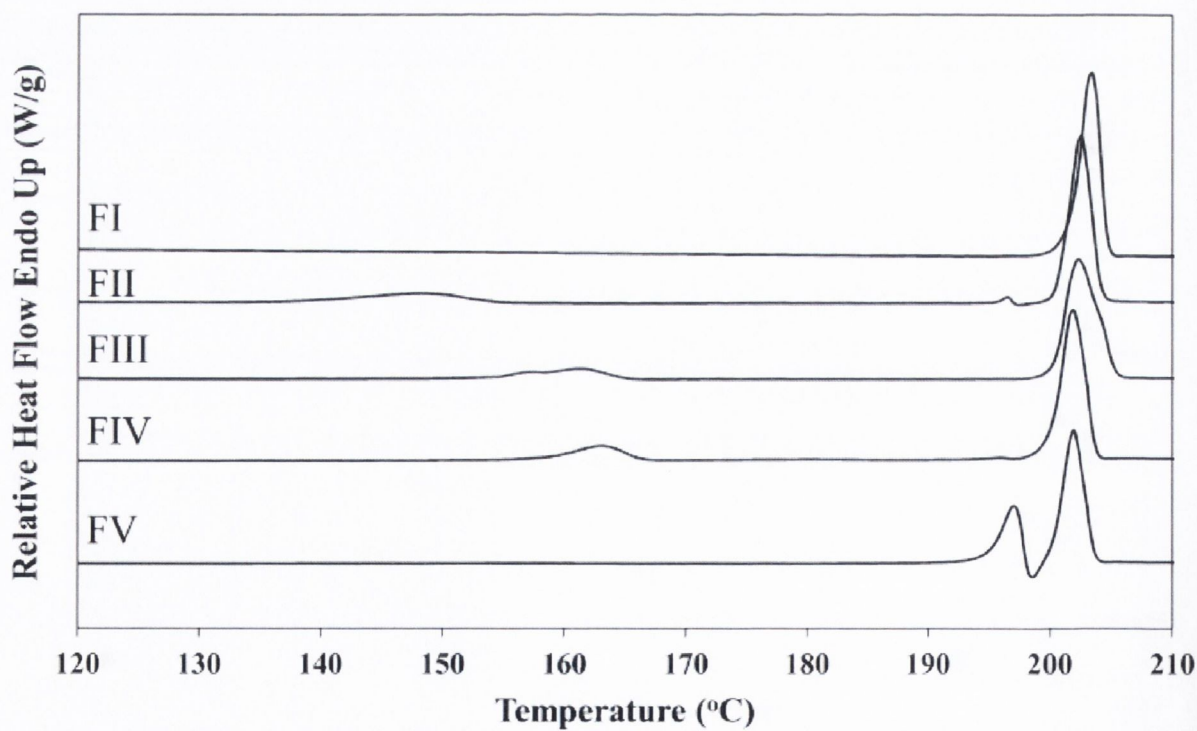


Figure 5.3: DSC profiles of the five different polymorphic forms reported by Munroe *et al.*, (2012).

Table 5.1: Onset transition temperatures and heat of transitions for each polymorph reported by Zeitler *et al.*, (2006). Note these polymorphs were re-named to correspond with the polymorphic forms discussed here.

	$T_{\text{poly}} (^{\circ}\text{C})$	$\Delta H_{\text{poly}} (\text{J/g})$
Form I	182	81.8
Form II	118	32.4
Form III	139	27.3
	177	114.2
Form IV	140	29.5
Form V	136	24.9
	177	1.0

5.1.3 Morphology and particle size

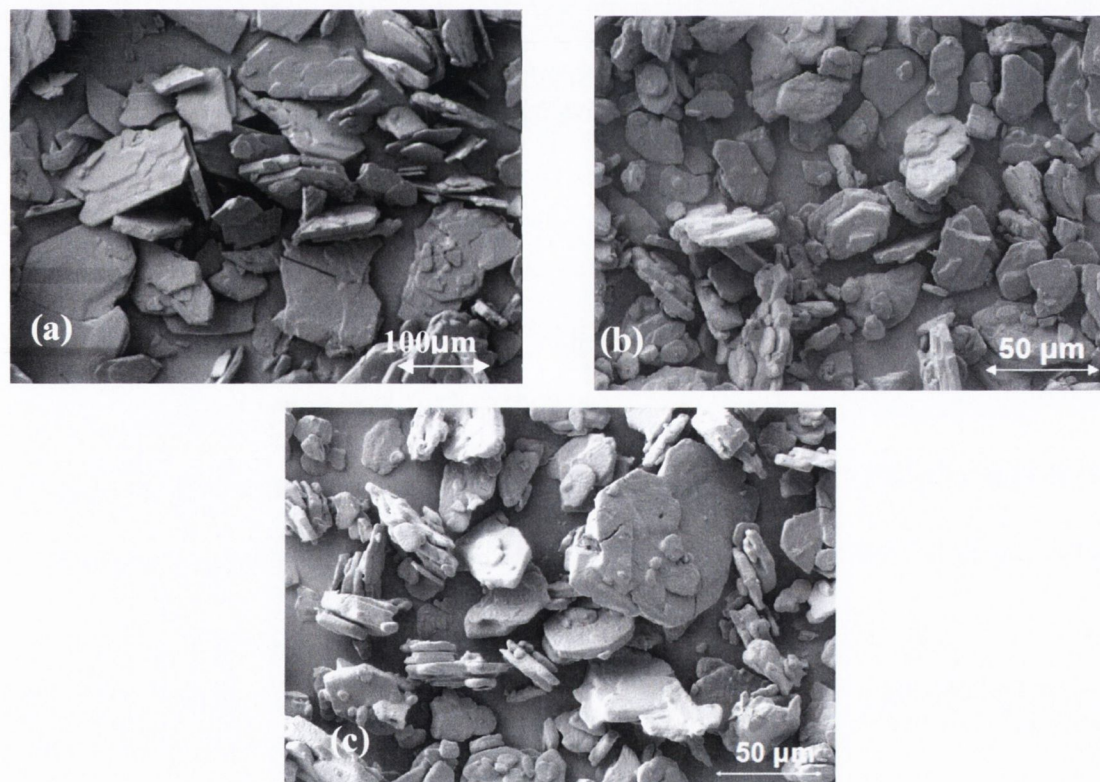


Figure 5.4: Morphology of STZ III (a) batch X (b) batch Y, both from Sigma, (Ireland) and (c) STZ I.

As can be observed from Figure 5.4 all SEM images show plate-like shaped particles that were irregular in size. Platelet shaped particles are characteristic of STZ III (Anwar *et al.*,

1989; Blagden *et al.*, 1998). STZ I was produced by heating to 180 °C and cooled, as described in section 2.1.1.4., and the morphology observed for STZ I (Figure 5.4 (c)) was very similar to that observed for STZ III-Y (Figure 5.4 b), with a plate-like structure and irregular sized particles with some plates having a diameter approximately 50 µm. Upon heating it was possible to maintain the plate-like morphology typical of Form III. Traditionally the morphology of Form I crystallised from solvent consists of a rod or needle shaped crystal habit (Anwar *et al.*, 1989 and Blagden *et al.*, 1998). However, Bianco *et al.*, (2012) produced spherical particles of STZ I by spray drying. The solvent free method used here, to induce crystallisation to produce Form I resulted in a material that had the physiochemical properties that are characteristic of sulfathiazole Form I polymorph but a morphology that was similar to Form III. Morphology will affect processes such as tableting and also powder flow properties.

Table 5.2: Particle size distribution determined by Malvern laser diffraction and the specific surface area (SSA) measured by BET of STZ III batch X and Y and STZ I.

	Particle size (µm)			SSA (m ² /g)
	d10	d50	d90	
STZ III -X	4.76 (0.15)	17.81 (0.34)	48.64 (1.33)	0.40 (0.14)
STZ III -Y	3.06 (0.36)	11.24 (1.38)	25.79 (0.63)	0.59 (0.11)
STZ I	2.47 (0.11)	7.58 (0.07)	16.42 (0.17)	1.66 (0.26)

Standard deviation is in parentheses, n=3

Table 5.2 shows the particle size distributions measured by Malvern laser diffraction and the specific surface area (SSA) as analysed by BET for STZ III batch X, Y (STZ III-X and STZ III-Y) unmilled and STZ I unmilled. The particle size distributions were monomodal for all samples. The median particle size for STZ III batch X was 17.81±0.34 µm while STZ III batch Y was 11.24±1.38 µm. This difference was also observed by SEM and is reflected by the SSA measurements for both batches (Table 5.2). STZ I had the narrowest size distribution ranging from 2.47±0.11 µm for the d₁₀ to 16.40±0.17 µm for the d₉₀ and a median of 7.58±0.07 µm. The SSA of 1.66±0.26 m²/g for STZ I is the highest of the three materials. Due

to the plate-like morphology of STZIII the particle size measured by laser diffraction is not consistent with SEM. The reason for this is that Malvern laser diffraction uses an algorithm that assumes spherical particles to calculate the particle size distribution, which may result in some error when the particles are platelet shaped.

5.1.4 Analysis of the polymorphic forms by NIR

Overall, the difficulty of polymorph characterisation of sulfathiazole by PXRD is associated with detecting minor peaks that are indicative of specific polymorphs. Thermal analysis allows the solid state transition temperature of a polymorphic form converting to another form to be observed as an endothermic event. This endotherm can take place over a region where several polymorphic transitions are possible. The wide temperature range over which this conversion can arise leads to difficulties in characterising which specific polymorph or polymorphs present in the sulfathiazole sample. Zeitler *et al.*, (2006) states that, using DSC analysis alone, it was not possible to distinguish between sulfathiazole polymorphic forms as their melting endotherms were all detected around a narrow temperature range. NIR analysis of the unmilled materials was carried out by researchers in National University of Ireland, Galway (NUIG). They compared the results to a calibration model of sulfathiazole Form I and III (Hu *et al.*, 2010). The limit of detection (LOD) and limit of quantification (LOQ) for the detection of low content of Form I in III were 0.43 and 1.30 %, respectively. This calibration curve only considered changes to mixtures containing Forms I and III and very distinct peaks that were characteristic of the other Forms. NUIG eliminated the presence of Form V of sulfathiazole, as it has a distinct peak that was not detected in either batch X or Y. They noted that NIR spectra of Form II, IV and III are very similar and Forms II and IV will partly mimic form III in mixtures. Consequently the Form I/III calibration model will predict incorrect Form III content when other forms are present. The NUIG team suggested that batch X was Form III and batch Y was predominantly III with traces of II and/or IV and concluded that Batch Y consisted of approximately 2% Form I and 98% Form III.

5.2 Binary mixtures

To investigate how an additional polymorphic form can influence the PXRD and thermal analysis, binary mixtures of Form I and III (STZ III-X) were prepared and analysed.

5.2.1 Powder X-ray diffraction

Figure 5.5 shows the PXRD of STZ III-X, Form I, the physical mixtures of form I and form III polymorphs and the CCDC simulated powder patterns from single crystal data, for Form I and III. The powder diffraction patterns obtained for the mixtures showed several peak changes as the concentration of Form I was increased, (indicated by arrows in Figure 5.5). The peak at 11.0 2 θ degrees (black arrow, Figure 5.5) detected in the Form I diffractogram was present for all mixtures. The characteristic peak at 17.7 2 θ degrees for Form I was detected when at least 10 %wt was added. Increasing the Form I content to 50 % resulted in the increased intensity of peak 17.7 2 θ degrees (green arrow, Figure 5.5). The doublet peak at 22.9 2 θ degrees, characteristic of Form III was detected for each mixture (red arrow, Figure 5.5). The peak at 24.15 2 θ degrees (blue arrow, Figure 5.5) detected in Form III diffractogram was not present for any of the mixed samples. Peaks detected between 30 2 θ degrees and 40 2 θ degrees were detected as minor peaks in both theoretical diffraction patterns. PXRD analysis is susceptible to problems with preferred orientation events which may prevent accurate classification of samples polymorphic forms (Morissette *et al.*, 2004).

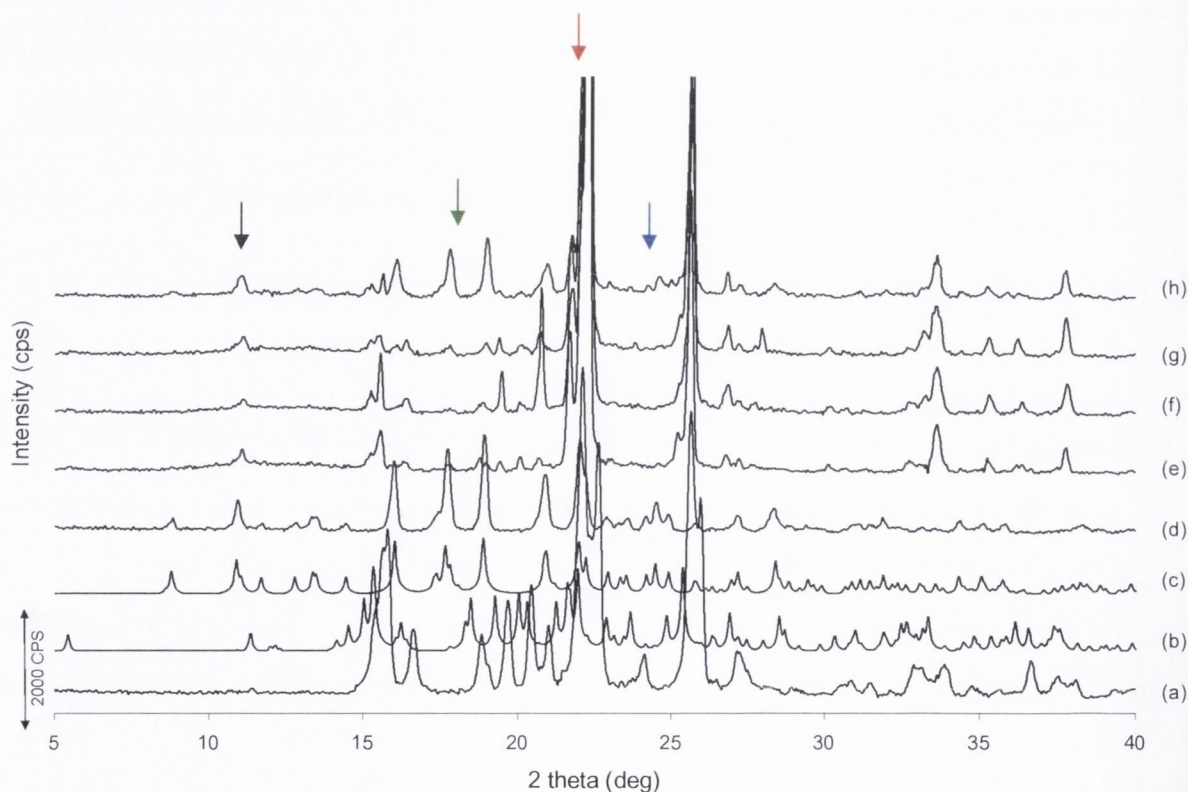


Figure 5.5: PXRD of sulfathiazole (a) 100% Form III (STZ III-X); the simulated powder patterns from single crystal XRD data obtained from CCDC for Form III (b), and Form I (c), 100 % Form I (d), and the binary mixtures of from I and III: (e) 3 %wt Form I and 97 %wt

From III; (f) 5 %wt Form I and 95 %wt Form III; (g) 10 %wt Form I and 90 %wt Form III; (h) 50 %wt Form I and 50 %wt Form III. The arrows indicate the characteristic peaks present in the diffractograms: black \rightarrow 11.0 2θ degrees indicating Form I, green \rightarrow 17.7 2θ degrees indicating Form I, red \rightarrow doublet peak at 22.9 2θ degrees indicating Form III and blue \rightarrow 24.15 2θ degrees indicating Form III

5.2.2 Thermal analysis

Figure 5.6 shows the thermograms for STZIII-X, STZ I and the physical mixtures of both polymorphs. Two thermal events were evident for STZIII-X and the binary mixtures, the first endotherm was attributed to the polymorphic transition of Form III to Form I and the second to the melting of Form I. Thermal analysis showed that by introducing 3, 5 and 10 %wt of Form I to Form III, the onset for the solid-state transition temperature shifted from ~ 162 °C to ~ 158 °C (Figure 5.6, Table 5.3). Adding equal quantities of Form I to Form III resulted in the detection of a solid state transition at ~ 157 °C. This indicates that a binary mixture can result in the solid state transition temperature shifting which may explain the difference between batch X and Y. The DSC transition temperature detected for STZIII-Y was detected at ~ 150 °C, which is several degrees lower than that observed for the physical mixture of 3 %wt Form I with Form III. Residual amounts of a third polymorph may be present which may explain the difference between the solid state temperature difference detected for the binary mixture and that observed for STZ III-Y. The difference between batch X and Y could also be attributed to several factors such as the length of time and conditions the material were stored in after manufacturing and/or the solvents used during manufacturing. Bianco *et al.*, (2012) showed that storage of spray dried sulfathiazole below 35 %RH resulted in the transformation of the amorphous phase to Form I while storage above 35 %RH led to crystallisation of the material that consisted of a mixture of Forms I, III and/or II. If the material processed by Sigma consisted of residual amount of Form I then the transformation of Form I to Form III may result in residual amounts of form II and/or IV within the material. Shakhtshneider and Boldyrev (1993) milled sulfathiazole and noted that factors that can contribute to low phase transition temperature may include the formation of a new polymorphic form, a combined number of polymorphs, small particles and/or an increased number of defects.

Table 5.3: Thermal properties of 100 %wt STZ III and STZ I and the physical mixtures of Form I (3 to 50 %wt) mixed with Form III.

	T_{poly}	ΔH_{poly}	T_{m}	ΔH_{m}
STZ III 100 %wt	162 (0.57)	28 (0.21)	201 (0.75)	111 (0.34)
3 %wt	158 (0.08)	26 (0.14)	201 (0.64)	107 (0.27)
5 %wt	158 (0.12)	24 (0.14)	201 (0.51)	111 (0.22)
10 %wt	158 (0.10)	22 (0.09)	201 (0.54)	109 (0.31)
50 %wt	157 (0.49)	12 (0.22)	201 (0.49)	110 (0.09)
STZ I 100 %wt			201 (0.18)	111 (0.51)

Standard deviation is in parentheses, n=3

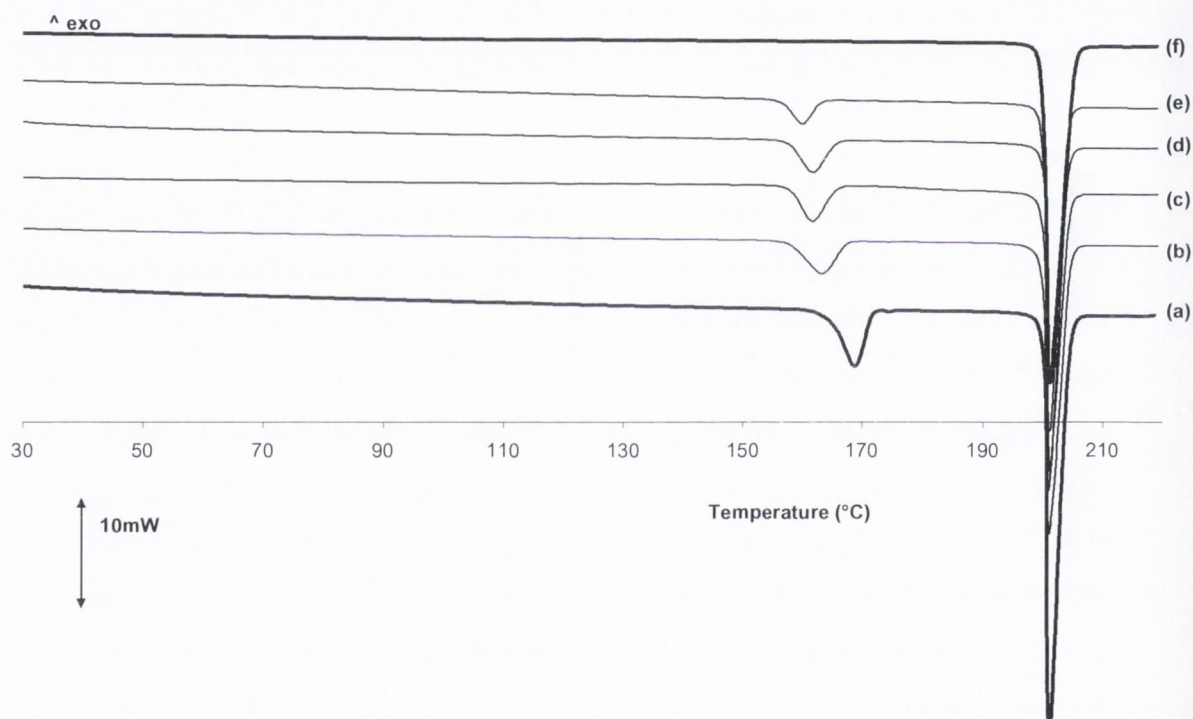


Figure 5.6: DSC thermograms of sulfathiazole (a) 100 % Form III (STZ III-X); (b) 97 %wt Form III and 3 %wt Form I; (c) 95 %wt Form III and 5 %wt Form I; (d) 90 %wt Form III and 10% Form I; (e) 50 %wt Form III and 50 %wt Form I; (f) 100 %wt Form I.

5.3 Ball milling STZ III

5.3.1 Investigating the affect of the ball-to-powder weight ratio of 20:1

5.3.1.1 Powder X-ray Diffraction

Figure 5.7 (a and b) illustrates the PXRD patterns of STZ III-X milled with a BTP weight ratio of 20:1 at RT and 4 °C respectively and CCDC patterns generated from the single crystal X-ray data of Form I and III. The unmilled material is characteristic of Form III and was discussed previously. Figure 5.7 (a) showed that ball milling for 5 minutes at RT resulted in the reduction of the total peak area intensity from 100 % for the unmilled milled material to 61.29 ± 1.64 %. Further milling for a total of 30 minutes reduced the crystallinity to 48.96 ± 0.63 %. There is no significant statistical difference between the total peak area obtained for the sample milled for a total of 30 minutes with the samples milled for a total of 60, 120 and 5 hours. Ball milling for 10 hours resulted in a statistically significant change in the peak area to 43.58 ± 1.50 % and further ball milling for a total of 15 and 20 hours resulted in no further significant statistical change in the total peak area.

The PXRD graphs of STZ III-X milled at 4 °C (Figure 5.7b) are very similar to those observed when milling at RT. The initial peak area decreased after 5 minutes of milling to 55.9 ± 1.89 %. Ball milling of STZIII-X for 20 hours resulted in a total peak area reduction to 35.84 ± 3.41 %. Table 5.3 and Figure 5.8 outline the change to the crystallinity of STZ III-X milled at 4 °C and RT with a BTP weight ratio of 20:1. Comparing the peak area for each time period (e.g. 5 min vs. 5 min, 30 min vs. 30 min etc.) milled at RT and 4 °C using Tukey's multiple comparison test showed that a statistical difference was observed for the samples milled for a total of 5 minutes and 30 minutes but there was no significant statistical difference observed between the samples milled for 60 minutes up to 20 hours at both temperatures. These results would indicate that the temperature used for ball milling the sulfathiazole samples induced a significant difference when shorter milling times were used and this difference was eliminated with ball milling times of 60 minutes or more.

No new distinct peaks were detected for the samples milled at RT or 4 °C and the broadness of the peaks prevented the clear identification of which polymorphs were present or of if there was a mixture. The doublet peaks at 20.0-20.03 2 θ , characteristic of the Form III (Munroe *et*

al., 2012), merged into one peak after milling for 30 minutes. This single peak was detected after each milling time thereafter, and at both temperatures.

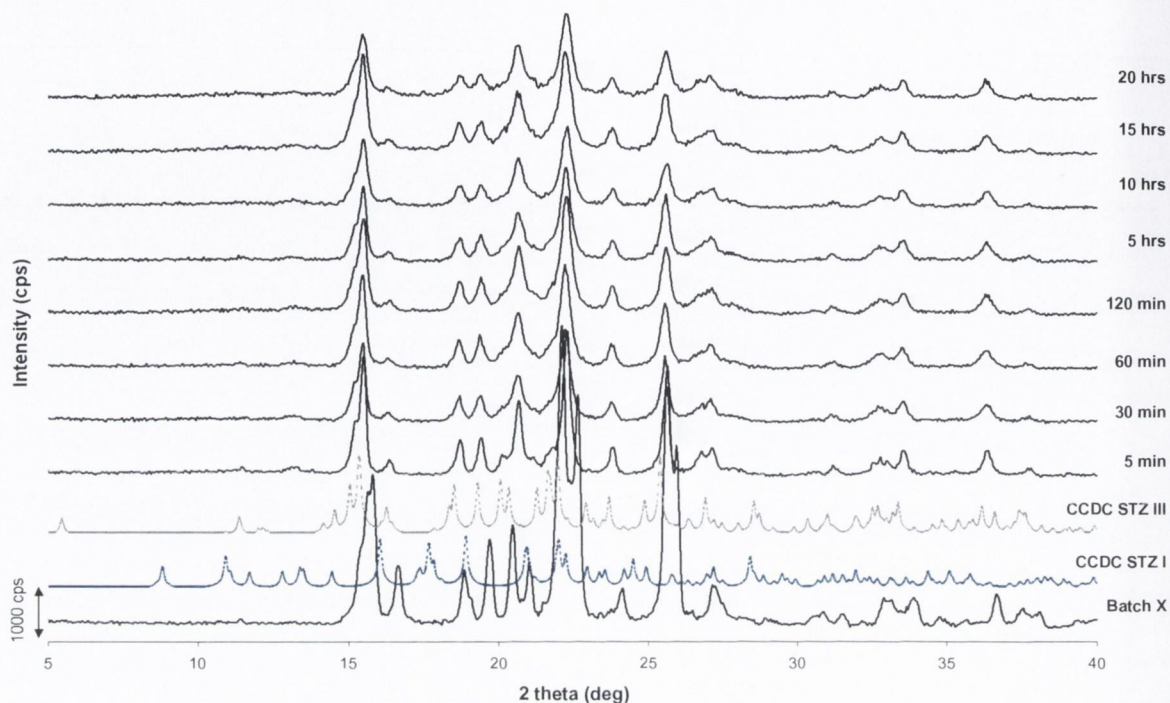


Figure 5.7 (a): PXR D of STZ III-X, CCDC STZ I and III and STZ III-X milled at RT with a BTP weight ratio 20:1 from 5 minutes to 20 hours.

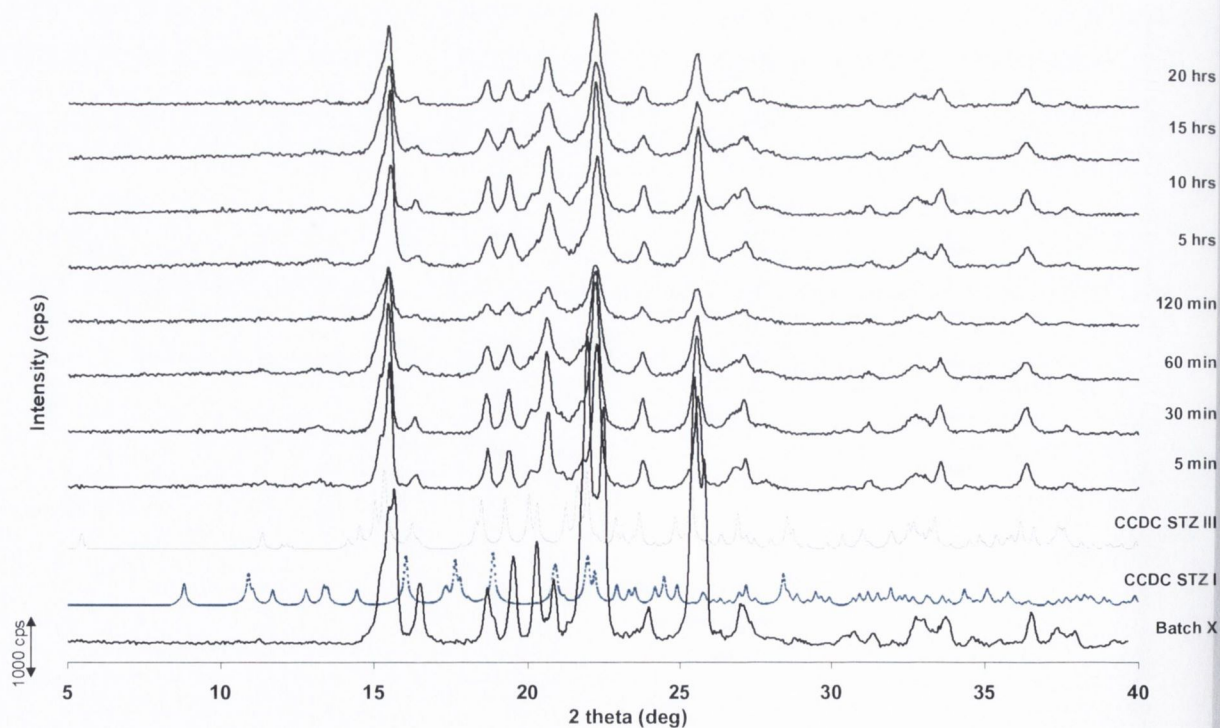


Figure 5.7 (b): PXR D of STZ III-X, CCDC STZ I and III and STZ III-X milled at 4 °C at 400 rpm with a BTP weight ratio 20:1 from 5 minutes to 20 hours.

Shakhtshneider and Boldyrev (1993) reported that milling sulfathiazole (Form III) for 1 minute with a planetary mill with a ball-to-powder weight ratio of 20:1 resulted in XRD peak broadening and an intensity decrease. They also suggested that after 1 minute of mechanical treatment up to 50 % of the sample appeared to be in a noncrystalline state. After 5 minutes, peaks for the Form I were observed and no further changes to the detected quantity of Form I was observed when the sample was milled for up to 3 hours. They found that prolonged milling resulted in the recrystallisation of the sample which was observed by the narrowing of the diffraction peaks and an increase in their intensity. They only discussed these data which were not presented in their publication. As no new peaks were observed for the STZ samples milled at both temperatures in this study it was not possible to confirm the results observed by Shakhtshneider and Boldyrev (1993). This study is an expansion of the one carried out by Shakhtshneider and Boldyrev (1993) as the ball milling was carried out at two different temperatures that were monitored as opposed to cooling the centrifugal ball mill with water which was done by Shakhtshneider and Boldyrev (1993). The results presented here show that ball milling with a ball to powder weight ratio of 20:1 results in similar peak area change regardless of the milling temperature but only if the milling time is 60 minutes or is up to a total of 20 hours. The most significant results were observed after ball milling for 5 and 30 minutes where ball milling at 4 °C resulted in a more significant change to the total peak area as opposed to ball milling with the same conditions at RT. Dujardin *et al.* (2008) investigated the effect of ball milling at two different temperatures (room temperature (RT) and at -15 °C). They believed that an amorphous phase was induced at both temperatures but it was only detected after ball milling at -15 °C. They accredited not finding an amorphous phase as a result of ball milling at RT, due to the fact that it readily recrystallised. Overall the results presented here show that a higher level of disorder was achieved at the lower temperatures and the peak area differences between the samples are negligible with prolonged milling.

The data outlined in Table 5.3, obtained from the PXRD diffractograms presented in Figure 5.7 (a and b), was graphed for comparison purposes in Figure 5.8. It was noted that the peak area decreased as a result of increased ball milling time but Figure 5.8 showed that as a result of ball milling at RT the total peak area increased after 5 hours of ball milling. As mentioned above Shakhtshneider and Boldyrev (1993) found that with prolonged milling of 3 hours the peaks became narrow indicating recrystallisation as a result of prolonged milling. In this study it is shown that with prolonged milling for up 10, 15 and 20 hours the peak area continues to

decrease and no other signs of recrystallisation are observed. These prolonged milling steps were not carried out by Shakhthshneider and Boldyrev (1993) and it was believed that prolonged milling of STZ form III resulted in the recrystallisation of the induced disordered phase. Ball milling at 4 °C prevented this recrystallisation event to occur. Figure 5.8 shows that a peak area drop was observed after 5 and 30 minutes and with prolonged milling of up to 20 hours a further drop to $35.84 \pm 3.41\%$ was achieved.

Table 5.3: Total peak area changes for STZ III-X milled from 5 minutes to 20 hours.

Milling time (minutes)	Peak area (%) at RT	Peak area (%) at 4 °C
5	61.29 (1.64)	55.95 (1.89)
30	48.96 (0.63)	53.53 (0.78)
60	48.40 (2.56)	47.79 (0.59)
120	45.29 (1.56)	44.85 (4.53)
300	47.86 (0.99)	44.52 (2.82)
600	43.58 (1.50)	45.07 (2.32)
900	42.12 (1.35)	43.18 (3.05)
1200	40.74 (1.29)	35.84 (3.41)

Standard deviation in parentheses, n=3

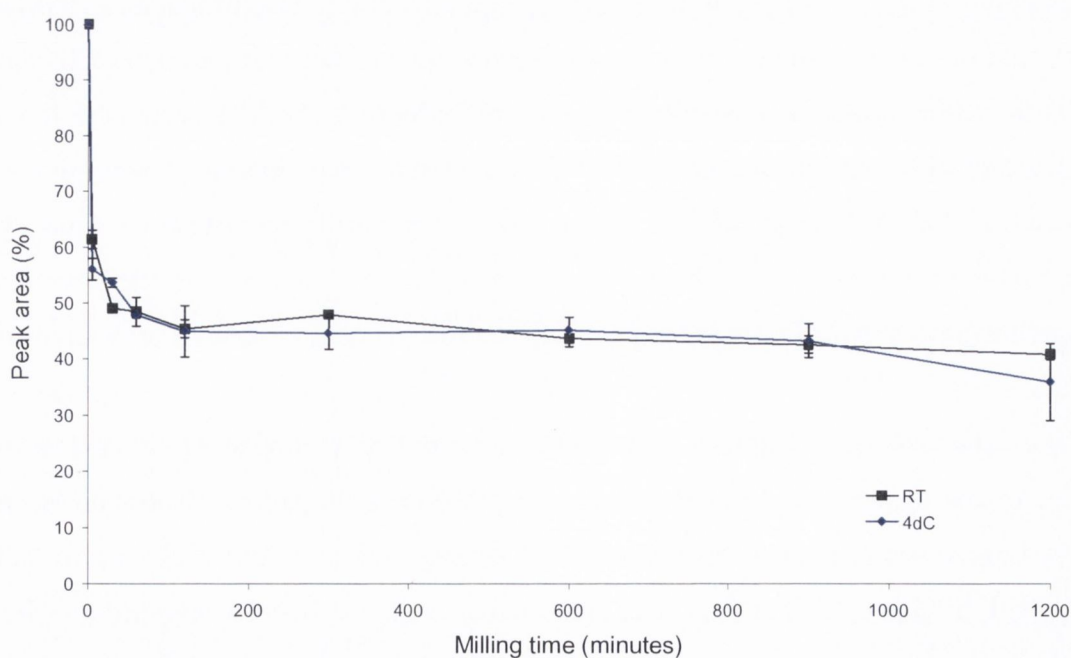


Figure 5.8: Illustrates the total peak area change to STZ III when milled with a BTP weight ratio of 20:1 from 5 minutes to 20 hours at RT and 4 °C.

5.3.1.2 Thermal analysis

Results of thermal analysis by DSC of STZ III-X milled with a BTP weight ratio of 20:1 at RT and 4 °C is illustrated in Figure 5.9a and 5.10, respectively. The onset temperature for the polymorphic transformation observed for STZ III-X unmilled at ~162 °C shifted when milled for 5 minutes to ~145 °C and the endotherm became broader in shape. This peak shift was observed for samples milled for 5 minutes to 15 hours and is followed by a melt endotherm associated with Form I with an onset at ~201 °C. Factors that contribute to lowering of the phase transition temperature include formation of a new polymorphic form, a combined number of polymorphs, small particles and/or an increased number of defects (Shakhtshneider and Boldyrev, 1993). These factors may also contribute to lower phase transition enthalpies. Figure 5.9b illustrates the DSC thermogram obtained for STZIII-X milled for 5 hours at RT and variable temperature X-ray diffraction (VT-XRD) patterns taken before and after the solid state transition. The VT-XRD analysis showed that before the transition the material was Form III with a characteristic peak detected at 20.04 2 θ degrees and after the transition Form I was present with peaks at 16.0 2 θ , 17.7 2 θ , 20.9 2 θ and 21.9 2 θ degrees detected. This transition is observed for all milled samples and confirms the transition to Form I.

STZ III-X ball milled for 20 hours resulted in three distinct thermal events. The first thermal event was an exotherm occurring at ~66 °C which indicated crystallisation of the induced amorphous phase. The second thermal event was an endotherm detected at ~121 °C corresponding to a solid state transition and the third thermal event was the melt endotherm at ~201 °C. Crystallisation was evident when disorder was induced as a result of milling. Low levels of amorphous content are often difficult to detect and an example of this is shown in Figure 5.9 for STZ III-X ball milled for up to 120 minutes as no crystallisation exotherm was observed when the thermograms are observed in its entirety (from 30 °C to 220 °C) but if the area of interest was examined alone (65 °C to 81 °C) an exothermic peak can be observed. Table 5.4 outlines the thermal events for each milled sample, the mass loss from 30 °C to the melt and the DSC amorphous content, calculated using the equation outlined by Lefort *et al.*, (2004). This method required the determination of the heat capacity measured by MTDSC for the 100 % crystalline sample (~1.13 J.C⁻¹.g⁻¹) and the 100 % amorphous sample obtained by melt quench (~1.261 J.C⁻¹.g⁻¹). The T_g for STZ has been previously reported to occur ~60 °C (Caron *et al.*, 2011) but in this study, due to the low level of disorder induced and the broad exotherm observed in Figure 5.9(a), it was not possible to detect the T_g for the samples that

had crystallisation exotherm present. The highest DSC amorphous content induced occurred after 20 hours of milling and reach 11.04 ± 2.09 %. The change in DSC amorphous content is shown in Figure 5.10. The amorphous content calculated is not dependent on milling time, as this fluctuates as milling time is increased. This was in contrast to PXRD peak area analysis where increased milling time resulted in a decrease of peak area (Table 5.3). Shakhshneider *et al*, (1997) also found that as milling time increased the level of amorphous content varied. They accredited this to the recrystallisation of the amorphous phase induced as a result of prolonged milling. The ball milled samples of STZ III-X showed that the mass loss determined by TGA ranged from below 1 % when milled for 20 hours to just above 1.6 % when milled for 10 hours. The average and standard deviation for each samples is presented in Table 5.4.

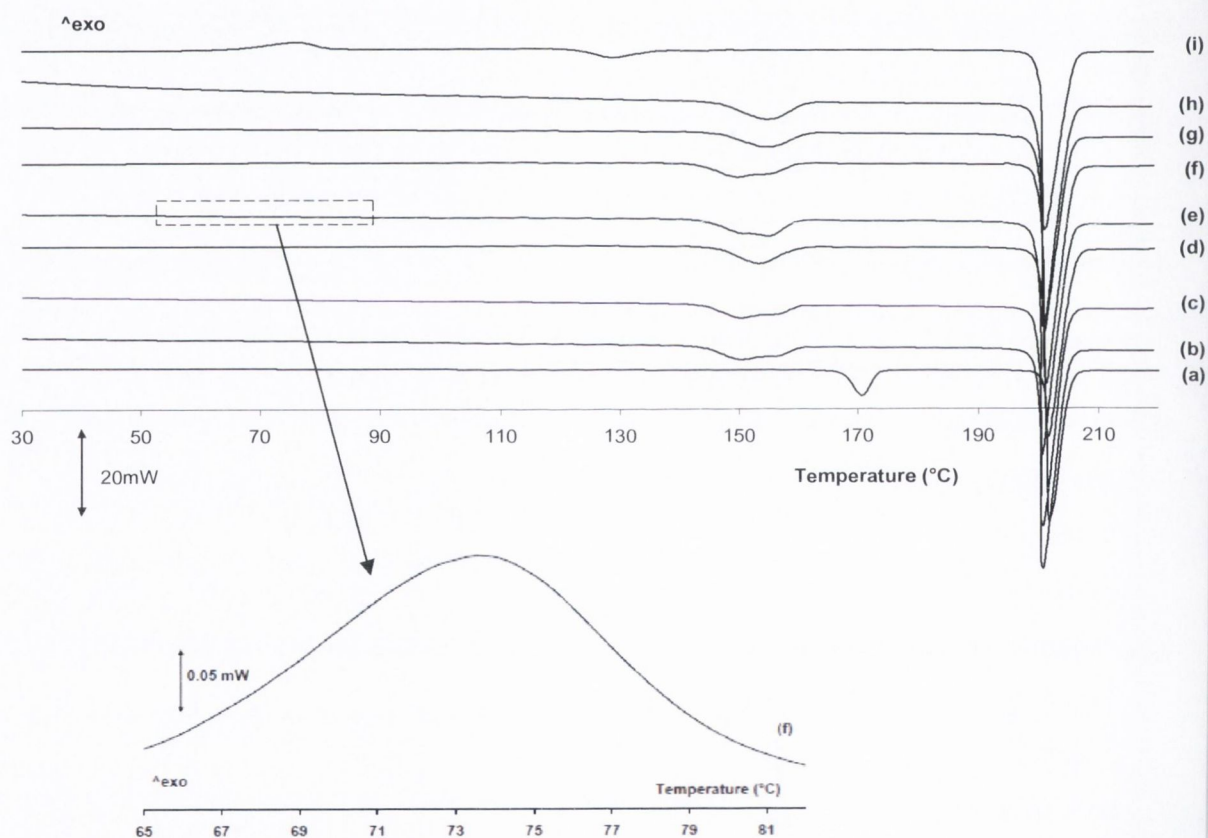


Figure 5.9 (a): DSC thermograms of STZ III-X unmilled (a) and milled at RT with a BTP weight ratio 20:1 for (b) 5 min; (c) 30 minutes (d) 60 minutes (e) 120 minutes (f) 5 hours (g) 10 hours (h) 15 hours (i) 20 hours. The highlighted section is the crystallisation exotherm of STZIII milled for 5 hours.

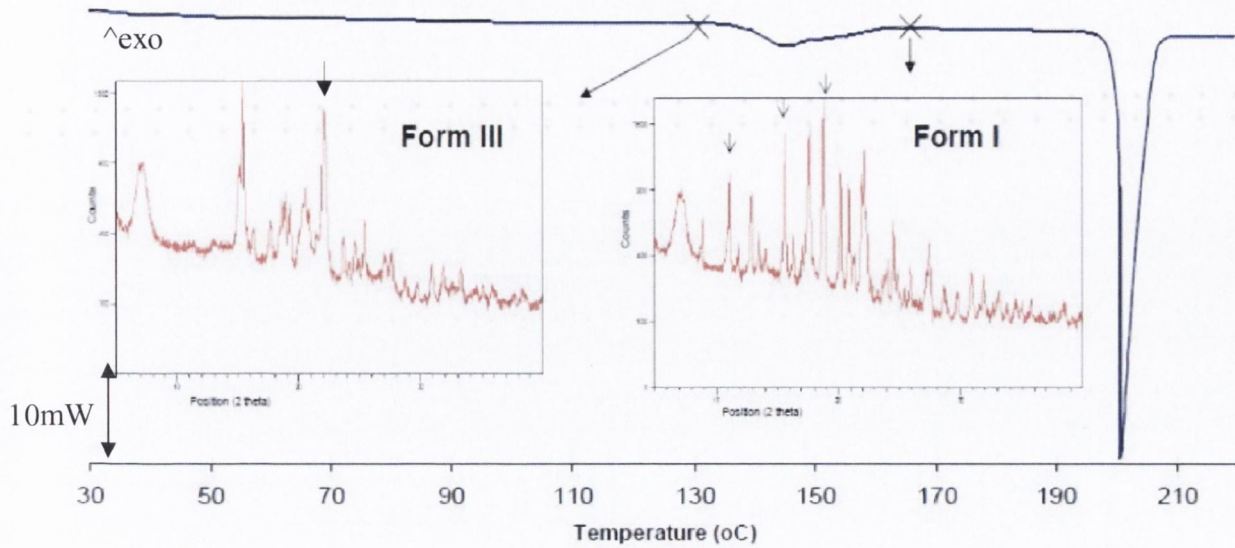


Figure 5.9 (b): DSC and VT-XRD analysis of STZ III-X milled for 5 hours with a BTP weight ratio of 20:1 at RT.

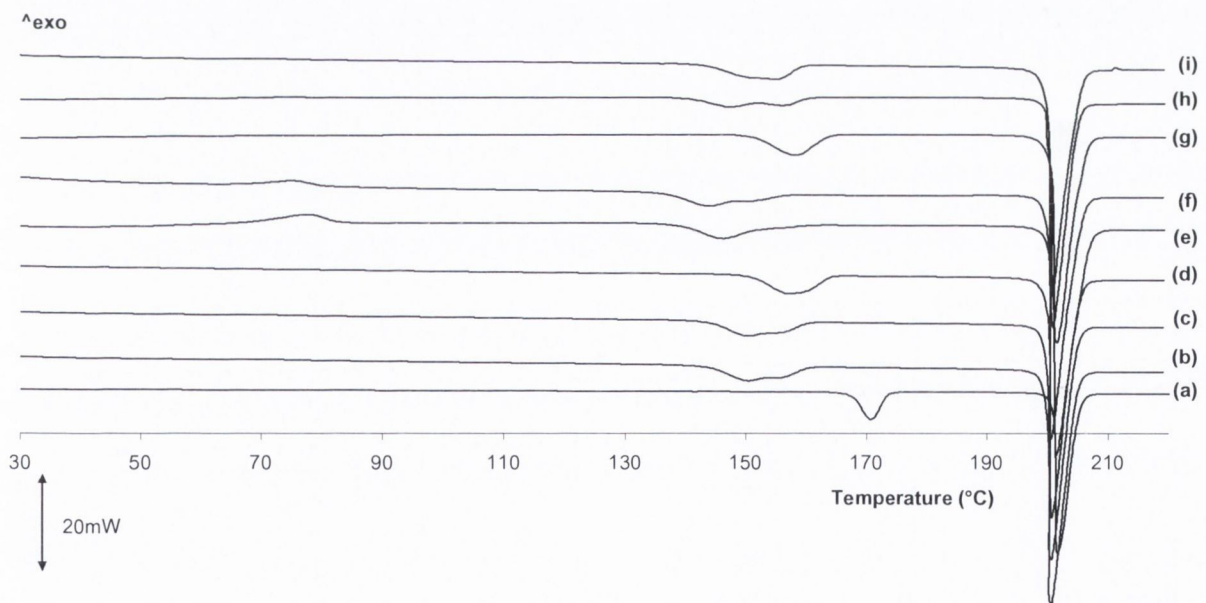


Figure 5.10: DSC thermograms of STZ III-X unground (a) and milled at 4 °C with a BTP weight ratio 20:1 for (b) 5 min; (c) 30 minutes (d) 60 minutes (e) 120 minutes (f) 5 hours (g) 10 hours (h) 15 hours and (i) 20 hours.

Figure 5.10 illustrates the thermograms for STZ III-X unground and milled at 4 °C with a BTP weight ratio of 20:1. The thermal events observed after milling at RT were also detected when

STZ III-X was milled at 4 °C, such as crystallisation exotherms, solid state transitions and melt endotherms, but the temperature at which they were detected was different for each sample. Table 5.4 outlines the temperature and enthalpy associated with the crystallisation event, the solid state transformation, the melt, the total mass loss from 30 °C to the melt and the calculated DSC amorphous content. The highest level of DSC amorphous content induced after two hours at 4 °C was 12.20 ± 1.32 % compared to 11.04 ± 2.09 % induced after 20 hours at RT. The highest DSC amorphous content level was reached after milling for 120 minutes at 4 °C, but as milling time was increased to 5 hours, this decreased. The occurrence of the crystallisation event resulted in an early onset temperature for the solid state transformation, as observed in Table 5.4 for STZ III-X milled for 120 minutes, 5, 10 and 20 hours at RT and for samples milled at 4 °C for 120 minutes, 5, 15 and 20 hours. As ball milling affects the particle size and results in induced defects into the structure, it is possible that the presence of the disordered phase may have facilitated the transition from one form to another at lower temperatures.

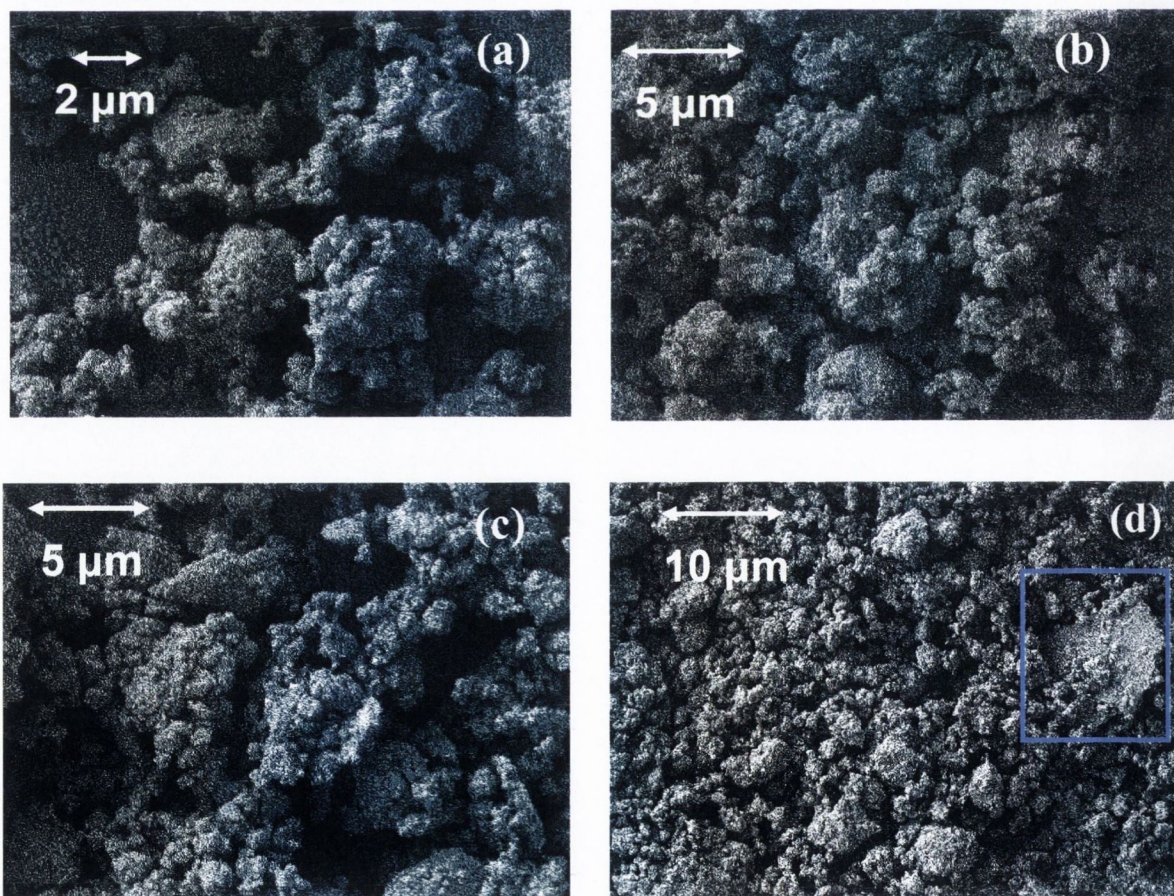
Table 5.4: Thermal properties of STZ III-X unmilled and milled samples at RT and 4 °C with a BTP weight ratio 20:1.

Milling time (minutes)	T_{poly} (°C)	ΔH_{poly} (J/g)	T_{cr} (°C)	ΔH_{cr} (J/g)	T_{m} (°C)	ΔH_{m} (J/g)	TG mass loss (%)	DSC amor. (%)
STZ III -X	162 (0.57)	28 (0.21)			201 (0.75)	111 (0.34)	0.71 (0.43)	0.00 (0.00)
5	145 (0.48)	26 (0.13)			201 (0.61)	110 (0.45)	0.89 (0.15)	0.00 (0.00)
30	145 (0.91)	24 (0.41)			201 (0.63)	110 (0.47)	1.40 (0.21)	0.94 (0.45)
60	147 (0.61)	24 (0.09)			201 (0.12)	108 (0.34)	1.55 (0.06)	0.83 (0.12)
120	138 (0.34)	22 (0.16)	64 (0.17)	6 (0.21)	201 (0.13)	111 (0.10)	1.29 (0.22)	4.86 (1.53)
300	142 (0.57)	24 (0.74)	64 (0.10)	2 (0.10)	201 (0.48)	110 (0.09)	1.25 (0.17)	1.42 (0.37)
600	140 (0.56)	20 (0.79)	63 (0.42)	8 (0.84)	201 (0.10)	110 (0.71)	1.61 (0.41)	6.73 (1.61)
900	141 (0.72)	23 (0.46)			201 (0.14)	111 (0.72)	1.41 (0.05)	0.00 (0.00)
1200	121 (0.91)	12 (0.87)	66 (0.41)	14 (0.37)	201 (0.14)	112 (0.10)	0.98 (0.61)	11.04 (2.09)
5	153 (0.21)	25 (0.15)			201 (0.71)	110 (0.24)	0.93 (0.21)	0.00 (0.00)
30	151 (0.42)	26 (0.31)			201 (0.34)	111 (0.10)	0.87 (0.39)	0.00 (0.00)
60	153 (0.37)	24 (0.17)			201 (0.56)	111 (0.41)	1.02 (0.83)	0.00 (0.00)
120	139 (0.39)	21 (0.81)	66 (0.46)	15 (0.38)	201 (0.49)	110 (0.17)	0.97 (0.08)	12.20 (1.32)
300	143 (0.27)	23 (0.97)	63 (0.41)	8 (0.22)	201 (0.48)	110 (0.11)	1.07 (0.09)	6.51 (0.97)
600	150 (0.61)	24 (0.58)			201 (0.21)	110 (0.15)	1.25 (0.11)	0.00 (0.00)
900	140 (0.14)	21 (0.49)	63 (0.16)	6 (0.34)	201 (0.23)	110 (0.63)	1.14 (0.01)	4.88 (0.67)
1200	140 (0.18)	12 (0.92)	65 (0.09)	6 (0.38)	201 (0.16)	111 (0.78)	1.77 (0.39)	4.83 (1.61)

T_{poly} = onset temperature of solid state transition, ΔH_{poly} = enthalpy of solid state transition, T_{cr} =onset temperature of crystallisation, ΔH_{cr} =enthalpy of crystallisation, T_{m} = onset temperature of melt, ΔH_{m} = enthalpy of melt. DSC amor. =DSC amorphous content. Standard deviation in parentheses. n= 3

5.3.1.3 Morphology and particle size

The morphology of STZ III-X milled at RT with a BTP weight ratio of 20:1 is shown in Figure 5.11 (a to f) and samples milled at 4 °C are shown in Figure 5.12 (a to f). Comparing all milled samples to the unmilled material (Figure 5.4) which was presented previously, an overall reduction of particle size was achieved. Ball milling yields particles that are irregular in shape and size, regardless of time and temperature. STZ III-X milled at RT (Figure 5.11 a to f) produced clusters or agglomerates of small particles, making it difficult to evaluate the particle size. A platelet shaped particle detected after 5 hours (Figure 5.11 d highlighted in the blue box) is characteristic of Form III and is similar in shape to the unmilled material. This could be attributed to inefficient milling or crystallisation of the milled material to STZ Form III. Milling for 10 hours at RT resulted in large particle clusters or/and agglomerations (Figure 5.11 e) and further milling of 20 hours resulted in an environment of agglomerated particles that appear to have agglomerated together.



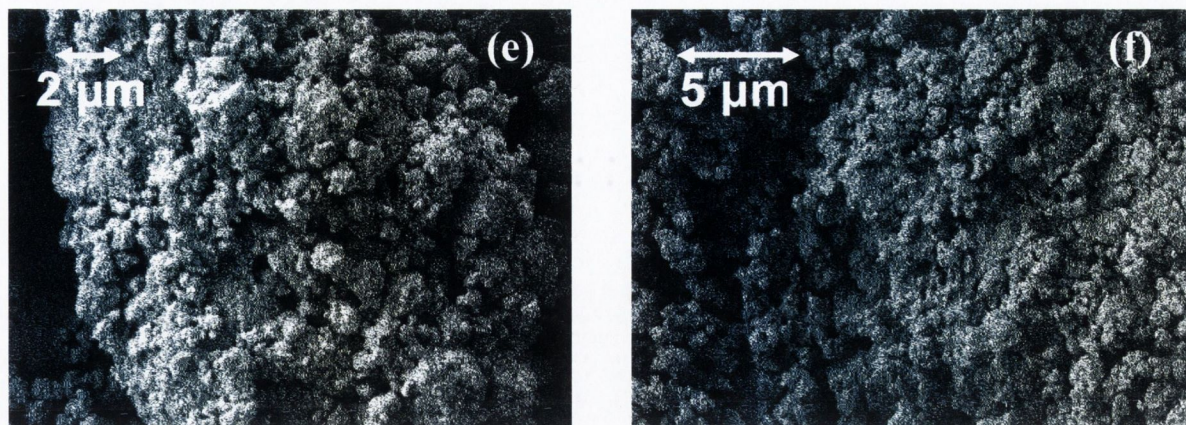


Figure 5.11: SEM of STZIII batch x milled with a BTP weight ratio of 20:1 at RT for (a) for 30 minutes; (b) 60 minutes; (c) 120 minutes; (d) 5 hours; (e) 10 hours; (f) 20 hours.

Figure 5.12: (a) illustrates the morphology of STZ III-X ball milled for 30 minutes. The particles were reduced in size and are irregular in shape as a result of the process. Figure 5.12a shows large particles covered in an array of smaller particles. The reduction of particle size was greater at RT than 4 °C when comparing samples milled for 30 minutes. Ball milling for 60 minutes at 4 °C yields structures made up of small particles that look agglomerated together. Ball milling for 120 minutes (Figure 5.12 c) resulted in an array of small particles. Some particles in this arrangement appear fused together, but agglomerated shaped structures observed in Figure 5.12 (b) are no longer evident. Ball milling for 5 hours (Figure 5.12 d) resulted in an assortment of irregular shaped particles significantly smaller than the starting material. Prolonged milling for 10 and 20 hours (Figure 5.12 e and f) resulted in irregular shaped and sized particles that are larger in size compared to those observed after milling for 5 hours. Characterisation of the polymorphic form is often achieved by the examination of the materials morphology, as each polymorphic structure has a characteristic shape. The micrographs shown in Figure 5.11 and 5.12 shows that milling destroyed the crystals characteristic shape making it almost impossible to use this method for polymorphic characterisation, but does allow the reduction in particle size to be observed.

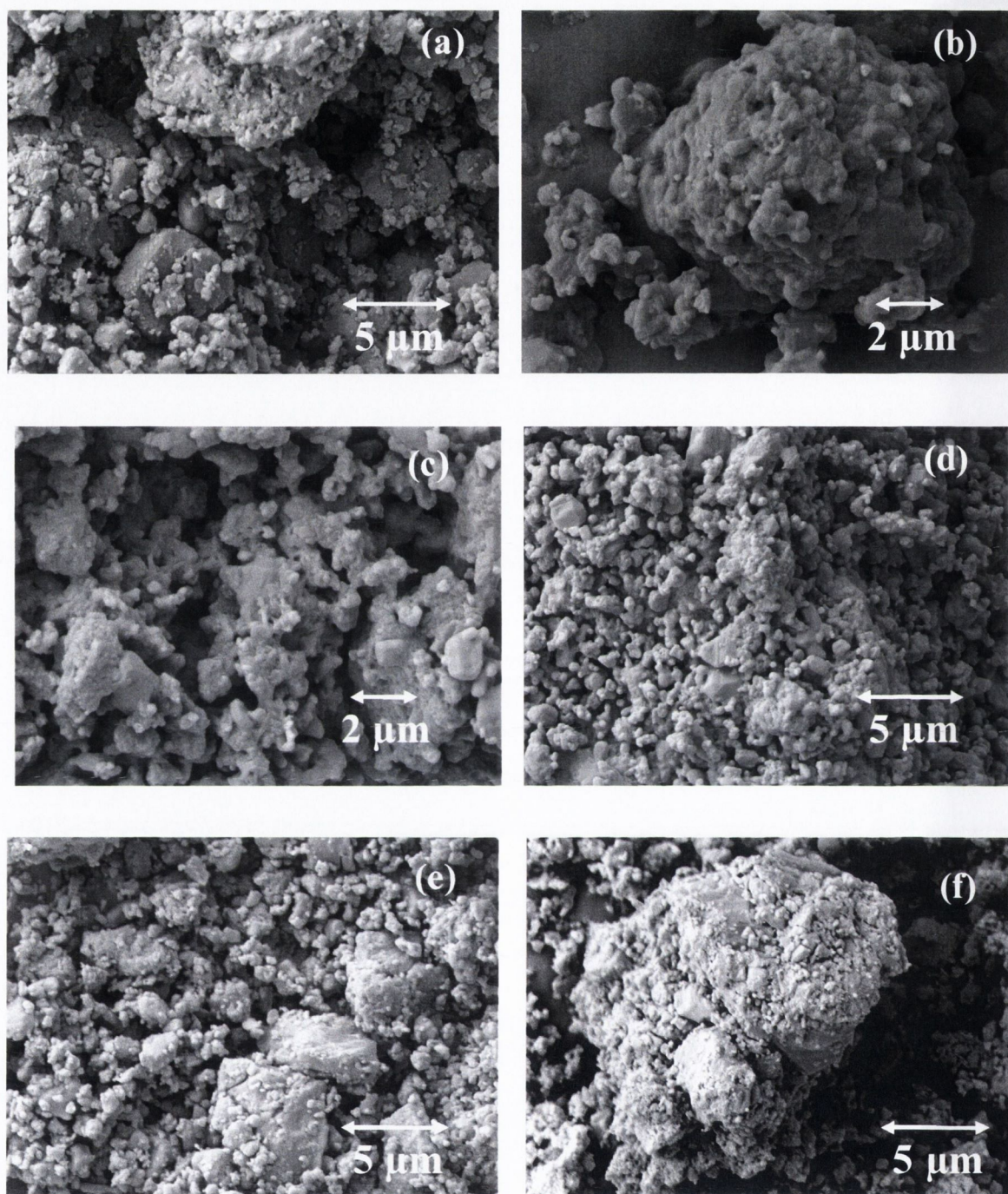


Figure 5.12: SEM of STZ III-X milled with a BTP weight ratio of 20:1 at 4 °C for (a) 30 minutes; (b) 60 minutes; (c) 120 minutes; (d) 5 hours; (e) 10 hours; (f) 20 hours.

A selection of ball milled samples were characterised by Malvern laser diffraction and their particle size range were compared to the unmilled material in Table 5.5. Samples milled for 30, 60 and 120 minutes at 4 °C resulted in a bimodal size distribution shown in Figure 5.13 unlike the monomodal size distribution obtained for the unmilled material. Ball milling for 30 minutes resulted in a decreased d_{10} and d_{50} measurement compared to the unmilled sample but an increase in the d_{90} from $48.64 \pm 1.33 \mu\text{m}$ to $72.01 \pm 6.54 \mu\text{m}$. This trend was also observed for samples milled for 60 and 120 minutes. As milling time is increased the particle size range increased which could be attributed to the agglomerated particle, observed by SEM.

Table 5.5: Particle size distribution obtained by Malvern laser diffraction for STZ III-X unmilled and milled at RT with a BTP weight ratio of 20:1 for 30, 60 and 120 minutes.

Milling conditions	Time (minutes)	Particle size		
		d_{10} (μm)	d_{50} (μm)	d_{90} (μm)
BTP weight ratio 20:1, 4°C	STZ III-X	4.76 (0.15)	17.81 (0.34)	48.64 (1.33)
	30	1.01 (0.17)	4.90 (0.14)	72.01 (6.54)
	60	1.59 (0.15)	9.05(2.29)	148.22 (33.11)
	120	1.90 (0.45)	12.69 (2.10)	219.75 (89.35)

Standard deviation in parentheses, n=3

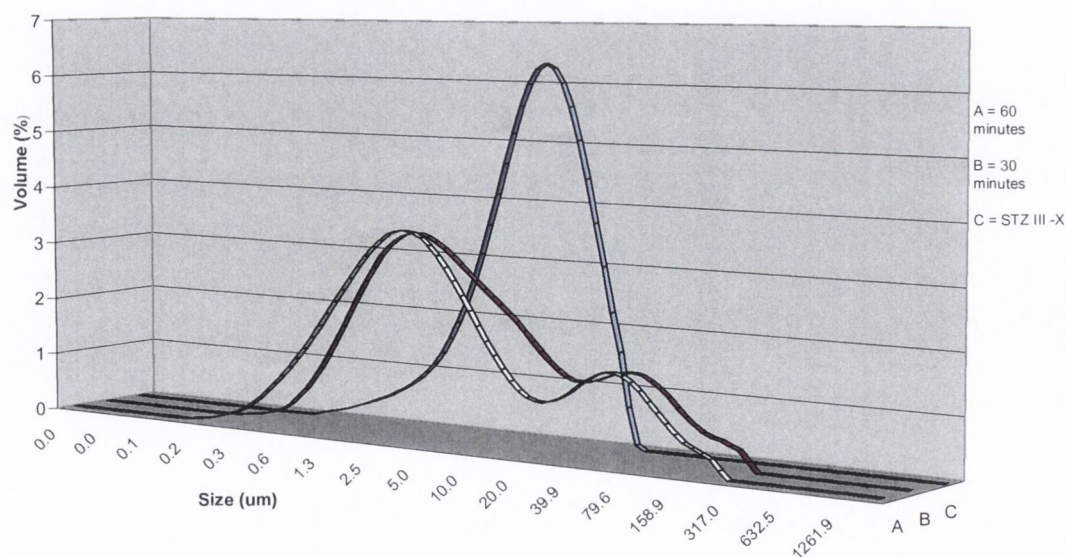


Figure 5.13: Particle size distribution obtained by Malvern laser diffraction of STZ III-X unmilled and milled at RT with a BTP weight ratio of 20:1 for 30 and 60 minutes.

5.4 Investigating the affect of the ball-to-powder weight ratio of 40:1

The level of DSC amorphous content induced when STZ was milled with a BTP weight ratio of 20:1 was < 15. Shakhtshneider and Boldyrev (1993) reported ball milled STZ III samples with a BTP weight ratio of 20:1 but failed to quantify the DSC amorphous content. While Caron *et al.*, (2011) ball milled STZ III with a Planetary ball mill with a BTP weight ratio of 32:1 using zirconium jar and milling balls but an amorphous phase was induced as a result of ball milling with PVP. Increasing the BTP weight ratio for SD and SDNa in the previous chapters yielded a higher level of disorder in comparison to the equivalent milling times with a BTP weight ratio of 20:1. Therefore, it was the aim to investigate the effect a higher BTP weight ratio (40:1) in order to induce higher levels of disorder into the material's structure. Materials investigated included STZ III-Y and STZ I.

5.4.1 Sulfathiazole Form III, batch Y

5.4.1.1 Analysis directly after milling

5.4.1.1.1 Powder X-ray diffraction

Figure 5.15 illustrates the PXRD for STZIII-Y unmilled, milled with a BTP weight ratio of 40:1 for different time periods from 5 minutes to 20 hours at RT tested directly after milling and the theoretical CCDC patterns generated from the single crystal X-ray data. As discussed previously the unmilled material is predominantly Form III (section 5.1). Ball milling for 5 minutes resulted in a decrease in peak intensity. As milling time was increased from 30 minutes to 20 hours, the doublet peaks at $25\ 2\theta$ and triplet peaks at $15\ 2\theta$ and $21\ 2\theta$ degrees merged into one peak. The peak intensity decreased and no new peaks characteristic of any other polymorphic form were detected (Table 5.6 and Figure 5.14). The change in peak area as milling time was increased is illustrated in Figure 5.15. This showed that the total peak area decreased to ~50 % after 5 minutes. Further milling resulted in a further peak area decrease until it reached a plateau at ~14 % after 10 hours.

With prolonged milling (10, 15 and 20 hours) the crystalline peaks gave way to a halo, characteristic of a disorder amorphous state with only minor peaks detected at $15.45\ 2\theta$, $18.95\ 2\theta$, $20.7\ 2\theta$, $22.25\ 2\theta$ and $25.55\ 2\theta$ degrees. These peaks are not characteristic of any specific

polymorph. For example, the peak detected at $15.45\ 2\theta$ could be characteristic of the Form III which has a peak at $15.3\ 2\theta$ or the Form IV which has a peak at $15.58\ 2\theta$. Anwar *et al.*, (1989) found that minor variations of the peak position reflected small variations in the unit cell. The lack of characteristic peaks detected in the milled samples made it difficult to determine the polymorphic forms present in the milled samples.

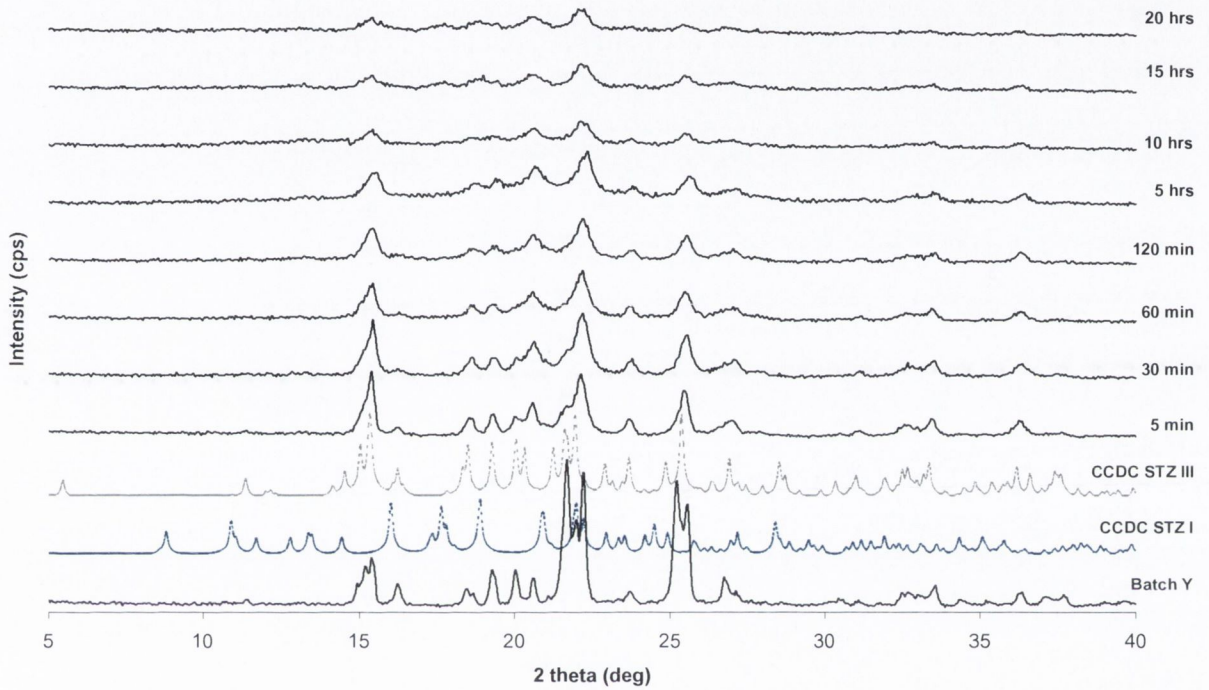


Figure 5.14: XRD of STZ III-Y as received and STZ III-Y form III milled for 5, 30, 60, 120 minutes and 5, 10 and 20 hours at RT with BTP weight ratio of 40:1 and a rotational speed of 400 rpm.

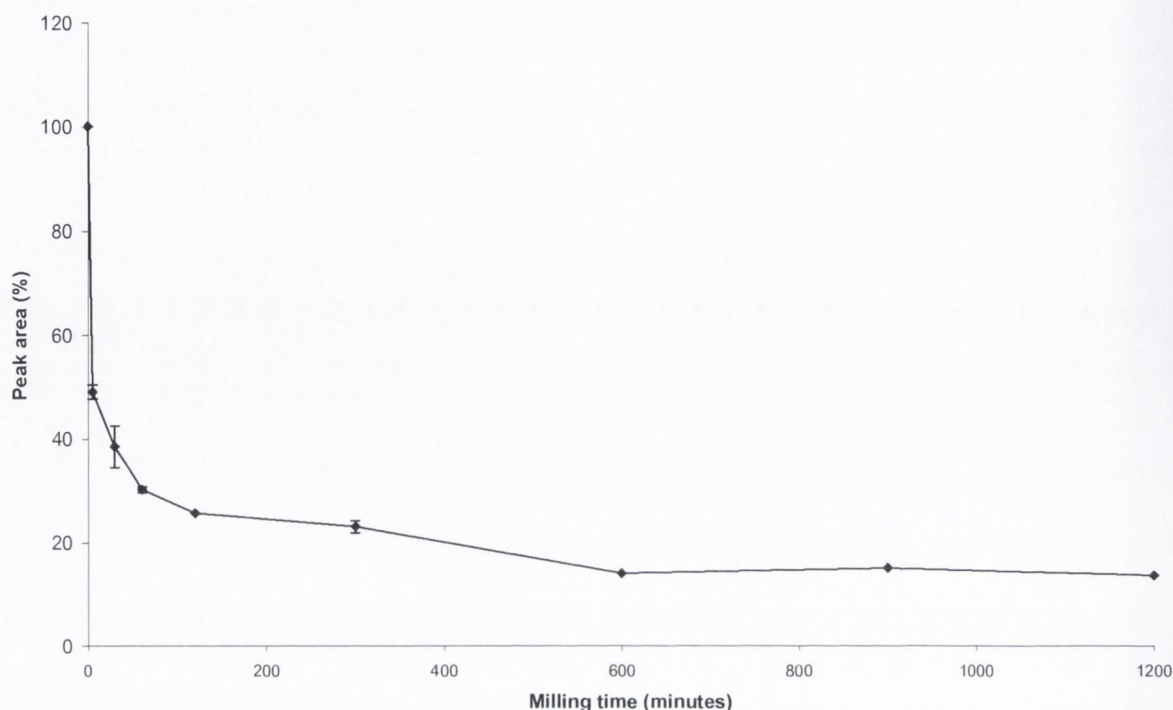


Figure 5.15: PXR D total peak area of STZ III-Y, unmilled and ball milled at RT with a BTP weight ratio of 40:1 for, 5, 30, 60, 120 minutes and 5, 10, 15 and 20 hours

5.4.1.1.2 Thermal analysis

Thermal analysis by DSC of STZ III –Y unmilled and milled at RT for different time periods from 5 minutes to 20 hours is shown in Figure 5.16. The NIR results of the unmilled materials discussed previously (section 5.1.4.) indicated that the unmilled batch Y was a binary mixture of approximately 2 % Form I and 98 % Form III. Ball milling for 5 minutes resulted in a shift of the phase transition to a lower temperature of ~ 131 °C from ~ 154 °C compared to the unmilled material and an enthalpy drop from ~ 29 to ~ 20 J/g (Table 5.6). The melt endotherm was detected at ~ 201 °C but the enthalpy ~ 108 J/g for the unmilled material appeared to increase to ~ 113 J/g after 5 minutes of milling. The crystallisation and solid state thermal events detected for each sample occurred at different temperatures but all samples converted to a predominantly Form I structure which melted at ~ 201 °C. The enthalpy of melt differs from sample to sample, which could indicate that the material did not completely convert to the Form I structure and/or could be due to the number of defects induced in the milling process (Zeitler *et al.*, 2006). Further milling for a total of 30 minutes resulted in a third thermal event detected at ~ 40 °C characteristic of a crystallisation exotherm and the solid state transition temperature was detected at ~ 126 °C. This was lower compared to the unmilled

sample and the 5 minute STZ III-Y milled sample. This event occurred over a shorter temperature range compared to STZ III-Y milled for 5 minutes. Ball milling for 60 minutes resulted in three thermal events, the first at ~ 35 °C, the second at ~ 136 °C and the third at ~ 201 °C which were related respectively to, crystallisation of the amorphous phase induced, a polymorphic transition phase and the melt endotherm of Form I. Comparing the 60 and 30 minute milled samples, it appeared that prolonged milling resulted in an increased level of disorder, with the crystallisation exotherm detected at lower temperatures and the phase transition shifted to higher temperatures (Figure 5.16 and Table 5.6).

Milling for 120 minutes did not follow this trend, as the crystallisation exotherm was detected at ~ 48 °C and the solid state transition temperature was detected at ~ 119 °C. The PXRD diffractograms of STZ III-Y milled for 120 minutes after the sample was heated to 95 °C and 130 °C is shown in Figure 5.16. These temperatures corresponded to the onset and end temperature of the phase transition. The sample heated to 95 °C consisted of peaks characteristic of STZ Form III detected at 18.75 2θ and 19.45 2θ degrees. While the sample heated to 130 °C had several peaks characteristic of the Form I; 10.9 2θ , 17.7 2θ , 18.8 2θ and 20.9 2θ degrees.

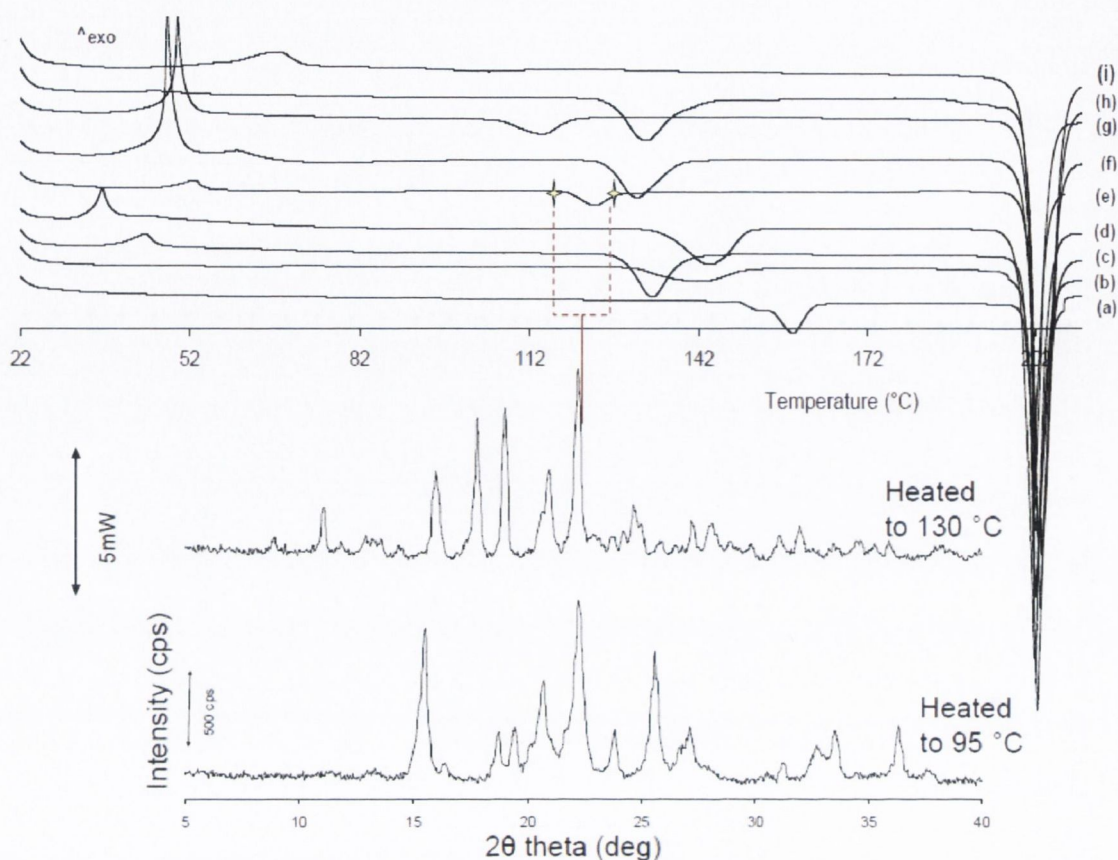


Figure 5.16: DSC thermograms (a) STZ III-Y unmilled and milled STZ III at RT for (b) 5, (c) 30, (d) 60, (e) 120 minutes and (f) 5, (g) 10, (h) 15 and (i) 20 hours. The inserted PXR patterns were taken after heating STZ III-Y milled for 120 minutes to 95 °C and 130 °C.

STZ III-Y milled for 5 hours resulted in the highest DSC amorphous content of 25.11 ± 2.67 %, compared with the samples milled for different time periods. Thermal events detected include a double exothermic peak at ~ 39 °C related to crystallisation of an induced amorphous phase, a phase transition at ~ 126 °C and a melt endotherm at ~ 201 °C. A similar double crystallisation event was observed for SD ball milled with a BTP weight ratio of 40:1 and it was attributed to a non-uniform distribution of energy within the sample Trasi *et al.*, (2010). In the case of SD it was thought that the difference in molecular mobility between the surface and the bulk, and the activation energy required for nucleation and/or growth resulted in the formation of the double crystallisation exotherm. This may be the case for STZ III-Y sample that was ball milled for up to 5 hours but it may also be attributed to the non-uniform distribution of energy associated with the different polymorphic forms that crystallise out as the temperature was increased. Further milling for 10 hours resulted in a decreased

amorphous content to 20.55 ± 0.91 % and the onset temperatures for the thermal events shifted to ~ 49 °C, ~ 106 °C, ~ 201 °C which correspond respectively to crystallisation, a phase transition and the melting of Form I.

No recrystallisation peak was detected in STZ III-Y milled for 15 hours which showed that the sample was constantly evolving as milling time was increased (Figure 5.16). Further milling of 20 hours resulted in three thermal events detected, similar to the ones observed previously. An amorphous phase was present, as indicated by the crystallisation event. This crystallisation event was followed by a phase transition temperature at ~ 93 °C with an enthalpy of ~ 5 J/g, which made it difficult to detect. Compared to the phase transitions detected for the other milling times investigated it occurred at the lowest temperature and it had the lowest enthalpy. This indicated that the sample was predominantly amorphous and this amorphous phase crystallised out to a predominantly Form I structure.

Unlike the PXRD diffractograms, where the peaks had low intensities and were broad in shape which made it difficult to determine the polymorphic form but did allow the loss of crystallinity to be determined, thermal analysis made it possible to determine the amorphous phase induced and the polymorphic form obtained after crystallisation.

The phase transition of Form III and IV to Form I is expected between the range of 150-170 °C according to Anwar *et al.*, (1989). Zeitler *et al.*, (2006) investigated the transition temperatures of each polymorph (Table 5.1) and they stated that, due to the range of transition temperatures and enthalpies, it was not possible to distinguish the different polymorphic forms by thermal analysis alone. The temperatures and enthalpy measurements reported by Zeitler *et al.*, (2006) (Table 5.1) are higher than those obtained for STZ III ball milled (Table 5.6). Apperley *et al.*, (1999) stated that the conversion of Form III to Form I is a defect driven process. The number of defects and the amorphous phase induced during ball milling may have affected the transition temperature onset and the energy required for a polymorphic transition (Table 5.6), which makes it difficult to characterise the polymorphic form by thermal analysis.

Table 5.6: Thermal properties of unmilled STZ III-Y and milled at RT with a BTP weight ratio of 40:1 for 5, 30, 60, 120 minutes and 5, 10, 15 and 20 hours, tested directly after milling.

Milling time (minutes)	T_{cr} (°C)	ΔH_{cr} (J/g)	T_{poly} (°C)	ΔH_{poly} (J/g)	T_m (°C)	ΔH_m (J/g)	DSC amorphous content (%)	TGA (%)
STZ III -Y			154 (0.31)	29 (0.05)	201 (0.11)	108 (0.04)	0.00 (0.00)	0.82 (0.4)
5			131 (0.11)	20 (0.05)	201 (0.14)	113 (0.13)	0.00 (0.00)	1.05 (0.1)
30	40 (0.21)	4 (0.35)	126 (0.14)	23 (0.04)	201 (0.09)	109 (0.11)	3.40 (1.71)	3.41 (0.5)
60	35 (0.19)	8 (0.27)	136 (0.42)	24 (0.12)	201 (0.09)	108 (0.07)	11.99 (2.46)	2.15 (0.2)
120	48 (0.15)	6 (0.48)	119 (0.71)	15 (0.09)	201 (0.12)	104 (0.02)	16.26 (2.01)	2.59 (0.3)
5 hours	39 (0.16)	31 (0.81)	126 (0.15)	25 (0.11)	201 (0.03)	108 (0.10)	25.11 (2.67)	5.26 (0.3)
10 hours	49 (0.22)	27 (0.22)	106 (0.67)	14 (0.08)	201 (0.14)	107 (0.11)	20.55 (0.91)	5.54 (0.9)
15 hours			127 (0.22)	22 (0.13)	201 (0.09)	108 (0.10)	0.00 (0.00)	2.29 (0.7)
20 hours	59 (0.04)	6 (0.32)	93 (0.29)	5 (0.07)	201 (0.10)	105 (0.07)	4.45 (0.04)	4.35 (0.2)

T_{poly} = onset temperature of solid state transition, ΔH_{poly} = enthalpy of solid state transition, T_{cr} = onset temperature of crystallisation, ΔH_{cr} = enthalpy of crystallisation, T_m = onset temperature of melt, ΔH_m = enthalpy of melt. TGA = thermogravimetric analysis. Standard deviation in parentheses. n=4

The amorphous content induced was not completely dependent on time as the amorphous phase was induced in increasing levels as milling time was increased (up to 5 hours), but further milling time (10 hours) resulted in a drop in the amorphous content detected within the samples by thermal analysis. This trend was also observed for STZ III-X milled with a BTP weight ratio of 20:1 in section 5.3.1.2. As previously mentioned Shakhtshneider *et al.*, (1997) also found that as milling time increased the level of amorphous content varied. They

attributed this to the recrystallisation of the amorphous phase induced as a result of prolonged milling.

The position and the broadness of the crystallisation exotherm prevented the detection of the T_g (glass transition temperature). Analysis of the T_g with the MDSC was not possible due to the slow heating rate and the readiness of the amorphous phase to crystallise. The T_g of an amorphous spray dried phase was reported by Bianco *et al.*, (2012) at 59 ± 0.8 °C. The crystallisation onset temperatures for the milled samples were all lower than the reported T_g temperature, apart from STZ III-Y milled for 20 hours.

There was approximately less than 1% weight loss by TGA for the STZ III-Y unmilled but as a result of milling this increased, Table 5.6. The milled samples that resulted with the highest DSC amorphous content, such as STZ III-Y 5 and 10 hours, had a corresponding high weight loss. This may suggest that the amorphous phase allows the absorption of moisture and a higher DSC amorphous content phase present within the same can result in a higher moisture content.

5.4.1.1.3 Particle size by laser diffraction

Changes to the particle size distribution as a result of milling is given in Table 5.7 and illustrated in Figure 5.17. The unmilled material had a monomodal distribution, but as a result of milling this was changed to a bi or trimodal distribution (Figure 5.17). The size distributions shown in Figure 5.17 shows an immediate change occurred as a result of milling for 5 minutes and this change was evident for all other milled samples. Ball milling for 5 minutes resulted in a decrease in d_{10} and d_{50} but an increase in the d_{90} . Overall, all d_{10} measurements for the milled samples are less than the unmilled material. Investigating the change by statistical analysis using the Tukey's multiple comparison test showed that changes to the median particle size were observed after 5 minutes of milling but further changes are only evident when milling is prolonged to 120 minutes. After 120 minutes the median particle size showed no statistical change until milling time of 15 hours was reached and the particle size obtained at this time was no different to the 20 hour milled sample.

Table 5.7: Particle size distribution obtained by Malvern laser diffraction for STZ III – Y unmilled and milled at RT with a BTP weight ratio of 40:1 from 5 minutes to 20 hours.

Milling conditions	Time (minutes)	Particle size		
		d10 (μm)	d50 (μm)	d90 (μm)
BTP weight ratio 40:1, RT	STZ III - Y	3.06 (0.36)	11.24 (1.38)	25.79 (0.63)
	5	1.55 (0.14)	9.39 (0.36)	80.48 (6.61)
	30	1.57 (0.09)	8.70 (0.77)	120.15 (19.77)
	60	1.69 (0.29)	7.31 (1.63)	75.76 (24.68)
	120	2.15 (0.22)	14.60 (0.28)	187.87 (12.75)
	300	2.30 (0.23)	15.05 (1.20)	138.01 (2.59)
	600	2.34 (0.36)	14.40 (3.09)	136.43 (21.16)
	900	1.40 (0.18)	7.75 (1.89)	68.53 (11.28)
	1200	2.19 (0.28)	10.39 (1.31)	85.71 (1.85)

Standard deviation in parentheses. n=3

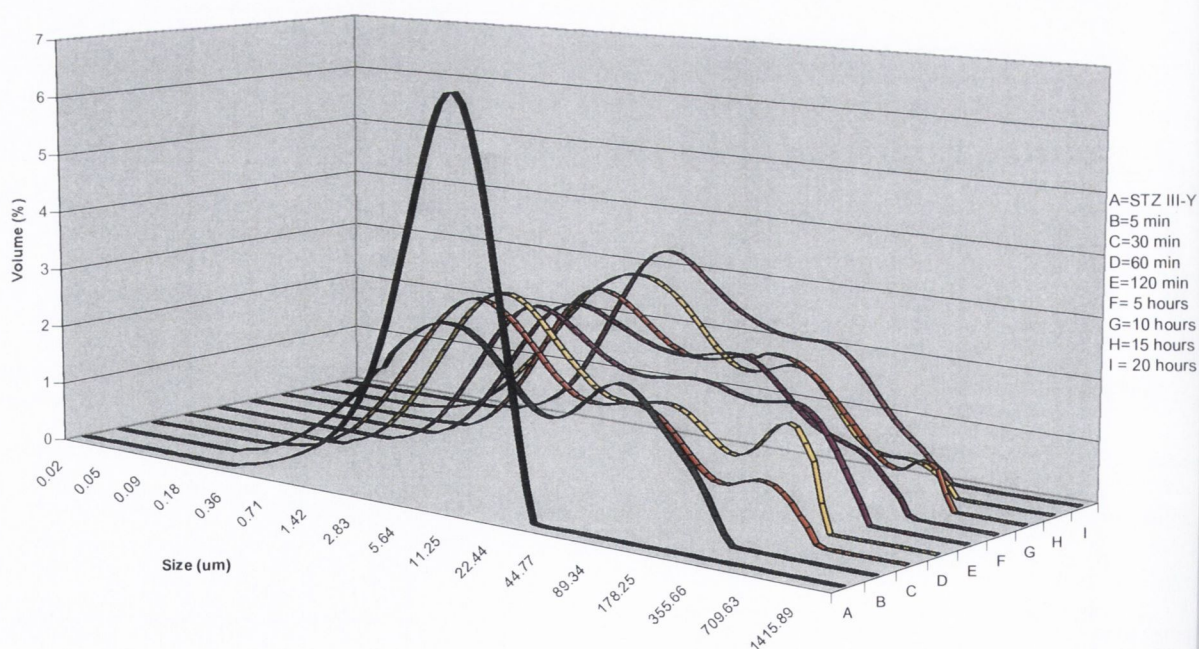


Figure 5.17: Particle size distribution obtained by Malvern laser diffraction of STZ III-Y unmilled and milled at RT with a BTP weight ratio of 40:1 from 5 minutes to 20 hours.

5.4.1.1.4 Morphology and specific surface area

The specific surface area (SSA) measured by BET after 5 minutes increased from 0.59 ± 0.11 m^2/g for the unmilled STZ III-Y to 5.14 ± 0.14 m^2/g (Table 5.8). As milling time was increased the SSA varies. therefore statistical analysis was used to determine the difference between the samples. Overall, STZ III-Y milled for 5 minutes was statistically different to all other samples with the exception of STZ III-Y, milled for 120 minutes. STZ III-Y milled for 30 minutes was only statistically different to samples milled for 120 minutes and 5 hours. STZ III-Y milled for 60 minutes was statistically different to those milled for 120, 300, 600, 900 and 1200 minutes. Samples milled for 120 and 300 minutes were different to each other and those milled for 600, 900 and 1200. No difference was observed between STZ III-Y milled for 600, 900 and 1200 minutes.

Table 5.8: Specific surface area by BET of STZ III-Y unmilled and milled from 5 minutes to 20 hours at RT with a BTP weight ratio 40:1

Ball milling time (minutes)	STZ III –Y (m^2/g)
0	0.59 (0.11)
5	5.1 (0.14)
30	3.83 (0.11)
60	4.33 (0.01)
120	5.41 (1.24)
300	6.94 (0.20)
600	3.52 (0.11)
900	3.48 (0.27)
1200	3.45 (0.06)

Standard deviation in parentheses, n=3

Changes to the materials' structure was evaluated by SEM and shown in Figure 5.18 (a and b). The platelet structure observed in Figure 5.4 was reduced to aggregates and/or agglomerates of smaller particles. Ball milling for 120 minutes (Figure 5.18 (a)) and 10 hours (Figure 5.18 (b)) resulted in a structure that was similar in nature to each other. Formation of agglomerated particles, as observed by SEM analysis, could contribute to the increased d_{90}

measurements and the change in SSA. The small agglomerated particles in Figure 5.18 (a) appear like they have coated a platelet shaped particle which could protect the Form III material from further milling and/or limit the amorphous phase induced.

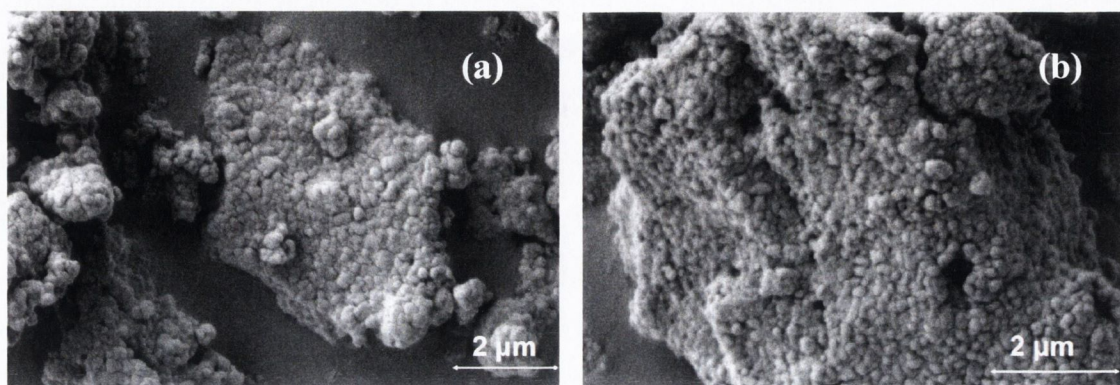


Figure 5.18: SEM morphology of STZ III milled (a) for a 120 minutes and (b) 10 hours at RT with a BTP weight ratio of 40:1.

5.4.1.2 Storage of the ball milled STZ III-Y

5.4.1.2.1 Powder X-ray diffraction

The samples were tested directly after milling, stored at 4 °C in a dessicator with phosphorous pentoxide for one hour and then a selection of samples tested again by PXRD and thermal analysis. Figure 5.19 shows PXRD analysis obtained after an hour of storage for STZ III-Y milled for a total of 30, 60 and 120 minutes and 5, 10 and 20 hours and these were compared to the CCDC Form I and III patterns and the unmilled STZ III-Y. Table 5.9 outlines the changes to the total peak area analysed for each of these samples. The results showed that the crystallinity increased as a result of storing the milled samples for an hour in comparison to the PXRD diffractograms obtained directly after milling. The STZ III-Y milled for 20 hours and stored for an hour resulted in the most dramatic change (Figure 5.19 i). Peaks detected for STZ III-Y milled for 20 hours and stored for an hour are characteristic of those detected in the unmilled material (Figure 5.19 c and i). Bianco *et al.*, (2012) found that amorphous sulfathiazole obtained by spray drying started to crystallise within an hour of collection. The PXRD analysis of the samples stored for an hour is proof that the amorphous phase induced by milling is as unstable as the form induced by spray drying. It also confirms that the amorphous phase produced by milling reverts back to the Form III.

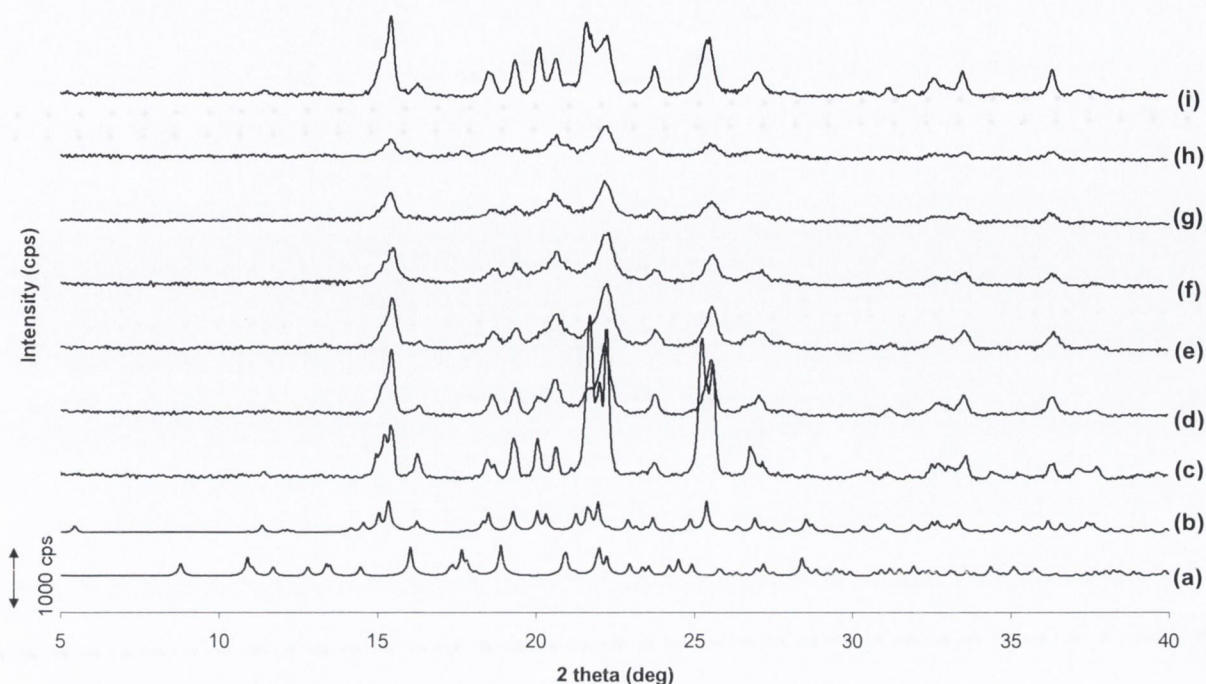


Figure 5.19: PXRD of STZ (a) CCDC form I; (b) CCDC Form III; (c) STZIII – Y unmilled and STZ III–Y ball milled samples stored for one hour at 4 °C; (d) milled for 30 minutes; (e) milled for 60 minutes; (f) milled for 120 minutes; (g) milled for 5 hours; (h) milled for 10 hours and (i) milled for 20 hours.

PXRD analysis of the STZ III-Y ball milled samples stored for one week at 4 °C in a desiccator with phosphorus pentoxide is shown in Figure 5.20 and peak area analysis is given in Table 5.9. Bragg peaks detected for the samples indicate the presence of a crystalline structure. The diffractogram for the milled samples was similar to the unmilled STZ III-Y material. Figure 5.21 compares the peak areas after each storage period with those obtained directly after milling. The readiness of each sample to crystallise indicated the instability of the induced amorphous phase but the intensity of the peaks after one week shows that a certain level of disorder remained within the structure.

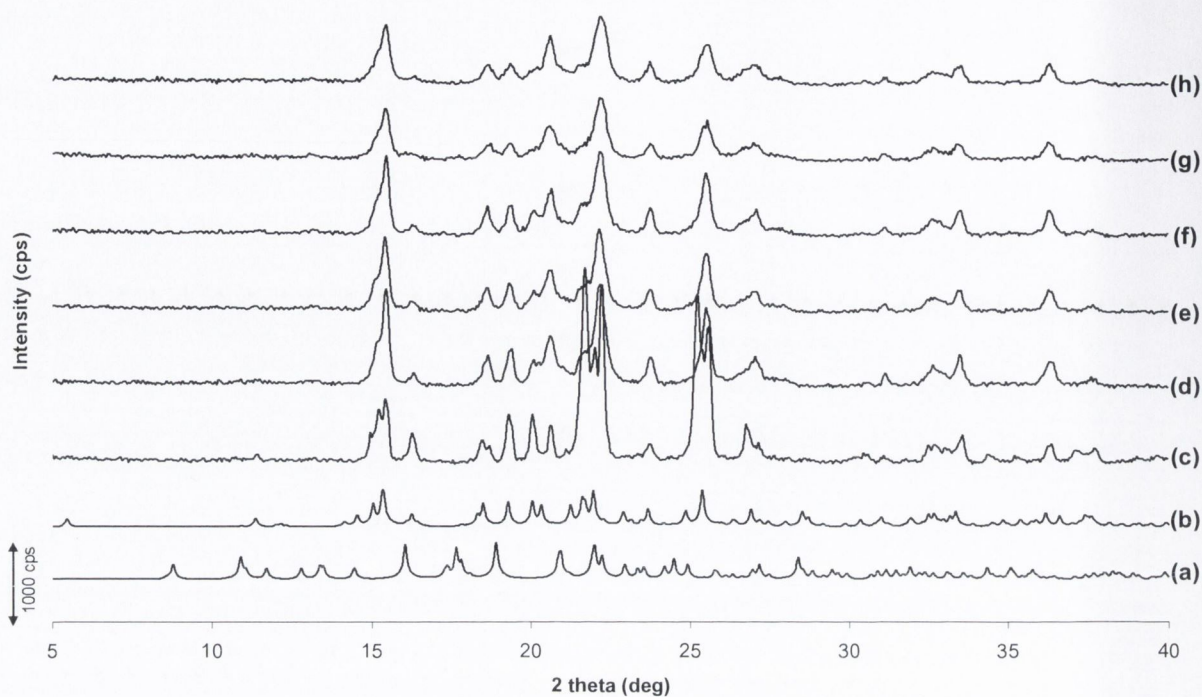


Figure 5.20: PXRD of STZ (a) CCDC Form I; (b) CCDC Form III; (c) STZ III–Y and STZIII–Y stored for one week; (d) milled for 30 minutes; (e) milled for 60 minutes; (f) milled for 120 minutes; (g) milled for 5 hours and (h) milled for 10 hours.

Table 5.6: The total peak area changes for STZ III batch Y milled from 5 minutes to 20 hours at RT. (NM = not measured)

Milling time (minutes)	Peak area (%)	Peak area (%)	Peak area (%)
	STZ III – Y	STZ III – Y	STZ III – Y
	40:1, RT	40:1, RT	40:1, RT
	Directly after milling (n=3)	After one hour (n=2)	After one week (n=2)
5	49.02 (1.33)	NM	NM
30	38.49 (4.05)	55.99 (1.64)	81.11 (0.14)
60	30.16 (0.57)	37.14 (2.48)	55.16 (3.16)
120	25.64 (0.03)	39.25 (3.30)	65.01 (4.92)
300	23.03 (1.17)	32.93 (2.76)	62.05 (1.91)
600	14.00 (0.07)	22.94 (1.53)	58.51 (1.65)
900	15.03 (0.04)	NM	NM
1200	13.60 (0.01)	73.24 (2.23)	NM

Standard deviation in parentheses.

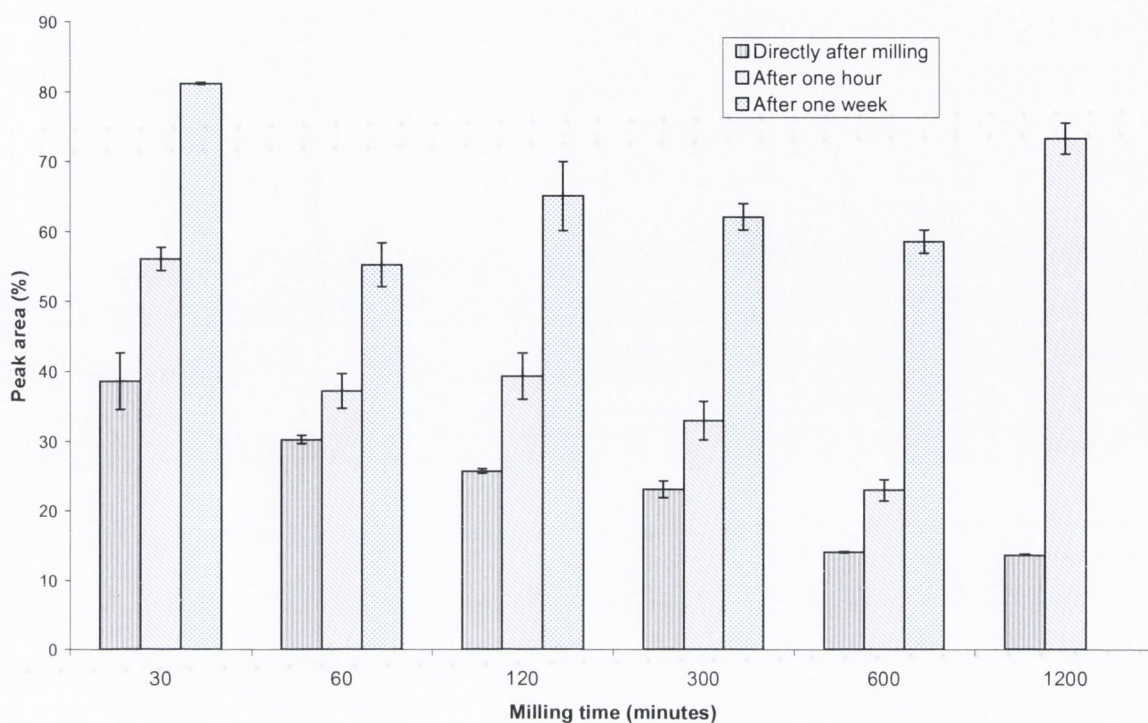


Figure 5.21: Total peak area analysis measured directly after milling, after one hour of storage and after one week of storage at 4 °C.

5.4.1.2.2 Thermal analysis

Thermal analysis of a selected number of samples was tested after one hour of storage (Figure 5.22) and one week of storage (Figure 5.23) after milling. This showed that the induced amorphous phase had either completely or partially crystallised (Figure 5.22 and 5.23 and Table 5.7). A comparison between the DSC amorphous content determined after testing the milled samples directly after milling and after one hour is shown in Figure 5.24. STZ III-Y milled for 60 minutes resulted in the phase transition temperature to shift to ~119 °C from ~134 °C after one hour, and after one week of storage the sample completely crystallised and the phase transition temperature was detected at ~126 °C. The phase transition temperatures measured after one hour of storage after milling for samples milled for 60, 120 minutes and 5 and 10 hours, were detected at lower temperatures compared to those determined directly after milling. Ball milling for 20 hours resulted in a phase transition temperature increased from ~94 °C to ~140 °C after one hour of storage and the amorphous phase had appeared to be completely crystallised as no crystallisation exotherm was detected. A crystallisation exotherm was not detected for the samples that were tested by thermal analysis after one week

of storage, indicating complete crystallisation of the amorphous phase. The phase transition temperature detected for each sample was at a higher temperature when compared to the transitions detected when the samples were analysed directly after milling (Figure 5.23 and Table 5.7).

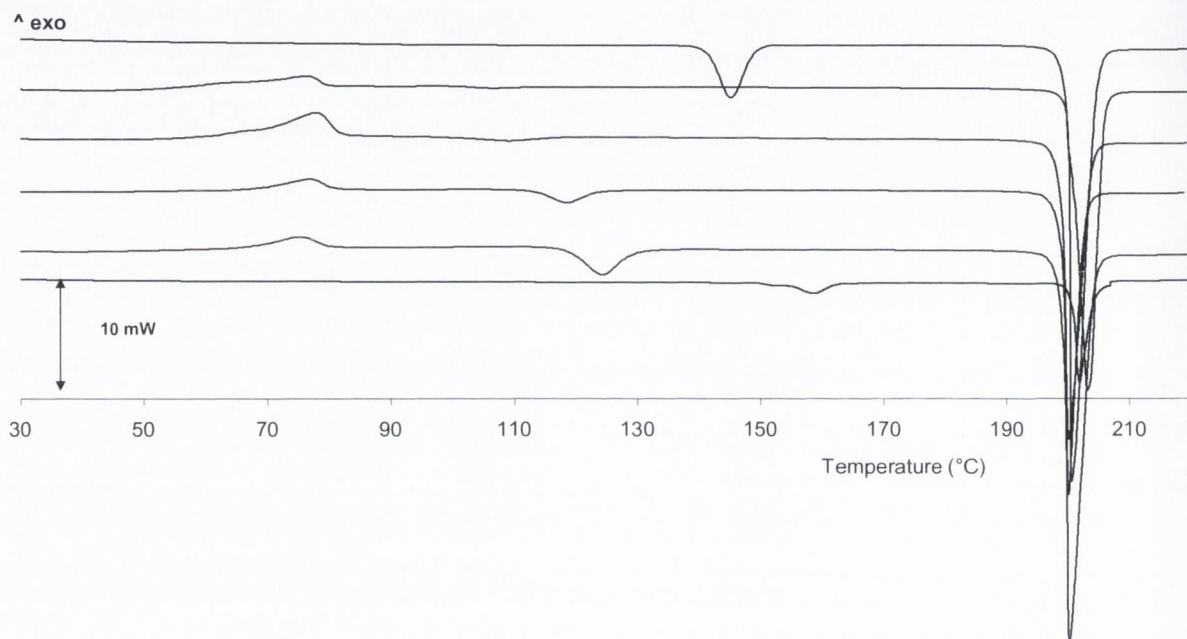


Figure 5.22: DSC thermograms of STZ III- Y unground (a), and STZ III –Y milled and tested one hour later (b) 60 minutes; (c) 120 minutes; (d) 5 hours; (e) 10 hours and (f) 20 hours.

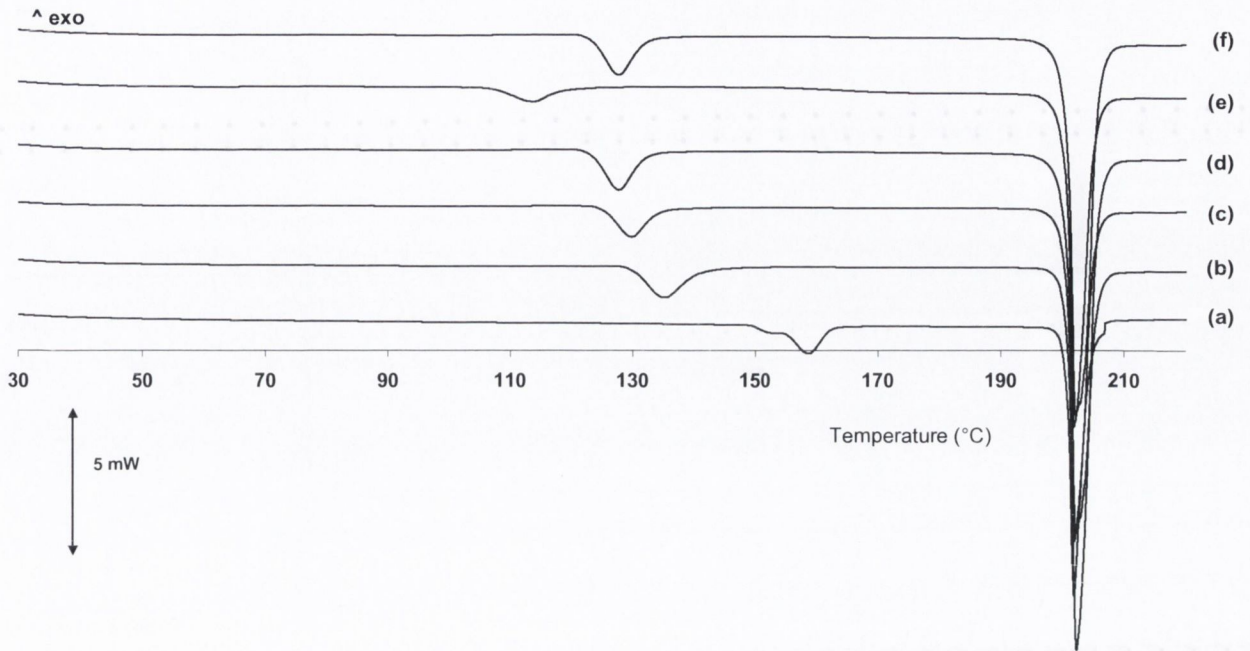


Figure 5.23: DSC analysis of (a) STZ III-Y unground and milled for (b) 30 minutes, (c) 60 minutes; (d) 120 minutes; (e) 5 hours and (f) 10 hours, tested after 1 week of storage.

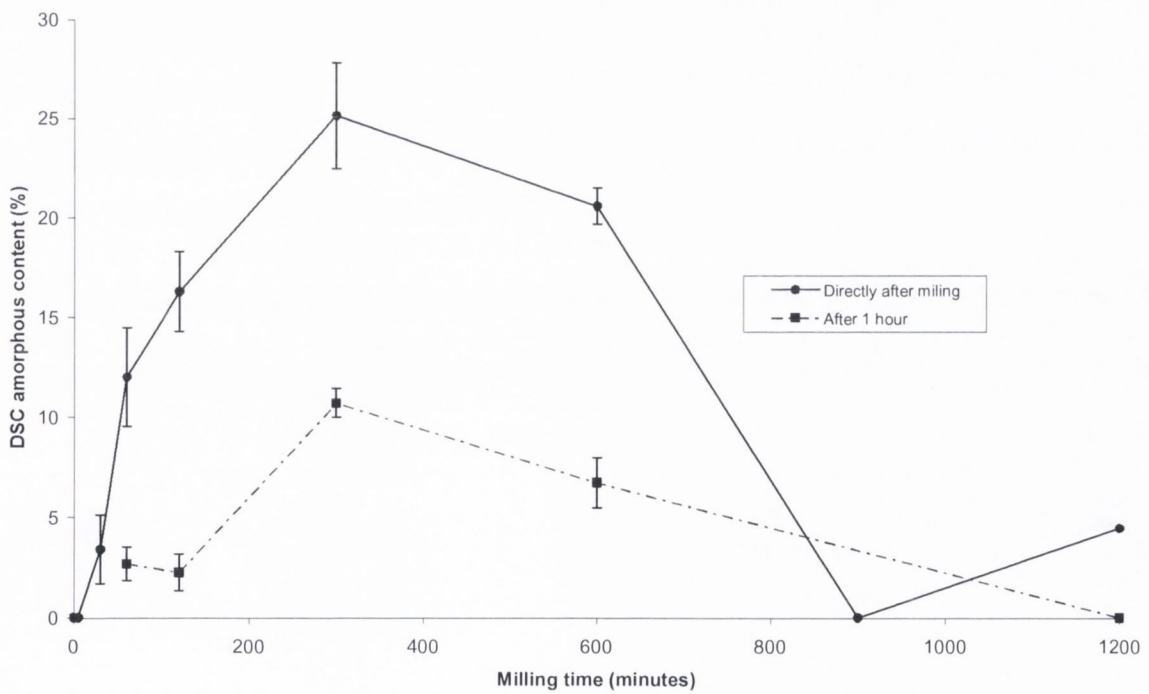


Figure 5.24: DSC amorphous content measured directly after milling and after one hour for STZ III-Y milled at RT with a BTP weight ratio of 40:1.

Table 5.9: Thermal properties of unmilled STZ III-Y and milled at RT with a BTP weight ratio of 40:1 for 5, 30, 60, 120 minutes and 5, 10, 15 and 20 hours. Stored samples.

	Milling time (minutes)	T_{cr} (°C)	ΔH_{cr} (J/g)	T_{poly} (°C)	ΔH_{pol} _y (J/g)	T_m (°C)	ΔH_m (J/g)	DSC amorphous content (%)
Tested after one hour	STZ III -Y			154 (0.31)	29 (0.05)	201 (0.11)	108 (0.04)	0.00 (0.00)
	60	68 (0.14)	6 (0.11)	119 (0.01)	17 (0.01)	200 (0.09)	117 (0.14)	2.68 (0.83)
	120	69 (0.09)	5 (0.41)	113 (0.14)	12 (0.04)	200 (0.09)	116 (0.17)	2.24 (0.92)
	300	48 (0.27)	24 (0.07)	102 (0.13)	9 (0.13)	201 (0.04)	107 (0.18)	10.68 (0.72)
	600	61 (0.94)	15 (0.56)	103 (0.17)	5 (0.04)	200 (0.75)	118 (0.16)	6.71 (1.24)
	1200			140 (0.19)	24 (0.04)	200 (0.69)	121 (0.21)	0.00 (0.00)
	Tested after one week	30			130 (0.34)	22 (0.11)	201 (0.54)	108 (0.22)
60				126 (0.17)	19 (0.13)	201 (0.34)	108 (0.24)	0.00 (0.00)
120				124 (0.18)	17 (0.04)	201 (0.61)	108 (0.23)	0.00 (0.00)
300				108 (0.09)	11 (0.01)	201 (0.57)	108 (0.19)	0.00 (0.00)
600				121 (0.22)	12 (0.07)	201 (0.49)	108 (0.28)	0.00 (0.00)

T_{poly} = onset temperature of solid state transition, ΔH_{poly} = enthalpy of solid state transition, T_{cr} = onset temperature of crystallisation, ΔH_{cr} = enthalpy of crystallisation, T_m = onset temperature of melt, ΔH_m = enthalpy of melt. Standard deviation in parentheses. n=2

Shakhtshneider (1997) investigated the effect when Form I and III were milled with an AGO-type planetary mill in which the vials were cooled with water but unfortunately the temperature and the milling speed was not given. Form III was milled with a BTP weight ratio of 20:1 for 1, 5, 10, 15, 25 and 40 minutes. The conversion of Form III to Form I was observed upon milling and the polymorphic forms followed the conversion outlined in Figure 5.25. Prolonged milling resulted in the crystallisation of the amorphous phase to Form I.

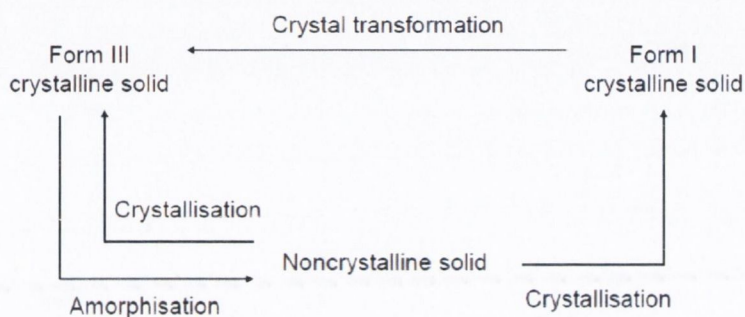


Figure 5.25: The pathway of crystalline form of sulfathiazole during mechanical treatment (Shakhtshneider, 1997)

In this study the thermogram obtained directly after milling for each ball milled sample resulted in a phase transition that was, detected in a temperature range, previously attributed by Zeitler *et al.*, (2006) to the transformation of Form II, III, IV and V to Form I. Thermal analysis showed that after one hour of storage the induced DSC amorphous phase was reduced and the polymorphic form reverted back to a more stable crystal form. This was evident by the change in the peak area detected for the STZ III-Y 20 hours ball milled samples after an hour of storage.

Storage of one week resulted in the elimination of the amorphous phase (Figure 5.23) and a shift of the phase transition temperature to higher temperatures. The PXRD diffractograms after the week of storage were similar to the unmilled STZ III-Y material. Bladgen *et al.*, (1998) states that sulfathiazole precipitated from aqueous solution follows Ostwald's rule of stages and that the stability of the polymorphs increased in the order: I to II to III and finally to IV. Ostwald's rule of stages stated 'when leaving a given state and in transforming to another state, the state which is sought out is not the thermodynamically stable one, but the state nearest in stability to the original state, this must be the next least stable state (Threlfall, 2003; Ostwald 1897). In the case of sulfathiazole the more unstable state, Form I, converts to

the more stable state, Form III, as a result of storage. Earlier solubility studies by Lagas and Lerk (1981) state the order of stability of sulfathiazole was V to I and I converted to III. Khoshkhoo and Anwar (1993) found that the stability of sulfathiazole followed I to V, V to IV and finally form IV converted to III. These studies did not include all the polymorphic forms because they were either not discovered at the time or were difficult to isolate. Munroe *et al.*, (2012) carried out extensive research on the stability of the individual polymorphs and binary mixtures of sulfathiazole, both from solution. They found that when samples were held at temperatures between 10-50 °C they followed the stability order of I to V, V to IV, IV to II and finally II to III, while above 100 °C the stability order changed completely to II to III, III to IV, and IV to V and this converted to I.

PXRD analysis of the stored milled STZ III-Y samples suggested that, the over time, the material would convert completely to the Form III. Shakhtshneider (1997) investigated the effect of ball milling sulfathiazole and found that the induced amorphous phase reverted back to the more stable crystal structure. They stated the amorphous phase facilitated the change in the polymorphic forms. This was evident for the samples here as the STZ III-Y 20 hours milled sample was converted to a mixture of amorphous phase and a predominately form I phase. Thermal analysis of the 20 hour milled sample after one hour showed that the amorphous phase was no longer detected and the detection of a solid-state transition at ~140 °C indicates the structure was no longer predominately Form I.

5.5 Sulfathiazole Form I (STZ I)

5.5.1 Directly after milling

5.5.1.1 Powder X-ray diffraction

Ball milling was found to induce changes such as induced DSC amorphous content and polymorphic conversion to the STZ III-Y structure. Regardless of the similarities between polymorphs they were shown to behave differently regarding tabletability (Picker-Freyer *et al.*, 2007). Therefore, it was of interest to investigate how the ball milling process affects the different polymorphs of sulfathiazole. Form I was investigated because it is easily formed and as a result of ball milling STZ III-Y for 20 hours with a ball to powder weight ratio of 40:1 it is possible to convert the Form III to Form I by ball milling and as it was possible to induce

this phase during ball milling it was of interest to investigate how this phase behaved during ball milling when it was the original phase before ball milling was undertaken.

Figure 5.27 shows the PXRD of STZ I unmilled, the CCDC theoretical patterns simulated from single crystal XRD data of STZ Form I and III and STZ I milled for 5, 30, 60, 120 minutes and 5, 10, 15 and 20 hours with a BTP weight ratio of 40:1 at RT. Ball milling for 5 minutes resulted in a reduction in the Bragg peak intensity (Figure 5.27 and Table 5.12).

The characteristic peaks of Form I were still detected at 10.9 2 θ , 16 2 θ , 17.7 2 θ , 18.8 2 θ and 20.9 2 θ degrees for samples milled from 5 minutes to 10 hours. Further milling of a total of 15 hours resulted in the elimination of the Form I characteristic peaks at 10.9 2 θ and 16.0 2 θ and 17.7 2 θ , while peaks at 15.4 2 θ and 25.4 2 θ degrees were detected. The peak at 15.4 2 θ were also present in the theoretical diffractograms of Form II, III and IV and the peak at 25.4 2 θ is present in the theoretical pattern of Form III. Ball milling for 20 hours resulted in a further loss of crystallinity with fewer crystalline peaks detected. Those detected were broad in shape but are predominantly characteristic of the Form I. The peak at 15.4 2 θ remained but 25.4 2 θ was eliminated.

The PXRD peak area obtained for the 15 hour STZ I milled samples was higher than the 10 hours STZ I milled material, due to new peaks, characteristic of a polymorphic change as milling time is increased. Ball milling for a total of 20 hours resulted in decrease of the PXRD peak area to 35.61 \pm 5.30 % compared to the of the original peak height of the unmilled STZ I samples of which were taken to be 100 %. The changes to the peak area are illustrated in Figure 5.28.

Table 5.12: PXRD total peak area for STZ I ball milled at RT with a ball to powder weight ratio of 40:1 at RT from 5 minutes to 20 hours.

Milling time (minutes)	Peak area (%) STZ I, 40:1, RT
5	62.85 (3.42)
30	62.08 (11.11)
60	46.86 (3.65)
120	37.57 (0.14)
300	37.18 (8.02)
600	34.83 (0.06)
900	38.42 (1.06)
1200	35.61 (5.30)

Standard deviation in parentheses. n =4.

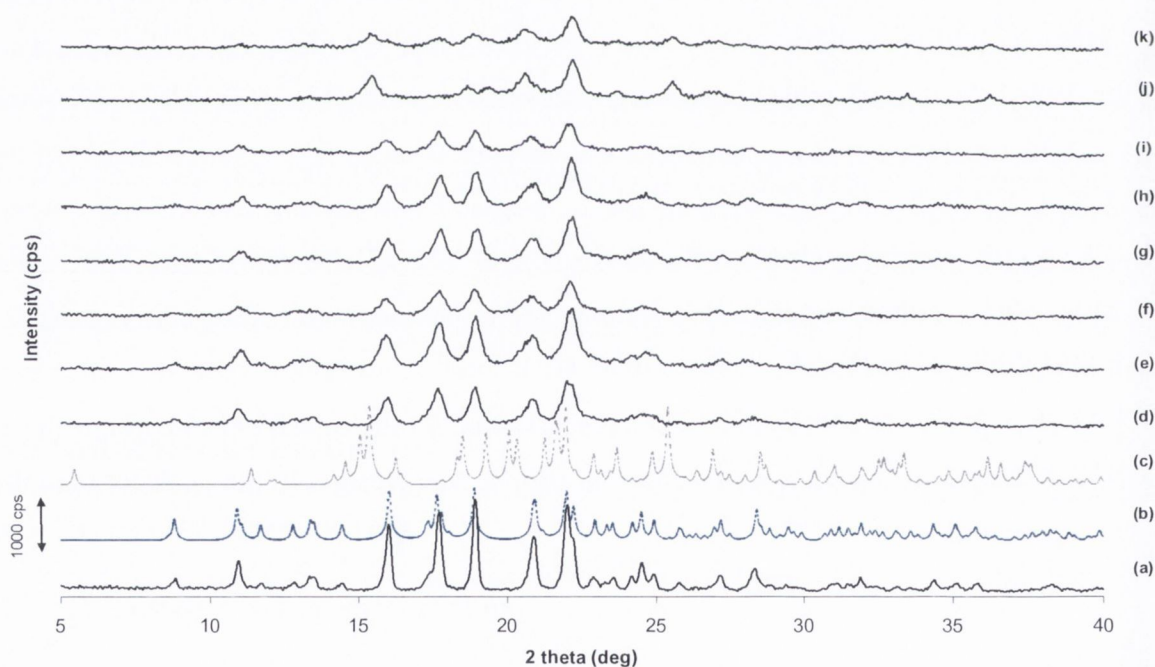


Figure 5.27: PXRD of (a) STZ I unmillied, (b) CCDC STZ I, (c) CCDC STZ III and STZ I milled at RT at speed of 400 rpm with a BTP weight ratio 40:1 (d) 5 minutes; (e) 30 minutes; (f) 60 minutes; (g) 120 minutes; (h) 5 hours; (i) 10 hours; (j) 15 hours and (k) 20 hours

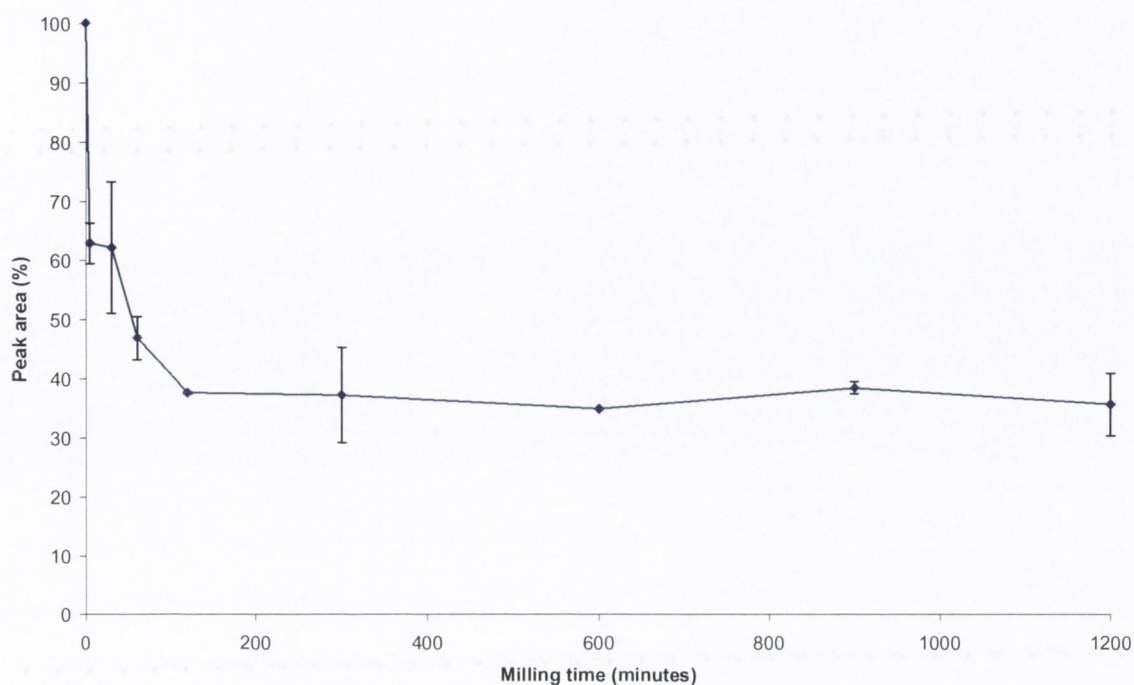


Figure 5.28: PXR D total peak area analysis of STZ I unmilled and milled at RT with a BTP weight ratio for 40:1 for 5, 30, 60, 120, 300, 600, 900 and 1200 minutes.

5.5.2 Thermal analysis

The thermal analysis of STZ I unmilled and milled is shown in Figure 5.30. Ball milling STZ I for 5, 30 and 60 minutes resulted in the detection of one thermal event attributed to the melting of Form I at ~ 201 °C. The enthalpy of melting (ΔH_m) is given in Table 5.13. The melt enthalpy was found to change as milling time was increased. This could be attributed to the increased number of defects induced into the crystallite size, and/or the reduction of the crystallite size, as a result of the ball milling process. Ball milling of STZ I for a total of 120 minutes resulted in a second thermal event being detected, characteristic of a crystallisation event at 87 °C, shown in Figure 5.29, which is followed by the melting of Form I. The level of DSC amorphous content induced as a result of ball milling for a total of 120 minutes was 2.02 ± 1.21 %. Further milling for 5 hours resulted in three thermal events detected, the first at ~ 61 °C, the second event was detected at ~ 95 °C and the third at ~ 201 °C, which were respectively related to the crystallisation of the amorphous phase, the phase transition and the melting of Form I. The phase transition temperature was detected over a large temperature range in which several phase transitions may occur. This made it difficult to determine the polymorphic phases present after crystallisation. The 5 hour milled sample was heated to

95°C and analysed by PXRD. This point is marked with a star in Figure 5.29 and shown as an insert below the thermograms. The diffractogram of this sample consisted of peaks characteristic of Form I, but a minor peak detected at 22.9 2θ degrees, characteristic of Form III, was also detected. Ball milling for 10 hours resulted in the highest DSC amorphous content of 15.03±1.42 % induced and three thermal events were detected. These events consisted of a crystallisation exotherm detected at ~66 °C followed by an endothermic event characteristic of a phase transformation at ~102 °C, and a melt endotherm at 201 °C. Further milling of 15 and 20 hours resulted in three similar thermal events. The DSC amorphous content induced for STZ I milled for 15 hours was 11.8±1.49 % and 7.78±0.73 % after 20 hours. The phase transition shifted from ~98 °C with an enthalpy of ~1 J/g to ~109 °C with an enthalpy of ~21 J/g for the 15 and 20 hours milled samples, respectively. The phase transition appeared to be affected by the quantity of amorphous content induced as a result of ball milling. As the DSC amorphous content increased the enthalpy for the phase transition increased. The data collected from the thermal analysis presented in Table 5.13 and the calculated amorphous content is also presented.

There was approximately less than 1% weight loss by TGA for the unmilled STZ I. As a result of ball milling STZ I at RT with a BTP weight ratio of 40:1, the weight loss by TGA was higher than the unmilled sample. This is outlined in Table 5.13. From the ball milled samples tested, the highest weight loss was observed for the STZ I sample ball milled for 10 hours at ~6 %, this sample was also found to have the highest level of DSC amorphous content. As ball milling time was increased the DSC amorphous content and mass loss determined by TGA decreased.

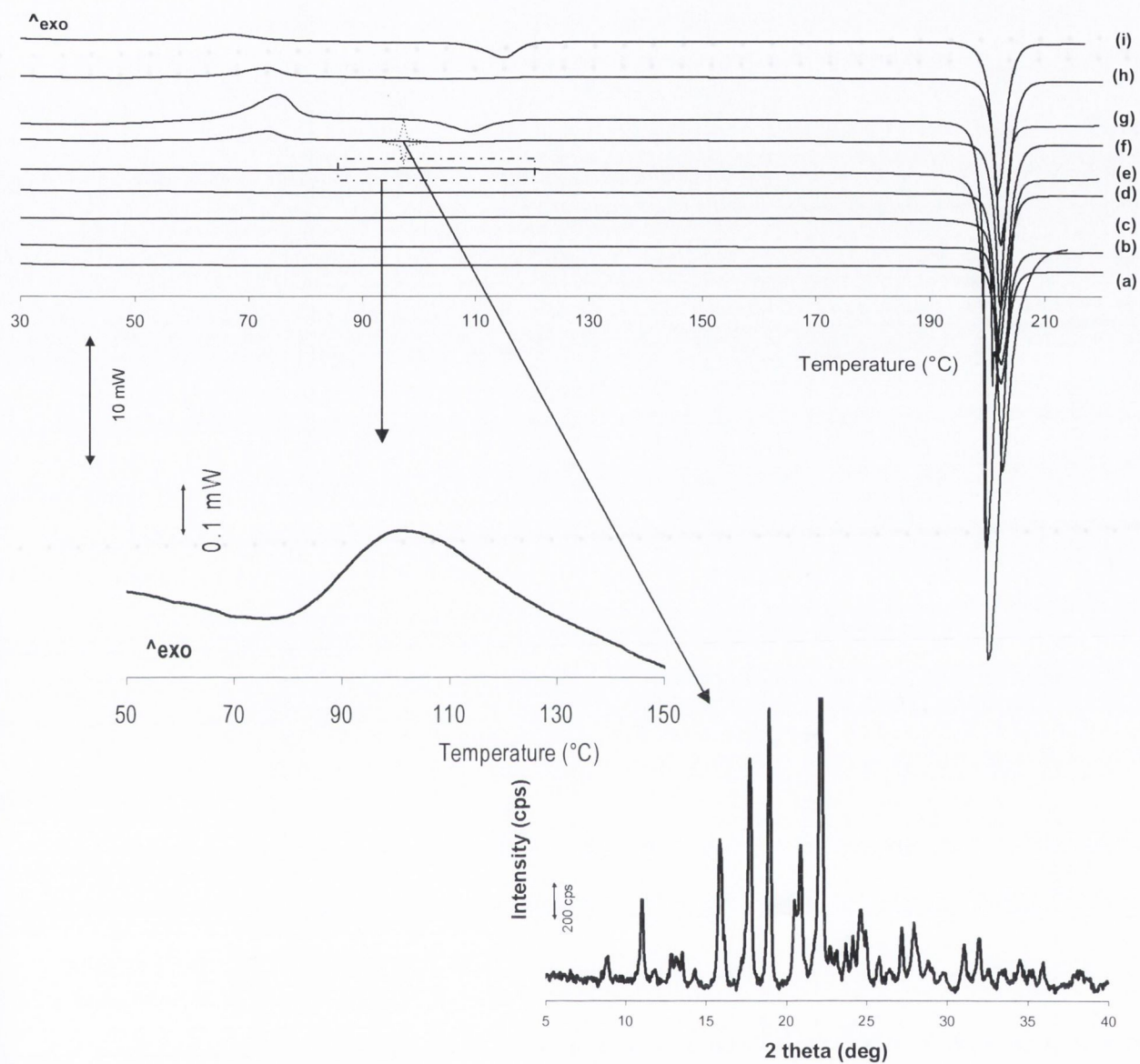


Figure 5.29: DSC thermograms STZ I unmilled (a) and milled STZ I at RT for (b) 5 minutes; (c) 30 minutes; (d) 60 minutes; (e) 120 minutes and (f) 5 hours; (g) 10 hours; (h) 15 hours and (i) 20 hours. The magnified image corresponds to the crystallisation exothermic event detected after 120 minutes. The PXRD was collected after the 5 hours milled sample was heated to 95 °C.

Table 5.13: Thermal properties of unmilled STZ I and STZ I milled samples at RT with a BTP weight ratio of 40:1.

Milling time (minutes)	T_{poly} ($^{\circ}\text{C}$)	ΔH_{poly} (J/g)	T_{cr} ($^{\circ}\text{C}$)	ΔH_{cr} (J/g)	T_{m} ($^{\circ}\text{C}$)	ΔH_{m} (J/g)	DSC amorphous content (%)	TGA (%)
STZ I					201 (0.18)	111 (0.51)	0.00 (0.00)	0.93 (0.28)
5					201 (0.19)	127 (0.48)	0.00 (0.00)	1.49 (0.31)
30					201 (0.19)	139 (0.91)	0.00 (0.00)	3.81 (0.29)
60					200 (0.22)	105 (0.84)	0.00 (0.00)	3.92 (0.41)
120			87 (0.54)	3 (0.18)	199 (0.17)	116 (0.37)	2.02 (1.21)	3.77 (0.18)
300	95 (0.15)	5 (0.14)	61 (0.43)	5 (0.37)	201 (0.16)	106 (0.97)	4.17 (0.94)	4.19 (0.48)
600	102 (0.27)	8 (0.11)	66 (1.07)	20 (1.11)	201 (0.19)	120 (0.33)	15.03 (1.42)	6.09 (0.72)
900	98 (1.31)	1 (0.02)	65 (0.93)	13 (0.82)	201 (0.27)	102 (0.21)	11.80 (1.49)	3.94 (0.63)
1200	109 (0.98)	21 (0.91)	62 (0.99)	9 (0.38)	201 (0.16)	106 (0.46)	7.78 (0.73)	3.55 (0.17)

T_{poly} = onset temperature of solid state transition, ΔH_{poly} = enthalpy of solid state transition, T_{cr} = onset temperature of crystallisation, ΔH_{cr} = enthalpy of crystallisation, T_{m} = onset temperature of melt, ΔH_{m} = enthalpy of melt. TGA = thermogravimetric analysis. Standard deviation in parentheses. n=4

5.5.3 Particle size, surface area and morphology

Particle size analysis by Malvern laser diffraction is given in Table 5.14 and the distribution trends for each sample are compared in Figure 5.30. Analysis of the particle size distribution showed that the d10 of the unmilled material was $2.47 \pm 0.11 \mu\text{m}$ and the d90 was $14.42 \pm 0.17 \mu\text{m}$. Ball milling resulted in a change to the distribution shape from monomodal for the unmilled STZ I samples to a bi- or tri- modal distribution for the ball milled STZ I powders (Figure 5.30). An particle size decrease was observed as a result of ball milling for 5 minutes as the median particle size was reduced to $7.06 \pm 0.22 \mu\text{m}$, from $7.58 \pm 0.07 \mu\text{m}$ for the unmilled STZ I powder. Further milling for 30 minutes resulted in the particle size to increase and as

milling time increased the particle size increased. This event was unusual as ball milling is commonly used to reduce the particle size, not to increase it.

Statistically comparing the median particle size by Tukey's multiple comparison test showed that there was no significant difference between the 5 and 30 minute milled samples. The 60 minute milled samples had a median particle size that was statistically the same as the median particle sizes obtained for 30 minutes and 120 minutes, but it was different to the median particle sizes measured for the samples milled for a total of 5 hours or longer. This suggests that ball milling of STZ I for 120 minutes or longer (up to 20 hours) results in an increased median particle size. Statistically comparing the d90 values by Tukey's multiple comparison test showed a difference between STZ I unmilled and STZ I milled sample for 60 minutes. STZ I milled for 60 minutes was statistically different to all other STZ I milled materials. The increased d90 value could also be attributed to the formation of the agglomerated structures. The presence of the agglomerated particles is shown in the morphology in Figure 5.31.

Table 5.14: Particle size distribution obtained by Malvern laser diffraction for STZ I unmilled and milled at RT with a BTP weight ratio of 40:1 from 5 minutes to 20 hours

Milling conditions	Time (minutes)	Particle size		
		d10 (μm)	d50 (μm)	d90 (μm)
BTP weight ratio 40:1, RT	STZ I	2.47 (0.11)	7.58 (0.07)	14.42 (0.17)
	5	1.40 (0.02)	7.06 (0.22)	65.91 (6.39)
	30	1.70 (0.20)	8.07 (0.76)	59.54 (0.10)
	60	1.68 (0.17)	9.20 (1.66)	185.36 (17.51)
	120	1.85 (0.15)	10.08 (0.95)	108.41 (25.32)
	300	2.21 (0.43)	10.45 (1.39)	84.91 (21.25)
	600	1.86 (0.05)	9.76 (0.73)	103.82 (11.39)
	900	1.85 (0.01)	10.94 (0.31)	156.04 (8.53)
	1200	2.24 (0.47)	13.70 (2.18)	151.39 (14.72)

Standard deviation in parentheses, n=3

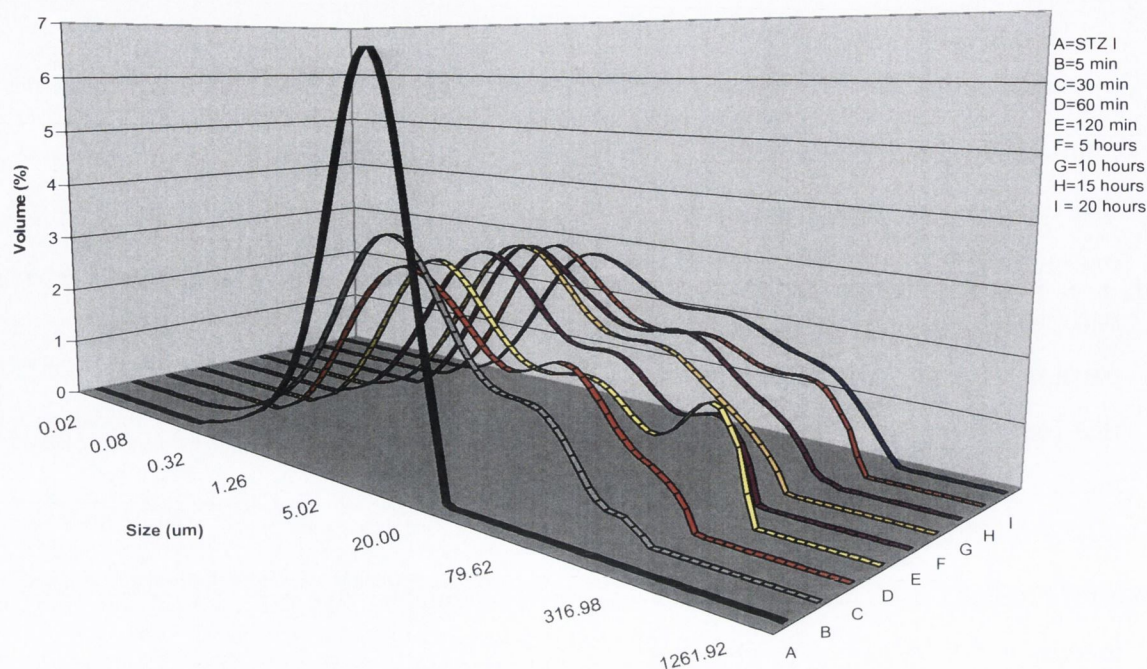


Figure 5.30: Particle size distribution measured by Malvern laser diffraction for STZ I unmilled and milled at RT with a BTP weight ratio 40:1 from 5 minutes to 20 hours.

A decrease in the particle size was reflected in the increased specific surface area (SSA) measured by BET (Table 5.15). As a result of milling for 5 minutes, the SSA of STZ I unmilled was $1.66 \pm 0.26 \text{ m}^2/\text{g}$, and this increased to $5.08 \pm 0.16 \text{ m}^2/\text{g}$. The change of the SSA and particle size distribution with milling time can be attributed to the formation of clusters and/or agglomerates which are observed by SEM analysis (Figure 5.31). Comparing these micrographs to the unmilled material (Figure 5.4) a clear reduction in particle size was evident. Unlike the particles that were observed as a result of ball milling STZ III-Y, which consisted of small round particles that appeared to coat a platelet structure, these were irregular in shape and appeared to be agglomerates of small particles. Therefore, the increased particle size may be attributed to the agglomerated particles.

Table 5.15: Specific surface area by BET of STZ I unmilled and milled from 5 minutes to 20 hours at RT with a BTP weight ratio 40:1.

Ball milling time (minutes)	STZ I (m ² /g)
0	1.66 (0.26)
5	5.08 (0.16)
30	3.54 (0.06)
60	4.91 (0.02)
120	5.22 (0.22)
300	3.98 (0.10)
600	4.48 (0.18)
900	4.96 (0.21)
1200	5.27 (0.19)

Standard deviation in parentheses, n=3

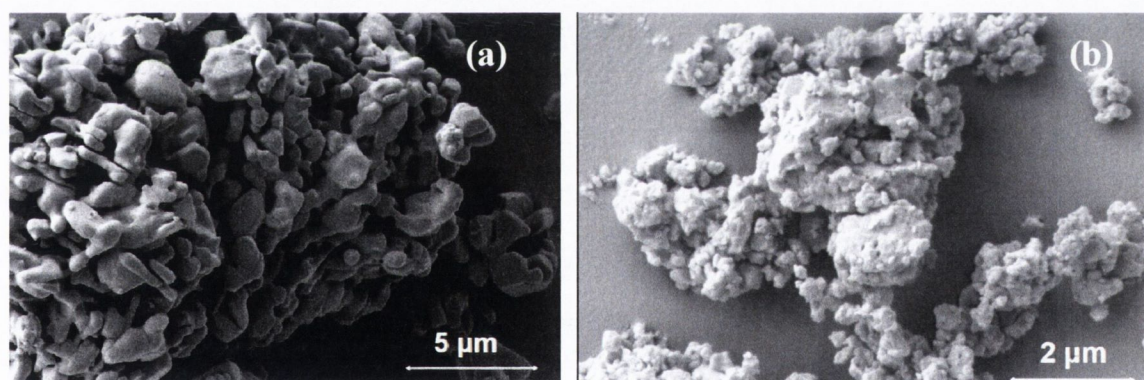


Figure 5.31: SEM morphology of STZ I milled (a) for a 120 minutes and (b) 10 hours at RT with a BTP weight ratio of 40:1.

5.5.2 Storage of the ball milled samples

5.5.2.1 Powder X-ray diffraction

Several ball milled STZ I samples were stored at 4 °C over phosphorous pentoxide for 24 hours. The samples analysed included those that were milled for 120 minutes, 5 and 20 hours with a BTP weight ratio of 40:1 at RT. This was carried out to observe the changes to the induced amorphous content and if there was a change in the polymorphic form as a result of

storage. The PXRD patterns are given in Figure 5.32 and they are compared to the Form I and III simulated x-ray patterns obtained from single crystal data obtained from CCDC theoretical and the unmilled PXRD of the STZ I. The diffractogram for STZ I milled for 120 minutes (Figure 5.32 (d)) consisted of Bragg peaks characteristic of Form I. The peaks were more distinct in comparison to those observed directly after milling (Figure 5.28 (g)). Peak area analysis showed that the total PXRD peak area measured after 24 hours of storage was 59.73 ± 3.41 %, compared to 37.57 ± 0.04 % measured directly after milling for STZ I milled for 120 minutes. The diffractogram for STZ I milled for 5 hours and stored is shown in Figure 5.32 (e) and was crystalline in nature as distinct Bragg peaks were detected. These peaks resemble more Form III than Form I, with peaks detected at 15.4 2θ and a doublet peak at 20.0 2θ . The peak area increased from 34.86 ± 0.06 % to 62.19 ± 1.72 %, indicating a change in crystallinity over the storage period. Ball milling for 20 hours and storage for 24 hours resulted in a predominately crystalline sample, with Bragg peaks characteristic of the Form I and Form III detected. Peak area measured directly after milling was 35.61 ± 5.30 % and after 24 hours it increased to 64.38 ± 4.98 %.

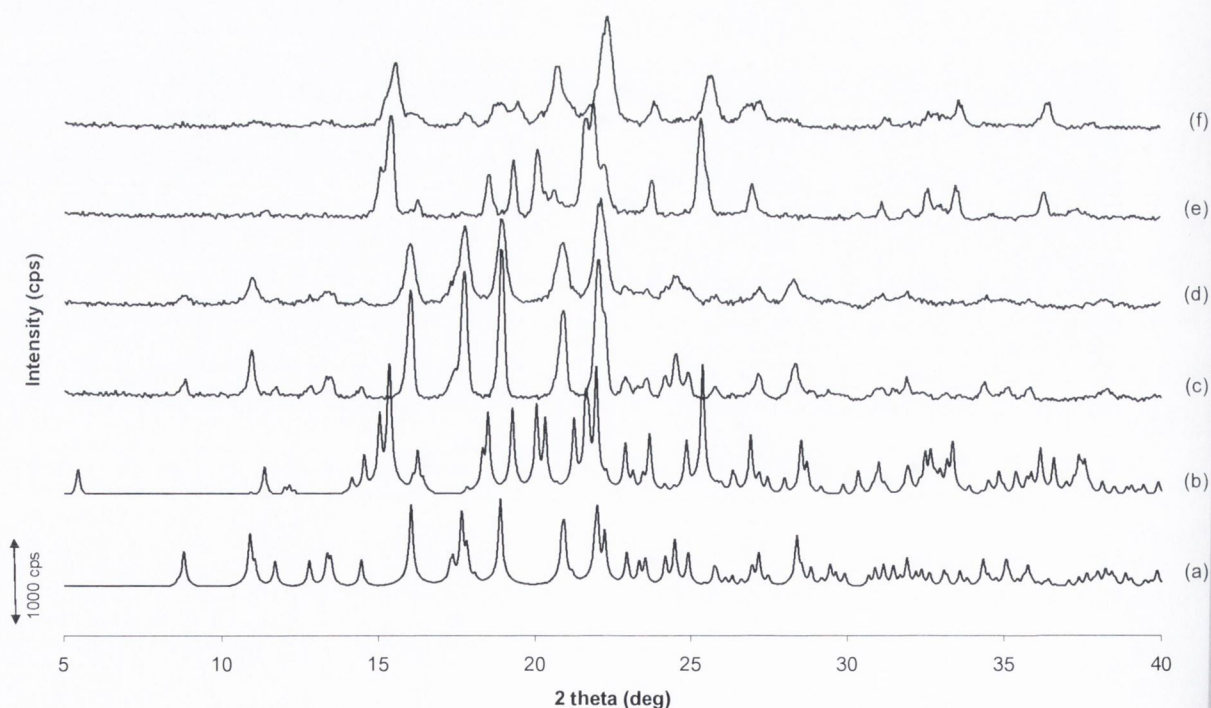


Figure 5.32: PXRD of (a) CCDC pattern of STZ I; (b) CCDC pattern of STZ III; (c) STZ I unmilled; (d) STZ I milled 120 minutes, tested after 24 hours; (e) STZ I milled for 5 hours, tested after 24 hours; (f) STZ I milled for 20 hours, tested after 24 hours.

5.5.2.2 Thermal analysis

Figure 5.33 shows the thermal analysis of the STZ I samples that were ball milled for 120 minutes, 5 hours and 20 hours and were stored at 4 °C over phosphorous pentoxide for 24 hours. Storage of the 120 minute ball milled STZ I samples had one thermal event, detected by DSC analysis, which was characteristic of a melt at ~201 °C. The DSC amorphous content present after milling crystallised, and the melt enthalpy changed from 116 J/g to 120 J/g over the storage period. Two thermal events were detected for the 5 hours and 20 hours milled STZ I after they were stored for 24 hours. The thermal events corresponded to a phase transition of one polymorphic form to Form I and the melting of Form I. The amorphous phase detected directly after milling completely crystallised for both samples. The phase transition detected for STZ I milled for 5 hours directly after milling was detected at ~95 °C with an enthalpy of ~5 J/g, after 24 hours this transition shifted to ~131 °C and the enthalpy increased to ~26 J/g. This indicated a decrease of Form I present within the sample and an increase of different polymorphic forms. The phase transition detected for STZ I milled for 20 hours shifted from ~109 °C with an enthalpy of ~21 J/g to ~103 °C, with enthalpy measured at ~10 J/g. This would suggest that the polymorphic forms changed during the storage period. The melt enthalpy for the three milled materials stored was ~120 J/g.

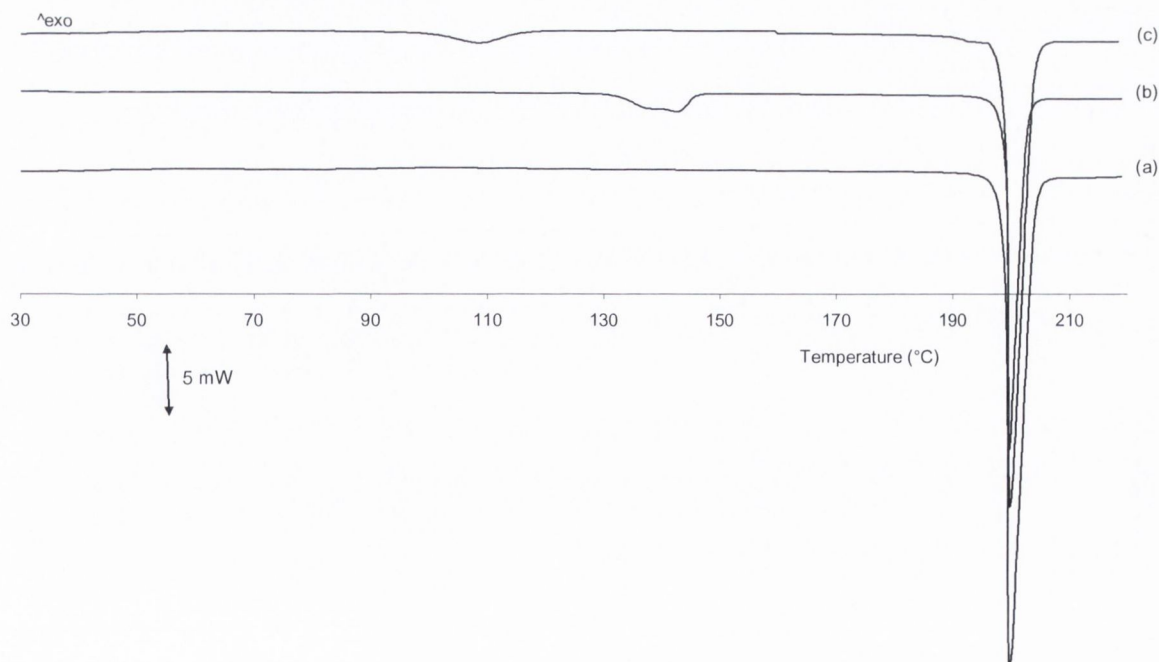


Figure 5.33: DSC thermograms of STZ I milled for (a) 120 minutes: (b) 5 hours and (c) 20 hours. Tested 24 hours after milling.

Changes to the solid state nature of sulfathiazole as a result of spray drying were described by Bianco *et al.*, (2012). An amorphous phase was detected directly after spray drying, characterised by PXRD and thermal analysis. Storage at ambient temperature over 24 hours resulted in two thermal events detected by DSC, the first attributed to the phase transition of Form II and/or Form III to Form I followed by a melt endotherm of Form I. The authors stated that endothermic transition detected were not the same for different samples, indicating a variable amount of polymorphs in the completely crystallised products.

Comparing the two polymorphs, STZ I and STZ III-Y, that were ball milled at RT with a BTP weight ratio of 40:1, showed that different levels of disorder were induced. Quantification of the induced amorphous content by DSC, showed that a level of disorder was easier to induced into the STZ III-Y structure. For example, 3.40 ± 1.71 % was induced after a total of 30 minutes of milling STZ III-Y, while a total of 120 minutes was required to induced a DSC amorphous content of 2.02 ± 1.21 % into the STZ I material. From the ball milling times investigated in this study, the highest level of DSC amorphous content obtained as a result of ball milling STZ III-Y for 5 hours was 25.11 ± 2.67 %. In contrast to this, STZ I required a total of 10 hours of ball milling to obtain a DSC amorphous content of 15.03 ± 1.42 %. This was the highest DSC amorphous content reached in this study for STZ I ball milled. Regardless of the different levels of amorphous content induced, prolonged ball milling eventually resulted in a fluctuation in the amorphous content measured. For example ball milling for 20 hours resulted in a DSC amorphous content of 7.78 ± 0.73 % and 4.45 ± 0.04 %, for STZ III-Y and STZ I, respectively. Form III is stable at RT while Form I is stable above 170 °C (Munroe *et al.*, 2012). These results showed a higher amorphous phase maybe induced into the more stable polymorphic form, as opposed to the metastable form, if ball milled. It is possible the induced amorphous phase, that was induced into the STZ I materials, was used as an intermediate phase, which resulted in crystallisation to the more stable form.

5.6 Sulfathiazole sodium salt (STZNa)

The level of disorder induced as a result of ball milling was different for the two sulfathiazole polymorphs. Therefore, it was of interest to investigate the affect ball milling had on the salt form of sulfathiazole. Sulfathiazole sodium salt was ball milled at RT with a ball to powder

weight ratio for 5, 30, 60 120 minutes and 5 and 10 hours and to investigate the changes incurred upon milling the effects of milling for 1 minute was also investigated.

5.6.1 Sulfathiazole sodium salt unmilled

5.6.1.1 Powder X-ray diffraction

The PXRD for STZNa (Sigma, Ireland) is shown in Figure 5.34 (a). The distinct Bragg peaks indicate a crystalline structure. The unmilled material was assumed to be 100% crystalline in nature. The PXRD obtained after exposing STZNa to a sorption-desorption cycle (0%RH up to 90%RH and back to 0%RH) by DVS confirmed that the unmilled material was crystalline in nature (data not shown). The crystallinity of the material was confirmed by DVS as no recrystallisation event was detected. The PXRD diffractogram obtained after the DVS analysis was different to the received material (Figure 5.34 (b)). The distinct Bragg peaks indicate a crystalline material. This shows that exposure to high humidity levels may result in the formation of a hydrate. Similar patterns were reported by Bianco *et al.*, (2012) for both the unmilled STZNa material and the sample collected after DVS analysis. The material exposed to high levels of humidity was reported to form a sesquihydrate structure (Bianco *et al.*, 2012).

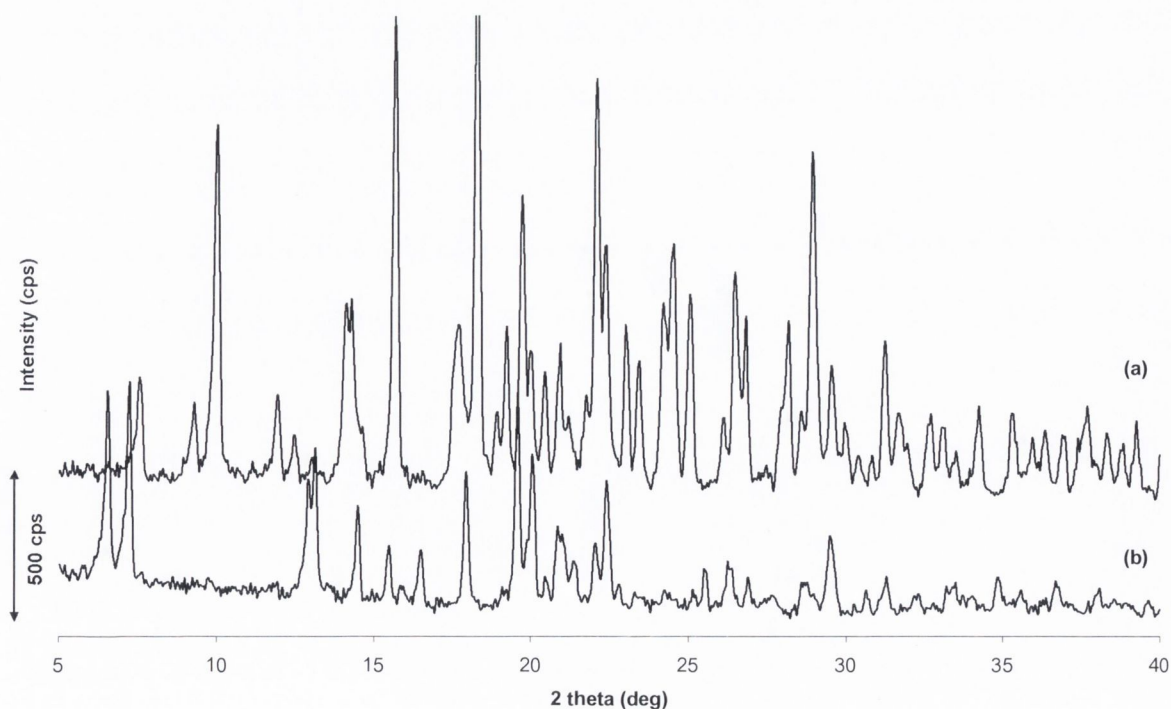


Figure 5.34: PXRD of STZNa (a) material received from Sigma, Ireland and (b) after DVS sorption, de-sorption cycle.

5.6.1.2 Thermal analysis

Thermal analysis by DSC (Figure 5.35 (a)) of the STZNa unmilled material showed an endothermic peak detected below 100 °C. This was attributed to the removal of residual solvent. This was followed by a melt endothermic event, with an onset of ~267 °C. The corresponding TGA thermogram, shown in Figure 5.35 (b) indicated that a mass loss of ~3.8 % (w/w) occurred between 25 to 110 °C. This mass loss was too low to be associated with a completely hydrated form. Therefore, it could be associated with a residual level of moisture that was adsorbed from the environment or it may be due to a partially hydrated structure that existed within the materials structure. As PXRD and DVS analysis confirmed a completely crystalline material, the change in mass loss was associated with a partially hydrated structure. Mass loss of ~5 % detected during melting indicated degradation of the material. This was confirmed by the burnt black substances collected from the TGA after heating to 280 °C. Comparing the non-salt forms with the sodium salt, showed a difference of ~65 °C between the melt temperatures.

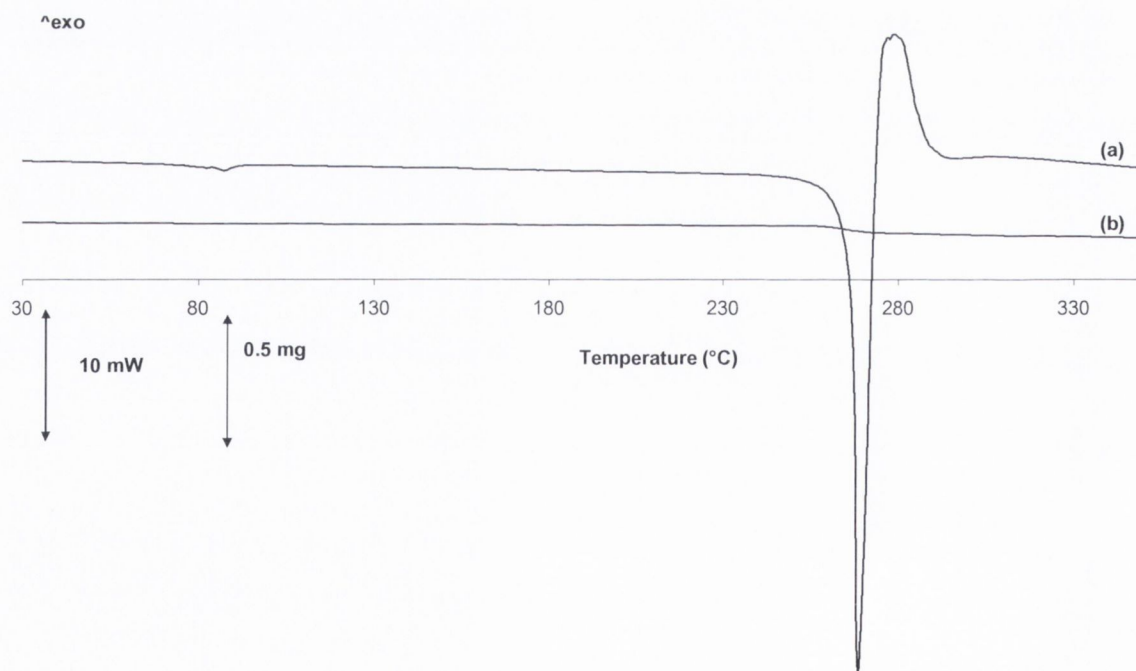


Figure 5.35: (a) DSC and (b) TGA thermogram of STZNa received from Sigma, Ireland.

5.6.1.3 Morphology

Figure 5.36 illustrates the micrographs obtained by SEM for STZNa material received from Sigma, Ireland. The particles are irregular in shape and size. Figure 5.36 (a), showed that the particle size range can exceed 100 μm . A closer look at the particle in Figure 5.36 (b), showed that the surface of the material has a number of pores. With a porous structure it is possible that residual water from the environment could become trapped within the structure, only to be released during heating or processing. The morphology of sulfathiazole Form I and III could be either needle or platelet like, depending on the polymorphic form or how the material was produced, which was very different to the irregularly shaped structure observed for the sodium salt.

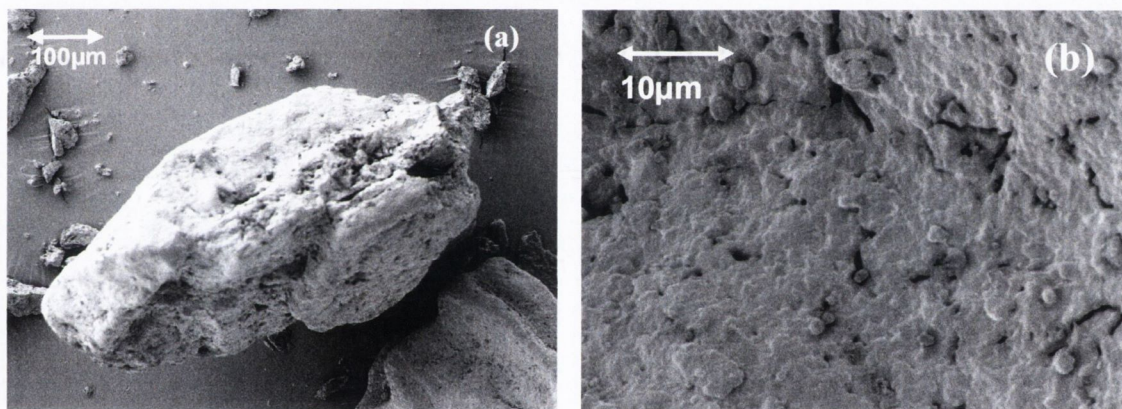


Figure 5.36: SEM of STZNa material received from Sigma Ireland.

5.6.2 Sulfathiazole sodium salt ball milled

5.6.2.1 Powder X-ray diffraction

PXRD patterns of sulfathiazole sodium salt (STZNa) received from Sigma and the samples that were ball milled at RT with a BTP weight ratio of 40:1 for 1, 5, 30, 60, 120 minutes and 5 and 10 hours are shown in Figure 5.37. Analysis was carried out immediately after each milling period. Distinct Bragg peaks detected for the received material indicated a crystalline structure. Ball milling for 1, 5, 30 and 60 minutes resulted in the PXRD peak intensity to decrease with increased milling time. Changes to the total peak area are outlined in Table 5.16 and Figure 5.38. Ball milling for 1 and 5 minutes resulted in the peak area decrease to $\sim 95\%$. Further milling for 30 and 60 minutes resulted in a decrease of the peak area to $64.32 \pm 1.61\%$ and $62.30 \pm 4.43\%$, respectively. According to Tukey's multiple comparison test, there was no

statistical difference between the peak areas measured for STZNa milled for 1 and 5 minutes and between STZNa milled for 30 and 60 minutes. Prolonged milling for 120 minutes resulted in minor Bragg peaks detected and the presence of an amorphous halo indicating a predominantly disordered phase and the total peak area was reduced to $12.70 \pm 1.57\%$ after 120 minutes. Further milling for a total of 5 hours resulted in no detected Bragg peaks, indicating a transformation to an amorphous phase. A disordered phase was also detected after 10 hours of ball milling. The halo observed for both disordered phases obtained after 5 and 10 hours of milling were slightly different (Figure 5.39). The pattern of the amorphous halo detected after milling for 10 hours had three distinct bumps unlike STZNa milled for 5 hours which had two bumps. This may suggest that a residual level of crystallinity remained in the STZNa material after a total of 5 hours of milling.

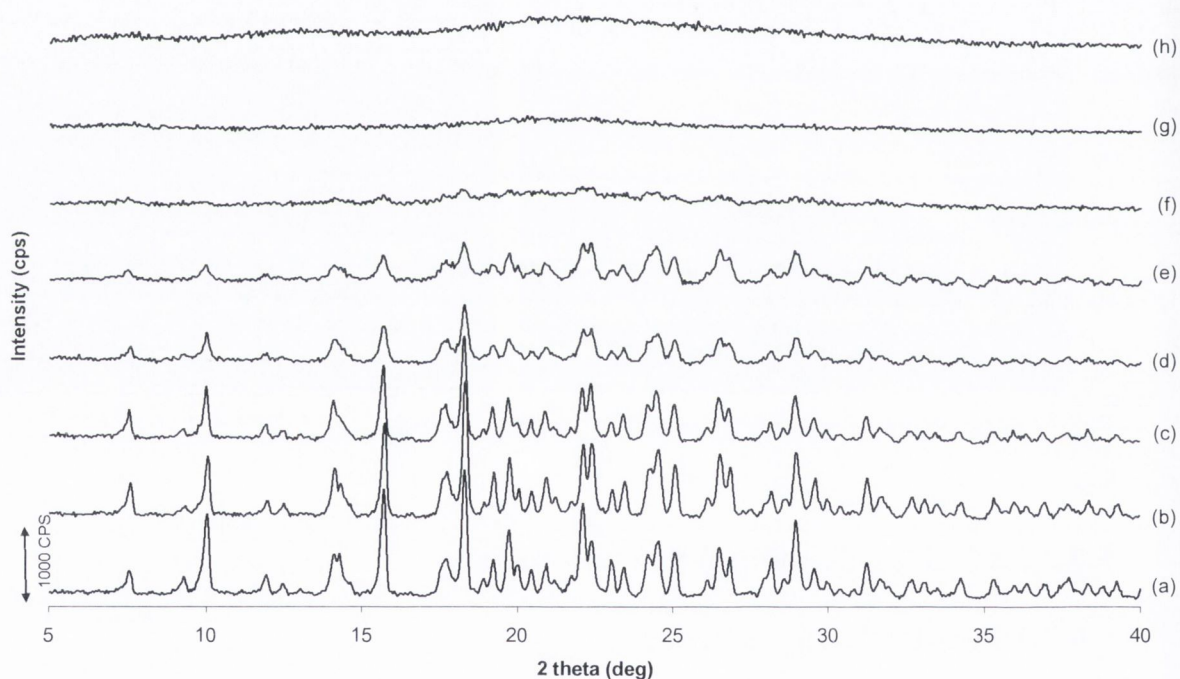


Figure 5.37: PXRD of (a) STZNa unmilled and milled at RT with a BTP weight ratio of 40:1 for (b) 1 minute; (c) 5 minutes; (d) 30 minutes; (e) 60 minutes; (f) 120 minutes; (g) 5 hours and (h) 10 hours.

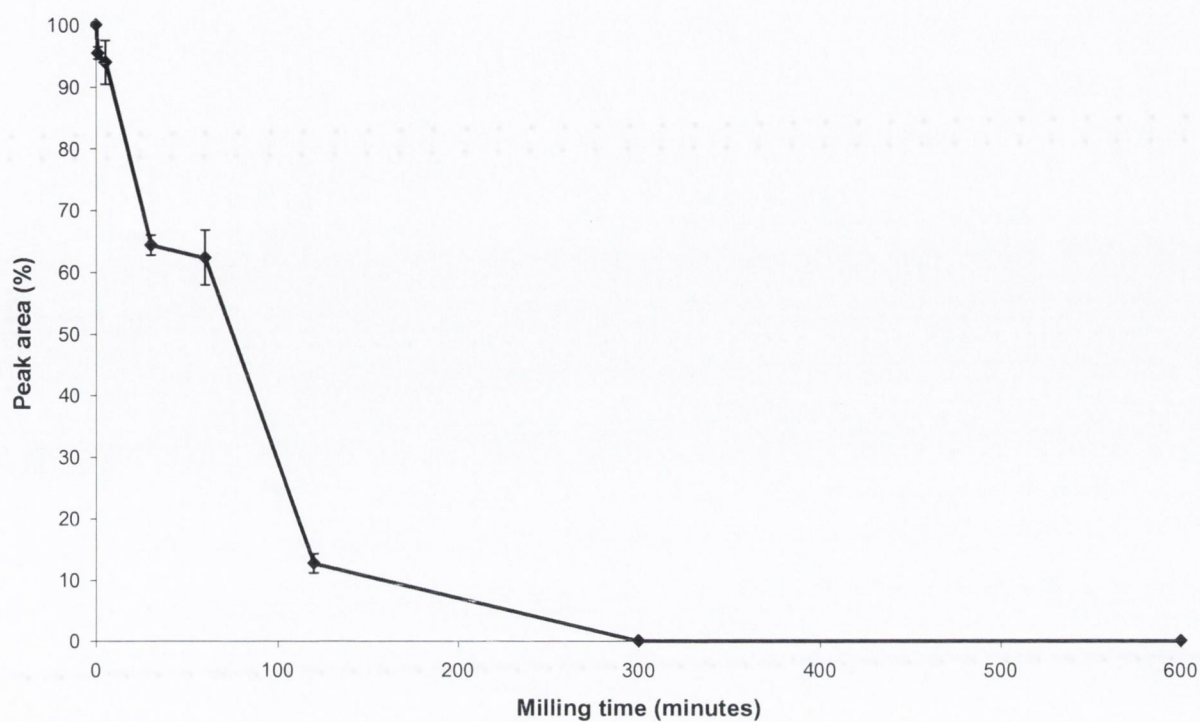


Figure 5.38: Total peak area change to STZNa as milling time is increased.

Table 5.16: PXRD total peak area changes for STZ I milled from 5 minutes to 20 hours at RT.

Milling time (minutes)	PXRD peak area (%)
0	100.00 (0.00)
1	95.44 (0.98)
5	93.92 (3.54)
30	64.32 (1.61)
60	62.30 (4.43)
120	12.70 (1.57)
300	0.00 (0.00)
600	0.00 (0.00)

Standard deviation in parentheses. n=3

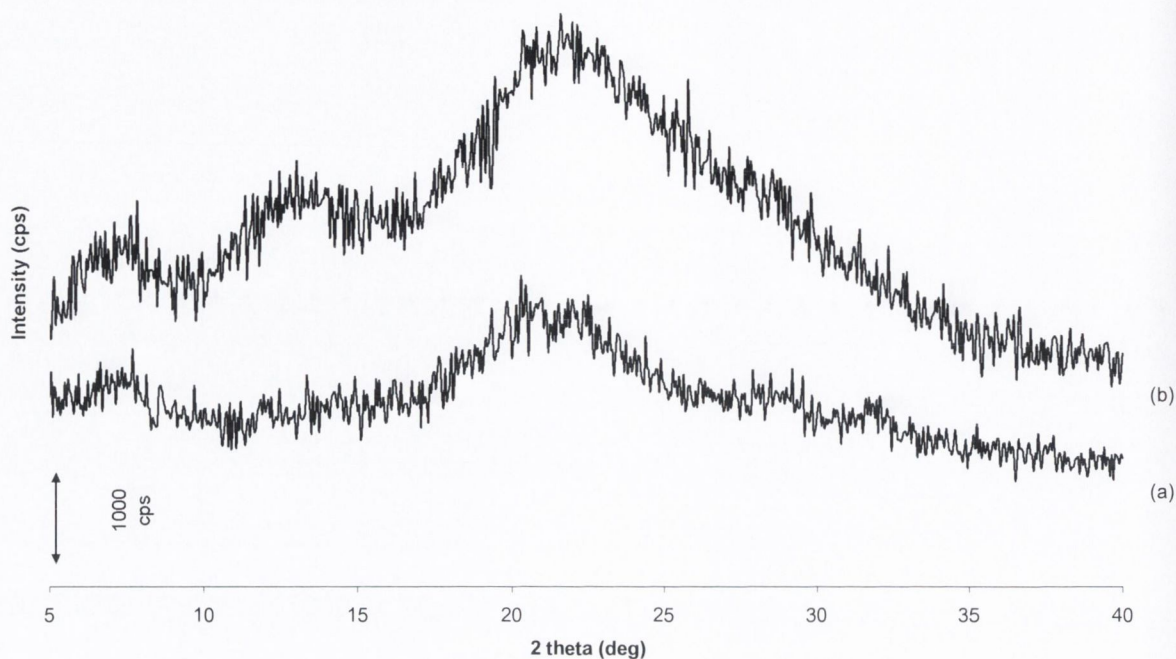


Figure 5.39: PXRD of STZNa milled for (a) 5 hours and (b) 10 hours at RT with a BTP weight ratio of 40:1.

5.6.2.2 Thermal analysis

Thermal analysis by DSC for STZNa unmilled and milled at RT for 1, 5, 30, 50, 120 minutes and 5 and 10 hours is shown in Figure 5.40. Part of the thermogram, from 25 and 160 °C, is also shown in Figure 5.40 so that the thermal events that were detected in this region could be observed clearly. The thermal properties of the STZNa received material (unmilled) were discussed previously (Section 5.6.1.3). STZNa milled for a total of 1, 5 and 30 minutes (b, c and d in Figure 5.40) resulted in two thermal events similar to those observed for the unmilled material. The first was related to a dehydration endothermic step, detected below 100 °C and the second event was associated with a melt endotherm, with an onset at ~268 °C. Ball milling for 60 and 120 minutes resulted in a double endothermic peak corresponding to the loss of moisture. The total loss of moisture measured by thermogravimetric analysis (TGA) showed that from 25 °C to 120 °C the mass loss for STZNa milled for 60 minutes was 3.98 ± 0.09 % and was 4.46 ± 0.01 % for STZNa milled for 120 minutes. No crystallisation peak was detected for the STZNa samples that were milled for a total of 1, 5, 30, 60 and 120 minutes. This change may suggest that the change in PXRD peak area could be attributed to the changes such as a reduction in crystallite size. Analysis of the melt onset temperature and enthalpy for the ball milled samples, given in Table 5.17, showed that as a result of increased milling time

a decrease in the melt temperature and enthalpy was observed. This change was first observed in this study for the ball milled sulfadimidine samples and the peak broadening observed in the PXRD diffractogram was attributed to the decrease in crystallites. The change in crystallite size was shown to result in a decrease of the melting temperature and was described as the Gibbs-Thomas law. Therefore, the initial peak area decrease, observed by PXRD, may be attributed to a decrease in crystallite size and not an induced amorphous phase.

Several factors have been found to affect the position of the melt onset and the enthalpy of melt. Ng *et al.*, (2010) investigated the effect milling had on the structure of adipic acid and found that as a result of residual moisture trapped within the samples structure, a decrease in melt onset and enthalpy were observed. Niraj *et al.*, (2010) found that ball milling of griseofulvin resulted in a decrease in melt enthalpy and onset temperature. They attributed the changes to structural changes that occurred upon milling such as new surfaces, cracks and defects. These two factors (surface changes and trapped moisture) could both contribute to the changes observed upon milling STZNa.

Ball milling for 5 and 10 hours resulted in four thermal events, the first was attributed to the loss of moisture from the sample detected between 25 and 110 °C, the second was a glass transition temperature (T_g) at ~123 °C for both samples, this was followed by a crystallisation exotherm at ~133 °C and then a melt endotherm at ~260 °C. The onset temperatures for these events were similar for both samples but the enthalpy was different (Table 5.17). Ball milling for 5 and 10 hours resulted in the induced DSC amorphous content of 70.54±1.16 % and 71.15±0.59 %, respectively. This suggests that with prolonged milling at RT with a BTP weight ratio of 40:1 for up to 10 hours, the majority of the STZNa crystalline order was replaced by an amorphous phase.

The mass loss determined by TGA between 25 and 120 °C and from 120 to 270 °C is given in Table 5.17. Mass loss at the lower temperature range can be associated with residual water bound to the surface of the material. Mass loss at the higher temperatures could be due to the fact that water was trapped as inclusions during the milling process and as the sample was heated it allowed the sample to release the water slowly (Ng *et al.*, 2010). Degradation of the sample during milling may result in a significant mass decrease. Each sample appeared burnt

after analysis indicating degradation occurred upon melting. High mass loss between the crystallisation exothermic event and the melt could indicate thermal decomposition.

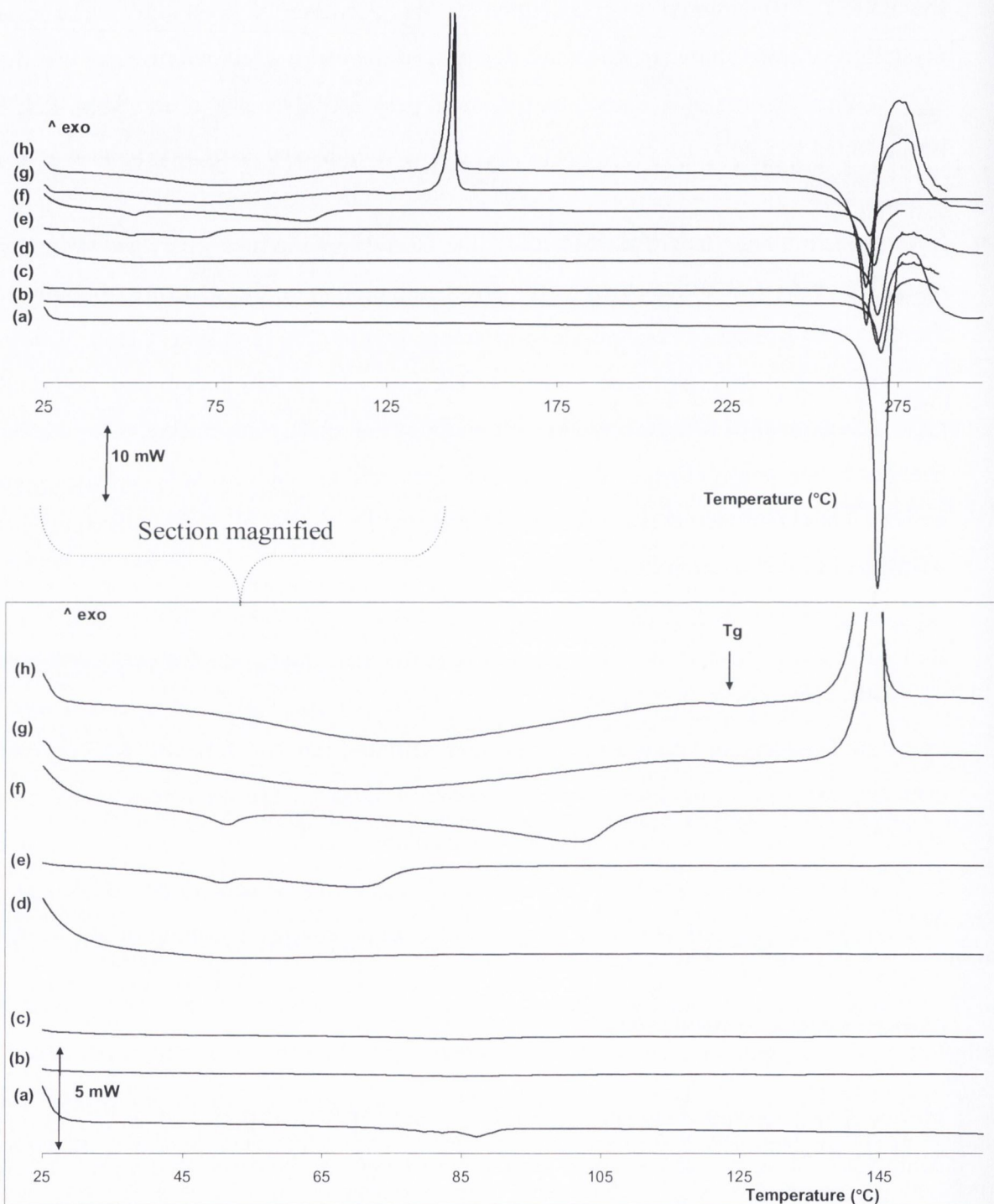


Figure 5.40: DSC thermograms of (a) STZNa received from Sigma (unmilled) and STZNa milled (b) 1 minute; (c) 5 minutes; (d) 30 minutes; (e) 60 minutes; (f) 120 minutes; (g) 5 hours and (h) 10 hours. The events between 25 and 160 °C are also shown.

Table 5.17: Thermal properties of unmilled STZNa and STZNa milled samples at RT with a BTP weight ratio of 40:1.

Milling time (minutes)	T _g (°C)	T _{cr} (°C)	ΔH _{cr} (J/g)	T _m (°C)	ΔH _m (J/g)	DSC	TG mass loss (%)	
						amor. content (%)	25-120 °C	120-270 °C
0				267	209	0.00	3.50	4.56
				(0.15)	(0.31)	(0.00)	(0.46)	(1.08)
1				267	168	0.00	2.60	3.20
				(0.09)	(0.14)	(0.00)	(0.07)	(0.08)
5				265	174	0.00	2.68	4.01
				(0.10)	(0.19)	(0.00)	(0.07)	(0.32)
30				263	205	0.00	2.82	2.43
				(0.08)	(0.16)	(0.00)	(0.27)	(0.45)
60				263	187	0.00	3.98	2.32
				(0.13)	(0.21)	(0.00)	(0.09)	(0.09)
120				262	142	0.00	4.46	2.34
				(0.14)	(0.28)	(0.00)	(0.01)	(0.01)
300	123	142	74	260	210	70.54	3.21	3.92
	(0.12)	(0.33)	(1.24)	(0.07)	(0.79)	(1.16)	(0.49)	(0.50)
600	123	142	78	260	211	71.15	4.01	4.56
	(0.17)	(0.47)	(0.33)	(0.04)	(0.15)	(0.59)	(1.07)	(0.46)

Standard deviation in parentheses. n=3 Note: amor. = amorphous content.

5.6.2.3 Particle size, specific surface area and morphology

Table 5.18 outlines the particle size measured by laser diffraction and the specific surface area determined by BET of STZNa unmilled and milled. A decrease in the particle size distribution was evident after one minute. The median particle size was reduced from $84.45 \pm 4.01 \mu\text{m}$ for STZNa unmilled to $9.22 \pm 0.64 \mu\text{m}$ as a result of ball milling for one minute. There was a significant particle size decrease, when comparing each milled sample to the unmilled material. The unmilled material had a monomodal distribution (Figure 5.41). As a result of milling a bi or tri-modal distribution was obtained. A statistically significant difference was

observed between STZNa milled for 1 minute and STZNa milled for all other time periods. Tukey's multiple comparison test showed a difference between the d_{10} value for STZNa milled for 5 and 60 minutes. A statistical difference between the median size ranges was observed between samples milled for 1 and 60 minutes; 5 and 60 minutes and 1 and 5 hours and. No statistical difference was found between any other median size measurements. The d_{90} values obtained for all samples milled were lower than the unmilled material. It can be seen from the distribution shown in Figure 5.41 that an overall reduction in the particle size was evident, but a fraction of the material exists as larger particles or as agglomerated structures.

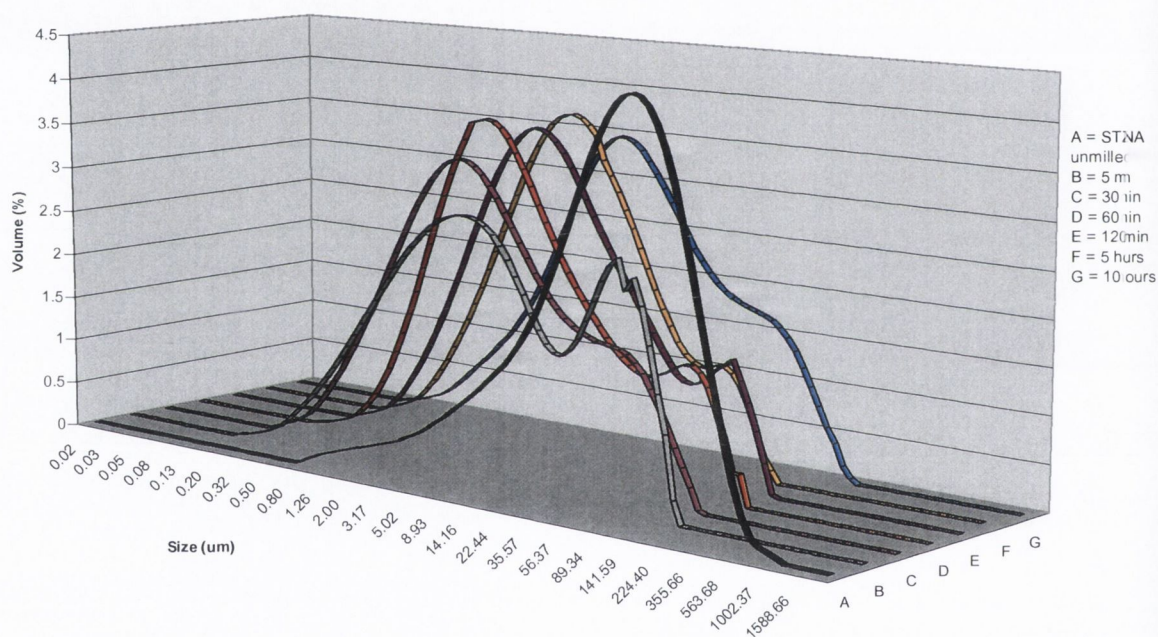


Figure 5.41: 3D representation particle size distribution determined by Malvern laser diffraction of STZNa unmilled and milled at RT from 5 minutes to 10 hours with a BTP weight ratio of 40:1 and a rotational speed of 400rpm.

Analysis of the specific surface area (SSA) by BET showed an increase from $0.34 \pm 0.04 \text{ m}^2/\text{g}$ for STZNa unmilled to 2.17 ± 0.11 and $3.11 \pm 0.11 \text{ m}^2/\text{g}$ after 1 and 5 minutes of milling, respectively. Increasing the milling time to 30 minutes resulted in a further increase in SSA to $8.21 \pm 0.09 \text{ m}^2/\text{g}$. Continued milling resulted in a decrease of the SSA, with a value of $7.37 \pm 0.24 \text{ m}^2/\text{g}$ obtained after 60 minutes of milling. Statistically comparing the SSA showed that no significant difference was detected between the samples milled for the following; 60

and 120 minutes, 60 and 5 hours and 60 and 10 hours and between 5 and 10 hours. An increase in the SSA of a material may result from the formation of agglomerated particles as a result of an increased amorphous phase.

Table 5.18: Particle size for STZNa obtained by Malvern laser diffraction, specific surface area (SSA) by BET for the unmilled and ball milled samples.

Time	Particle size			BET SSA
	d10 (μm)	d50 (μm)	d90 (μm)	m^2/g
Unmilled	11.02 (0.49)	84.45 (4.01)	250.12 (37.93)	0.34 (0.04)
1 min	1.54 (0.17)	9.22 (0.64)	66.09 (3.57)	2.17 (0.11)
5 min	1.28 (0.04)	8.54 (0.27)	75.08 (2.76)	3.11 (0.02)
30 min	1.05 (0.09)	5.09 (0.11)	41.66 (2.66)	8.21 (0.09)
60 min	1.04 (0.06)	4.40 (0.07)	38.82 (5.14)	7.37 (0.01)
120 min	1.10 (0.02)	5.37 (0.32)	54.19 (12.51)	7.78 (0.24)
5 hr	1.07 (0.11)	4.71 (0.62)	30.31 (0.04)	7.20 (0.10)
10 hr	1.27 (0.02)	6.86 (0.13)	53.47 (3.23)	6.97 (0.16)

Standard deviation in parentheses. n=3

The morphology of ball milled STZNa after 5, 120 minutes and 10 hours is shown in Figure 5.42 (a), (b) and (c), respectively. Ball milling for 5 minutes produced a morphology that consisted of smaller particles ranging from 1 to 5 μm in size which assembled in agglomerated structures; these were dispersed throughout the material among the finer particles and among them was an occasional larger particle (Figure 5.42 (a)). After milling for 120 minutes the morphology consisted of a mix of fine particles and agglomerates. Unlike the agglomerates observed in Figure 5.42 (a), the top layer of the finer particles appeared to have melted. Examination of the morphology of STZNa milled 10 hours consisted of a powder that appeared to be a result of deliquescence. The high level of amorphous content within the structure of the 10 hours milled samples may have resulted in the sorption of atmospheric moisture which resulted in the consistency observed in Figure 5.42 (c).

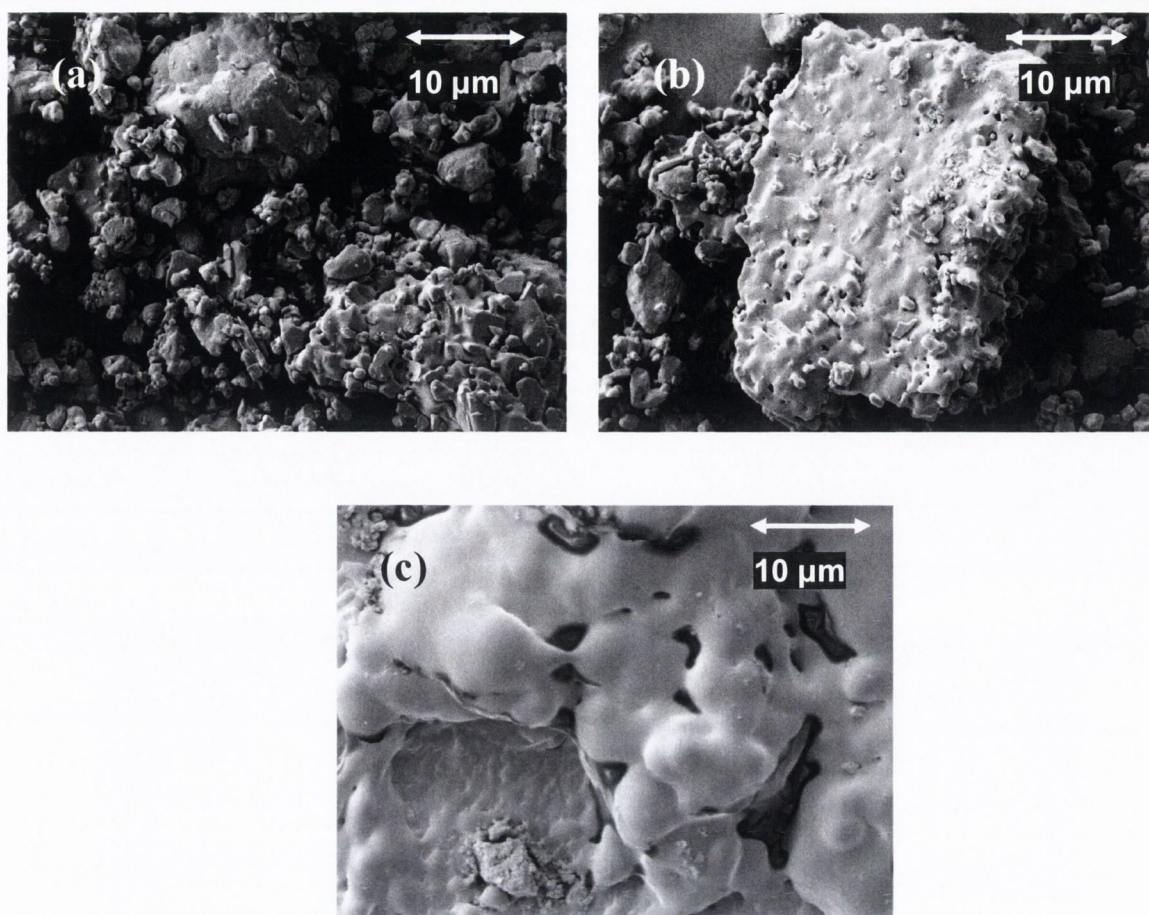


Figure 5.42: Morphology of STZNa milled for (a) 5 minutes; (b) 120 minutes and (c) 10 hours.

5.7 Conclusions

Analysis of the binary mixtures showed that as little as 3 % of Form I present in a predominantly Form III material resulted in a lowering of the transition temperature determined by DSC. All binary mixtures resulted in the transition temperature shift towards a lower temperature (~ 158 °C) regardless of the quantity of Form I added, while the enthalpy required for the transition decreased with increasing quantities of Form I. The thermal properties of the binary mixture were different to the thermal properties of STZ III-Y, which was believed to be a mixture of polymorphs.

The Form I polymorphic structure was obtained by heating STZ III-Y to above the transition temperature. Analysis by PXRD and DSC showed that the material had physicochemical

properties characteristic of the Form I but micrographs consisted of platelet morphology which is characteristic of the Form III. These morphology changes may impact on the tablet and powder flow properties.

Analysis of the unmilled materials indicated that STZ III-X, STZ III-Y, STZ I and STZNa were crystalline in nature. Ball milling of the non-salt forms resulted in a change in particle size, surface area and morphology. An induced amorphous phase was possible but this was not dependent on time. For the three non-salt forms the induced amorphous phase fluctuated with time. Thermal analysis indicated that a change in the polymorphic form was detected. Identification of the phase(s) present was difficult as the solid state transition temperature was lower than any other reported transition. This may have been due to the change in crystallite size which was indicated by the change in PXRD peak area. Storage of the samples for a day resulted in a change in the polymorphic form and the DSC amorphous content suggesting that the ball milling process results in a metastable phase that changes over a short period to a more stable form.

Ball milling of sulfathiazole sodium salt resulted in a decrease PXRD peak area as milling time was increased. Thermal analysis suggested that the change observed to the PXRD peak area may be attributed to the decreased crystallite size but disorder was induced as a result of milling for 5 and 10 hours. Unlike the non salt form, increased ball milling in this study resulted in an increased level of disorder.

Powder flow and tablet hardness

6.0 Introduction

Powder flow is not an inherent material property but is a result of a combination of material physical properties. Flow properties of pharmaceutical powders are critical to manufacturing. Poor flow may cause undesirable process break down, thereby directly impacting the product uniformity (Jallo *et al.*, 2012). Manufacturing of pharmaceutical solid dosage forms involves several processes including flow through hoppers, sieving, pouring, blending, die filling and compaction (Guerin *et al.*, 1999). The cohesive nature of powders results in the tendency for particles to agglomerate which subsequently gives rise to poor flowability, low bulk density and may lead to an increased tendency for electrostatic charging, thus adversely affecting downstream processing and handling (Han *et al.*, 2011).

The most commonly used pharmaceutical dosage forms today are tablets (Armstrong, 2007). Direct compression is the most efficient process used in tablet manufacturing because it is fast, simple and comparatively inexpensive (Liu *et al.*, 2008). Factors affecting the tensile strength may include mechanical properties of the material, particle size and shape, moisture content, solid-state nature and the compression speed and force used for compaction (Roberts and Rowe, 1987a; Eirksson and Alderborn, 1995; Sun and Grant, 2001). The mechanical strength of tablets is an important parameter, as it is important to produce a product with sufficient strength to withstand handling. An awareness of how different manufacturing processes affect material properties which may further influence the product's properties is essential.

Using several different α -cyclodextrin samples, Maggi *et al.* (1998) demonstrated that flowability and compactability of the powder could be related to the material's crystallinity or amorphous nature and the amount and state of water present within the crystal structure. These conclusions were drawn from the analysis of the samples by angle of repose measurements and measuring the tensile strength of the tableted materials. Their research was limited, in the sense that the materials were either completely amorphous or crystalline, while ball milling has been shown to induce partial and/or a completely disordered phase (Zhang *et al.*, 2004).

To date little has been shown in the literature that relates the solid state changes induced by ball milling to the material's ability to flow or compact. Muzzio *et al.*, (2002) suggested that the flow properties of the powder might change significantly during various stages of processing, thus affecting the quality of the final product, and noted that the mechanisms responsible for these changes are poorly understood.

The work in this chapter follows on from results presented and discussed in chapters 3, 4 and 5, where milling conditions were investigated and found to induce disorder into the crystalline structure. The bulk and tap densities of the powders were measured in order to calculate the Carr's compressibility Index, which will indicate the type of flow a powder has. The hardness of compacts made from each material was also determined. A correlation between the powder flow and tableability with the characteristic changes that were previously evaluated and discussed in the aforementioned chapters; these include the DSC amorphous content, PXRD total peak area, the median particle size determined by laser diffraction and the specific surface area determined by BET, was investigated. The overall aim was to determine if there was any relationship between the solid state changes incurred as a result of milling and the material's ability to flow and compact. The materials tested included sulfadimidine, sulfadimidine sodium salt, sulfathiazole I and III and sulfathiazole sodium salt.

6.1 Powder flow

The bulk and tapped densities were used to calculate the Carr's compressibility Index. These tests were carried out using the unmilled powders and the powders obtained after milling. From the results presented and discussed in chapter 3, 4 and 5, the induced amorphous phase into the SD, STZ I, STZ III-Y and STZNa crystallises over a short period of time, therefore a new sample was used for each test to limit the impact of crystallisation of the amorphous phase and to ensure consistency.

6.1.1 Carr's compressibility index (CI)

The Carr's compressibility Index (CI) indicates the capability of the particles to consolidate with minimal amounts of excess air in the bulk. It utilises the powders tapped and bulk densities within the calculation (discussed in detail in section 1.3.1) and is expressed as a

percentage. The value obtained for the CI can be related to a flow type, as outlined in Table 6.1. A low CI is typical of a powder where the inter-particle cohesive forces are low (Han *et al.*, 2011).

Table 6.1: Carr's Index table (Carr, 1965)

Carr's Index (%)	Type of flow
5-15	Excellent
12-16	Good
18-21	Fair to passable
23-35	Poor
33-38	Very poor
>40	Extremely poor

The bulk density and CI calculated values for the unmilled and milled powders are outlined in Table 6.2. The majority of the powders appear to show poor, very poor or extremely poor flowability. There were two exceptions; the first with the lowest CI of 13.15 % was measured for the STZNa unmilled powder, which suggested good powder flow. The second exception, with fair powder flow properties was STZ I ball milled for 20 hours. Lower compressibility indicates there is efficient packing of the particles and a minimal amount of excess air in the bulk, which is a desirable property for pharmaceutical powders intended for solid dosage forms (Carr, 1965). Han *et al.*, (2011) suggested this typically occurred when the inter-particle cohesive forces are low in comparison to the particles own inertial forces. These results would then suggest that comparing all Carr Index results of the powders tested, the STZNa unmilled powder had the lowest inter-particle cohesive forces in contrast to the STZNa powder that was milled for 10 hours and SDNa powder milled for 5 minutes, which resulted in a CI of 40.59 and 42.65 %, respectively. The increase of the CI values for these two materials would suggest that the change to the interparticle cohesive forces for these samples were the most significant, which resulted in the highest CI obtained in comparison to the other ball milled and unmilled material.

Bulk density is a function of particle shape and surface smoothness (Carstensen *et al.*, 1993). Ghoroi *et al.*, (2012) suggested that the similarities between the bulk densities could be attributed to the similar particle shapes, since the packing of the same shaped particles in a

fixed volume was likely to produce the same or similar void space irrespective of their size. Other factors that may influence a powder's bulk density including their cohesive properties and the internal porous structure. If these properties were similar from material to material it could result in obtaining similar volume for a fixed mass. The bulk densities of the powders are given in Table 6.2 and these similarities between the bulk densities are reflected in the comparable CI results. Similarities between the powders particle shape and size distributions were observed and previously discussed in chapter 3, 4 and 5 and these similarities may have contributed to a similar void space present when packing the ball milled powders, which resulted in comparable CI and bulk density measurements for a number of powders.

Jallo *et al.* (2012) found that the CI was dependent on the particle size and regardless of the material properties, powders with a particle size $<30 \mu\text{m}$ were classified as having poor flow and particles $>30 \mu\text{m}$ were categorised as having good flow. This statement may be applied to powders investigated for this study as the median particle size for the majority of the powders, milled and unmilled, was less than $30 \mu\text{m}$. The only material that was found to have good flow properties was STZNa unmilled powder which had a median particle size of $84.45 \pm 4.01 \mu\text{m}$, confirming the results reported by Jallo *et al.* (2012).

The CI of the powders appeared to have fluctuated with increasing milling time, in comparison to the unmilled powder. Statistical analysis by ANOVA showed that there was no statistical significant difference between the CI's of the SD powders analysed ($p = 0.4343$) but this was not the case for the other powders investigated. ANOVA analysis suggested that a statistically significant difference was detected for the samples of SDNa ($p < 0.0001$), STZ I ($p < 0.0001$), STZ III-Y ($p = 0.0002$) and STZNa ($p < 0.0001$). The behaviour was unpredictable but the majority of the ball milled powders was classified as having poor flow properties. Han *et al.*, (2011) micronized ibuprofen reducing its particle size from $102.8 \mu\text{m}$ to below $20 \mu\text{m}$ and found that, as a result, the CI increased.

It can be concluded that, over the range of ball milled powders tested for each of the materials over the given milling times investigated, the CI obtained for the majority of the powders indicated that poor flow properties were inevitable. For each material, one ball milled powder resulted in a CI that was close to the 'fair to passable' powder flow category but ball milling time required to obtain these results were not the same for every material, making it difficult

to predict which ball milling time may result in a low CI. This indicates continuous change within the inter particle forces as milling time was increased and that the ball milling process affected each material differently.

Table 6.2: Carr's compressibility Index and bulk density for the unmilled and milled powders

Milling time (minutes)		0	5	30	60	300	600	1200
Carr's Index (%)	SD	33.26 (3.14)	31.67 (2.36)	29.33 (0.94)	35.83 (3.54)	38.13 (2.65)	26.29 (3.23)	30.95 (3.37)
	SDNA	31.25 (0.53)	42.65 (1.39)	35.42 (2.95)	34.85 (2.14)	23.25 (1.06)	29.55 (3.21)	
	STZ III - Y	37.50 (0.45)	33.87 (3.53)	40.00 (5.15)	30.69 (0.97)	29.32 (3.78)	30.50 (4.92)	23.03 (2.79)
	STZ I	29.63 (1.29)	36.36 (2.15)	38.45 (1.34)	30.95 (3.37)	25.00 (5.05)	26.14 (1.61)	22.50 (3.54)
	STZNa	13.15 (0.91)	38.51 (2.10)	36.54 (2.72)	35.48 (1.52)	34.52 (1.68)	40.59 (0.83)	
Bulk density (g/cm ³)	SD	0.59 (0.03)	0.58 (0.01)	0.58 (0.03)	0.66 (0.06)	0.58 (0.16)	0.55 (0.12)	0.42 (0.01)
	SDNA	0.57 (0.05)	0.61 (0.00)	0.69 (0.04)	0.59 (0.09)	0.67 (0.01)	0.68 (0.04)	
	STZ III - Y	0.64 (0.04)	0.74 (0.03)	0.81 (0.13)	0.76 (0.02)	0.79 (0.04)	0.76 (0.10)	0.59 (0.07)
	STZ I	0.48 (0.01)	0.66 (0.04)	0.67 (0.02)	0.62 (0.02)	0.66 (0.09)	0.68 (0.01)	0.76 (0.05)
	STZNa	0.66 (0.04)	0.78 (0.13)	0.54 (0.01)	0.53 (0.06)	0.62 (0.03)	0.70 (0.01)	

Standard deviation in parentheses. n=3.

6.2 Compaction

This section investigates how the changes induced as a result of ball milling at RT with a BTP weight ratio of 40:1 influenced the hardness of compacts/tablets prepared from pure API. Initial studies examined the critical formation pressure required to form a solid tablet. This was followed by evaluation of the tablet geometry, hardness, tensile strength and specific surface area for tablets prepared from the unmilled materials, to investigate the different compaction properties of the unprocessed materials. The hardness and specific surface area of tablets prepared from samples milled for different time periods (from 5 minutes up to 20 hours) was then investigated in order to evaluate if a relationship existed between the changes incurred as a result of milling and the compact hardness and the tablet specific surface area. The material properties considered with respect to the tablet hardness include: the crystallinity/amorphicity of the material as evaluated by PXRD and DSC analysis, particle size as determined by Malvern laser diffraction and the powder's specific surface area as evaluated by BET analysis. Tablets consisted of 100 % of the API and a dusting of magnesium stearate was used as a lubricant.

6.2.1 Determination of the critical formation pressure

In order to investigate the hardness of a tablet it is essential to form a tablet that does not laminate or result in capping once the compaction pressure is released. The compaction pressure and speed used has been found to influence tablet hardness (Roberts and Rowe, 1887a; de Lourdes Garzón and Villafuerte, 2002). To compare the tablet hardness of one material to the other and to eliminate the effect of varied compaction pressures, it was necessary to find a pressure at which a solid tablet could be produced for all materials investigated. In order to do so, the unmilled SD, SDNa, STZ III-Y and STZNa powders were compressed under different pressures and the tablet hardness of the resulting components were investigated.

Figure 6.1 illustrates the tablet hardness as a function of increasing compaction pressures (73, 146, 219 and 292 MPa) of compressed SD, SDNa, STZ III-Y and STZNa powders. A compaction pressure of 73 MPa resulted in tablets with hardness values below 40 N for all samples. At this pressure the tablets that were produced lacked uniformity and the edges of the tablets crumbled when held, which suggested that this pressure was not sufficient to

produce robust tablets for compression testing. Increasing the compaction pressure to 146 MPa resulted in an increase in tablet hardness for all samples (Figure 6.1). One out of three SD and STZ III-Y tablets demonstrated capping or lamination when compacted with 219 MPa pressure. Compaction of all SD tablets with a compaction pressure of 292 MPa resulted in capping or laminating, limiting the compaction pressure that produced robust tablets for further testing.

Armstrong (2007) stated that the physical strength of a tablet is dependent on the extent and strength of interparticulate bonds and these in turn are related to the compressive force which is applied. Therefore, as the compaction pressure of 146 MPa produced uniform tablets, which was an essential requirement for this study, it was used for further analysis of the milled materials.

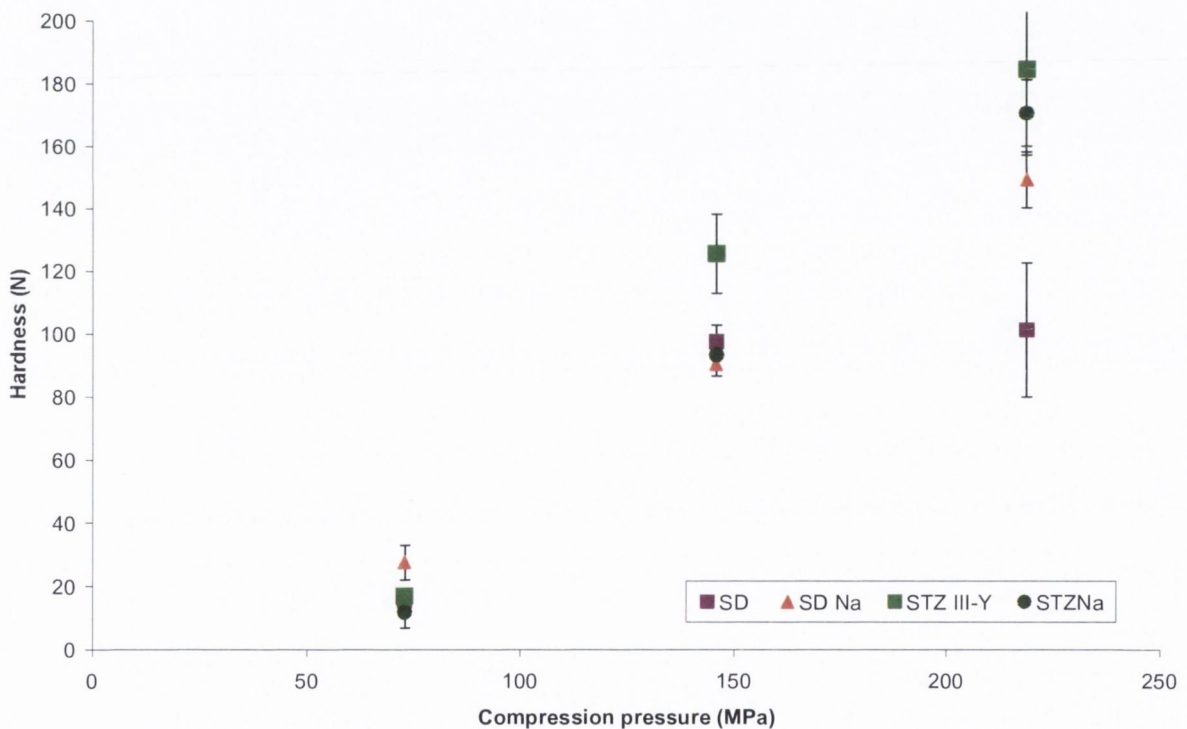


Figure 6.1: Tablet hardness of SD, SDNa, STZ III-Y and STZNa when compressed at different pressures. $n = 5$

6.2.1 Tableting properties of the unmilled materials

Table 6.6 outlines the tablet geometries, hardness and tensile strength for tablets prepared from SD, SDNa, STZ I, STZ III-Y and STZNa powders before they were milled. The tablet hardness for the sodium salts was between 90 and 95 N while SD, STZ I and STZ III-Y yielded tablet hardness values between 104 and 113 N (Table 6.6), when compressed with a pressure of 146 MPa.

Table 6.6 Tablet geometries, hardness and tensile strength of the unmilled materials. (SSA_{Tab} : specific surface area of the tablet).

Material	Height (cm)	Diameter (cm)	Tablet hardness (N)	Tensile strength (MPa)	SSA_{Tab} (m^2/g)
SD	0.53 (0.02)	1.28 (0.01)	104.00 (2.65)	0.96 (0.03)	1.30 (0.02)
SDNa	0.53 (0.01)	1.28 (0.02)	90.20 (3.76)	0.94 (0.03)	2.24 (0.27)
STZ III-Y	0.52 (0.01)	1.27 (0.01)	112.75 (11.59)	1.13 (0.12)	0.98 (0.09)
STZ I	0.52 (0.02)	1.28 (0.01)	107.00 (9.00)	1.09 (0.09)	1.04 (0.08)
STZNa	0.52 (0.03)	1.28 (0.02)	94.00 (3.46)	0.91 (0.33)	1.57 (0.19)

Standard deviation in parentheses, n=3

Determination of the tensile strength of a tablet considers the geometry and hardness of the tablet. As the difference between the tablets geometries was statistically insignificant (Table 6.6), the tensile strength followed the same trend as the tablet hardness. It has been suggested that the mechanical strength is governed by the interparticulate bonding mechanism and the area over which these bonds interact (Nyström *et al.*, 1993; Sebhatu and Alderborn, 1999). Bonding mechanisms can include attraction forces such as van der Waals forces and solid

bridges. Nyström *et al.* (1993) proposed that the dominating bonding mechanisms are reflected by the specific surface area. Mattsson (2000) further explained that there is an assumed proportionality between the tablet surface area and the surface area participating in bonding. Therefore, a tablet with a high specific surface area should indicate that the particles are held together by weaker attractive forces and a low value would indicate that the material's bonding mechanism could be attributed to the formation of strong bonds such as solid bridges. Olsson and Nystrom (2000) found that the bonding mechanism was not the only factor to influence the tensile strength, as differences in the particle size were also found to influence the tablet strength. The sodium salts had the highest SSA_{Tab} and the lowest tensile strength, while STZ III-Y had the lowest SSA_{Tab} and the highest tensile strength, indicating a difference between the samples' bonding mechanisms. The median particle size measured by laser diffraction (Table 6.6) varied and could not be directly related to the change in tablet hardness.

6.2.2 Tablet hardness

Hardness is the force required to fracture a tablet and it is an expression of the tablet's physical strength or mechanical strength. Measurement of tablet hardness can be used to compare tablets of the same size and shape and as an in-process control. Table 6.7 lists the hardness values obtained after each material both milled and unmilled were compressed and then hardness tested. Tablets produced from the milled powders were prepared within an hour after each ball milling process was completed.

Tablets that were produced from the materials that were ball milled generally resulted in an increased tablet hardness when compared to the tablets produced from powders that were not milled (Table 6.7, and SD and STZ III-Y were graphed to show as an example of this, Figure 6.2). The increase of tablet strength may be influenced by properties associated with the solid state nature and the material's micrometric properties and these will be correlated to determine the possible influencing factors in the following sections. Two observations were evident from the tablet hardness data; the first was a significant increase of the tablet hardness and tensile strength evident after 5 minutes of milling and the second was that the increase in tablet hardness and strength was not directly proportional to increased ball milling time.

The tablet hardness increase was especially apparent in tablets composed of the two sodium salts, as they both increased from under 100 N for the unmilled powders to over 400 N after the powders were ball milled for 5 minutes. There was a statistically significant difference when comparing the tablet hardness obtained from the tablets produced from the unmilled (STZNa and SDNa) powders with those produced using the ball milled powders. As milling time was increased, the tablet hardness obtained from the tablets produced from the ball milled powders remained high (~200 N to ~400 N) in comparison to the tablets produced from the unmilled powders (~100 N). Further analysis of the data by Tukey's multiple comparison test showed that there was a significant statistical difference for SDNa tablets produced from the 5 minute ball milled powder and the tablets produced from the samples ball milled for 30 and 120 minutes. SDNa tablets produced from the powder ball milled for 120 minutes was statistically significantly different to the tablets produced from the powders ball milled for 5 and 10 hours. No statistical difference was observed between the other SDNa powders.

Analysis of the STZNa materials by Tukey's multiple comparison test showed that several samples produced tablets with hardness values that were statistically the same. The STZNa samples that appeared to have no statistical significant difference are outlined in Table 6.8.

Table 6.7: Tablet hardness (N) of tablets produced from unmilled and ball milled powders.

Milling time (minutes)	0	5	30	60	120	300	600	900	1200
	SD	104 (2.65)	152 (9.17)	199 (11.73)	201 (9.20)	225 (26.65)	254 (23.11)	275 (8.68)	257 (8.66)
SDNA	90 (3.76)	404 (16.26)	334 (43.13)	343 (28.28)	295 (56.57)	352 (42.43)	378 (3.54)		
STZ III - Y	113 (11.59)	199 (3.54)	254 (15.56)	314 (11.31)	301 (7.78)	302 (12.73)	304 (24.04)	229 (33.23)	333 (29.70)
STZ I	107 (9.00)	240 (4.24)	224 (10.61)	229 (14.14)	241 (12.02)	276 (31.82)	237 (9.19)	260 (15.56)	308 (21.92)
STZ Na	94 (3.46)	428 (19.09)	422 (24.75)	363 (17.68)	400 (4.24)	377 (30.41)	419 (9.19)		

Standard deviation in parentheses, n=3.

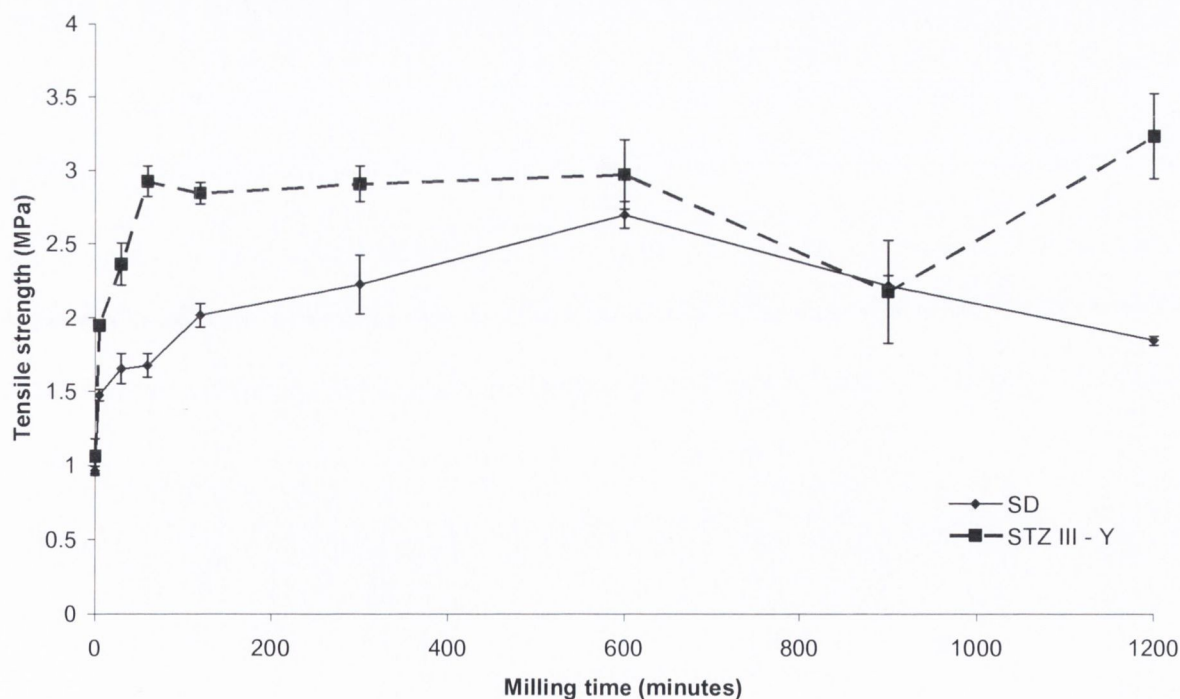


Figure 6.2: Tensile strength of SD and STZ III-Y tablets as a function of milling time. Tablets were compacted with a pressure of 146 Mpa.

Tablets prepared from both STZ III-Y and STZ I powders that were milled for 5 minutes were at least twice as hard as the tablets produced from the unmilled powders, as the tablet hardness increased from 107 N to 240 N for STZ III-Y and 113 N to 199 N for STZ I. The tablets produced from the SD powders that were milled for 5 minutes only increased by ~ 50 %, as the tablet hardness obtained from the tablets produced using the unmilled SD powder was 104 N and the hardness of the tablet produced from the SD powder milled for 5 minutes was 152 N.

The tablet hardness varied as milling time was increased. Differences between the tablet hardness of the samples were difficult to identify. Therefore, Tukey's multiple comparison test was used to identify the similarities and differences between the tablets' hardness. Table 6.8 outlines the samples that are deemed not statistically different for SD, STZ I and STZ III-Y. The correlation studies, which are discussed later, should suggest what solid state changes, which incurred as a result of the milling, affected the tablet hardness.

Table 6.8: Tukey's multiple comparison test results indicating comparisons that are not statistically significant (min = minutes and hr = hour)

SD	30 min vs. 60 min and 20 hr 60 min vs. 120 min and 20 hr 120 min vs. 5 hr and 20 hr 5 hr vs. 60 min and 20 hr
STZ I	5 min vs. 30, 60, 120 min, 10 hr and 15 hr 30 min vs. 60 min, 5 hr and 10 hr 60 min vs. 10 hr 120 min vs. 5, 10, and 15 hr 5 hr vs. 15 hr 10 hr vs. 15 hr
STZ III-Y	5 min vs. 15 hr 30 min vs. 15 hr

	60 min vs. 120 min, 5 hr, 10 hr and 20 hr 120 min vs. 5 hr, 10 hr and 20 hr 5 hr vs. 10 hr and 20 hr 15 hr vs. 20 hr
STZNa	5 min vs. 30 min and 10 hrs 30 min vs. 120 min and 10 hrs, 60 min vs. 120 min and 5 hrs 120 min vs. 5 and 10 hrs

Sebatu and Alderbron (1999) reported the differences between the tablet strength of amorphous and crystalline lactose and found that amorphous lactose tablets were considerably higher in strength. They related the changes in tablet strength to the interparticulate contact area. These workers suggested that the amorphous lactose formed stronger interparticulate bonds than crystalline lactose. They proposed that the amorphous lactose might have a larger number of intermolecular bonding sites over an effective contact area. It was suggested that the difference between the tensile strength and interparticulate contact area relationship for amorphous and crystalline lactose could be explained by differences in elastic deformation during compression (Sebatu and Alderborn 1999). The results from the previous chapters showed that a higher amorphous phase was induced after ball milling the sodium salts for 5 minutes in-comparison to the non-salt forms. Relating the work done by Sebatu and Alderborn (1999) to the results obtained in the current study suggests that the amorphous phase induced after 5 minutes formed stronger interparticulate bonds, which produced tablets with a higher hardness value. The increase in tablet hardness as a result of milling may be related to the change in the number of bonds and the bonding forces between the particles, as suggested Eriksson and Alderborn, (1995).

The change to the degree of crystallinity was not the only change observed as milling time was increased. Particle size and surface area changes were also evident. The hardness results showed that as milling time was increased the tablet hardness varied. As the amorphous phase induced, determined by PXRD analysis, was dependent on time for all the materials milled in

this study but the tablet hardness was not. This would suggest that other factors influenced the tensile strength of these materials. For this reason all results were correlated together and discussed below.

Picker-Freyer *et al.* (2007) evaluated the tableting performance of STZ Form I, II and III. They produced flat faced tablets without lubricant and these were tested by nanoindentation and their compaction properties were evaluated. This group showed that the microstructural difference between the polymorphic forms affected their compaction properties. Their results showed that Form III displayed a significantly greater hardness and elasticity in comparison to Form I and II. They suggested that the hexagonal plates of the Form III crystals compacted better than the needle shaped Form I crystals. The morphology for both the unmilled polymorphs in the current set of experiments were very similar due to the method used to produce Form I and, as a result of ball milling for 5 minutes the morphology for both sulfathiazole polymorphs consisted of irregular shaped particles that agglomerated together. These similarities resulted in tablet hardness values that were not statistically significantly different ($p = 6010$) when comparing the two polymorphic forms.

6.2.3 Tablet specific surface area

The specific surface area (SSA_{Tab}) evaluated by BET analysis for each of the tablets produced from the unmilled and milled powders is given in Table 6.9. All powders that were ball milled for 5 minutes resulted in an increase of the SSA_{Tab} in comparison to their unmilled counterparts. The SSA_{Tab} for both sodium salts was higher than the unmilled non-salt forms tested and this was observed for both the unmilled samples and those milled for 5 minutes. For all of the materials tested here there was no obvious relationship between the SSA_{Tab} and ball milling time, as the SSA of the tablets fluctuated as time was increased.

Table 6.9: Specific surface area (m^2/g) (SSA_{Tab}) determined by BET obtained from the tablets produced using unmilled and milled powders.

Milling time (minutes)		0	5	30	60	120	300	600	900	1200
Specific surface area (m^2/g)	SD	1.30 (0.02)	2.81 (0.54)	4.10 (0.21)	4.90 (0.19)	4.18 (0.47)	7.34 (1.27)	8.05 (0.48)	7.45 (1.11)	4.42 (0.22)
	SDNA	2.24 (0.27)	3.11 (0.44)	3.56 (0.07)	2.53 (0.61)	2.63 (0.53)	3.15 (0.41)	3.12 (0.39)		
	STZ III-Y	0.98 (0.09)	1.76 (0.06)	1.93 (0.01)	2.04 (0.14)	3.02 (0.04)	1.40 (0.09)	1.64 (0.41)	1.65 (0.43)	1.63 (0.01)
	STZ I	0.91 (0.48)	1.83 (0.44)	2.20 (0.32)	1.57 (0.16)	2.51 (0.42)	1.96 (0.25)	1.95 (0.12)	1.32 (0.06)	1.59 (0.05)
	STZ Na	1.58 (0.18)	2.14 (0.32)	2.98 (0.39)	3.16 (0.49)	2.94 (0.68)	2.87 (0.42)	2.98 (0.17)		

Standard deviation in parenthesis, $n=3$.

Westermarck *et al.*, (1999) investigated the effect of increased compression pressure on microcrystalline cellulose and found that the specific surface area decreased with increasing compression pressure as a result of plastic deformation. Adolfsson *et al.*, (1999) studied the change in the SSA of the tablets in relation to the tensile strength for two sets of materials in order to determine a relationship between the bonding forces, tablet surface area and the tensile strength. The first set (potassium chloride, sodium chloride, bicarbonate chloride and spray dried amorphous lactose) were chosen because they consolidated by plastic deformation and the second set (crystalline lactose and sucrose) formed tablets by fragmentation (Adolfsson *et al.*, 1999). From the results they concluded that, as compaction pressure increased (25 to 100 MPa), sodium chloride and potassium chloride formed the strongest tablets with the least increase in surface area and they associated this with the strong bonds, such as solid bridges or ionic bonds, that were formed. Sucrose and crystalline lactose were found to produce weak tablets and the surface area increased extensively during compaction. They attributed this to the development of interparticulate attractions that acted over greater relative distances. The other materials tested were found to be difficult to classify, which was thought to be due to even weaker bonds created during compaction. Adolfsson *et al.*'s

conclusions were difficult to evaluate and they focused on trying to relate the surface area to the materials hardness properties but had difficulties doing so and stated that factors other than surface area must affect the tensile strength of compacts (Adolfsson *et al.*, 1999).

The difference between the SSA_{Tab} of the tablets composed of the unmilled and ball milled materials may be attributed to the difference in the bonding mechanism during compaction. As milling time was increased the SSA_{Tab} increased in comparison to their unmilled counterpart. Overall it was clear that a change to the tablet's SSA was affected by ball milling; correlating these results with the other properties measured may suggest factors that influence a tablet's SSA.

6.3 Correlations

A correlation study quantifies the association between two variables without fitting a curve or line. No clear trend was apparent when comparing the powder flow or the tablet properties measured as milling time was increased to the solid state and particle size properties of each powder. A Spearman correlation study was undertaken to determine if relationships between the evaluated material's property changes that occurred as a result of milling and the powder flow and tablet properties could be observed. As powder flow is not an inherent property but reliant on several material characteristics it was of interest to investigate the correlation between the CI and the properties of the unmilled and milled materials. The material properties would include crystallinity as determined by PXRD peak area, amorphous content as determined by DSC, median particle size as evaluated by laser diffraction, the BET specific surface area of the powders (SSA_{Pow}) and the weight loss determined by thermogravimetric analysis. A similar study was then carried out with the tablet hardness, and SSA of the tablets.

6.3.1 Spearman correlation

The Spearman correlation allows the evaluation of a relationship between two fluctuating variables. Correlation studies are used when comparing two variables measured experimentally in order to observe how these variables vary in relation to one another. This is unlike linear regression where one variable is often experimentally manipulated (e.g. time, concentration etc.). The correlation coefficient, r , quantifies the direction and magnitude of

correlation, suggesting the degree of change of one variable in relation to another measured variable. The correlation coefficient, r , ranges from -1.0 to +1.0, Table 6.10 outlines the interpretation of r . It is not appropriate to apply the Spearman correlation if one variable may be manipulated, such as time, concentration etc. The Spearman correlation makes no assumptions regarding the sample distribution and can be used when comparing small sample sets, unlike the Pearson correlation, which assumes a Gaussian distribution and a large sample is preferred (Prism, 2007).

Correlating the material characteristic changes measured as a result of increased milling time with the powder flow, tablet hardness and the surface area was carried out in order to investigate possible relationships between the changes incurred as a result of milling to the powder flow, tablet hardness and surface area so that an understanding as to how one process (i.e. ball milling) may affect further processing steps (i.e. powder flow and tableting)

Table 6.10: Interpretations for the value correlation coefficient, r .

Value of r	Interpretation
1.0	Perfect correlation
0 to 1	The two variables tend to increase or decrease together
0.0	The two variables do not vary together at all
0 to -1	One variable increases as the other decreases
-1.0	Perfect negative or inverse correlation

To ensure that the correlations of interest were truly correlated, a significant test was carried out. The numbers of pairs tested is equal to eight, these are also known as the degrees of freedom (df) in a spearman study. Using a one tailed test to analysis the significance of the correlation results in the degrees of freedom is equal to six ($n-2$). Therefore, the null hypothesis can be rejected for any correlation with a coefficient value of 0.6571 or more. By rejecting the null hypothesis it suggests that there is a true correlation between the variables, and if the null hypothesis is accepted then the sample size may have to be increased to ensure no relationship truly exists.

6.3.2 Powder flow correlation study

Table 6.11 shows the correlation coefficients (r) obtained from the Spearman correlation study. The samples milled for 5, 30, 60 minutes and 5, 10 and 20 hours at RT with a BTP weight ratio of 40:1 were included in the analysis. Correlations that were close to -1.0 and $+1.0$ are highlighted in grey (Table 6.11) to distinguish the strong correlations; these include all figures between ± 0.9 and ± 1.0 . The strong correlations for this study all yielded negative correlations, indicating that as one property increased the other decreased or *vice versa*. To compare the strong correlations further the material characteristics of interest were graphed against ball milling time. Correlations that were between ± 0.80 and ± 0.89 are also highlighted in green (Table 6.11), with the intention that other less influencing factors would not be overlooked. The point of interest for this study was to explore the properties that correlated with powder flow CI. As a result of this correlation study other relationships were highlighted such as, the decrease of crystallinity determined by PXRD which correlated strongly with an increase in the DSC amorphous content for certain materials. This correlation will be discussed in the next chapter (General discussion).

There were two significant correlations found when comparing the CI analysis data with the material property changes incurred as a result of ball milling. Table 6.10 shows that, from the Spearman correlation analysis, the CI measurements were correlated with the median particle size measurements (d_{50}) for STZ I with an r value of -0.82 . This is not a strong correlation but the high minus r value does indicate that as one property increases the corresponding property decreases or *vice versa*. The CI and median particle size for STZ I milled at RT with a BTP weight ratio of 40:1 is graphed against ball milling time in Figure 6.3. As the median particle size decreased, due to ball milling STZ I for 5 minutes, the CI increased. This suggested that the decreased particle size resulted in a powder with poor flow properties. As milling time was increased the median particle size continued to fluctuate; these changes were reflected in the CI measurements. This relationship was not as significant for the other materials studied, but analysis carried out in previous chapters showed the change to the median particle size as milling time was increased was not as significant for all powders. A decrease in the median particle size results in the higher number of interparticle interactions which can contribute to a high cohesive nature which in turn results in the poor flow properties. These results are similar to those reported previously by Jallo *et al.* (2012) where smaller particles have poorer flow properties in comparison to larger particles.

Table 6.11: Results of Spearman correlation study comparing the powder flow properties and the material property changes incurred as a result of ball milling at RT with a BTP weight ratio of 40:1. (CI = Carr' Index, DSC amor. = DSC amorphous content, PXRD cry. = PXRD crystallinity, d50 = median particle size (laser diffraction), TGA = thermogravimetric analysis and SSA_{Pow} = specific surface area of the powder (BET)).

		CI	DSC amor.	PXRD cry.	d50	SSA_{Pow}
Sulfadimidine	DSC amor.	-0.32				
	PXRD cry.	0.10	-0.92			
	d50	-0.33	-0.06	0.17		
	SSA_{Pow}	-0.32	0.37	-0.43	-0.60	
	TGA	-0.23	-0.24	0.18	0.395	0.06
Sulfadimidine sodium salt	DSC amor.	-0.64				
	PXRD cry.	0.64	-0.97			
	d50	0.49	-0.12	0.12		
	SSA_{Pow}	0.15	0.43	-0.43	0.38	
	TGA	-0.60	0.79	-0.79	-0.08	0.49
Sulfathiazole Form I	DSC amor.	-0.54				
	PXRD cry.	0.71	-0.74			
	d50	-0.82	0.78	-0.93		
	SSA_{Pow}	-0.32	0.22	-0.61	0.43	
	TGA	-0.25	0.79	-0.643	0.57	0.14
Sulfathiazole Form III	DSC amor.	-0.67				
	PXRD cry.	0.86	-0.74			
	d50	-0.47	0.43	-0.29		
	SSA_{Pow}	-0.14	0.51	-0.07	-0.11	
	TGA	-0.71	0.67	-0.54	0.07	0.75
Sulfathiazole sodium salt	DSC amor.	0.34				
	PXRD cry.	-0.32	-0.82			
	d50	0.03	-0.14	0.67		
	SSA_{Pow}	0.14	-0.03	-0.46	-0.83	
	TGA	0.03	0.68	-0.20	0.49	-0.74

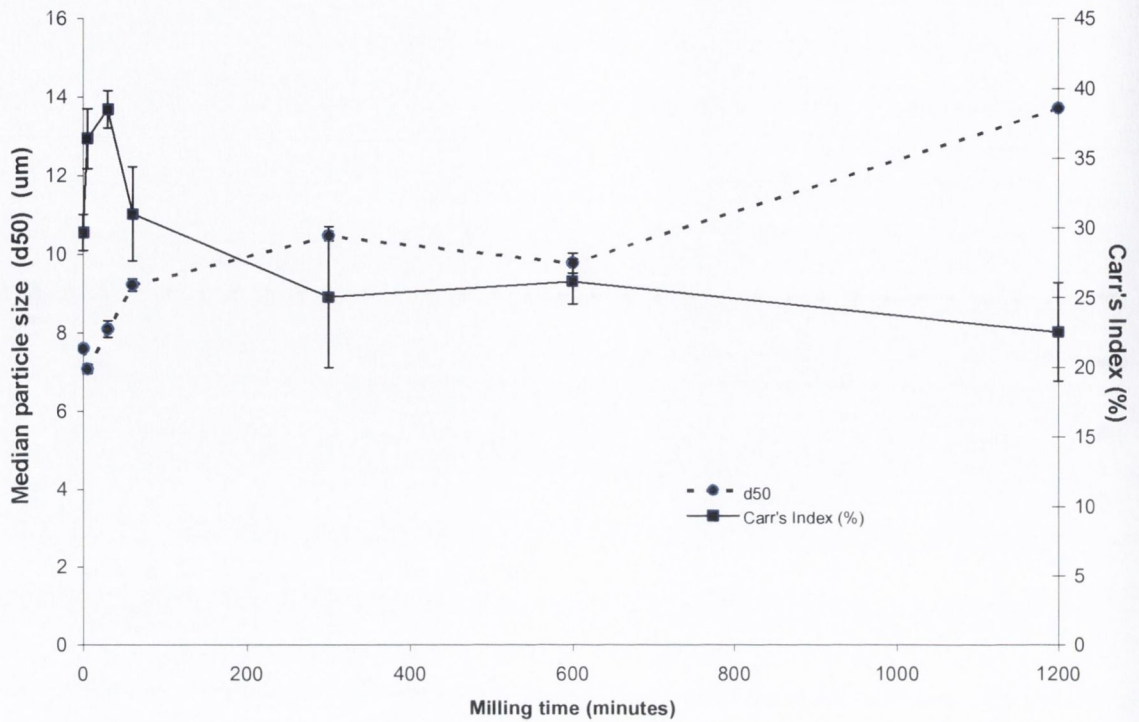


Figure 6.3: Median particle size (d50) and Carr's Index values for STZ I unmilled and milled from 5 minutes to 20 hours at RT.

Carr's Index was also correlated with the PXRD peak area analysis for STZ III-Y with an r value of 0.86, suggesting a reasonable correlation between these two parameters. A positive correlation indicated that the two variables increased or decreased together. These two variables are graphed against milling time in Figure 6.4. From the graph, a distinct drop is observed for both parameters as the ball milling time is increased from time 0 (unmilled) to 60 minutes of milling. No statistically significant change was observed for the Carr's Index measurements from 60 minutes to 10 hours, but there was a change after 20 hours. A gradual decline in the material's PXRD peak area was evident from time 0 up to 20 hours. This suggested that the loss of PXRD crystallinity, which is represented by the reduction in peak area that occurred as a result of ball milling for 5, 30 and 60 minutes and 20 hours, affected the powder's Carr's Index. The loss in crystallinity is thought to reflect an increased level of disorder within the structure. Therefore these results were unexpected as the presence of an amorphous phase has been found to result in poor flow properties (Maggi *et al.* 1998). Sulfathiazole has five known polymorphic forms and ball milling has been known to induce both amorphisation and solid state transformation during the process (Shakhtshneider, 1997). The change to the PXRD peak area may have been a result of both a change in crystallite size

and a polymorphic change. A change in a material's polymorphic form may result in changes such as surface energy and interparticulate bonds (York *et al.*, 1998). The correlation coefficient for DSC amorphous content with CI for STZ III-Y of $r = -0.67$ suggests that as the amorphous content increases the CI decreases; this trend would be expected. The results suggested that the change in the PXRD peak area that affected the decrease in CI could be related to the loss of crystallinity and the change in the polymorphic form. Sun and Grant (2001) noted that different orientations of slip plans in tablets are responsible for different tensile strengths of tablets as a result of differently-shaped crystals. This may also affect powder flow properties as the packing and flow of particles may be influenced by crystal shape.

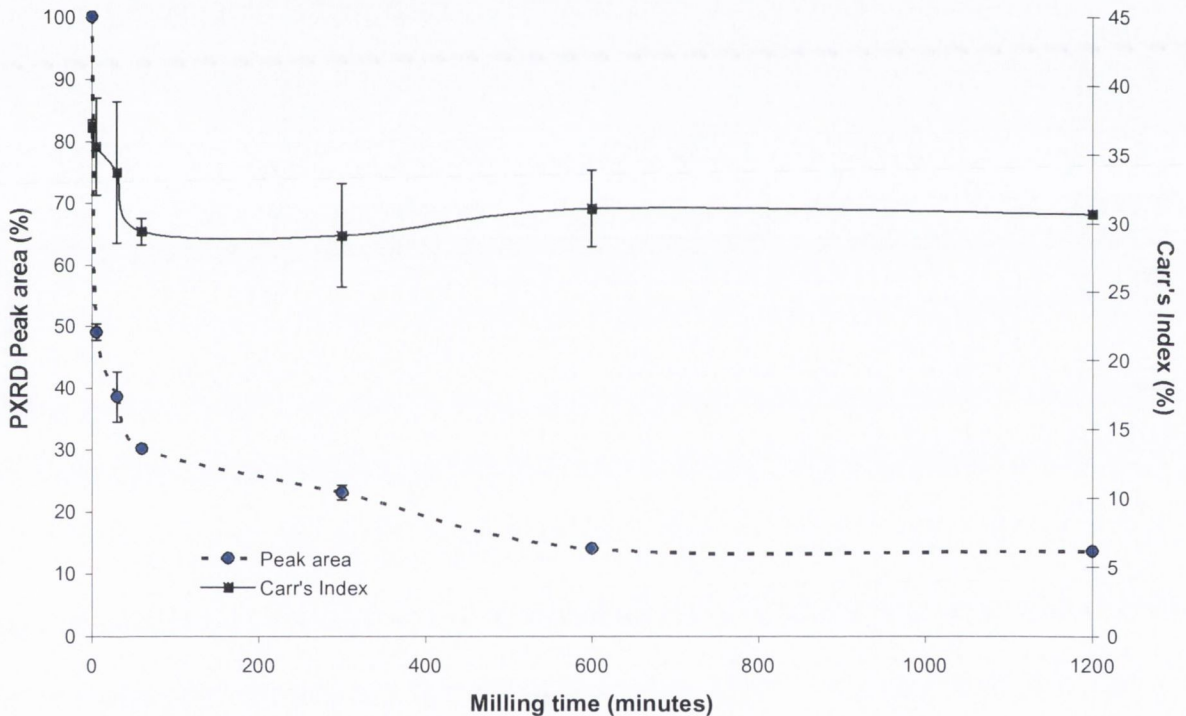


Figure 6.4: Carr's Index and PXRD peak area of STZ III-Y unmilled and milled from 5 minutes to 20 hours at RT.

Analysis of the STZ I correlations showed a relationship between the d_{50} and the PXRD peak area ($r = -0.93$) (Figure 6.5). The correlation suggests that as one property increases the other decreases and *visa versa*. The PXRD peak area analysis suggests that the crystallite size, orientation or lattice strain has changed. These changes can result in an increased surface

energy which can impact on how particles behave towards one another, in terms of inter-particle forces (Buckton and Gill 2007; Ohta and Buckton, 2004).

The morphology of the ball milled samples (reviewed in the previous chapter) showed that the powder consisted of fine particles agglomerated together. The formation of the agglomerated particles could be attributed to the increased surface energy or cohesion between the fine particles. It may be surmised that, as the crystallite size decreases, the ball milling process induces amorphous ‘hot spots’ within the material structure which is reflected in a decrease in the PXRD peak area; it may also result in an increased surface energy. This increased surface energy influences the formation of agglomerated particles which could be seen as an increased median particle size. This is merely conjecture and further studies would have to be done to confirm the relationship between the two properties in order to understand their relationship.

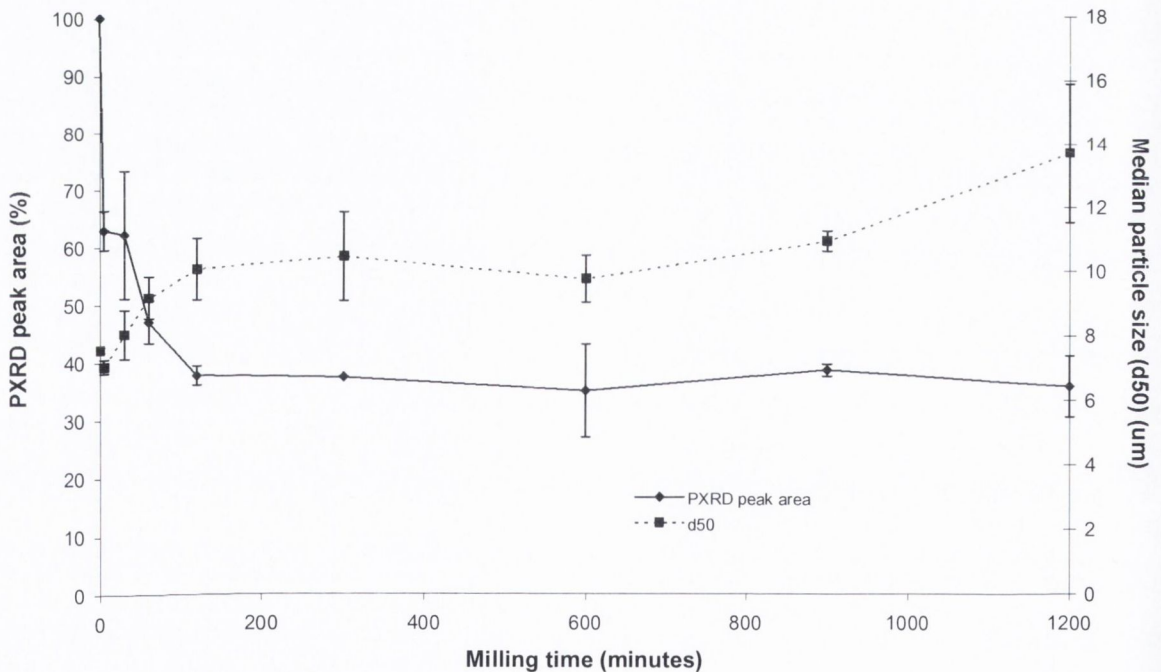


Figure 6.5: PXRD peak area and Median particle size (d50) for STZ I unmilled and milled from 5 minutes to 20 hours at RT.

Moisture has been shown to affect a materials powder flow properties (Ganesan *et al.*, 2008). Pharmaceutical materials maybe hygroscopic in nature which can result in them gaining or losing moisture depending on the humidity conditions they are processed in or stored in.

Moisture can cause cohesiveness as a result of interparticle liquid bridge formations. The sodium salts were found to have a larger weight loss by TGA which and some of this weight loss was attributed to the loss of moisture within the samples. The correlation studies show a relationship between the materials weight loss and the CI for most of the samples investigated but no strong correlations were evident.

6.3.3 Tablet hardness and surface area correlation study

The Spearman correlation coefficients (r) obtained after comparing the tablet properties with the materials' properties for sulfadimidine, sulfadimidine sodium salt, sulfathiazole Form I and Form III and sulfathiazole sodium salt are shown in Table 6.12. The tablet properties that were included in the correlation were hardness and the tablet specific surface area (SSA_{Tab}) and the material properties were PXRD peak area, DSC amorphous content, median particle size (d_{50}) and the powder specific surface area (SSA_{pow}). The correlations highlighted in grey represent the strong correlations that were between ± 0.9 and ± 0.99 , and correlations that were between ± 0.80 and ± 0.89 were highlighted in green.

Significant correlations that were observed included the relationship between the SSA_{Tab} and the hardness of the SD tablets. SSA_{Tab} and tablet hardness obtained from the tablets produced from SD unmilled and milled powders are shown in Figure 6.6 as milling time was increased from time 0 (unmilled) up to 20 hours. The graphs show that as one parameter increased the other increased accordingly ($r = 0.93$). Sebhata and Alderborn (1999) noted a similar trend when comparing the tensile strength of amorphous and crystalline lactose samples. They suggested that the amorphous lactose sample had a higher bonding capacity in comparison to the crystalline sample. They suggested that during the compaction of the powders, the fragmentation of the particles will increase the tablet's surface area, which results in an increased number of contact sites and the number of bonds formed, producing a harder tablet. This trend was only observed for the SD material, which may be because other materials formed compacts as a result of plastic deformation and/or a combination of fragmentation and plastic deformation.

The results also show that for sulfadimidine, the SSA_{Tab} was also correlated with the changes observed to the PXRD peak area, with an r value of -0.82. The PXRD peak area and the SSA_{Tab} obtained for SD unmilled and milled powders are graphed together in Figure 6.7 in relation to the milling time. The negative correlation indicates that as one parameter increases the other decreases or *vice versa*. The graph shown in Figure 6.7 demonstrated that as PXRD peak area decreased as milling time was increased, the SSA_{Tab} also increased. This correlation was only observed for sulfadimidine. The SSA_{Tab} was thought to be influenced by the bonding strength between the particles in the tablet (Aldolfsson *et al.*, 1999; Sebatu and Alderborn 1999). It was thought that as the surface area of a tablet increases the bonding between the particles is thought to occur by weak bonds which results in a decreased tablet hardness. However, the results suggest that the increased SSA_{Tab} resulted in an increased tablet hardness. The change in the PXRD peak area decrease observed as milling time was increased suggests that there was a decrease in the material's crystallite size and an increase in the material's loss of crystallinity. These changes can impact on a material's surface properties and the tableting results here suggest that this impact results in increased tablet hardness which may be attributed to the formation of a number of strong bonds that are created due to the changes indicated by the change in PXRD peak area (i.e. crystallite size and loss of crystallinity).

Factors that affect the SSA_{Tab} include the bonding mechanism (fragmentation or /and plastic deformation) and the strength and type of bonds produced. Adolfsson *et al.*, (1999) found that tableting sodium chloride and potassium chloride resulted in an increased SSA_{Tab} , as a result of strong bonds formed during compaction.

Sun and Grant (2001) stated that a lower crystallinity improves the binding properties of a powder due to a greater plastic flow at the points of contact and an increased bonding area would result in stronger tablets. This was apparent for SD, as the decreased PXRD peak area which indicated a loss in crystallinity and a decreased crystallite size which resulted in an increased SSA_{Tab} (Figure 6.7) and the increase observed for the SSA_{Tab} was reflected by an increase in the tablet hardness (Figure 6.6). These results indicated that as SD was ball milled and its crystallinity and particle size was reduced an increased number of contact areas were created allowing for a stronger tablet to be produced.

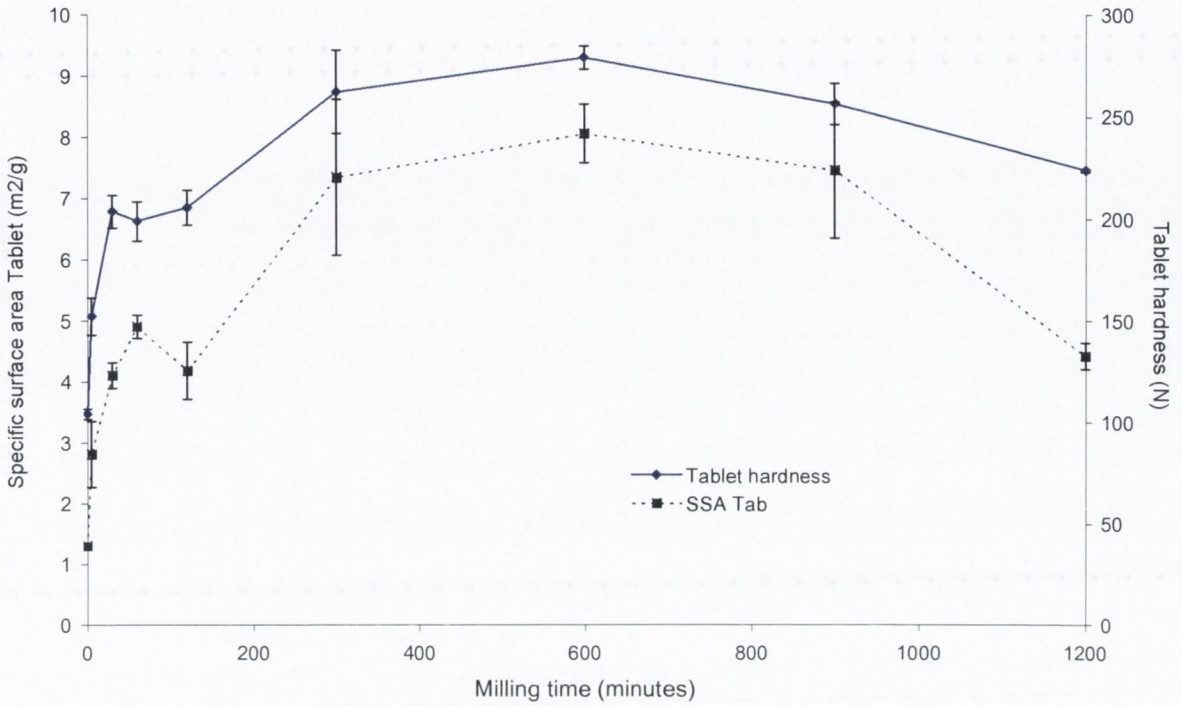


Figure 6.6: Specific surface area of the tablets (SSA_{Tab}) and the tensile strength of SD unmilled and milled from 5 minutes to 20 hours at RT.

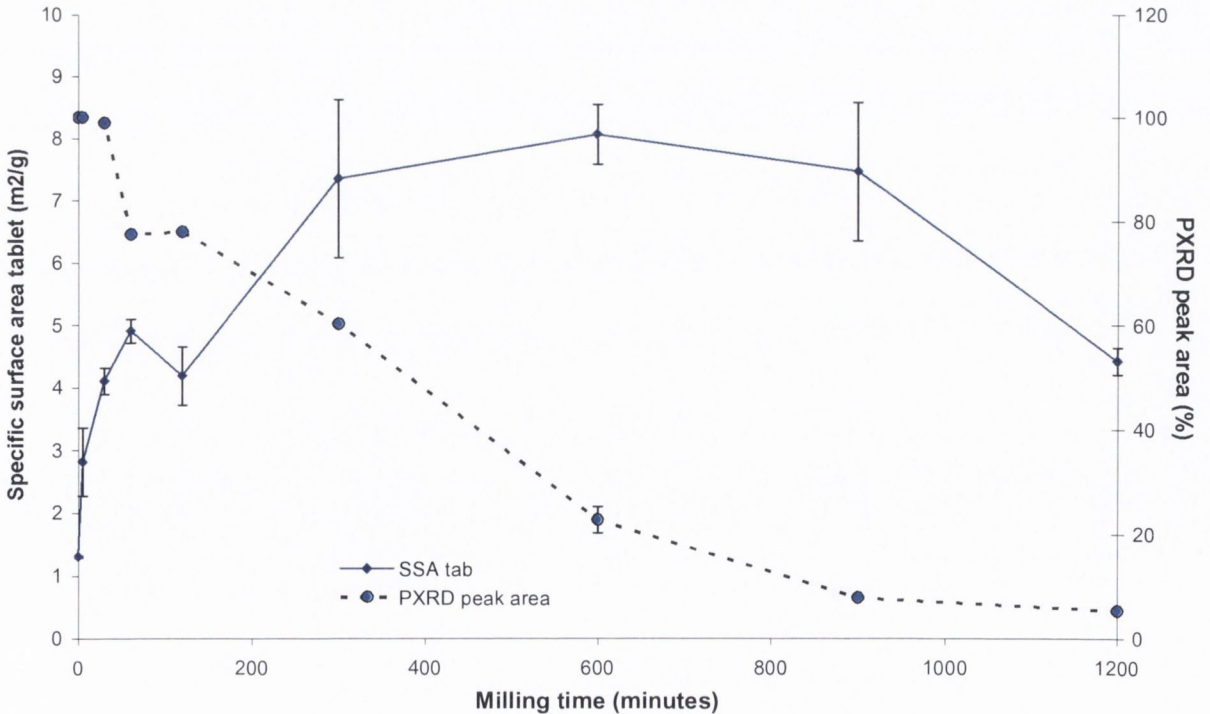


Figure 6.7: Specific surface area of the tablets (SSA_{Tab}) and the PXRD peak area of SD unmilled and milled from 5 minutes to 20 hours at RT.

Table 6.12: Spearman correlation study comparing the tablet properties and the material property changes incurred as a result of ball milling at RT with a BTP weight ratio of 40:1.

		Hardness	SSA _{Tab}	PXRD cry.	DSC amor.	d50
Sulfadimidine	SSA _{Tab.}	0.93				
	PXRD cry.	-0.78	-0.82			
	DSC amor.	0.79	0.73	-0.95		
	d50	-0.10	-0.13	-0.02	0.10	
	SSA _{Pow.}	0.70	0.63	0.63	0.40	-0.45
	TGA	0.03	-0.04	0.18	-0.24	0.40
Sulfadimidine sodium salt	SSA _{Tab.}	0.43				
	PXRD xry	-0.22	-0.37			
	DSC amor.	0.22	0.37	-0.99		
	d50	0.43	0.68	0.07	-0.07	
	SSA _{Pow.}	0.74	0.09	-0.41	0.41	0.22
	TGA	0.43	0.39	-0.79	0.79	-0.21
Sulfathiazole I	SSA _{Tab.}	0.17				
	PXRD xry	-0.65	-0.35			
	DSC amor.	0.62	0.04	-0.85		
	d50	0.82	0.05	-0.77	0.77	
	SSA _{Pow.}	0.68	0.03	-0.47	0.44	0.63
	TGA	0.23	0.27	-0.65	0.63	0.43
Sulfathiazole Form III	SSA _{Tab.}	0.12				
	PXRD xry	-0.72	0.13			
	DSC amor.	0.70	0.05	-0.49		
	d50	0.05	-0.38	-0.18	0.59	
	SSA _{Pow.}	0.13	0.42	0.08	0.37	-0.02
	TGA	0.65	-0.13	-0.77	0.76	0.47
Sulfathiazole sodium salt	SSA _{Tab.}	0.09				
	PXRD xry	-0.04	0.46			
	DSC amor.	0.04	0.13	-0.79		
	d50	0.14	-0.72	0.52	-0.09	
	SSA _{Pow.}	0.21	0.68	-0.34	-0.18	-0.71
	TGA	-0.32	-0.40	-0.32	0.67	0.50

(SSA_{Tab} = specific surface area of the tablets, SSA_{Pow} = specific surface area of the powders, both determined by BET, TGA = thermogravimetric analysis, d50 = median particle size determined by laser diffraction).

Analysis of the data showed that a limited number of strong correlations existed. One of the only other strong Spearman correlations detected was between the median particle size (d_{50}) measurements of the STZ I unmilled and milled powders and the hardness values obtained after tableting the unmilled and ball milled powders. The correlation coefficient (r) of 0.82 was obtained when correlating the median particle size and hardness. Figure 6.12 shows that as the median particle size increase so does the tablet hardness increase.

Adolffson *et al.*, (1999) considered the effect of particle size on the tensile strength of the materials they tableted and found that the particle size had a considerable effect on certain materials. They stated that materials that compacted via solid bridges such as sodium chloride, potassium chloride and sodium bicarbonate resulted in an increased tensile strength associated with an increased particle size. The compacts that were formed as a result of weak distant forces appeared not to be influenced by the different particle sizes; these materials included microcrystalline cellulose, crystalline lactose and sucrose. This may suggest that the STZ I material formed compacts via solid bridges, as the tablet hardness increases with increasing particle size.

Sun and Grant (2001) examined the effect of particle size on the tableting properties of L-lysine monohydrochloride dehydrate powder as the compaction speed varied. They found that compacts produced from powders with a small particle size had an increased tensile strength. They associated this relationship with the fact that smaller particles have a greater compressibility and the ability of smaller particles to reduce their volume under pressure with a lower number of porous structures introduced. This conclusion was only an assumption as they did not look at the bonding types formed during compaction. These studies would indicate that particle size will influence the tablet hardness but the bonding mechanism that occurs between the particles may have a stronger impact as suggested by the change in the PXRD peak area and SSA_{Tab} correlation that was observed for the SD ball milled samples.

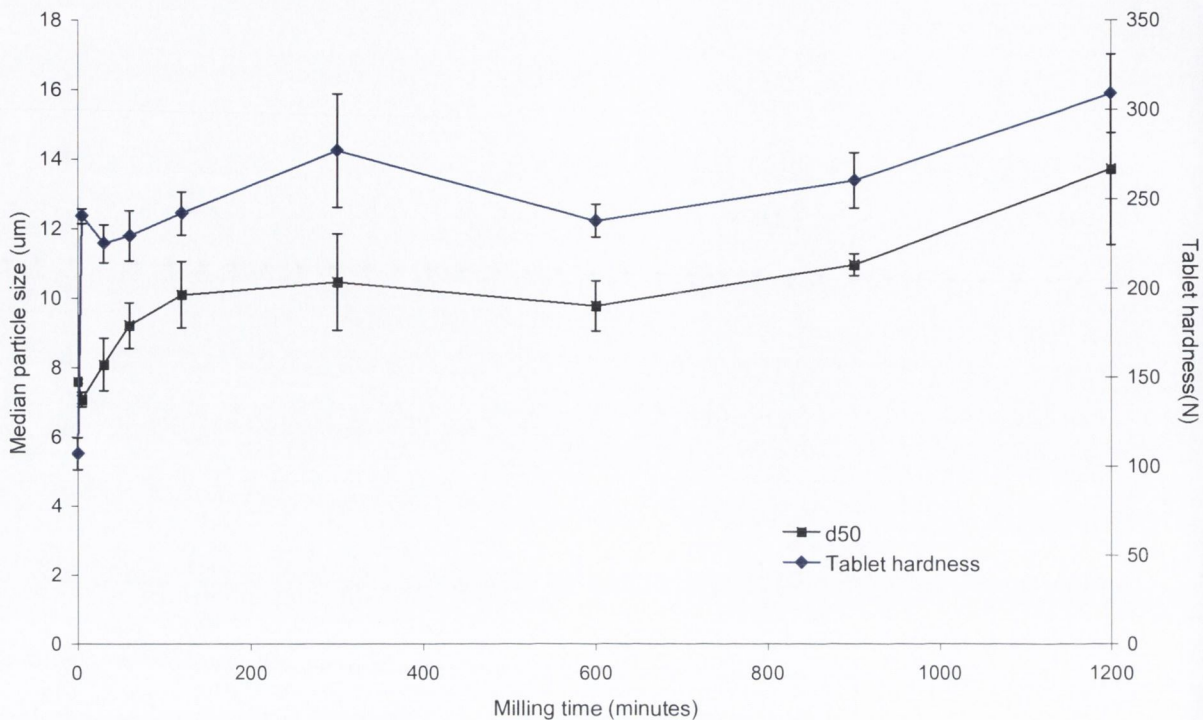


Figure 6.12: Median particle size (d50) determined by laser diffraction of the powders and the tablet hardness of STZ I unmilled and milled from 5 minutes to 20 hours at RT.

Moisture has been shown to affect a material's ability to form a tablet. The addition of water in tablets has been found to increase the hardness of the tablets as a result of increased adhesion of the particles to one another. The presence of moisture within the samples was confirmed by the weight loss determined by TGA. The correlation study shows that as TGA may not have a strong correlation with the tablet hardness but it has been shown to affect the tablet hardness (Westermarck *et al.*, 2009).

For both powder flow and tableting, the correlations that were discussed above were those where the r value was greater than ± 0.8 . However, from the correlation tables (Table 6.9 and 6.10) it was clear that the majority of the coefficients (r) obtained from the Spearman correlation study were less than ± 0.8 but none of the coefficients (r) were determined to be zero. This suggests that all of the changes to the material's properties incurred as a result of ball milling influenced the flowability and tablet hardness of each material to a certain degree. The weaker correlations are graphed and presented in Appendix III to show the relationships between the changes incurred as a result of milling at RT with a BTP weight ratio of 40:1,

including the PXRD crystallinity, DSC amorphous content, the particle size distributions, specific surface area, tablet hardness, and the tablet specific surface area.

6.4 Storage and tablet hardness

Storage of powders for an indefinite period of time before they are processed into a tablet form is often required in the pharmaceutical industry. The powder may be stored onsite or it may be transported, during this period of storage the solid state properties may be affected.

The ball milling of SD was discussed in chapter 3 and the results showed that as milling time was increased the amorphous content also increased. The ball milled powders were stored over an 84 day period and their amorphous content was evaluated by DSC and PXRD to investigate changes. To recap, the results showed that over time the induced amorphous phase crystallised but the rate at which this occurred was different for each sample and it depended on the initial level of disorder induced in the sample. Ball milling, tableting and storage are three tasks carried out regularly in the pharmaceutical industry. It was of interest to investigate if a difference was evident between the tablet hardness obtained from the tablets produced using the powders collected directly after the ball milling process was completed to the tablets produced from the ball milled powders that were milled and stored over an 84 day period.

Research published by Riepma *et al.*, (1992) regarding the affects of storage on already compressed tablets found that, α -lactose monohydrate and roller dried β -lactose tablets stored in a dry atmosphere did not absorb any moisture and the crushing strength and the specific surface area was not changed. The tablets that were stored at $45 \pm 5\%$ RH showed a decrease in both the crushing strength and BET specific surface area. They attributed the decrease of the crushing strength of the α -lactose monohydrate tablets to the sorbed moisture and stated that the moisture promotes relaxation of stress within a tablet and they found that if the tablets were stored in a dry atmosphere after their storage period at 45% RH the crushing strength increased. The storage of roller dried β -lactose tablets showed similar results where the tablet strength was reduced as a result of storage at high RH, whereas drying of the compacts over silica at 50°C for one night yielded stronger tablets. They stated that the stronger tablets could

be attributed to a relationship between the tablet strength and storage humidity and that high humidity environments may cause the dissolution of contact points between the individual lactose particles, while drying of the tablets may result in interparticulate crystallisation within the compacts resulting in new contact points and hence stronger tablets.

This study was very limited to testing the tablet hardness of stored tablets and a further study carried out by Riepma *et al.*, (1993) looked closely at how moisture content affected the specific surface area of the tablets. No research has been published regarding the investigation how a stored ball milled powder behaves when it is tableted. For this study the ball milled SD powders that were milled with a BTP weight ratio of 40:1 at RT for 5, 30, 60, 120 minutes and 5, 10, 15 and 20 hours were stored. These powders were then tableted after a definite period of storage (Table 6.13) then compressed into a tablet and the tablet hardness was evaluated. The powders were stored and tested after 7, 14, 21, 28, 56 and 84 days. A new powder was milled for each test and the characterisation by DSC and PXRD was previously discussed in chapter 3 section 3.5.

Table 6.13 outlines the tablet hardness obtained after the stored powders were compressed and their tablet hardness obtained. The stored samples were kept in desiccant conditions at 4 °C over phosphorous pentoxide. The temperature and RH conditions were monitored and these were presented in chapter 3. Not all of the samples were statistically significantly different, as a result of storing the powders for 84 days, but gradual changes were evident. Figure 6.13 shows the change in the tablet hardness obtained for the samples milled from 5 minutes to 120 minutes and stored over an 84 day period. ANOVA statistical analysis indicated a significant difference between the samples that were milled for 5 minutes, stored and then tableted ($p=0.0022$). Further analysis by Tukey's multiple comparison test showed that over the storage period of 21 days there was no significant statistical difference in the tablet hardness of the compressed milled powders but further storage of the samples for another 28 days resulted in a significant change in the tablet hardness obtained. Figure 6.13 shows that after the additional 28 days of storing the 5 minute ball milled SD sample resulted in a drop in the tablet hardness value obtained. There was no further statistically significant change in the tablet hardness as storage time was increased.

Analysis of the SD samples that were milled for 30 minutes and tableted directly after milling and after storage showed that the tablet hardness fluctuated when comparing the results obtained from T_0 to T_{28} . As a result of further storage the tablet hardness obtained from the tablets produced from the powders stored for 56 and 84 days appeared to decrease as seen in Figure 6.13. ANOVA statistical analysis of the tablet hardness values obtained from the SD samples milled for 30 minutes and tableted was $p=0.0252$. ANOVA statistical analysis of the tablets produced from the SD material that was milled for 60 and 120 minutes, analysed directly after milling and after storage, showed that there was no significant difference as storage time was increased with a p values of 0.6891 and 0.0788, respectively.

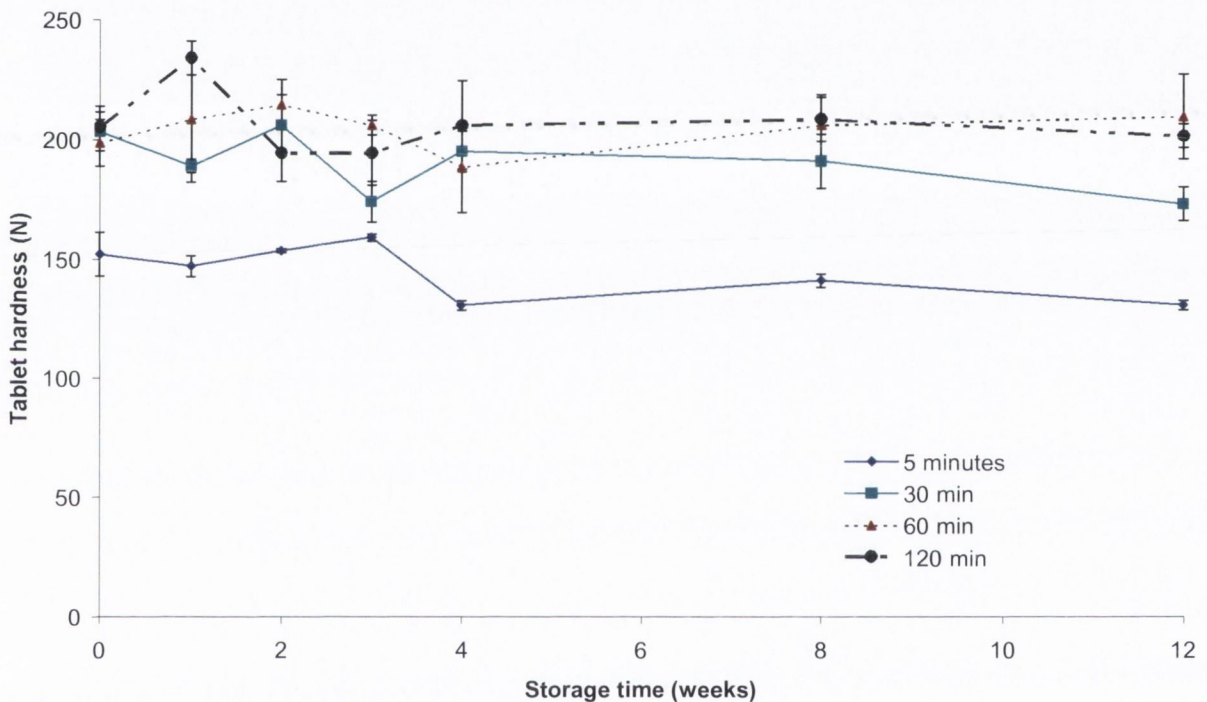


Figure 6.13: Tablet hardness obtained for the SD ball milled powders that were tableted directly after milling and after storage. The samples presented in this graph were milled for 5, 30, 60, and 120 minutes at RT with a BTP weight ratio of 40:1.

Figure 6.14 illustrates the change in tablet hardness obtained for the 5, 10, 15 and 20 hours SD ball milled samples that were tested directly after milling and after storage. Analysis of the SD ball milled samples that were milled for 5 hours and tableted, showed that there was no significant statistical difference, determined by ANOVA analysis, between the tablet hardness obtained from the milled, stored and tableted powders ($p=0.0511$). Figure 6.14 and

the data outlined in Table 6.13 shows that the hardness values fluctuated for each of the samples, as storage time was increased. The most significant change in the tablet hardness was observed for the 10 hr SD ball milled samples. The tablet hardness obtained for the SD ball milled sample that was tested at T_0 was significantly statistically different to the tablets produced from the all of the stored and tableted samples. This was confirmed by ANOVA ($p=0.0001$) and Tukey's multiple comparison test. The tablet hardness fluctuated with storage time, but a significant drop was evident after storing for 84 days, as the tablet hardness obtained after tableting the 10 hr SD ball milled samples dropped to 209 ± 16.97 N after 84 days in comparison to the tablet hardness obtained from the milled powder that was tableted directly after milling (275 ± 8.68 N).

Comparing the samples that were milled for 15 hours and stored and tableted, showed that a statistically significant difference was observed (ANOVA $p= 0.0048$). After 7 and 21 days of storage the tablet hardness obtained after the powders were stored, tableted and tested appeared to decrease. Tukey's multiple comparison test showed that these samples were the only samples statistically significantly different to the T_0 sample. Analysis of the 20 hours SD ball milled powder showed that there was significant changes when comparing the tablet hardness obtained from the tableted powders (ANOVA $p= 0.0047$). Further analysis of the results showed that the tablet hardness showed an initial increase after one week (T_7) of storing the powders. Testing of the samples after further storage (T_{14} and T_{21}) resulted in a decrease in tablet strength, while no significant change in the tablet hardness was observed between the samples stored for 4 weeks (T_{28}) or longer.

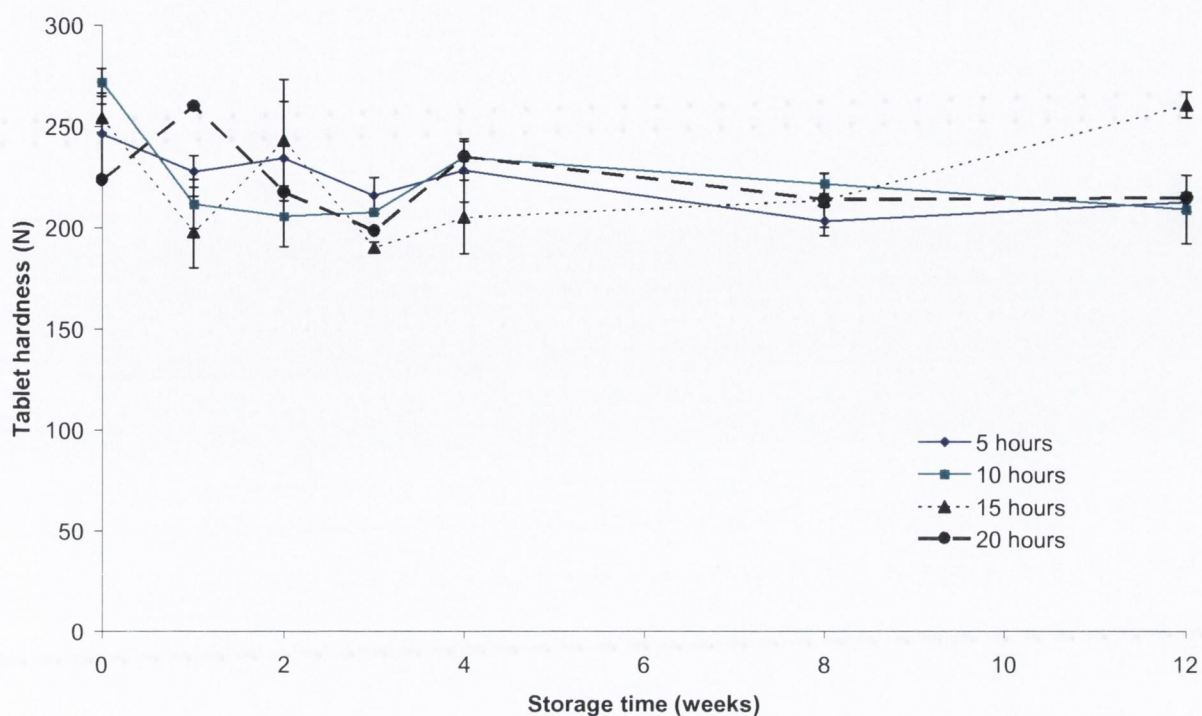


Figure 6.14: Tablet hardness obtained for the SD ball milled powders that were tableted directly after milling and after storage. The samples presented in this graph were milled for 5, 10, 15 and 20 hours at RT with a BTP weight ratio of 40:1.

The change to the tablet hardness as a result of storage was evident after 7 days of storage and as storage time was increased the tablet hardness obtained fluctuated. Overall the tablet hardness after storage appeared to decrease when compared to the hardness obtained after tableting the powder directly after milling (T_0). As storage time increased the change was gradual but over the 84 day period no sample that was tested resulted in a similar tablet hardness that was measured for the unmilled SD tablets (104 ± 2.65 N). This may have been due to the decreased particle size induced as a result of the ball milling process. The results in chapter 3 indicated that the amorphous phase crystallised over time as result of storage. This suggested that the each ball milled sample was continuously changing during this storage period. The RH of the storage chamber was kept below 4.5 % (section 3.5.1), which suggests that the RH may not have contribute to the decreased tablet strength. The loss of the amorphous phase may have resulted in a decreased attractive force between the particles resulting in the change in tablet hardness, reinforcing the importance of evaluating the change in crystallinity as a result of processing.

Table 6.13: Tablet hardness for the SD milled samples analysed directly after milling and stored over 12 weeks at 4 °C over phosphorus pentoxide. T_0 , T_7 , T_{14} , T_{21} , T_{28} , T_{56} and T_{84} represent the total peak area measured directly after mill, after 7, 14, 21, 28, 56 and 84 days respectively.

Ball milling time (minutes)	T_0	T_7	T_{14}	T_{21}	T_{28}	T_{56}	T_{84}
5	152 (9.17)	147 (4.24)	153.5 (0.71)	159 (1.41)	130.5 (2.12)	141 (2.83)	130.5 (2.12)
30	199 (11.73)	189 (2.83)	206 (12.73)	174 (8.49)	195 (8.62)	191 (11.31)	173 (7.07)
60	201 (9.20)	208.5 (26.16)	214.5 (10.61)	206 (4.24)	188.5 (19.09)	206 (12.73)	209.5 (17.68)
120	225 (26.65)	234 (7.07)	194.5 (12.02)	194.5 (13.44)	206 (18.39)	208.5 (9.19)	201.5 (4.95)
300	254 (23.11)	227.5 (7.78)	234 (28.28)	215.5 (9.19)	228 (15.56)	203 (7.07)	212.5 (4.95)
600	275 (8.68)	211.5 (12.02)	205.5 (14.85)	207.5 (0.71)	234.5 (7.78)	221.5 (4.95)	209 (16.97)
900	257 (8.66)	198 (17.79)	243 (30.04)	190 (2.83)	210 (18.17)	213.5 (13.44)	260.5 (6.36)
1200	223 (3.54)	260 (12.73)	217.5 (2.12)	198.5 (0.71)	235 (4.24)	214 (9.90)	215 (16.97)

Standard deviation in parentheses. n=3

6.5 Conclusions

The powder flow of the unmilled and ball milled materials were analysed by Carr's Index. The results showed that, of the materials tested, the STZNa unmilled powder had the lowest CI and the highest median particle size, indicating good flow properties. As a result of ball milling the median particle size of STZNa was decreased and the CI increased. Han *et al.*, (2011) suggests that a low CI is a result of low interparticle cohesive forces between the particles. The results in this study would suggest the interparticulate forces are high for the majority of the materials and as a result of ball milling they were increased in the case of STZNa.

Tableting of the unmilled and ball milled powders showed that the most significant change in tablet hardness was obtained after the powders were milled for 5 minutes. The most significant result was the increased tablet hardness obtained as a result of tableting the 5 minute ball milled sodium salt samples, indicating that the addition of a sodium ion and ball milling for 5 minutes may result in a significant increase in the tablet hardness when compared to the non-salt form.

Correlating the powder flow properties with the previously characterised property changes that were incurred as a result of ball milling using the Spearman correlation tables yielded results that were either positive or negative but no correlation was zero. This suggested that no one property affected the powders' ability to flow but rather a combination of several material properties. Properties that strongly influenced the powder flowability which had an r value of between ± 0.80 or ± 0.99 were only considered for further analysis as they were deemed more influential. As a result of ball milling STZ I the particle size appeared to increase with ball milling time which resulted in a decreased CI. The particle size has been found to affect the powder flow properties previously (Sun and Grant 2001; Kaerger *et al.*, 2004), as a result of changes to the interparticle bonds. Correlating the changes of the CI with PXRD peak area for STZ III ball milled suggested that the change to the polymorphic form induced as a result of ball milling may have affected the CI.

Correlation of the tablet hardness with the property changes that were incurred as milling time was increased suggested that no one factor affected the tablet hardness. Analysis of the sulfadimidine samples indicated that as tablet hardness increased the SSA_{Tab} also increased,

but this correlation was not apparent for the other materials investigated. The correlation of the sulfadimidine data also suggested a relationship between the increase of SSA_{Tab} and the decrease in PXRD peak area as milling time was increased. The only other correlation that was observed for the tableting data was the relationship between median particle size and the tablet hardness of STZ I as milling time was increased. These three relationships indicated that tablet hardness can be affected by several parameters and, depending on the material, one parameter may be more influential than another.

The fact that no two materials were found to have the same correlating factors could suggest that the bonding mechanism might be different for each material resulting in different properties affecting the tablet hardness and powder flow.

The impact an induced amorphous phase on a materials tablet hardness property was shown as both of these properties changed with storage. This indicated the influence the amorphous phase has in the interparticle bonds which can result in a loss in tablet strength if the amorphous phase is lost.

General discussion

7.0 Introduction

The main focus of this thesis was to determine the impact the ball milling process had on the solid-state properties of the Sulfa materials and to evaluate how these changes affected the material's ability to flow and to evaluate the effect these changes had on the tablets produced from the ball milled powders. The research presented in this thesis focused on the effect ball milling had on API characteristics and the combination of parameters required to induce an amorphous phase as a result of the ball milling process. Previous research in this area was focused on the material's thermal properties, milling time and temperature (Lefort *et al.*, 2004; De Gusseme *et al.*, 2008; Desprez and Descamps, 2006). In the current work, time and temperature were evaluated, along with the effect of the ball to powder weight ratio on the ability to produce an amorphous phase during milling. The sulfa drugs that were ball milled were: sulfadimidine, sulfadimidine sodium salt, sulfathiazole Form I and III and sulfathiazole sodium salt. This series of sulfa drugs were selected to investigate the potential of inducing an amorphous phase in a class of similar compounds and to identify potential similarities in physicochemical and micromeritic properties which could be correlated to powder flow and tablet hardness.

The effect of several different ball milling parameters were tested using sulfadimidine (Chapter 3) and to a lesser extent, sulfadimidine sodium salt (Chapter 4). Different levels of amorphous content were induced into the sulfadimidine structure as a result of increasing the ball milling time. To evaluate the behaviour (i.e. stability) of the induced amorphous phases, the samples were stored at 4 °C over phosphorus pentoxide and the crystallisation kinetics using a modified Avrami equation were evaluated. The change in the amorphous phase over the storage period was evaluated by PXRD peak area analysis and the DSC amorphous content. Form I and III of sulfathiazole and sulfathiazole sodium salt were then milled (Chapter 5). The powder flowability and tabletability properties of the ball milled powders were determined. Correlation studies were used to identify and determine the relationship between the property changes incurred as a result of ball milling to the powder flowability and tabletability properties.

7.1 Physicochemical changes incurred as a result of ball milling

7.1.1 Methods of evaluating change

The unprocessed sulfa materials analysed in this thesis were crystalline in nature before ball milling. When possible, the unmilled samples were compared to the powder X-ray diffractograms obtained from the Cambridge crystallography data centre (CCDC). Feng *et al.* (2008) stated that, as a result of milling crystalline active pharmaceutical ingredients (APIs), the mechanical stress inherent to the process often produces structural changes in the crystal. These structural changes may include loss of crystallinity and/or polymorphic transformations, both of which may be characterised by PXRD analysis. The peak intensity is related to the formation of atoms, as X-ray diffraction intensity corresponds to the number of atoms present at their relevant positions within the crystal motif. Brittain (2002) stated that the milling process causes a variety of deformations and fractures in a solid. Deformations include line defects, surface defects or point defects which can be classified as vacancies (i.e. lattice sites from which units (e.g. atoms, ions, molecules) are missing) and/or interstitials (i.e. molecules that have slipped into voids between lattice sites). Brittain states that with sufficient magnitude, ball milling will result in destroying the long-range order characteristic of a crystal and leave only the short-range order of an amorphous material (Brittain, 2002). Lucks *et al.* (2004) reiterates this point by stating that the XRD peak broadening can be attributed to a reduction of crystallite size and an introduction of defects (microstrain) because of the milling process. The crystallite size reduction has been shown to reduce the intensity and increase the broadening of the Bragg peaks (Willart *et al.*, 2006). Determining the crystallite size is possible by using the Scherrer equation (Scherrer, 1918), if no tailing at the end of the Bragg peaks is present and the peaks analysed are detected for each sample. These requirements were not met during this study, preventing determination of the crystallite size. Hancock (2007) states that at the molecular level, an amorphous material lacks the three-dimensional long range order that is characteristic of crystalline solids; instead their molecules are randomly arranged in space and the interactions between neighbouring molecules are not repeated with any regularity throughout the sample. By inducing an amorphous phase by ball milling, numerous defects are induced, to the point where the crystalline solid is no longer detected. The mechanical properties of the material and the time spent milling will govern the rate and extent at which these defects are induced into the crystalline structure.

The initial experiments which were carried out on binary mixtures consisting of known quantities of amorphous and crystalline SD samples, outlined in chapter 3, confirmed that PXRD could be used to evaluate the change in crystallinity of the material compared to the unmilled sample from the calibration curve constructed, which is shown in Chapter 3. The total peak area change was evaluated and was related to the crystallinity within the samples. This method of analysis is outlined in by the B.P. (2010). The LOD and LOQ obtained for evaluating the crystallinity in an amorphous phase were 2 % and 5 %, respectively. Thermal analysis was used to evaluate the level of amorphous content. The calibration curve constructed in Chapter 3 showed that it was possible to evaluate low levels of a disordered phase. Physical mixtures of known quantities of the crystalline and amorphous SD samples were mixed and tested. The method for evaluating the DSC amorphous content was outlined by Lefort *et al.* (2004) and the LOD and LOQ obtained from the calibration curve for the amorphous phase present in the sample was 3 % and 7 %, respectively.

From both calibration curves it was possible to illustrate the usefulness of these methods with regard to amorphous quantification and the evaluation of the degree of crystallinity within a sample. A discrepancy between the two techniques was evident when the milled samples were evaluated. For example, characterisation of the degree of crystallinity by PXRD total peak area analysis for the majority of the materials, regardless of the milling parameters used, showed that after 5 minutes of milling a loss of crystallinity was apparent. This was in contrast to the thermal analysis data collected for the samples, as milling for 5 minutes did not always result in the detection of the amorphous phase, as indicated by a crystallisation exotherm. The discrepancy observed between the two analytical techniques was detected for several samples as milling time was increased. Caron *et al.* (2011) noted a very similar problem when analysing ball milled alpha lactose by PXRD, NMR and DSC. They stated that as these techniques can easily distinguish pure crystalline matter from pure amorphous matter, which was observed when evaluating the calibration curves in this study. Caron *et al.* (2011) reported that these methods were unable to give a clear determination of an amorphous fraction when there was a 'mix' of phases. The milled samples cannot be considered as a mixture of perfect crystallites and amorphous matter but as an intermediate between these two states. For this reason DSC and PXRD analysis should both be considered when evaluating the changes induced by milling. Caron *et al.*, (2011) suggested that the crystalline defects induced by the milling process results in a static disorder which is not expected to contribute

to a change in the heat capacity at the glass transition temperature. They stated that the reason the change in the crystallinity is not reflected in the thermal analysis is because the molecules near the defects are still partially bonded to crystalline matter which results in difficulties detecting these changes upon heating (Caron *et al.*, 2011). The decrease of crystallite size as a result of ball milling can be reflected by a broadening of the diffraction peaks and may be confirmed by a decrease in the melting temperature according to the Gibbs-Thomas law (Descamps *et al.*, 2007). Therefore the initial peak area decrease observed on milling at earlier time points could be attributed to a decrease in crystallite size. Due to the difficulties in determining the amorphous fraction when the phases were 'mixed' as a result of the milling process, it was not possible to utilise the calibration curves for evaluating the changes within the milled samples.

The correlation studies in Chapter 6 (section 6.3.2) showed that DSC amorphous content and the change in PXRD peak area were strongly correlated for most of the materials with *r* values of -0.92, -0.97, -0.74, -0.74 and -0.82 obtained for ball milled SD, SDNA, STZ I, STZ III-Y and STZNa samples, respectively. The negative correlation value indicated that as one variable increased the other decreased. The results showed that as the DSC amorphous content increased the PXRD peak area decreased as a result of ball milling and that the loss of crystallinity observed by PXRD was reflected by the increased amorphous content determined by DSC.

7.1.2 The effect of the ball to powder weight ratio and temperature

A review of how different parameters affected the change in crystallinity and their ability to induce an amorphous phase was undertaken. The parameters investigated included temperature (RT and 4 °C), ball to powder weight ratio (20:1, 30:1, 35:1 and 40:1) and time (5, 30, 60, 120 minutes and 5, 10, 15 and 20 hours). The quantity of powder that could fit in the milling jars was limited and enough power had to be milled to allow subsequent testing such as tableting and powder flow to be carried out. With this in mind the lowest ball to powder weight ratio (20:1) was investigated first. This allowed 5 g to be milled at once. Ball milling with a BTP weight ratio of 20:1 was carried out at RT and 4 °C from 5 minutes up to 20 hours. The results showed as a result of ball milling sulfadimidine with a BTP weight ratio of 20:1, a partial amorphous phase was induced at either temperature of milling, with the

highest level of disorder obtained at 4 °C. After 20 hours of milling 1.08±0.70 % and 2.01±0.84 % DSC amorphous content was calculated as a result of milling carried out at RT and 4 °C, respectively. Therefore, the initial experiments proved that a higher amorphous phase was induced at 4 °C as opposed to milling at RT conditions. Dujardin *et al.* (2008) reported similar behaviour upon ball milling glucose at RT and -15 °C. They found that after milling at RT the Bragg peaks were broader but they suggested there was no trace of amorphisation. Further studies showed that as a result of ball milling at -15 °C, the Bragg peaks nearly disappeared giving way to a large diffusive bump, indicating that a large part of the material had been amorphised (Dujardin *et al.*, 2008). It was suggested that milling at temperatures lower than the glass transition temperature of the materials of interest increased the chance of obtaining an amorphous phase. Amorphisation at lower temperatures is possible due to the low molecular mobility which prevents the recrystallisation from counterbalancing the mechanical disordering which results in an amorphous state (Dujardin *et al.*, 2008).

Three possible methods were hypothesised, and discussed in Chapter 1, as to how the amorphous phase is induced during the ball milling process. Shakhtshneider and Boldyre (1999) stated that the amorphous phase is induced by a melt/quench process. They described this hypothesis, where at elevated temperatures, induced by the collision incurred by the milling balls resulted in local 'hot spots'. These 'hot spots' are thought to exceed the melting temperature of the material. The temperature of the material should return to RT at the end of the milling process and this rapid change in temperature acts as a quench mechanism, resulting in total amorphisation of the sample. If the hypothesis described by Shakhtshneider and Boldyre (1999) were true, then performing the ball milling process at lower temperatures should hinder the amorphisation process, as the temperature difference between the melting temperature and the milling temperature is greater. The results in this thesis suggest the opposite to the aforementioned melt/quench hypothesis. The results of the current work demonstrated that ball milling SD at 4 °C resulted in a higher amorphous phase than at RT. An example of this was observed when comparing the results obtained after ball milling the SD powder for 5 hours at RT and 4 °C. Ball milling with a ball to powder weight ratio of 20:1 resulted in a DSC amorphous phase of 1.23±0.36 % and 6.73±3.09 % when milling was carried out at RT and 4 °C, respectively. Increasing the ball to powder weight ratio of 40:1 and ball milling for 5 hours showed that an induced amorphous phase of 50.64±3.59 at RT and 79.80±2.01 % at 4°C was obtained. If the hypothesis described by Shakhtshneider and Boldyre (1999) was true, then these results should have produced a higher amorphous phase

at RT and not at 4°C. This difference was observed regardless of the milling time investigated for SD (Chapter 3).

Evaluation of the effect of using different BTP weight ratios was carried out at 4 °C with sulfadimidine. The results indicated that as the BTP weight ratio increased (from 20:1 to 40:1) the level of disorder increased. Rubinstein and Gould (1987) observed that the particle size measurements would be affected by the sample loading but reported no details in relation to the change of crystallinity as sample load decreased. The effect of the BTP weight ratio on the physicochemical properties of sulfadimidine is reported for the first time in this thesis. The details are described in Chapter 3, but the results suggest that as milling time and the ball to powder weight ratio was increased, the level of amorphous content as evaluated by thermal analysis increased, while the crystallinity of the material, as characterised by PXRD total peak area, decreased. This change in the crystalline order could be attributed to the fact that if there is less powder in the jars, the number of ball-to-powder collisions within the milling jars increases. Suryanarayana (2001) suggested that a higher BTP weight ratio will increase the weight proportion to the balls and the number of collisions per unit time increases; as a result more energy is transferred to the powder particles. The shearing effect of the balls and the lower temperature results in a higher level of amorphous material being produced.

The production of an amorphous form of sulfadimidine obtained by ball milling it alone is reported for the first time in this thesis. Amorphisation of sulfadimidine via ball milling was reported by Caron *et al.* (2011) but was only obtained as a result of ball milling with PVP. In Caron *et al.*'s work, a weight fraction of PVP of 0.6 or higher was required in the mixture in order to achieve an amorphous phase by ball milling with a Planetary PM100 ball mill at RT with zirconium oxide milling jars and balls using a BTP weight ratio of 32:1 and the samples were milled for a total to 10 hours. Complete amorphisation in the current study was achieved by milling at 4 °C for a total of 20 hours with a BTP weight ratio of 40:1. The difficulty in obtaining a pure amorphous sulfadimidine sample was previously attributed to its readiness to crystallise. The readiness of the amorphous sulfadimidine to crystallise was also observed in this study, as the sample showed signs of crystallisation within an hour of the ball milling process finishing. Similar events were described by Dujardin *et al.* (2008), who reported that the amorphised glucose sample readily recrystallised at RT after it was amorphised at the lower milling temperature (-15 °C).

To ensure the effect of the ball to powder weight ratio was not isolated to sulfadimidine the influence of BTP weight ratio of 20:1 and 40:1 was carried out with sulfadimidine sodium salt and sulfathiazole Form III. In both cases the samples were more readily amorphised when a BTP weight ratio of 40:1 was used.

7.1.3 The effect of ball milling time

To ensure that crystallisation of the induced amorphous phase after ball milling did not influence the characterisation analysis (i.e. PXRD peak area and DSC amorphous content), a new sample was milled for each set of tests. This resulted in a requirement to produce a large number of samples. Therefore, ball milling at RT resulted in a more practical practice compared to milling at 4 °C. As a more disordered phase could be produced from ball milling with a BTP weight ratio of 40:1, ball milling was carried out for all materials using this BTP weight ratio at RT and ball milling time was increased.

Evaluation by PXRD peak area analysis and the calculated DSC amorphous content for the sulfa materials of interest as milling time was increased is shown in Figure 7.1 (A) and 7.1 (B), respectively. These graphs allow the comparison between both methods used to determine the lack of crystalline order and the level of disorder induced for each of the milled materials compared to their unmilled counterpart.

Complete amorphisation characterised by PXRD and DSC, was achieved as a result of ball milling sulfadimidine sodium salt after 120 minutes at RT (Figure 7.1 A and B) as opposed to a decreased PXRD peak area to 77.40 ± 0.01 % and a DSC amorphous content of 11.85 ± 0.72 % for sulfadimidine after 120 minutes of milling. There is a difference of ~ 75 °C difference between the T_g of SDNa ($T_g = \sim 156$ °C) and SD ($T_g = \sim 78$ °C). A higher T_g than the processing temperature has been shown to produce an amorphous phase more readily (Willart *et al.*, 2006; Dujardin *et al.*, 2008; De Gusseme *et al.*, 2008). Molecular mobility is reduced when processing is carried out at temperatures well below the material's T_g . The greater the temperature difference between the processing temperature and a material's T_g , the higher the chance an induced amorphous phase may remain within the samples structure.

Therefore a higher level of disorder was induced into the SDNa materials when compared to the SD samples as the difference between the processing temperature and the material's T_g was higher. This also explains why a higher level of disorder was induced as a result of ball milling at 4°C in contrast to ball milling at RT.

Caron *et al.* (2007) reported that in the case of ball milling trehalose and mannitol, the nature of the transformation observed upon milling is governed by the position of the expected T_g with respect to T_{mill} (i.e. the milling temperature). They explained that in certain cases, but not all, for amorphisation to occur milling should be carried out below the T_g and polymorphic transformations are achievable when milling above the material's T_g .

A similar observation to that seen with sulfadimidine and sulfadimidine sodium was found when comparing both sulfathiazole polymorphs (Form I and III) and its sodium salt in terms of propensity to amorphise. The results indicated that, as a result of prolonged milling (up to 10 hours), the peak area in comparison to the unmilled materials was reduced to 34.33 ± 0.06 % and 14.00 ± 0.07 % for STZ I and STZ III-Y, respectively. An amorphous halo was detected by PXRD analysis of the sodium salt as a result of ball milling for 10 hours. Thermal analysis showed differences between DSC amorphous content obtained for the 10 hours milled samples with 15.03 ± 1.42 %, 20.55 ± 0.91 %, and 71.15 ± 0.59 % obtained for STZ I, STZ III-Y and STZNa, respectively. The discrepancy between the thermal analysis and the PXRD analysis was apparent for the sulfathiazole materials, but the most significant difference between the analytical methods was regarding the STZNa milled samples. Complete disorder indicated by PXRD analysis may include a mixture of the effects of decreased crystallite size and amorphous content, while thermal analysis evaluated the amorphous content only within the sample. The dramatic difference illustrates the importance of using both analytical techniques when evaluating the changes induced by ball milling. There was ~ 60 °C difference between the T_g s, with STZNa having the higher T_g of ~123 °C and as a higher amorphous phase was induced into the sodium salt structure the results reinforces the influence that the materials' thermal properties have on their ability to amorphise upon milling.

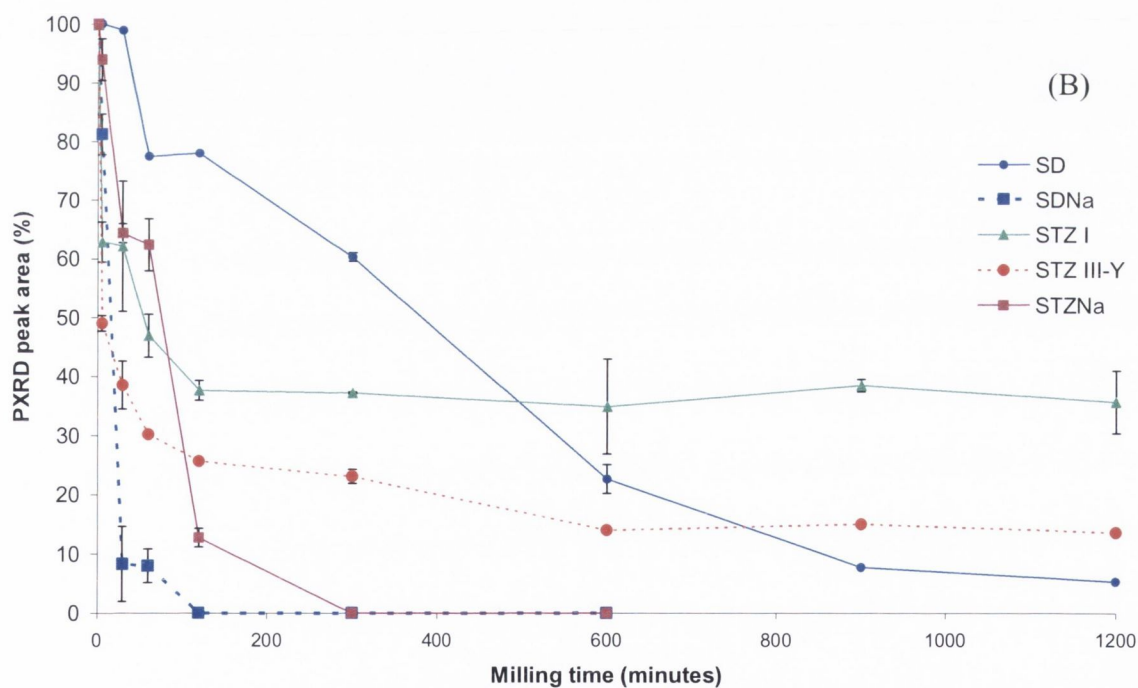
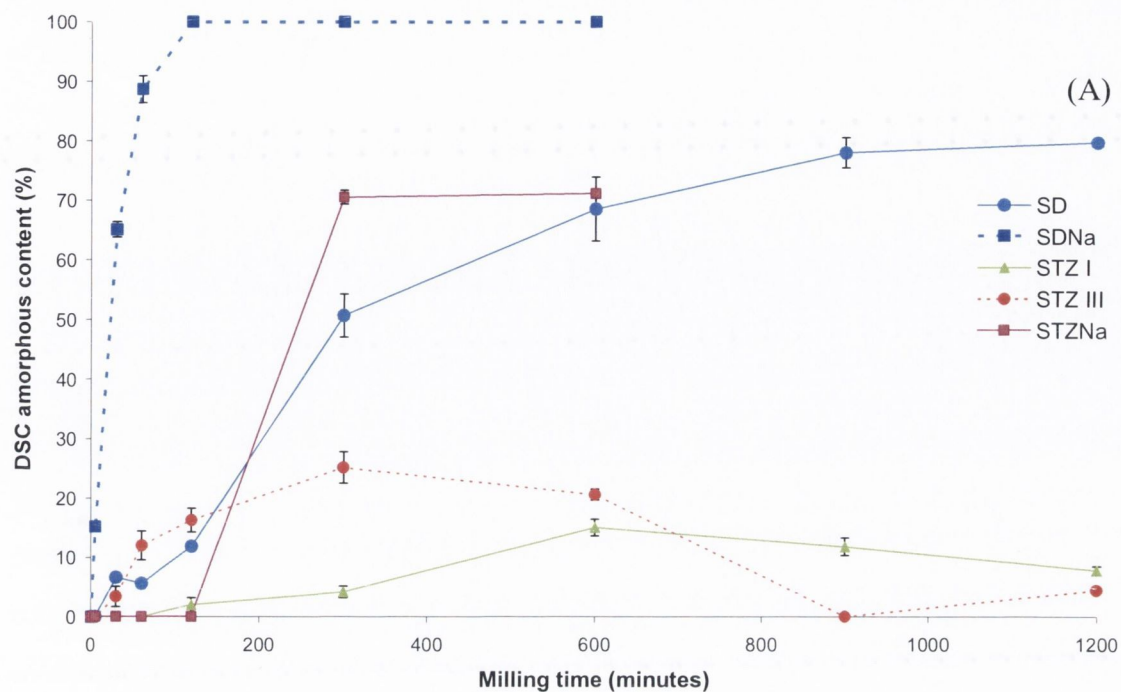


Figure 7.1 (A): Comparison of the total PXRD peak areas and (B) Comparison of the DSC amorphous content, of the unprocessed and ball milled sulfadimidine (blue circle), sulfadimidine sodium salt (blue square), sulfathiazole Form I (green triangle), sulfathiazole Form III (red circle) and sulfathiazole sodium salt (wine square) as milling time was increased. The ball to powder weight ratio was 40:1, the speed was 400 rpm and milling was carried out at RT.

In contrast to sulfadimidine, which resulted in an increased amorphous content as milling time was increased; ball milling of the sulfathiazole polymorphs did not follow the same trend. The quantity of amorphous content fluctuated as milling time was increased, and this was observed for both polymorphic forms. Several studies have shown that ball milling can induce a change in the polymorphic form (Prittimaki *et al.*, 1993; Zhang *et al.*, 2002; Talekar *et al.*, 2005). Due to the broad Bragg peaks it was difficult to evaluate the change in polymorphic form as milling time was increased but a thermal transition confirmed a transformation from one form to another had occurred. Byrn *et al.*, (1999) suggested that the polymorphic change in the solid state requires three steps; molecular loosening, solid solution formation and crystallisation of a new phase. The thermogram of Form III has two distinct events; the first is detected between 130-170 °C which is attributed to the solid state transition of Form III to Form I and the second is the melting of Form I, at 201 °C. The thermogram of Form I only contains the melt endotherm attributed to Form I. Analysis of the ball milled STZ III-Y samples suggested that a mixture of polymorphic forms was present, as two endothermic transition peaks characteristic of a solid state transition and a melt were detected (Chapter 5, section 5.4.1.1.2.)

Analysis of the STZ I milled samples suggested that the amorphous phase acted as an intermediate phase from which a different polymorphic form can crystallise. Analysis of STZ I showed that after a milling time of 120 minutes, 2.01 ± 1.21 % DSC amorphous content was present and only one endothermic melt peak was detected. Ball milling for 5 hours resulted in the detection of a solid-state transition at ~ 95 °C and an amorphous phase of 4.17 ± 0.94 %. The amorphous phase induced after 120 minutes may not have been sufficient for the production of a new polymorphic form but the level of disorder induced after 5 hours appeared to be adequate. The transition temperature was found to be lower than those quoted in the literature but, as a reduced crystallite size has been shown to decrease the melt temperature, in this case it may have also contributed to the position change of the solid state transition temperature. It was not possible to determine the polymorphic forms as none have been reported with such low transition temperatures and the broadened Bragg peaks prevented the detection of characteristic polymorphic peaks. Munroe *et al.* (2012) carried out extensive research on the stability of the sulfathiazole polymorphs and reported that the materials held at temperatures between 10-50 °C would follow Ostwald's rule of stages (Threlfall, 2003; Ostwald 1897), where Form I would convert to Form V, Form V to Form IV, Form IV to Form II and then Form II to FIII. The rate of this process may be very fast or slow depending

on the temperature and the number of seed crystals. These conversions are thought to have occurred for the ball milled STZ samples as a result of an intermediate amorphous phase. An intermediate amorphous phase induced as a result of ball milling has been reported by De Gusseme *et al.* (2008) as a result of ball milling fananserine which has four reported polymorphs. De Gusseme *et al.* reported that as a result of ball milling Form IV at different times an intermediate amorphisation stage was detected and this was followed by a transformation towards the metastable crystalline phase I.

Other changes observed as milling time was increased include the different presentation of the crystallisation exotherms observed for SD, SDNa and STZNa, which showed that as milling time was increased the crystallisation exotherm became increasingly larger and shifted towards higher temperatures. To illustrate this as SD was ball milled for 30 minutes the crystallisation exotherm was detected at ~ 53 °C, after 60 minutes of milling the crystallisation onset temperature of ~ 65 °C was measured and as milling time was increased to 20 hours crystallisation was detected at ~ 88 °C.

Caron *et al.* (2011) reported a similar event upon ball milling lactose and found that, as a result of prolonged milling, the crystallisation exotherm shifted towards higher temperatures. Caron *et al.* (2011) stated that this revealed an increase of the stability of the amorphous material against crystallisation. They thought that this behaviour was likely to be due to one of two reasons; the first reason suggested was that the shift towards higher temperatures may be attributed to the disappearance of the very last remaining crystalline nuclei, which were not milled during the first 12 hours; the second suggestion was that, due to the evolution of a local order in the amorphous material, a change in the nucleation and growth mechanisms driving the recrystallisation process occurred (Caron *et al.*, 2011). Trasi *et al.* (2010) ball milled griseofulvin and found the opposite effect that is increasing milling time resulted in a recrystallisation peak shifting to lower temperature. They attributed this to a change in specific surface area. With the huge surface area generated as a result of the fragmentation process during milling, recrystallisation was possible at the lower temperatures.

The results in this thesis suggest that the changes incurred as a result of ball milling are not only influenced by the different milling parameters but are also contributed to by the different physicochemical properties of the materials, which makes it difficult to predict the outcome of the milling process.

7.1.4 Stability of the induced amorphous phase

Inducing different levels of an amorphous phase or a loss of crystallinity by ball milling was the main aim for the first section of this thesis. The second section evaluated the effect the induced amorphous phase had on the powder flow and tableability properties, as presented in Chapter 6. In order to test the effect the amorphous phase had on the sample's tableability and powder flow properties, the stability of the induced amorphous phase was evaluated.

Thermal stability of the induced amorphous phase was different for each sample. Over an 84 day period the amorphous phase induced to the SD structure showed signs of crystallisation, characterised by thermal analysis. In contrast to this, the amorphous phase induced to the SDNa material appeared stable over the 84 days. This may be attributed to the higher level of disorder induced into the SDNa structure as a result of ball milling as well as, the significant difference between the storage temperature and the T_g of SDNa. The samples were stored in desiccant conditions at 4 °C; a profile of these monitored conditions over a long period was presented in Chapter 3. Hancock and Zografi (1997) stated that below the T_g the material is 'kinetically frozen' into a thermodynamically unstable glassy state with respect to both the equilibrium liquid and the crystalline phase. Yoshioka *et al.*, (1994) reported that a T_g close to the storage temperature may allow molecular mobility which results in crystallisation. Therefore, to slow this process down the T_g should be at least 50 degrees higher than the temperature of storage. The storage temperature never exceeded 5.4 °C and the relative humidity was kept below 4.5 %. This storage temperature is at least 50 degrees below the reported T_g 's of the materials investigated. The fact that SD was not completely amorphised may contribute to the crystallisation of the amorphous phase which could be attributed to the existence of residual nuclei of the crystalline material that survived the milling process and which promoted the crystallisation process.

To understand the mechanism of the transformations, the crystallisation kinetics for the SD milled samples at RT with a BTP weight ratio of 40:1 were evaluated by using a modified version of the Avrami equation described by Yang *et al.* (2010). From this analysis the best fit Avrami exponent (n) and the crystalliation rate constant (k) were calculated. The exponent (n) depends on the nucleation mechanism and the number of dimensions in which growth occurred. The calculated rate constants for each of the milled and stored samples analysed by both DSC and PXRD are given in Table 7.1. Roulet *et al.* (1988) reported that increasing intensities and areas of peaks in X-ray diffraction patterns describes the development of

crystallisation. For the analysis of the peak area, the total diffractogram was used, as individual peaks were difficult to isolate. Thermal analysis was used to determine the loss of amorphous content on storage.

The plots fitted in Chapter 3 showed that the crystallisation kinetics followed the modified Avrami equation. The value for the Avrami exponent n was found to result in the best fit if it was kept at 3, which assumes that all of sulfadimidine amorphous samples had the same or similar three dimensional growth. The rate of crystallisation was different depending on the analytical method used. Analysis of the PXRD data suggests that the amorphous content induced as a result of ball milling for 60 minutes recrystallised the fastest ($k=6.0 \times 10^{-5} \text{ days}^{-1}$). The results showed that the rate for crystallisation was different for each sample (Table 7.1).

A more significant difference was observed for the DSC amorphous contents data (Table 7.1). As discussed previously, the longer ball milling time produced a higher level of disorder into the material's structure. The crystallisation kinetics suggest that the amorphous content induced after 60 minutes of milling recrystallised at a faster rate when compared to the amorphous content induced after 20 hours with k values of $8.2 \times 10^{-2} \text{ days}^{-1}$ and $5.0 \times 10^{-4} \text{ days}^{-1}$ obtained, respectively. Analysis of all the samples suggests that the crystallisation kinetics are not directly proportional to the increased level of amorphous content induced but they do appear to slow with higher levels of amorphous content induced. Yang *et al.* (2010) stated that the S-shaped curve of recrystallisation produced for each material (shown in Chapter 3) was due to the presence of a small number of nuclei at the very beginning, followed by a rapid recrystallisation and a decline in the recrystallisation rate observed at the later stages of storage, due to the consumption of nucleation sites..

The results suggested that the DSC amorphous content proved to be a better method for analysing the changes to the amorphous phase induced as a result of ball milling. PXRD peak area analysis evaluates several changes such as the crystallite size, stress and strain to the lattice structure and the loss of crystallinity. Therefore, it was difficult to evaluate the crystallisation kinetics using the PXRD peak area, as the peak area changes were not exclusively associated with the amorphous phase.

Table 7.1: Crystallisation rate constants, k (day^{-1}) analysed for SD milled and stored samples, characterised by DSC and PXRD. Note the Avrami exponent $n=3$

Time (minutes)	k (day^{-1})	R^2	k (day^{-1})	R^2
	PXRD analysis		DSC analysis	
60	6.0×10^{-4} (7.1×10^{-5})	0.7806	8.2×10^{-2} (3.0×10^{-4})	0.8139
120	1.2×10^{-4} (4.02×10^{-5})	0.8733	7.3×10^{-3} (7.2×10^{-5})	0.8993
300	3.8×10^{-4} (4.31×10^{-5})	0.7936	1.1×10^{-3} (2.4×10^{-5})	0.8471
600	3.0×10^{-4} (1.2×10^{-5})	0.6960	1.2×10^{-3} (4.8×10^{-5})	0.8416
900	3.3×10^{-4} (1.5×10^{-5})	0.7245	3.3×10^{-3} (4.3×10^{-5})	0.8714
1200	2.3×10^{-4} (1.8×10^{-5})	0.8996	5.0×10^{-4} (3.9×10^{-5})	0.8174

Standard deviation in parentheses, $n = 3$

Analysis of the STZ ball milled samples found that change in the PXRD peak area and DSC amorphous content was detected after an hour of storage. This was evident for STZ III-Y as the PXRD peak area increased and the DSC amorphous content decreased. For example, STZ III-Y milled for 60 minutes with a BTP weight ratio of 40:1 at RT resulted in the phase transition temperature shifting to ~ 119 °C from ~ 134 °C after one hour of storage and after one week the sample completely crystallised and the phase transition temperature was detected at ~ 126 °C. A similar change in the solid state transition temperature was apparent for the other STZ III-Y milled samples (120 minutes, 5, 10, 15 and 20 hours) and was discussed in Chapter 4).

Analysis of the STZ I samples demonstrated a similar behaviour observed for STZ III-Y ball milled samples, where the induced amorphous phase showed signs of crystallisation after 1 day of storage. Thermal analysis showed that as the amorphous content decreased, a solid state transition temperature indicating the formation of a new polymorphic form was detected. This was discussed above and it is thought that the induced amorphous phase acted as an intermediate phase between the polymorphic form of the unmilled material (STZ I or STZ III) and the phases that crystallised out after the ball milling process was completed and the samples were stored.

In terms of the materials ball milled in this study, it was only possible to determine the crystallisation kinetics of SD over the period of interest. Unlike SDNa which retained a high level or complete amorphous content, depending on the sample, STZNa resulted in a phase that readily crystallised. Zhou *et al.* (2008) suggested that differences between materials' molecular mobility can result in certain materials crystallising faster than others. The presence of seed crystals remaining within the STZNa structure after prolonged ball milling may have contributed to the recrystallisation of the amorphous phase.

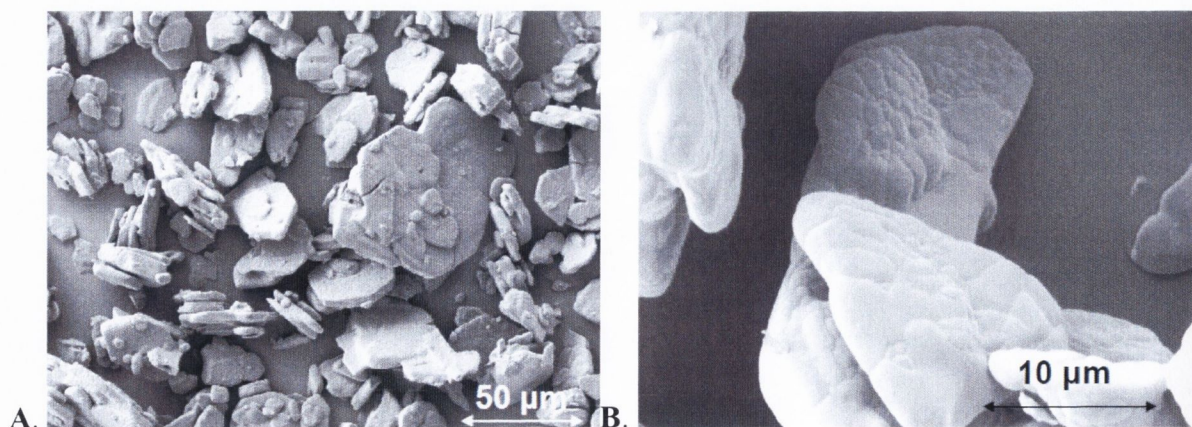
The readiness of certain materials to crystallise to a more thermodynamically stable state may have contributed to the fact that a significant difference was not always apparent between the powder flow and tablet properties of the crystalline samples and the samples that contained high levels of an amorphous phase, as was expected. This is discussed further below.

7.2 A review of the morphology and particle size changes incurred as a result of ball milling

7.2.1 Morphology

The morphologies of the unmilled materials were all different and are shown in Chapters 3, 4 and 5, but regardless of the ball milling time investigated the morphology of the samples changed in comparison to their unmilled counterpart. The morphology of the milled samples were, in general, irregular in both size and shape and the particles appeared to agglomerate. The change to the morphology was apparent after 5 minutes of milling, for all materials. In certain cases, such as STZNa, SDNa and STZ III prolonged (120 minutes or longer) milling resulted in the detection of larger particles these were shown in the morphology section of each chapter. Brodka-pfeiffer *et al.* (2003) reported on the formation of agglomerated fine particles as a result of ball milling salbutamol sulphate, which consisted of a needle like morphology before milling. They stated that the agglomerates were 15-140 μm in diameter and the agglomerated particles were loosely bound together and could be easily dispersed. The agglomerates found in the ball milled sulfa samples were within this diameter range. Brodka-pfeiffer *et al.* (2003) found that the fine particles ($<1 \mu\text{m}$) had a cohesive nature and attributed this to their electrostatic charge.

The identification of a polymorphic form is possible from its morphology. STZ Form I is described as needle shaped and Form III is described as hexagon shaped (Blagden *et al.*, 1998). Form III is the commercial stable polymorph and Form I can be obtained by heating the commercial raw form III material to above 180 °C for 30 minutes (Chan *et al.*, 1999) or by recrystallising from *n*-propanol at 80 - 90°C (Grove and Keenan, 1941). The reported morphology for STZ I has been produced from the recrystallisation method from solution. The polymorphic Form I material produced for ball milling in this study was obtained via heating the commercially available Form III material to above 180 °C for 30 minutes. The conversion was shown to be successful as PXRD analysis produced a diffractogram that was characteristic of Form I and thermal analysis indicated that only one thermal event was detected which was attributed to the characteristic melt endotherm of Form I. The morphology still resembled the hexagonal plates that were detected for the form III material. The conversion from Form III to Form I was confirmed by PXRD and DSC analysis for several samples and in every case the hexagonal crystals were detected. The SEM images for unmilled STZ III-Y compared with Form I produced by heating are shown in Figure 7.2. These results have never been presented before as no SEM images have been previously reported for the Form I sulfathiazole material produced via heating. The morphology of a material has been reported to affect material flow and tablet properties (Podczek and Miah, 1996; Sun and Grant 1999; Sun and Grant 2001). If it is possible to manipulate a polymorphic form by heating to above a transition temperature in order to produce the more desirable form that consists of a morphology that is easier to handle during processing, it may result in a more efficient process.



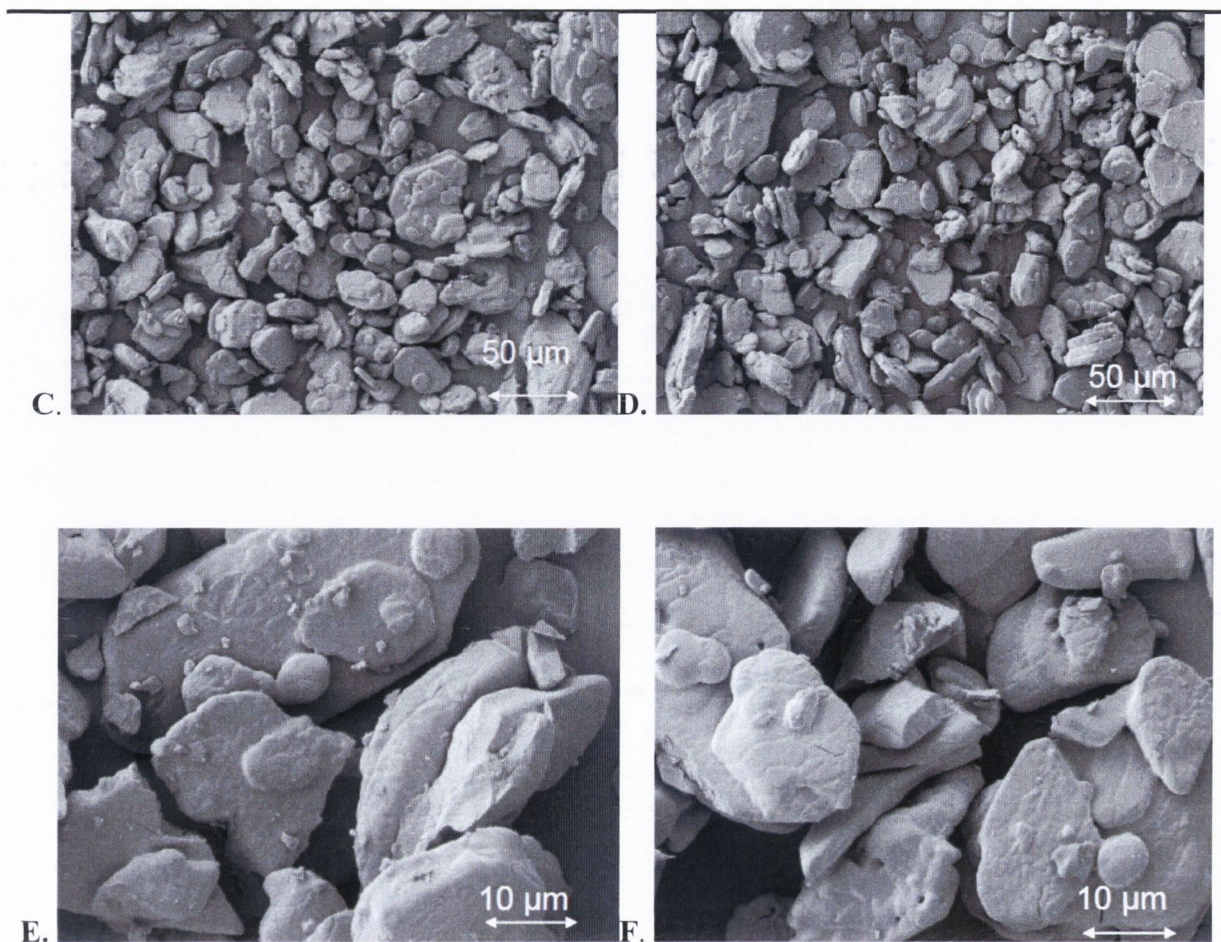


Figure 7.2: SEM analysis of (A and B) STZ III-Y unmilled obtained from Sigma and (C, D, E and F) STZ I unmilled produced in the lab.

7.2.2 Particle size

The particle size analysis of the unmilled and milled sulfa powders was carried out by Malvern laser diffraction. As a result of ball milling bi- or tri modal distributions were obtained regardless of the material, time or ball to powder weight ratio used. The agglomerated particles that were detected by SEM analysis may have contributed to the distribution profiles. As previously mentioned, Brodka-pfeiffer *et al.* (2003) reported an increase in the particle size as milling time was increased. They found that the agglomerates which consisted of particles that were less than 1 μm in size were difficult to de-agglomerate, as these structures were very cohesive in nature. Therefore the pressure used during the particle size analysis may not have been sufficient in de-agglomerating all of the fine particles. These agglomerated particles would contribute to the increased d90 measurements as well as a bi- or –tri distribution profile.

Ball milling for 5 or 30 minutes, depending on the material, resulted in a decreased median particle size. For certain materials increased milling time resulted in an increased median particle size. Figure 7.3 presents a comparison of the median particles sizes of SD, SDNa, STZ I and STZ III-Y unmilled and their corresponding samples milled for 5 minutes. To illustrate the increased particle size as milling time was increased the median particle size for SD and STZ I ball milled for 20 hours, SDNa milled for 10 hours and STZ III-Y milled for 120 minutes is also presented in Figure 7.3. These different times were used as they illustrate the best example for the change in particle size. STZNa was not presented in Figure 7.3 as the large median particle size would increase the y-axis scale, making it difficult to observe the changes incurred by the other materials. STZNa unmilled median particle size was $84.45 \pm 4.01 \mu\text{m}$, which was reduced after milling. Comparing the samples in Figure 7.3 shows that prolonged milling of both sulfathiazole polymorphs resulted in an increased particle size, unlike for ball milling of SD, where prolonged milling resulted in no statistically significant change in the particles size was observed when compared to the 5 minute milled sample and the SDNa prolonged mill sample increased in size in comparison to it's 5 minute milled sample but it was still smaller then the unmilled SDNa material. Thermal analysis of the ball milled polymorphs indicated that the ball milling process resulted in a solid state transformation and storage of the samples for 1 day indicated that the induced amorphous phase acted as an intermediate phase. It is possible that the increased particle size could be due to the new polymorphic form that was caused by the ball milling process but it may also be attributed to the agglomeration of fine particles ($\leq 1 \mu\text{m}$). Crystallisation of an amorphous phase requires the presence of nuclei. Brodka-pfeiffer *et al*, (2003) reported the particle size changes incurred as a result of ball milling time for salbutamol sulphate. They found that an initial decrease in the particle size distribution was evident when the sample was milled for 10 minutes. Further milling of 5 hours resulted in the particle size distribution increasing. They suggested that this phenomenon could be the simultaneous recrystallisation of the amorphous material and therefore particle growth. Humphreys and Hatherly, (1995) stated that once a viable nucleus exists, it grows; consuming the deformed and recovered material around it and a driving force behind this growth was attributed to the strain energy of dislocation. The results presented in Figure 7.3, showed that the median particle size increased as milling time was increased. This change is important to consider as the particle size as been shown to affect several aspects of the drug manufacturing and delivery process and ball milling is commonly used to decrease particle size, not to increase it.

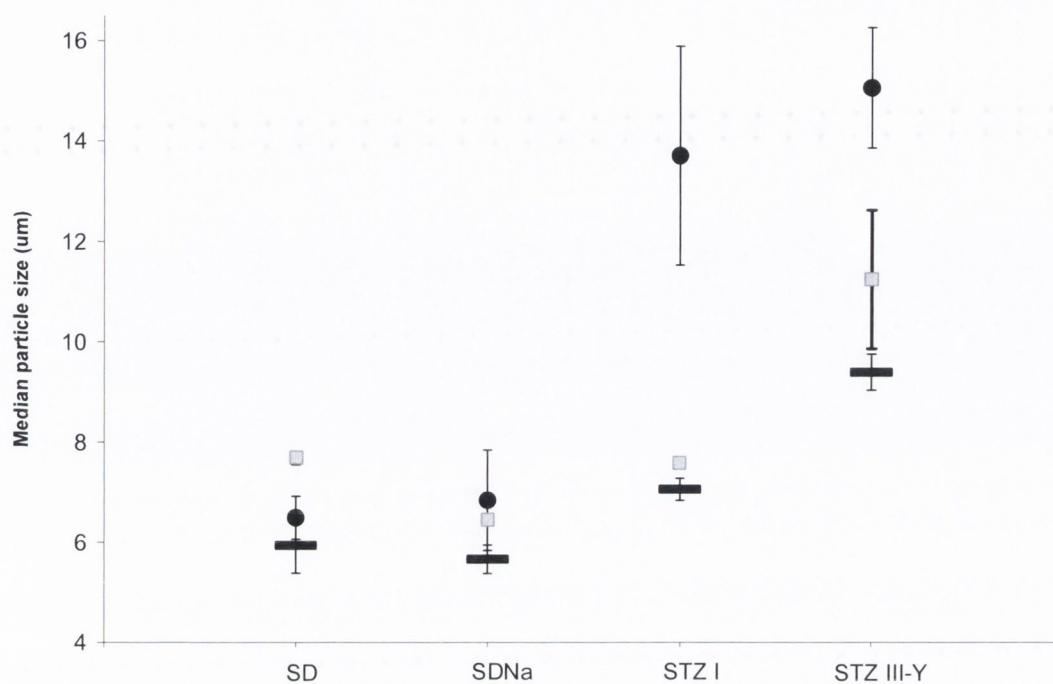


Figure 7.3: The median particle size (d50) determined by Malvern laser diffraction of unmilled sulfadimidine, sulfadimidine sodium salt, and sulfathiazole form I and sulfathiazole form III illustrated by the grey squares. The d50 determined after 5 minutes of milling for each material which is illustrated by the black rectangle. The black circles indicates the d50 obtained for SD and STZ I ball milled for 20 hours; SDNa milled for 10 hours and STZ III-Y milled for 120 minutes. All ball milled samples were milled at RT with a BTP weight ratio of 40:1.

7.3 Powder flow and tablet hardness

7.3.1. Powder flow

The powder flow properties of the unmilled and ball milled sulfa materials were evaluated using Carr's compressibility index (CI). The powders tested included the unmilled materials and the materials ball milled at RT with a BTP weight ratio of 40:1 and mill time was increased from 5 minutes up to 20 hours. The results showed that, as characterised by the CI classification system, the majority of the materials tested, unmilled and milled, were classified as having poor, very poor or extremely poor flowability. STZNa unmilled powder was classified as having good flow properties. Jallo *et al.*, (2012) reported that the CI was dependent on the particle size, regardless of the other material properties. They found that if

the median particle size was $<30\ \mu\text{m}$, the powders were classified as having poor flow, and if the median particle size was $>30\ \mu\text{m}$ it resulted in a material with good flow. This was consistent with the results presented in this study as STZNa was found to have a considerably larger median particle size ($\sim 80\ \mu\text{m}$) in comparison to the other materials (milled and unmilled; ~ 5 to $12\ \mu\text{m}$) indicating that the particle size was an influencing factor. Ball milling of STZNa for 5 minutes or longer resulted in a reduced median particle size to below the $30\ \mu\text{m}$ threshold described by Jallo *et al.*, (2012) accompanied by a change to the materials powder flowability properties to very poor. Several studies have shown that a reduced particle size results in poor flow properties (Liu *et al.*, 2008; Kaerger *et al.*, 2004; Luukkonen *et al.*, 1999). Mullarney *et al.*, (2003) suggested that the flow is hindered as a result of reduced particle size as the smaller particles have a larger true contact area between the particles that can contribute to an increased friction coefficient which would result in a decreased ability to flow.

Analysis by SEM showed that, as a result of ball milling, the particle size decreased but the formation of agglomerated structures was inevitable; however not all of the particles participated in these agglomerates. Mokkapati (2006) stated that agglomerates form in order to minimise the particles' energy and as a result of agglomeration the surface energy should decrease. The formation of the agglomerated particles may have been as a result of an induced amorphous phase and the reduced particle size, which has been shown to increase surface energy (Buckton and Gill 2007; Ohta and Buckton, 2004). The formation of the agglomerated particles may have also resulted in a decreased cohesiveness between the particles. The CI of the ball milled materials indicated poor flow which suggests that the formation of the agglomerated particles did not decrease the particles cohesiveness significantly. Bolhuis *et al.* (2009) found that agglomerated milled isomalt particles with a d_{50} of $240\ \mu\text{m}$ had excellent flow in comparison to milled particles with a d_{50} of $22\ \mu\text{m}$ which had poor flow properties. They determined particle size by laser diffraction which would suggest that the agglomerated structures had sufficient bonding strength to withstand the forces and pressures used for this analysis.

The ball milled sulfa materials in this study resulted in low d_{50} values (~ 5 to $12\ \mu\text{m}$) but high d_{90} values (~ 30 and $200\ \mu\text{m}$) and all ball milled particle size distribution histograms were bi- or tri- modal. This would suggest that a small number of agglomerates may have withstood

the forces and pressures applied during particle size analysis while the majority may not. The agglomerates that were bound tightly together may have improved flow while the reduced particle size and the induced amorphous phase resulted in materials that had poor flowability.

The correlation studies showed that no one property correlated strongly with powder flow but each property appeared to contribute, as a correlation coefficient of zero was never obtained. A negative Spearman correlation coefficient was obtained as a result of comparing the CI and the DSC amorphous content. The r values obtained were -0.32, -0.64, -0.54, -0.67 for ball milled SD, SDNA, STZ I and STZ III-Y. The negative results suggest that as one variable increased the other decreased. Therefore, the Spearman correlation showed that as the DSC amorphous content increased, as a result of ball milling, the CI decreased and the lower the CI, the poorer the powder flow properties. An induced amorphous phase is cohesive in nature and this increased cohesiveness impacts on powder flow properties.

7.4 The influence ball milling had on the tableability

As tablets are the most commonly used pharmaceutical dosage form today (Armstrong, 2007), it was of interest to investigate if and how the changes that occurred as a result of ball milling affected the compact/tablet hardness. An induced amorphous phase into an API's structure may only have an affect if the tablet consists of a high dosage form. In a low dosage form the the excipients added will have more influence than the API. The changes to the API as a result of ball milling were only investigated in this study. After different compression pressures were evaluated using only the unmilled material in order to determine the best pressure to use to ensure a solid robust compact/tablet was formed, the milled powders were compressed using the same compression pressure. The tablets produced were tested for their hardness and specific surface area. The physical strength of a tablet is dependent on the extent and strength of interparticulate bonds and these in turn are related to the compressive force which is applied (Armstrong, 2007). The effect that different compressive forces has on a tablet has been well documented (Sebhati and Alderborn, 1999; Busignies *et al.*, 2011; Sun 2005; Picker-Freyer *et al.*, 2007) and was therefore not considered for this study. Heistand (1997) stated that tableting is the process of sliding, fracturing and deforming particles enough to fit them closely together, the attraction is inherent.

As a result of ball milling the powders for only 5 minutes and tableting them under the same compression pressure a statistically significant increase in the tablet hardness was apparent when compared to the tablets produced using the unmilled materials. Ball milling for 5 minutes resulted in a decreased particle size distribution and an amorphous phase was detected for both sodium salts. Bolhuis *et al.*, (2009) noted a similar trend, where the particle size reduction resulted in poor flow properties but the crushing strength of the milled material increased enormously. They attributed the increased crushing strength to the increased surface area and stated that the milled isomalt material had a much higher surface for bonding, which resulted in a higher crushing strength. Similar results were reported by Mullarney *et al.* (2003) where they attributed the poor tablet strength obtained from tableting the larger particles to the low interparticulate bonding strength. They stated that the smaller particle size would increase particle-to-particle interactions and improve tensile strength.

As mentioned previously, prolonged milling affected the median particle size as well as the induced amorphous phase and in the case of sulfathiazole, a polymorphic change was observed. Tablet hardness also varied. Hancock *et al.*, (2002) found that the amorphous phase appeared to have a lower compaction strength than its crystalline counterpart which was attributed to the brittle 'glassy' nature of amorphous materials. These previous reports would suggest that the tablet hardness should increase as a result of the decrease in particle size and the increased surface area but that the induced amorphous phase should increase the brittle nature of the compacts. The most significant change to the tablet hardness and particle size was observed after the samples were milled for 5 minutes. As a result of ball milling for 5 minutes the median particle size decreased and the tablet hardness increased. Further ball milling often resulted in unpredictable changes to the median particle size, as discussed in section 7.2.2. Correlating the tablet hardness of the ball milled SD, SDNA, STZ III and STZNa powders with the changes in the median particle size resulted in a low r values, indicating a weak correlation between the properties. The specific surface area determined by BET and the DSC amorphous content were found to have a greater impact on the tablet hardness properties, as the correlation coefficient was higher. Comparing the specific surface area to the tablet hardness resulted in a positive r value for all of the materials. This indicated that as the surface area increased the tablet hardness would increase. This would suggest that as the surface area increased a larger number of bonds could be formed resulting in a stronger compact. Comparing the induced amorphous phase to the tablet hardness by means of a

correlation study showed a positive correlation between these properties existed. Therefore, an increased level of amorphous content would result in increased tablet hardness. This may be attributed to the cohesive nature of an amorphous material. This correlation was stronger for the non-salt forms. The r values obtained as a result of correlating the tablet hardness and the DSC amorphous content were 0.79, 0.22, 0.62, 0.70, 0.04, for SD, SDNA, STZ I, STZ III and STZNa. The tablet hardness obtained from the compressed 5 minute milled powder for both sodium salt powders was significantly higher than their unmilled counterparts. However, the induced amorphous phase increased as milling time increased. The low amorphous phase induced into the sodium salt structures as a result of ball milling for 5 minutes may have been an adequate change, necessary in increasing the tablet hardness. The change to the DSC amorphous content and the tablet hardness as milling time was increased were disproportional. As both sodium salted were completely amorphised as a result of milling, the tablet hardness under go such did not significantly change as milling time was increased. This may have resulted in the low correlation values.

Similar to the powder flow results the correlations studies did not indicate one particular physicochemical property that affected the tablet hardness of all the materials tested, but as no correlation resulted in zero it suggested that the tablet hardness is influenced by a number of interacting physicochemical properties. Over all, these results suggest that properties that affect powder flow may improve tablet hardness and *vice versa*.

Processing, such as ball milling, has been shown to affect the tablet hardness of the compressed powders. More often than not these ball milled powders are stored. Compression of the stored ball milled powders showed that the tablet hardness varied with storage time but the results were unpredictable (Chapter 6). The induced DSC amorphous content decreased over time and overall the tablet hardness of the stored powders decreased. This suggests that the decrease in DSC amorphous content reduces the tablet hardness of the compacted powders. This study showed that each material is different and familiarity of the material's properties before large scale processing and after a prolonger storage period is essential.

7.5 Conclusion

One of the main aims of this thesis was to determine how the induced amorphous phase incurred as a result of the ball milling process affected a material's ability to flow and its tableability. This proved more difficult than expected as the ball milling process did not always induce an amorphous phase but regardless of whether or not this disordered phase was induced. To evaluate the data and the relationships between the properties the Spearman correlation was used. The Spearman correlation studies also found that the median particle size and the specific surface area impacted on flowability and tablet hardness properties. This was suggested as no correlation was determined to be zero. As mentioned previously in Chapter 6, the Spearman correlation is used when two variables are experimentally determined such as DSC amorphous content and powder flow. The correlation coefficient, r , quantifies the direction and magnitude of the correlation, suggesting the degree of change of one variable in relation to another measured variable. The correlating factors included the CI, DSC amorphous content, PXRD peak area, the median particle size determined by laser diffraction and the specific surface area determined by BET analysis. The results were unexpected as the DSC amorphous content measured for each sample as a result of increased ball milling time did not strongly correlate with the CI or tablet hardness; however the non-zero correlation coefficient confirms that tablet hardness and powders flow is not an inherent material property but is a result of a combination of material physical properties.

Overall the study showed that as a result of ball milling solid-state property changes are possible and these will affect further processes that involve flow and tableting. The study suggests that a more rigid parameter controlled experiment is needed where the particle size, morphology, surface area are kept constant and the level of disorder is varied systematically.

7.6 Main findings:

- An amorphous phase is more readily induced at 4 °C than at room temperature.
- A higher ball to powder weight ratio resulted in a higher level of disorder induced into the material's structure.
- The sodium salt materials resulted in higher levels of amorphous content when compared to their non-salt forms. This was attributed to the difference in T_g .
- Ball milling of the sulfathiazole polymorphs does not result in an increased amorphous phase as milling time is increased. The amorphous phase induced acts as an intermediate state from which new polymorphs may crystallise.
- Differences in the kinetics of crystallisation was possible to determine by thermal analysis but not by evaluating changes to the PXRD total peak area.
- Changes to the materials investigated were apparent after 5 minutes of milling but the DSC amorphous content, median particle size and the specific surface area changes were not directly proportional to an increased milling time. These parameters changed unpredictably as milling time was increased.
- Prolonged ball milling was found to result in an increased median particle size.
- The tablet hardness and powder flow properties were significantly changed as a result of ball milling. This was observed for all of the sulfa materials milled and the change was evident after the powders were milled for as little as 5 minutes.
- The correlation studies showed that no correlation was zero which suggested that the powder flow and tablet hardness were affected by the different changes induced to the solid-state nature of the powders as a result of the ball milling process. These changes included the induced amorphous phase, the decrease in crystallinity and the median particle size and the change to the powders specific surface area BET.
- Storage of the SD ball milled powders over the 84 day period resulted in tablet hardness of the compacts produced from these powders to change. These changes were found to be unpredictable.

7.7 Future work:

- To investigate the changes to the crystallinity by PXRD peak area analysis using different APIs with the intention of evaluating the degree of change and to investigate if this change has the same significant effect on the material tablet hardness.
- Evaluation of the crystallite size changes by slower PXRD scans.
- Evaluate the crystallite size of the polymorphs to see if they not only affect the melt temperature but if they influence the solid state transition temperature also.
- Investigation into the different crystallisation kinetics to determine the difference between the crystallisation rates and nucleation mechanisms for several sulfa drugs to deduce if a correlation could be made between their different solid-state properties and the rate at which they crystallise. This would be with the aim to further understand the influencing factors that affect the recrystallisation kinetics of a material.
- The changes that incurred to the ball milled materials prevented a clear understanding of how an amorphous phase may affect the tablet hardness and powder flow properties; therefore it may be of interest to analyse materials that have a more stable amorphous phase to evaluate the effect of a disordered phase may have on these parameters. The other solid-state properties that have been shown to influence powder flow such as particle size, morphology and surface area should be kept constant.

References

Reference

- Abdelloui M. and Gaffet E. (1996) 'The physics of mechanical alloying in a modified horizontal rod mill: mathematical treatment', *Acta Materialia*, 44(2), 725-734.
- Adi H., Larson I and Stewart P. (2007) 'Laser diffraction particle sizing of cohesive lactose powder', *Powder Technology*, 179, 90-94.
- Adolfsson A., Gustafsson C., and Nystrom C. (1999) 'Use of tablet tensile strength adjusted for surface area and mean interparticulate distance to evaluation dominating bonding mechanisms', *Drug development and Industrial Pharmacy*, 25(6), 753-764.
- Admond D.A., and Grant D.J.W. (2001) 'Hydrogen bonding in sulfonamides', *Journal of Pharmaceutical Sciences*, 90(12), 2058-2007.
- Amidon G.E., Secreast P.J., Mudie D., (2009) Particle, powder, and compact characterization. In: Developing solid oral dosage forms: pharmaceutical theory and practice. *Academic press, Burlington, USA*, page 169.
- Anwar, J., Tarling, S.E., Barnes, P. (1989) 'Polymorphism of sulphathiazole', *Journal of Pharmaceutical Science*, 78, 337-342.
- Apperley D. C., Fletton R. A., Harris R. K., Lancaster R., W., Tavener S. and Threlfall T. L. (1999) 'Sulfathiazole polymorphism studied by Magic-Angle spinning NMR', *Journal of Pharmaceutical Science*, 88(12), 1275-1280.
- Armstrong N.A. (2007a) 'Tablet manufacturing by direct compression', *Encyclopaedia of Pharmaceutical Technology*, page 3673-3682.
- Armstrong N.A. (2007b) 'Tablet Manufacture', *Encyclopaedia of Pharmaceutical Technology*, page 3653-3672.
- Adolfsson A., Carmella C. and Nysrrom C. (1998) 'The effect of milling and addition of dry binder on the interparticulate bonding mechanisms of sodium chloride tablets', *International Journal of Pharmaceutics*, 160, 187-195.
- Avrami M. (1939) 'Kinetics of Phase Change, I. General Theory', *Journal of Chemical Physics*, 7(12), 1103-1112.

- British Pharmacopeia (2010) 'Characterisation of crystalline and partially crystalline solids by X-ray powder diffraction. Vol. I. London, UK: Pharmaceutical Press.
- Black D.B. and Lovering E.G., (1977) 'Estimation of degree of crystallinity in digoxin by X-ray and infrared methods', *Journal of Pharmacy and Pharmacology*, 29, 684-687.
- Blagden, N., Davey, R.J., Lieberman, H.F., Williams, L., Payne, R., Roberts, R., Rowe, R., Docherty, R. (1998) 'Crystal chemistry and solvent effects in polymorphic systems: sulfathiazole', *Journal of Chemical Society, Faraday Transactions*, 94, 1035-1044.
- Bogda M. J. (2007) 'Tablet compression: machine theory, design, and process troubleshooting', *Encyclopaedia of Pharmaceutical Technology*, page 3611-3629.
- Boldyrev V. V. and Tkáčová K. (2000) 'Mechanochemistry of solids: past, present and prospects', *Journal of Materials Synthesis and Processing*, 8(3/4), 121-132.
- Bolhuis G. K. Engelhart J.J.P. and Eissens A.C. (2009) 'Compaction properties of isomalt', *European Journal of Pharmaceutics and Biopharmaceutics*, 72, 621-625.
- Brittain H.G. (2002), 'Minireview: Effects of mechanical processing on phase composition', *Journal of Pharmaceutical Science*, 91(7), 945-954.
- Bianco S., Caron V., Tajber L., Corrigan O.I., Nolan L., Hu Y and Healy A. M. (2012) 'Modification of the solid-state nature of sulfathiazole and sulfathiazole sodium by spray drying', *AAPS Pharmaceutical Science Technology*, 13(2), 647-660.
- Brodka-Pfeiffer K., Langguth P., Grab P. and Häustler H. (2003) 'Influence of mechanical activation on the physical stability of salbutamol sulphate', *European Journal of Pharmaceutical and Biopharmaceutics*, 56, 393-400.
- Buckton G. and Darcy P., (1995) 'The use of gravimetric studies to assess the degree of crystallinity of predominantly crystalline powders', *International Journal of Pharmaceutics*, 123, 265-271.
- Buckton G. and Gill H. (2007), 'The importance of surface energetics of powders for drug delivery and the establishment of inverse gas chromatography', *Advanced Drug Delivery Reviews*, 59, 1474-1479.

- Buckton G., Choularton A., Beezer A.E., Chatham S.M., (1988) 'The effect of the comminution techniques on the surface energy of a powder'. *International Journal of Pharmaceutics*, 47, 121-128.
- Burger A. and Ramberger R. (1979) 'On the polymorphism of pharmaceuticals and other molecular crystals I', *Mikrochimica Acta*, 259-271.
- Busignies V., Leclec B., Truchon S. and Tchoreloff P. (2011) 'Changes in the specific surface area of tablets composed of pharmaceutical materials with various deformation behaviours', *Drug Development and Industrial Pharmacy*, 37(2), 225-233.
- Byrn, S., Pfeiffer, R.R., Stowell, J.G., (1999) *Solid State Chemistry of Drugs*. SSCI Inc., Indiana.
- Callister (1998) *Introduction to Material Science*, Wiley and sons, New York.
- Caron V., Willart J.F. Danede F., and Descamps M. (2007) 'The implication of the glass transition in the formation of trehalose/mannitol molecular alloys by ball milling', *Solid State Communication*, 144, 288-292.
- Caron V., Willart J.F., Lefort R., Derollex P., Denede F. and Descamps M. (2011) 'Solid state amorphization kinetic of alpha lactose upon mechanical milling', *Carbohydrate Research*, 346, 2622-2628.
- Carr R.L. (1965) 'Evaluating flow properties of solids', *Chemical Engineering*, 72, 69-72
- Carstensen J. T., and Ertell C., Geoffroy J.M. (1993) 'Physio-chemical properties of particulate matter', *Drug Development Industrial Pharmaceutics.*, 19, 195-219.
- Chan, F.C., Anwar, J., Cernik, R., Barnes, P., Wilson, R.M. (1999) 'Ab initio structure determination of sulfathiazole polymorph V from synchrotron X-ray powder diffraction data', *Journal of Applied Crystallography*, 32, 436-441.
- Charkho A., Kazemian H. and Kazemini M. (2010) 'Optimized experimental design for natural clioptilolite zeolite ball milling to produce nano powders', *Powder Technology*, 203, 389-396.

- Chieng N., Zujovic Z., Bowmaker G., Rades T. and Saville D. (2006) 'Effect of milling conditions on the solid state conversion of ranitidine hydrochloride from 1'. *International Journal of Pharmaceutics*, 327, 36-44.
- Chikhaliya V., Forbes R.T., Storey R.A., Ticehurst M. (2006) 'The effect of crystal morphology and mill type on milling induced crystal disorder', *European Journal of Pharmaceutical Science*, 27 (1), 19-25.
- Corrigan O. I. (2007) Salt forms: pharmaceutical aspects, *Encyclopaedia of Pharmaceutical Technology*, page 3187-3177.
- Crowley K. J. and Zografi G., (2002) 'Water vapor absorption into amorphous hydrophobic drug/poly(vinylpyrrolidone) dispersions', *Journal of Pharmaceutical Sciences*, 91(10), 2150-2165.
- Crusellas J., (1942) 'The vapour pressure of some hydrates of sulfathiazole sodium', *Journal of the American Pharmaceutical Association*, 31(5), 157-158.
- Davies P.N., Newton J.M. (1996) 'Mechanical strength. In Alderborn, G. and Nyström, C. (Eds.), *Pharmaceutical powder compaction technology*, Marcel Dekker Inc., New York, page. 165-191.
- De Gusseme A., Neves C., Willart J.F., Rameau A. and Descamps M. (2008) 'Ordering and disordering of molecular solids upon mechanical milling: The case of fananserine', *Journal of Pharmaceutical Sciences*, 97(11), 5000-5012.
- De Lourdes Garzón M. and Villafuerte L. (2002) 'Compactability of mixtures of calcium carbonate and microcrystalline cellulose', *International Journal of Pharmaceutics*, 231, 33-41.
- Duberg M., Nyström C. (1986) 'Studies on direct compression of tablets. XVII. Porosity-pressure curves for the characterisation of volume reduction mechanisms in powder compression', *Powder Technology*, 46, 67-75
- Descamps M., Willart J. F., Dudognon E., Caron V. (2007) 'Transformation of pharmaceutical compounds upon milling and comilling: The role of Tg', *Journal of Pharmaceutical Sciences*, 96, 1398-1407.

- Desprez S. and Descamps M. (2006), 'Transformation of glassy indomethacin induced by ball milling', *Journal of Non-Crystalline Solids*, 352, 4480-4485.
- Doelker E. (1994) 'Assessment of powder compaction', Powder technology and pharmaceutical processes, (eds). D. Chulia, M. Deleuil, and Y. Pourcelot. Amsterdam: Elsevier. 403-471
- Dubinskaya A. (1999) 'Transformation of organic compounds under the action of mechanical stress', *Russian Chemical Reviews*, 68(8), 637-652.
- Dugognon E., Willart J.F., Caron V., Capet F., Larsson T. and Descamps M. (2006) 'Formation of budesonide/ α -lactose glass solutions by ball milling', *Solid state communications* 138, 68-71.
- Dujardin N., Willart J.F., Dudognon E., Hedoux A., Guinet Y., Paccou L., Chazallon, Descamps M. (2008) 'Solid state vitrification of crystalline α and β -D-glucose by mechanical milling', *Solid state communications*, 148, 78-82.
- Eirksson M. and Alderson G. (1995) 'The effect of particle fragmentation and deformation on the interparticulate bond formation process during powder compaction', *Pharmaceutical Resources*, 12, 1031-1039.
- Erizal S., Yeyet Cahyati S., Nurono S. and Halim A. (2008) 'Effect of milling on solid state transformation of sulfamethoxazole', *International Journal of Pharmacology*, 4(2), 140-144.
- Fecht H.J. (1992) 'Defect-induced melting and solid-state amorphisation', *Nature*, 356, 133-135
- Fiebich K. and Mutz M.,(1999) 'Evaluation of calorimetric and gravimetric methods to quantify the amorphous content of desferal', *Journal of Thermal Analysis and Calorimetry*, 57 75-85.
- Fell J.T. and Newton J.M. (1970) 'Determination of tablet strength by the dimetral compression test', *Journal of Pharmaceutical Science*, 59 (5), 688-691.
- Feng T. Rodolfo P. And Carvajal M.T. (2008) 'Process induced disorder in crystalline materials: Differentiating defective crystals from the amorphous form of griseofulvin', *Journal of Pharmaceutical Science*, 95, 3207-3221.

- Frenchini M.K. (2007) Particle engineering, *Encyclopaedia of Pharmaceutical Technology*, page 2567-2581.
- Ganesan V., Rosentrater K.A. and Muthukumarappa K. (2008) 'Flowability and handling characteristics of bulk solids and powders – a review with implications for DDGS', *Biosystems Engineering*, 101, 425-435.
- Geldart D., Abdullah E.C. and Verlinden A. (2009) 'Characterisation of dry powders', *Powder Technology*, 190, 70-74.
- Ghoroi C., Gurumurthy L., McDaniel D.J., Jallo L.J. and Dave R. N. (2012) 'Multi-faceted characterization of pharmaceutical powders to discern the influence of surface modification', *Powder Technology*.
- Giron D., Remy P., Thomas S. and Vilette E. (1997) 'Quantisation of amorphicity by microcalorimetry', *Journal of Thermal Analysis and Calorimetry*, 48, 465-472.
- Giron D and Grant D. J. W (2002). In: Stahl PH and Wermuth CG, editors. *Hand-book of Pharmaceutical Salts: Properties, Selection, and Use*, page. 41-81. Weinheim: Wiley.
- Giron D., Goldbronn C., Mutz M., Pfeffer S., Piechon P. and Schwab P. (2002) 'Solid state characterisation of pharmaceutical hydrates', *Journal of Thermal analysis and Calorimetry*, 68, 453-465.
- Giron D., Mutz M. and Garnier S., (2004) 'Solid-State of pharmaceutical compounds - Impact of the ICH Q6 guideline on industrial development', *Journal of Thermal Analysis Calorimetry*, 77, 709-747.
- Grant D.J.W. (1999) Theory and origin of polymorphism, in H.G. Brittain (Ed.), *Polymorphism in pharmaceutical solids*, Vol. 95, Marcel Dekker, New York, page 1-33.
- Gregg, S. and Sing, K., *Adsorption, Surface Area and Porosity*, 2nd edition, Academic Press, NY (1982).
- Grisedale L. C. and Jamieson M. J., Belton P. S., Barker S. A., and Craig D. Q. M. (2008) 'Characterisation and quantification of amorphous material in milled and spray-dried salbutamol sulphate: a comparison of thermal, spectroscopic, and water vapour sorption approaches', *Journal of Pharmaceutical Sciences*, 1-16.

- Grove, D.C., Keenan, G.L., (1941) 'The dimorphism of sulfathiazole', *Journal of American Chemical Society*, 63, 97-99.
- Guerin E., Tchoreloff P., Leclerc B., Tanguy D., Deleuil M. and Couarraze G. (1999) 'Rheological characterization of pharmaceutical powders using tap testing, shear cell and mercury porosimeter', *International Journal of Pharmaceutics*, 189, 91-103.
- Haleblain J.K. and McCrone W.C. (1969) 'Pharmaceutical application of polymorphism', *Journal of Pharmaceutical Sciences*, 58, 911-929.
- Han X., Ghoroi C., To., D Chen Y. and Dave R. (2011) 'Simultaneous micronisation and surface modification for improvement of flow and dissolution of drug particles', *International Journal of Pharmaceutics*, 415, 185-195.
- Hancock B. (2007), Amorphous pharmaceutical systems, *Encyclopaedia of Pharmaceutical Technology*, page 83-91.
- Hancock B.C. and Zografi G. (1997) 'Characterisation and significance of the amorphous state in pharmaceutical systems', *Journal of Pharmaceutical Science*, 89(1), 1-12.
- Hancock B. C., Carlson G.T., Ladipo D. D., Langdon B.A. and Mullarney M.P. (2002) 'Comparison of mechanical properties of the crystalline and amorphous forms of a drug substance', *International Journal of Pharmaceutics*, 241, 73-85.
- Heistand E.N. (1997) 'Principles, tenets and notions of tablet bonding and measurements of strength', *European Journal of Pharmaceutics and Biopharmaceutics*, 44, 229-242.
- Hiatt A. N., Taylor L.S. and Mauer L.J. (2011) 'Effects of co-formulation of amorphous maltodextrin and deliquescent sodium ascorbate on moisture sorption and stability', *International Journal of Food Properties*, 14(1), 726-740.
- Hogan S. E. and Buckton G. (2001) 'Water sorption/desorption – near IR and calorimetric study of crystalline and amorphous raffinose', *International Journal of Pharmaceutics*, 227, 57-69.
- Hu Y., Erxleben A., Ryder A.G. and McArdle P (2010) 'Quantitative analysis of sulfathiazole polymorphs in ternary mixtures by attenuated total reflectance infrared, near-infrared and Raman spectroscopy', *Journal of Pharmaceutical and Biomedical Analysis*, 53, 412-420.

- Huang L. F. and Tong W. Q., (2004) 'Impact of solid state properties on developability assessment of drug candidates', *Advanced Drug Delivery Reviews*, 56, 321-334.
- Humphreys F.J. and Hatherly M. (1995) 'Recrystallisation and related annealing phenomena'; Elsevier Science.
- Jackson C.L. and McKenna G.B. (1990) 'The melting behaviour of organic materials confined in porous solids', *Journal of Chemical Physics*, 93(12).
- Jallo L.J., Ghoroi C., Gurumurthy L., Utsav P. and Davé R.N. (2012) 'Improvement of flow and bulk density of pharmaceutical powders using surface modification', *International Journal of Pharmaceutics*, 423, 213-225.
- Kaerger S.J., Edge S. and Price R. (2004) 'Influence of particle size and shape on flowability and compactability of binary mixtures of paracetamol and microcrystalline cellulose', *European Journal of Pharmaceutical Science*, 173-179.
- Khatirkar R.K. and Murty B.S. (2010), 'Structural changes in iron powder during ball milling', *Materials Chemistry and Physics*, 123, 247-253.
- Khoshkhoo S. and Anwar J. (1993) 'Crystallization of polymorphs: The effect of solvent', *Journal of Physical Development: Applied Physics*, 26, B90-B93.
- Kwon Y.S., Gerasimov K.B. and Yoon S.K. (2002) 'Ball temperatures during mechanical alloying in planetary mills', *Journal of Alloys and Compounds*, 346,276-281.
- Lagas, M., Lerk, C.F., (1981) 'The polymorphism of sulphathiazole', *International Journal of Pharmaceutics*, 8, 25-33.
- Lappalainen M. and Karppinen M. (2010) 'Techniques of differential scanning calorimetry for quantification of low contents of amorphous phases', *Journal of Thermal Analysis and Calorimetry*, 102, 171-180.
- Lefort R., De Gusseme A., Willart J.F. Danède F. and Decamps M. (2004) 'Solid state NMR and DSC methods for quantifying the amorphous content in solid dosage forms: an application to ball-milling of trehalose', *International Journal of Pharmaceutics*, 280(1-2), 209-219.

- Liu L.X., Marziano I., Bentham A. C. Litster J. D., White E.T and Howes T. (2008) 'Effect of particle properties on the flowability of ibuprofen powders', *International Journal of Pharmaceutics*, 362, 109-117.
- Lucks L., Lamparter P. and Mittemeijer E.J. (2004) 'An evaluation of methods of diffraction-line broadening analysis applied to ball-milled molybdenum', *Journal of Applied Crystallography*, 37, 300-311.
- Luukkonen P., Schaefer T., Hellen L., Juppo A.M. and Yliruusi J. (1999) 'Rheological characterisation of microcrystalline cellulose and silicified microcrystalline cellulose wet masses using a mixer torque rheometer', *International Journal of Pharmaceutics*, 188, 181-192.
- Mackin L., Sartnurak S. Thomas I and Moore S. (2002) 'The impact of low levels of amorphous material (<5%) on the blending characteristics of a direct compression formulation', *International Journal of Pharmaceutics*, 231, 213-226.
- Maggi L. Conte U. and Bettinetti G.P. (1998) 'Technological properties of crystalline and amorphous α -cyclodextrin hydrates', *International Journal of Pharmaceutics*, 172, 211-217.
- Mallick S., Pattnail S., Swain K., De P. K., Saha A., Ghoshal G. and Mandal A. (2008), 'Formation of physically stable amorphous phase of ibuprofen by solid state milling with kaolin', *Journal of Pharmaceutics and Biopharmaceutics*, 68, 346-351.
- Martin A (1993), *Physical Pharmacy*, 4th ed. Williams & Wilkins, Baltimore
- Masteau J.C. and Thomas G. (1999) 'Modelling to understand porosity and specific surface area changes during tableting', *Powder Technology*, 101, 204-248.
- Mattsson S. (2000) *Pharmaceutical binders and their function in directly compressed tablets*, Submitted to the University of Upsaliensis.
- Milkhailenko M. A., Shakhtshneider T.P. and Boldyrev V.V. (2007) 'Acylation of sulfathiazole with maleic anhydride under mechanochemical activation', *Mendeleev Communications*, 17, 315-317.
- Mokkapat S. P. (2006) 'Simulation of particle agglomeration using dissipative particle dynamics', Master Thesis submitted to Texas A&M University.

- Morissette S L., Almarssona O., Peterson M. L., Remenara J. F., Read M. J., Lemmo A. V., Ellisa S., Cimab M. J. and Gardner C. R (2004) 'High-throughput crystallization: polymorphs, salts, co-crystals and solvates of pharmaceutical solids' *Advanced Drug Delivery Reviews*, 56 275– 300.
- Morris K. R., Schlam R. F., Cao W., Short M. S. (2010) 'etermination of average crystallite shape by X-ray diffraction and computational methods', *Journal of Pharmaceutical Sciences*, 89(11), 1432-1442.
- Mullarney M.P., Beach L.E., Davé R.N., Langdon B.A., Polizzi M. and Blackwood D.O. (2011) 'Applying dry powder coatings to pharmaceutical powders using a comil for improving powder flow and bulk density', *Powder Technology*, 212, 397-402.
- Munroe Á., Rasmuson Å. Hodnett K. and Croker M. (2012) 'elative stabilities of five polymorphs of sulfathiazole', *Crystal Growth and Design*, 12(6), 2825-2835.
- Muzzio F.J., Shinbrot T. and Glasser B.J. (2002) 'Powder technology in the pharmaceutical industry: the need to catch up fast', *Powder Technology*. 124 1–7.
- Nerurkar M.J., Duddu S., Grant D.J.W. and Rytting J.H. (2000) Properties of the solids that effect transport in G.L. Amidon, P.I. Lee, E.M. Topp (Eds.), *Transport processes in pharmaceutical systems*, Vol. 102, Marcel Dekker, New York, page 575-611.
- Newman A. W. and Byrn S.R. (2003) Solid-state analysis of the active pharmaceutical ingredient in drug products, *Drug Discovery Today*, 8(19), 898-905.
- Ng W.K., Kwek J.W., Yuen A., Tan C.L. and Tan R. (2010) 'Effect of milling on DSC thermogram of excipients adipic acid', *AAPS Pharmaceutical Science Technology*, 11(1), 159-167.
- Niraj S., Boerrigter S. X. M. and Byrn S.R. (2010) 'Investigation of the milling-induced thermal behaviour of crystalline and amorphous griseofulin', *Pharmaceutical Research*, 27, 1377-1389.
- Nokodchi A., Maghsoodi M., Hassan-Zadeh D., Barzegar-Jalali M. (2007) 'Preparation of agglomerated crystals for improving flowability and compactability of poorly flowable and compactable drugs and excipients', *Powder Technology*, 175, 73-81.

- Nolan L, (2008) 'The production and characterisation of spray dried nanoporous microparticles (NPMPs) intended for dry powder inhalation drug delivery systems' Thesis submission, Trinity College, Dublin.
- Nyström C., Alderborn G., Duberg M. and Karehill P.G. (1993) 'Bonding surface area and bonding mechanism –two important factors for the understanding of powder compactability', *Drug Development Industrial Pharmaceutics*, 19, 2143-2196.
- Ohta M. and Buckton G. (2004) 'Determination of the changes in surface energetics of cefditoren pivoxil as a consequence of processing induced disorder and equilibration to different relative humidities' *International Journal of Pharmaceutics*, 269, 81-88.
- Olsson, H. and Nyström, C. (2001) 'Assessing tablet bond types from structural features that affect tablet tensile strength', *Pharmaceutical Research*, 18(2), 203-210.
- Ostwald W. (1897) 'Studien über die Bildung und Umwandlung fester Körper', *Journal of Physical Chemistry*, 22, 289-330.
- Parrott E. (1974) 'Milling of pharmaceutical solids', *Journal of Pharmaceutical Sciences*, 63(6), 813-829.
- Patel A.D., Luner P.E. and Kemper M.S. (2001) 'Low-level determination of polymorph composition in physical mixtures by near-infrared reflectance spectroscopy', *Journal of Pharmaceutical Sciences*, 90(3), 360-370.
- Patel U. H. (1995) 'The crystal structure of Na-sulfadimidine', *Crystal Research and Technology*, 30(3), 381-387.
- Patterson J.E., James M.B., Foster A.H., Lancaster R.W., Butler J.M. and Rades T. (2005) 'The influence of thermal and mechanical preparative techniques on the amorphous state of four poorly soluble compounds', *Journal of Pharmaceutical Sciences*, 94(9), 1998-2012.
- Peleg M (1983). Physical characteristics of food powders. In: Physical Properties of Foods (Peleg M; Bagley E eds), page. 293–323. AVI, New York.
- Pfannkuch F. P., Rettig H. and Stahl P.H. (2011), Chapter 5: Biological effects of the API salt form. From Handbook of pharmaceutical salts properties: selection and use, 2nd ed.

- Picker-Freyer K. M., Liao X., Zhang G. and Wiedmann T. (2007), 'Evaluation of the compaction of sulfathiazole polymorphs', *Journal of Pharmaceutical Sciences*, 96(8), 2111-2124.
- Podczeczek F., Miah Y. (1996) 'The influence of particle size and shape on the angle of internal friction and the flow factor of unlubricated and lubricated powders', *International Journal of Pharmaceutics*, 144, 187-194.
- Prescott J.K. and Barnum R.A (2000) 'On powder flowability', *Pharmaceutical Technology*, 85-60.
- Prism, (2007) 'Interpreting results: Correlations', San Diego California USA, www.graphpad.com [accessed: 23/05/12]
- Pirttimäki J. Laine E., Ketolainen J., Paronen P., (1993) 'Effects of grinding and compression on crystal structure of anhydrous caffeine', *International Journal of Pharmaceutics*, 95 (1-3), 93-99
- Ramlakhan, M., Wu, C.Y., Watano, S., Dave, R.N., and Pfeffer, R. (2000) 'Dry particle coating using magnetically assisted impaction coating: modification of surface properties and optimization of system and operating parameters', *Powder Technology*, 112,137-148
- Retsch, (2009) Operation instruction manual for the PM 100 Planetary mill, Retsch, Germany.
- Riepma K.A., Dekker B.G. and Lerk C.F. (1992) 'The effect of moisture sorption on the strength and internal surface area of lactose tablets', *International Journal of Pharmaceutics*, 87, 149-159.
- Riepma K.A., Dekker B.G., Jager R.S., Elberse P.A. and Lerk C.F. (1993) 'Rapid communication: The effect of storage at ambient humidity on the BET-specific surface area of tablets compacted from different materials', *International Journal of Pharmaceutics*, R1-R4
- Roberts R.J., Rowe R.C. (1987a) 'The compaction of pharmaceutical and other model materials – a pragmatic approach', *Chemical Engineering Science* 42, 903-911.
- Rodes M. (1998) *Introduction to Particle Technology*, second ed. Wiley and sons Ltd. New York.

- Roulet P., Macinnes W.M., Wursch P., Sanchez R.M. and Raemy A. (1988) 'A comparative study of the retrogradation kinetics of gelatinized wheat starch in gel and powder from using X-rays, differential scanning calorimetry and dynamic mechanical analysis', *Food hydrocolloids*, 2, 381-396.
- Rubino J.T. (1989) 'Solubilities and solid state properties of the sodium salts of drugs', *Journal of Pharmaceutical Sciences*, 78, 485-489.
- Rubinstein H.M. and Gould P. (1987) 'Particle size reduction in the ball mill', *Drug Development and industrial Pharmacy*, 13(1), 81-92.
- Rudnick A., Hunter A. R. and Holden F. C., (1963) 'An analysis of the diametral compression test', *Material Research Standards*, 3, 283-289
- Scherrer P. (1918) Nachrichten von der Gesellschaft der Wissenschaften zu Göttingen 98-100.
- Schmitt E.A. Law D., Zhang G.G. (1999) 'Nucleation and crystallisation kinetics of hydrated amorphous lactose above the glass transition temperature', *Journal of Pharmaceutical Sciences*, 88, 291-296.
- Schulze D. (2011) Flow Properties of Powders and Bulk Solids (2011) <http://www.dietmar-schulze.de/grdle1.pdf> [accessed 23/08/12]
- Sebhatu T. and Alderborn G. (1999) 'Relationship between the effective interparticular contact area and the tensile strength of tablets of amorphous and crystalline lactose of varying particle size', *European Journal of Pharmaceutical Science*, 8, 235-242.
- Shah B., Kakumanu K V. and Bansal K. A., (2006) 'Analytical techniques for quantification of amorphous/crystalline phases in pharmaceutical solids', *Journal of Pharmaceutical Sciences*, 95(8), 1641-1665.
- Shakhtshneider T. P. (1997) 'Phase transformations and stabilization of metastable states of molecular crystals under mechanical activation', *Solid State Ionic's*, 101(103), 851-856.
- Shakhtshneider T. P. and Boldyrev V. V. (1999) 'Reactivity of Molecular solids', Wiley Ltd. Chichester, page 271.

- Shakhtshneider T. P. and Boldyrev V. V. (1993) 'Phase transformation in sulfathiazole during mechanical activation', *Drug Development and Industrial Pharmacy*, 19(16), 2055-2067.
- Shakhtshneider T.P., Vasilchenko M.A., Politoc A.A. and Boldyre V.V. (1997) 'Mechanochemical preparation of Drug-carrier solid dispersions', *Journal of Thermal Analysis*, 48, 491-501.
- Shakhtshneider T. P. (1997) 'Phase transformations and stabilization of metastable states of molecular crystals under mechanical activation', *Solid State Ionic's*, 101-103, 851-856.
- Shekunov B. Y., Chattopadhyay P., Tong H. H. Y and Chow A. H. L. (2007) Particle size analysis in pharmaceuticals: principals, methods and application', *Pharmaceutical Research*, 24(2), 203-227.
- Staniforth J. N. (2002) Chapter 2: Powder flow', *Aulton's Pharmaceutics: The Science of Dosage Form Design*. Ed.: Aulton ME, Churchill Livingstone, Edinburgh London.
- Staniforth J.N. and Aulton M. E. (2007) Chapter 10: Particle size reduction. *Aulton's Pharmaceutics; The design and manufacture of medicines*, 3rd eds. Hungary.
- Sun C.C. (2005) 'Quantifying errors in tableting data analysis using the Ryshkewitch equation due to inaccurate true density', *Journal of Pharmaceutical Sciences*, 94(9), 2061-280.
- Sun C. and Grant D.J.W. (2001) 'Effects of initial particle size on the tableting properties of L-lysine monohydrochloride dihydrate powder', *International Journal of Pharmaceutics*, 215, 221-228.
- Sun, C., Grant, D.J.W., (1999) 'Influence of crystal shape on the compaction properties of L-lysine monohydrochloride dehydrate', *AAPS Pharmaceutical Science Technology*, 2894, 325S.
- Sun C. and Grant D.J.W. (2001) 'Effects of initial particle size on the tableting properties of L-lysine monohydrochloride dihydrate powder', *International Journal of Pharmaceutics*, 215, 221-228.
- Sun C.C. (2008) 'Mechanism of moisture induced variations in true density and compaction properties of microcrystalline cellulose', *International Journal of Pharmaceutics*. 346, 93-101.

- Suryanarayana C. (2001) 'Mechanical alloying and milling', *Progress in Material Science*, 461-184.
- Tajber L., Corrigan O. I. and Healy A. M. (2005) 'Physiochemical evaluation of PVP-thiazide diuretic interactions in co-spray-dried composites-analysis of glass transition composition relationships', *European Journal of Pharmaceutical Science*, 24, 553-563.
- Talekar M.V., Jin C.Y. Dunkel U., Rades T. Saville D. 'Influence of milling on polymorphic transformation of ranitidine hydrochloride form 1, in Proceedings of the controlled release society conference, Miami US (2005).
- Threlfall T. (2003) 'Structural and Thermodynamic Explanations of Ostwald's Rule', *Organic Process Research and Development*, 7(6), 1017-1027.
- Ticehurst M. D., Basford P. A., Dallman C. I., Lukas T. M., Marshall P. V., Nichols G., and Smith D. (2000) 'Characterisation of the influence of micronisation on the crystallinity and physical stability of revatropate hydrobromide', *International Journal of Pharmaceutics*, 193, 247- 259.
- Tiwari R. K., Haridas M. and Singh T.P. (1984), 'Structure of 4-Amino-N (4,6-dimethyl-2-pyromodonyl) benzenesulphonamide (Sulfadimidine), C₁₂H₁₄N₄O₂S', *Acta Crystallographica C*, 40, 655-657.
- Tiway A.K. (2007) 'Crystal habit changes and dosage form performance', *Encyclopaedia of Pharmaceutical Technology*, page 820-833.
- Tong P. and Zografi G., (1999) 'Solid state characteristics of amorphous sodium indomethacin relative to the free acid', *Pharmaceutical Research*, 16(8), 1186-1192.
- Trasi N. S., Boerrigter S. X. M., Byrn S. R. (2010) 'Investigation of the Milling induced thermal behaviours of crystalline and amorphous griseofulvin', *Pharmaceutical Research*, 27(7), 1377-1389
- Vatsaraj N.B., Gao D and Kowalski D.L. (2006) 'Optimization of the operating conditions of a lab scale Aject mill using lactose and sucrose: A technical note', *AAPS Pharmaceutical Science Technology*, 4(2), article 27, 1-7.

- Vippagunta S.R., Brittain H.G. and Grant D.J.W. (2001) 'Crystalline solids', *Advanced Drug Delivery Reviews*, 48, 3-26.
- Ward G.H. and Schultz R.K. (1995) 'Process-induced crystallinity changes in albuterol sulphate and its effects on powder physical stability', *Pharmaceutical Resources*, 12(5), 773-779.
- Westermarck S., Juppo A., Kervinen L., Ylirussi J. (1999_A) 'Microcrystalline cellulose and its microstructure in pharmaceutical processing', *European Journal of Pharmaceutical Biopharmaceutics*, 48, 199-206.
- Wildfong P.L.D., Hancock B.C., Moore M.D. and Morris K.R. (2006) 'Towards and understanding of the structurally based potential for mechanically activated disordering of small molecular organic crystals', *Journal of Pharmaceutical Sciences*, 95(12), 2645-2656.
- Willart J.F., DeGusseme A., Hemon S., Odou G., Danede F. and Descamps M. (2001) 'Direct crystal to glass transformation of trehalose induced by ball milling', *Solid state Communication*, 119, 501-505.
- Willart J.F., Caron V., Lefort R., Danede F., Prevost D. and Descamps M. (2004) 'A thermal character of the solid state amorphisation of lactose induced by ball milling', *Solid State Communication*, 132, 693-696.
- Willart J.F., Lefebvre J. and Danede F., Comini S., Looten P. and Descamps M. (2005) 'Polymorphic transformations of the Γ -form and D-sorbitol upon milling: structural and nanostructural analyses', *Solid State communications*, 135, 519-524.
- Willart J.F., Descamps N., Caron V., Capet V., Danede F., Descamps M. (2006) 'Formation of lactose-manitol molecular alloys by solid state vitrification', *Solid State Communication*, 138, 194-199.
- Willart, J.F., Caron, V. and Descamps, M. (2007) 'Transformation of crystalline sugars upon milling'. *Journal of Thermal Analysis and Calorimetry*. 90,125-130
- Wujiang Bolin Industry, (2007) 'Sulfadimidine', ww.bolinchina.com [accessed: 19/06/2011]

- Yang J., Grey K. and Doney J. (2010) 'An improved kinetics approach to describe the physical stability of amorphous solid dispersions', *International Journal of Pharmaceutics*, 384, 24-31.
- Yang J., Sliva A., Banerjee A., Dave R.N. and Pfeffer R., (2005) 'Dry particle coating for improving the flowability of cohesive powders', *Powder Technology*, 158, 21-33.
- York P., Ticehurst M.C., Osborn J.C, Roberts R.J. and Rowe R.C, (1998), 'Characterisation of the surface energetic of milled dl-propranolol hydrochloride using inverse gas chromatography and molecular modelling', *International Journal of Pharmaceutics*, 174 179-186.
- York P. (1978) 'Particle slippage and rearrangement during compression of pharmaceutical powders', *Journal of Pharmacy and Pharmacology*, 30, 6-10.
- Yoshioka M., Hancock B.C. and Zografi G. (1994) 'Crystallisation of indomethacin from the amorphous state below and above its glass transition temperature', *Journal of Pharmaceutical Science*, 83, 1700-1705.
- Yu L. (2001) 'Amorphous pharmaceutical solids: preparation, characterisation and stabilization', *Advanced Drug Delivery*, 48, 27-42.
- Zeitler, J.A., Newnham, D.A., Taday, P.F., Threlfall, T.L., Lancaster, R.W., Berg, R.W., Strachan, C.J., Pepper, M., Gordon, K.C., Rades, T., (2006) 'Characterization of temperature induced phase transitions in five polymorphic forms of sulfathiazole by terahertz pulsed spectroscopy and differential scanning calorimetry', *Journal of Pharmaceutical Science*, 95, 2486-2498.
- Zhang G.G.Z., Gu C.H. Zell M.T., Burkhardt R.T., Munson E.J. and Grant D.J.W. (2002) Crystallisation and transformations of sulfamerazine polymorphs. *Journal of Pharmaceutics Science*, 91 (4), 1089-1100.
- Zhang G. G., Law D., Schmitt E. A. and Qui Y. (2004), Phase transformation considerations during process development and manufacture of solid oral dosage forms, *Advanced Drug Delivery Reviews*, 56: 371-390.

Zhou D., Zhang G.G.Z., Law D., Grant D.J.W. and Schmitt E.A. (2008) 'Thermodynamics, molecular mobility and crystallisation kinetics of amorphous griseofulvin', *Molecular Pharmaceutics*, 5(6), 927-936.

Zhu L, Wong L and Yu L. (2008) 'Surface-enhanced crystallization of amorphous nifedipine', *Molecular Pharmaceutics*, 5(6), 921-926.

Appendices

Appendix I

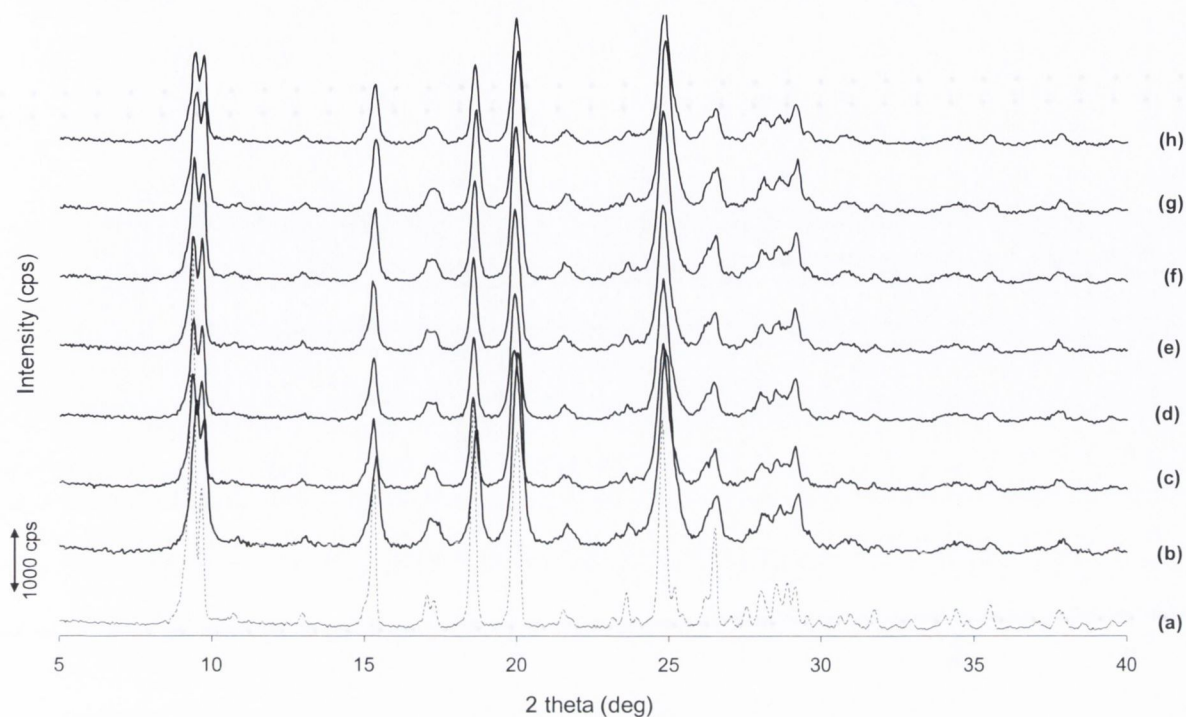


Figure 1: PXR D of (a) SD unmilled (Sigma, Ireland), (b) SD milled for 30 minutes and tested directly after milling and SD milled for 30 minutes (c) stored for 1 week, (d) stored for 2 weeks, (e) stored for 3 weeks, (f) stored for 4 weeks, (g) stored for 8 weeks (h) stored for 12 weeks.

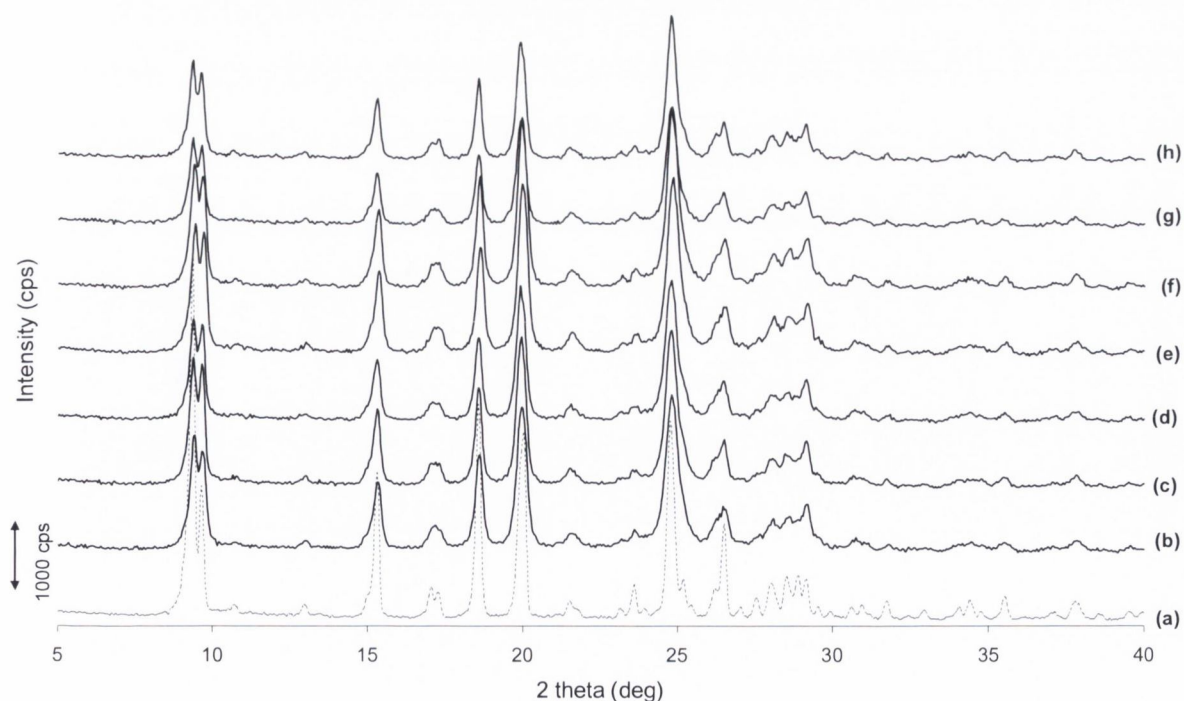


Figure 2: PXR D of (a) SD unmilled (Sigma, Ireland), (b) SD milled for 60 minutes and tested directly after milling and SD milled for 60 minutes (c) stored for 1 week, (d) stored for 2

weeks, (e) stored for 3 weeks, (f) stored for 4 weeks, (g) stored for 8 weeks (h) stored for 12 weeks.

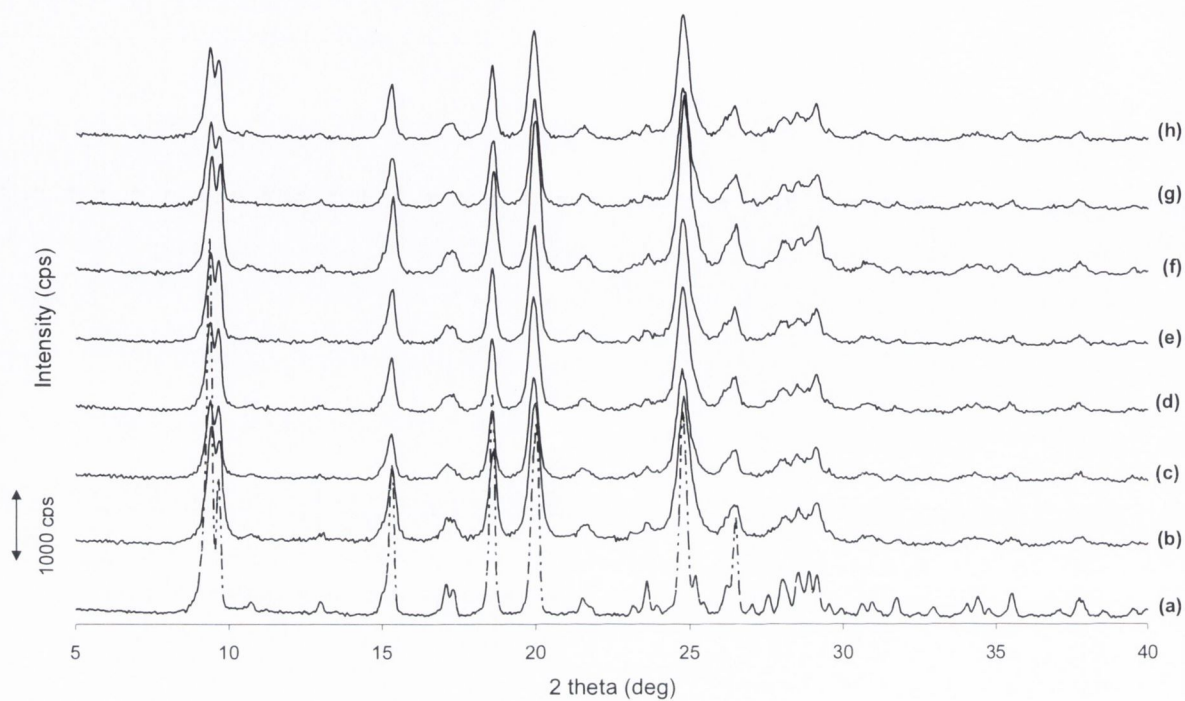


Figure 3: PXRD of (a) SD unmilled (Sigma, Ireland), (b) SD milled for 120 minutes and tested directly after milling and SD milled for 120 minutes (c) stored for 1 week, (d) stored for 2 weeks, (e) stored for 3 weeks, (f) stored for 4 weeks, (g) stored for 8 weeks (h) stored for 12 weeks.

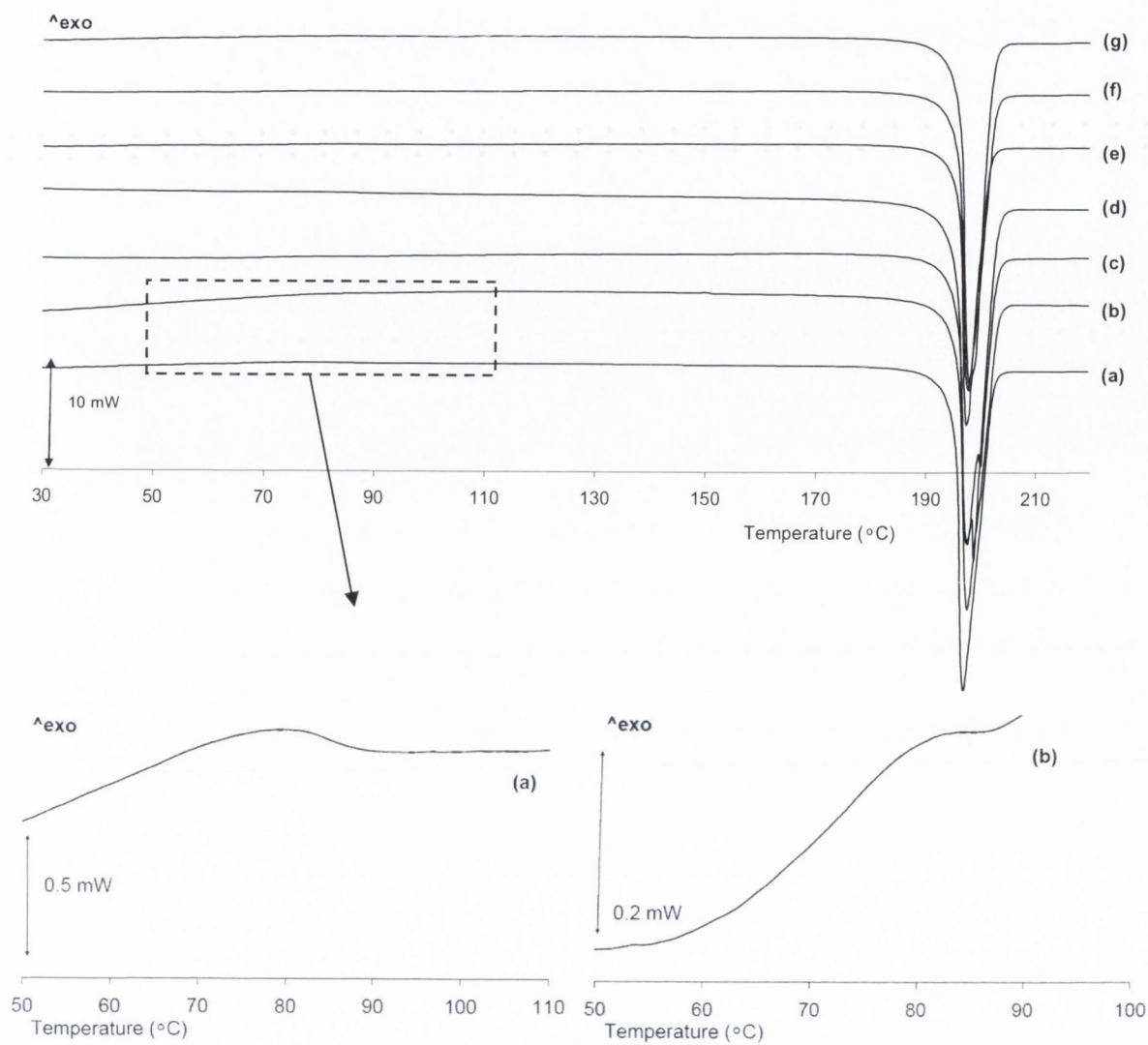


Figure 4: Illustrates the DSC thermograms for (a) SD milled for 30 minutes and tested directly after milling, the magnified region below shows the crystallisation exotherm and SD milled for 30 minutes and stored at 4 °C, for (b) 1 week, the magnified region displaying the exotherm is given below; (c) 2 weeks; (d) 3 weeks; (e) 4 weeks; (f) 8 weeks and (g) 12 weeks.

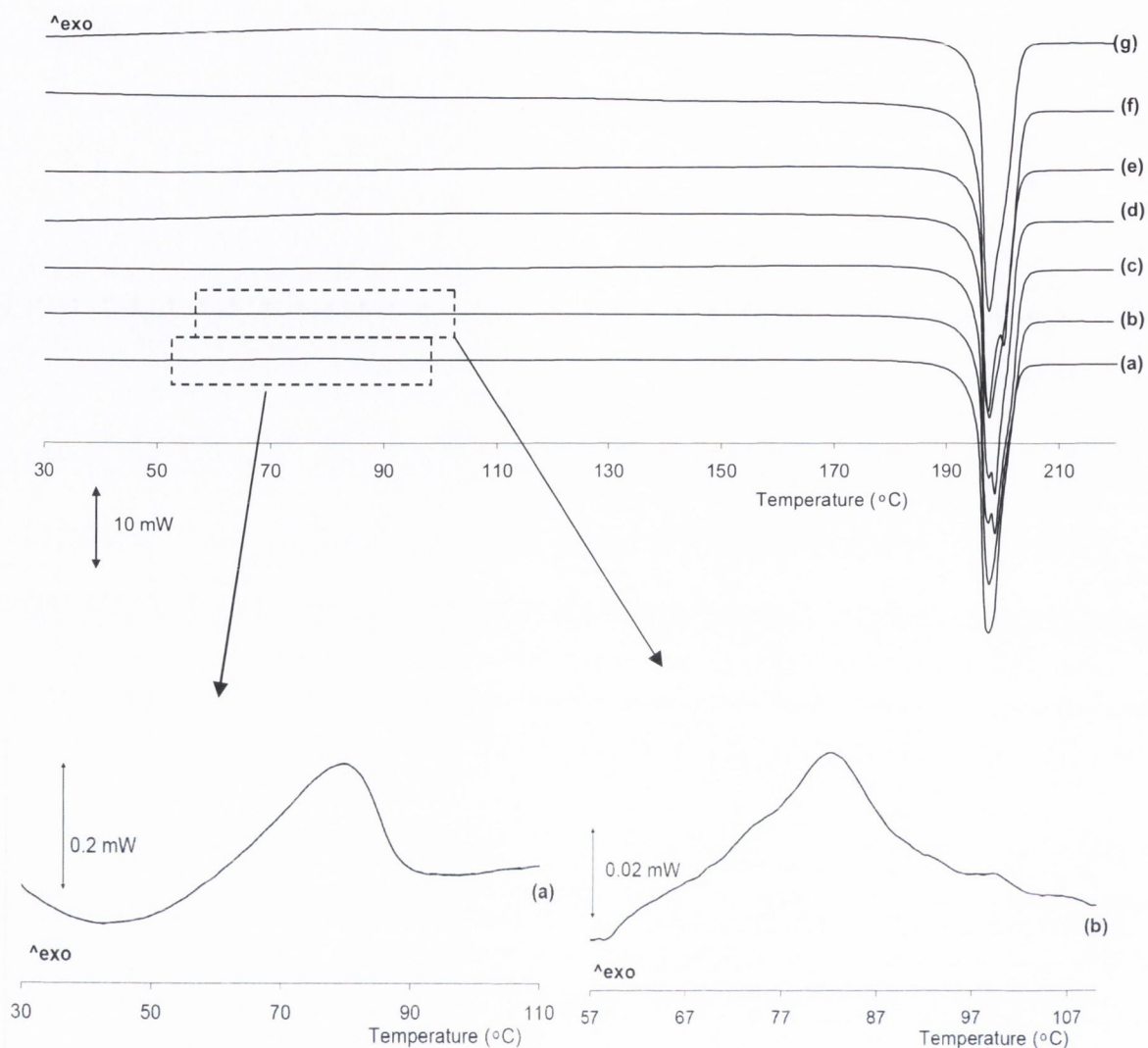


Figure 5: Illustrates the DSC thermograms for (a) SD milled for 60 minutes and tested directly after milling, the magnified region below shows the crystallisation exotherm and SD milled for 60 minutes and stored at 4 °C, for (b) 1 week, the magnified region displaying the exotherm is given below; (c) 2 weeks; (d) 3 weeks; (e) 4 weeks; (f) 8 weeks and (g) 12 weeks.

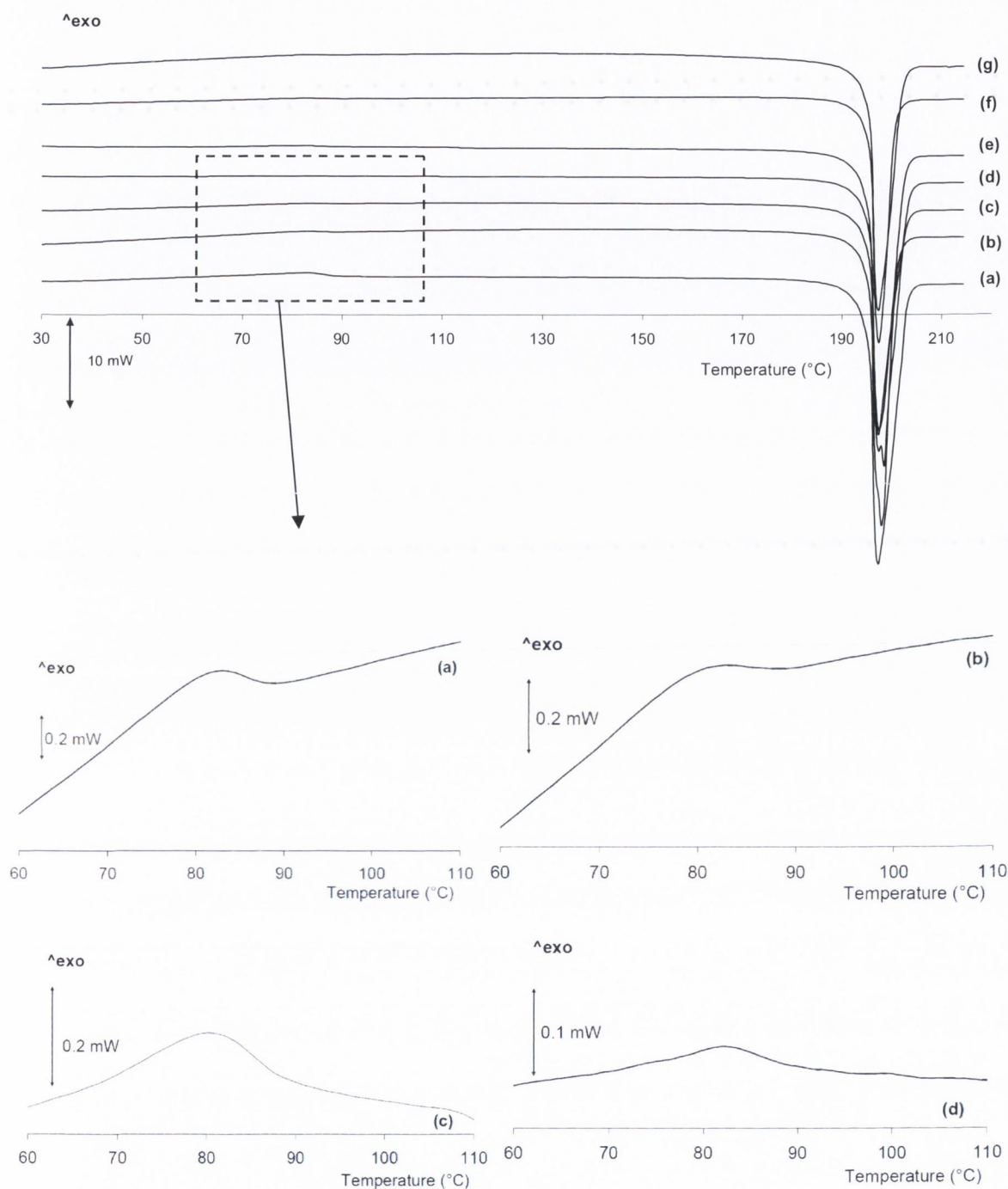


Figure 6: Illustrates the DSC thermograms for (a) SD milled for 120 minutes and tested directly after milling, the magnified region below shows the crystallisation exotherm and SD milled for 120 minutes and stored at 4 °C, for (b) 1 week, the magnified region displaying the exotherm is given below; (c) 2 weeks, the magnified region displaying the exotherm is given below; (d) 3 weeks, the magnified region displaying the exotherm is given below; (e) 4 weeks; (f) 8 weeks and (g) 12 weeks.

Appendix II

Multivariable analysis from NUIG investigated the purity of sulfathiazole unmilled samples received from Sigma Ireland. Batch X, shown in figure 1 was found to be 100% form III and batch Y, shown in figure 2 was a mix of 97-98% form III with 3-2% form I. The circled areas in figure 2 indicate the peaks characteristic of form I.

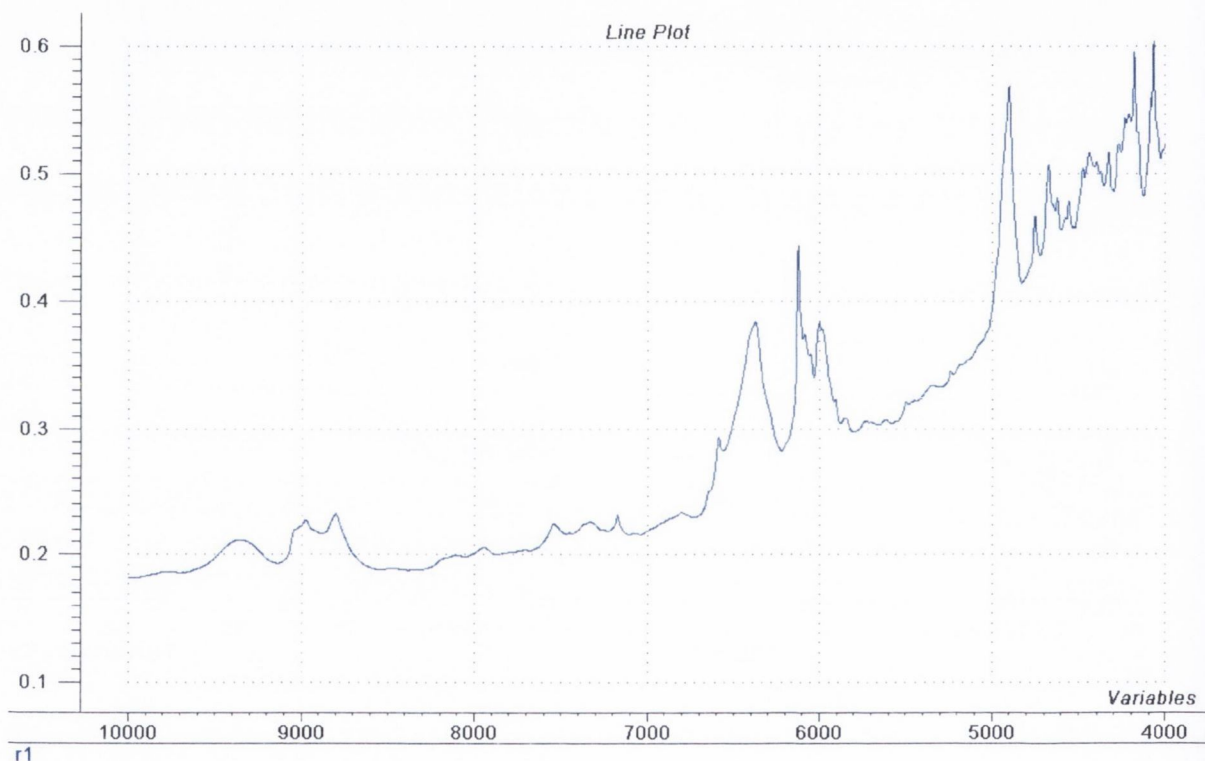


Figure 1: Results from multivariable analysis for batch X, indicating a pure form III STZ material.

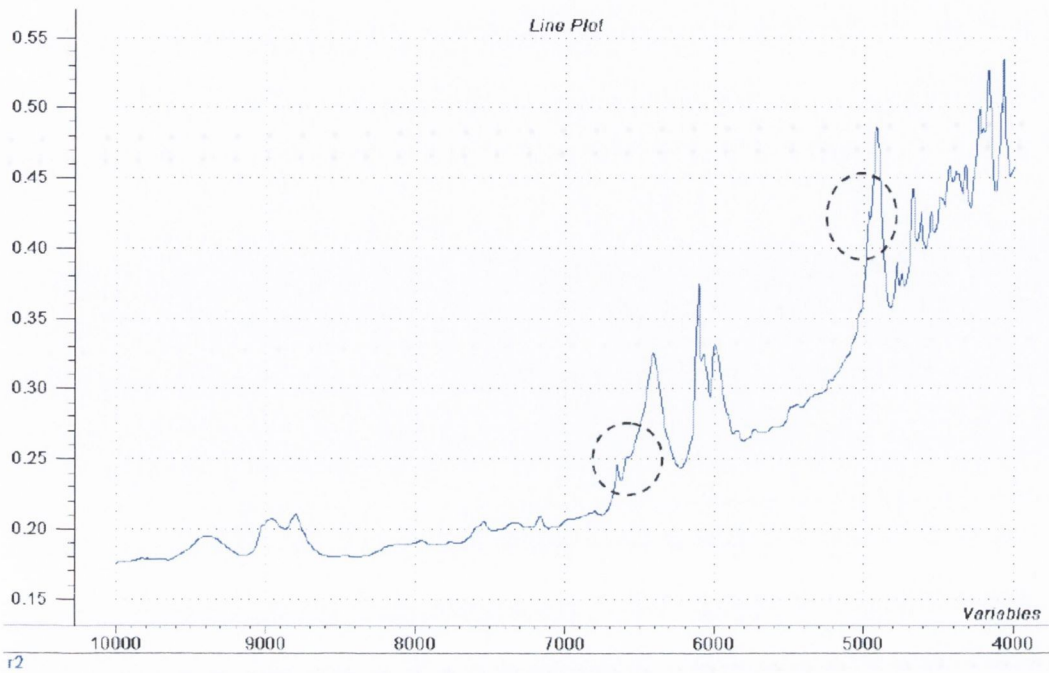


Figure 2: Results from multivariable analysis for batch Y, indicating a mixture of form III STZ and form I.

Appendix III

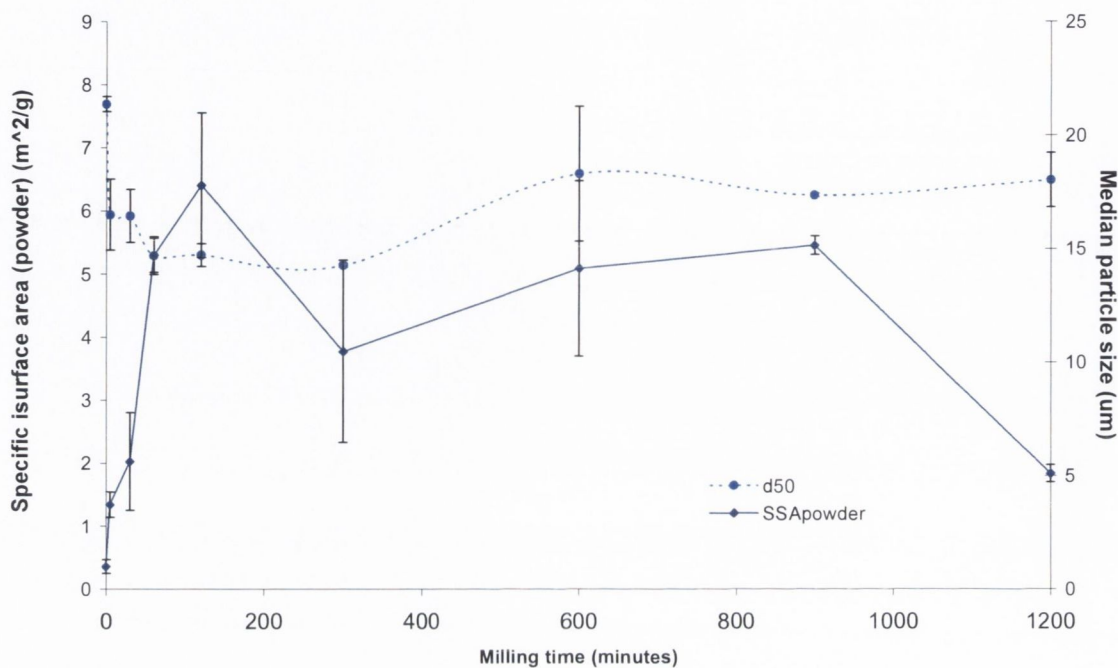


Figure 1: Specific surface area determined by BET and the median particle size determined by Malvern particle size for the unmilled and ball milled SD powder. The ball milled SD powder was done at RT with a BTP powder weight ratio of 40:1 from 5 minutes to 20 hours. The Spearman correlation coefficient (r) was -0.60 obtained when these variables were compared.

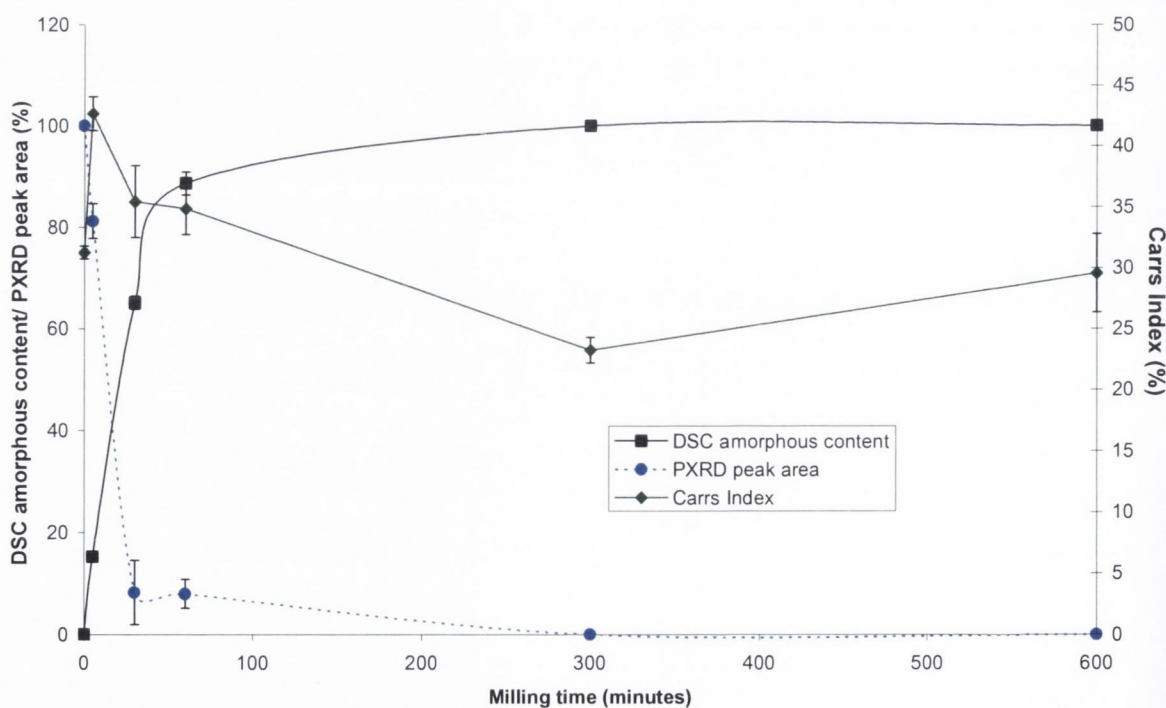


Figure 2: DSC amorphous content and the PXR peak area and the Carr's Index for the unmilled and ball milled SDNa powder. The ball milled SD powder was done at RT with a BTP powder weight ratio of 40:1 from 5 minutes to 20 hours. The Spearman correlation coefficient (r) obtained when comparing DSC amorphous content with the Carr's Index was -0.64 and the r obtained when comparing PXR peak area and Carr's Index was 0.64.

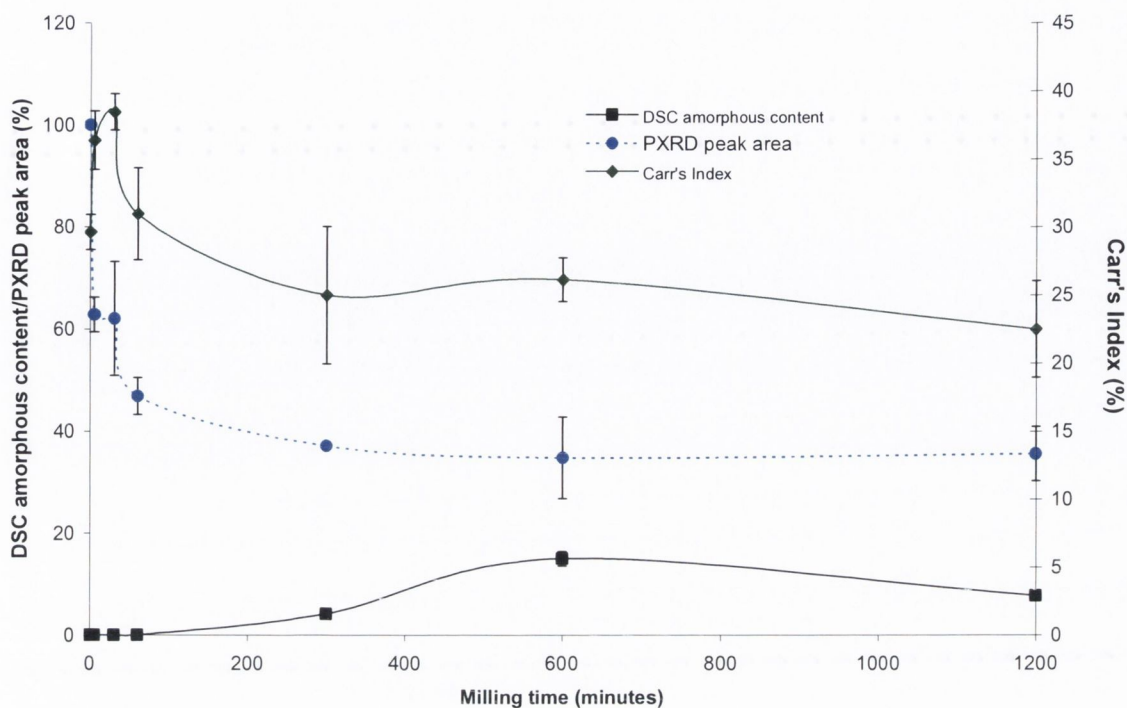


Figure 3: DSC amorphous content and the PXR peak area and the Carr's Index for the unmilled and ball milled STZ I powder. The ball milled SD powder was done at RT with a BTP powder weight ratio of 40:1 from 5 minutes to 20 hours. The Spearman correlation coefficient (r) obtained when comparing DSC amorphous content with the Carr's Index was -0.54 and the r obtained when comparing PXR peak area and Carr's Index was 0.71 .

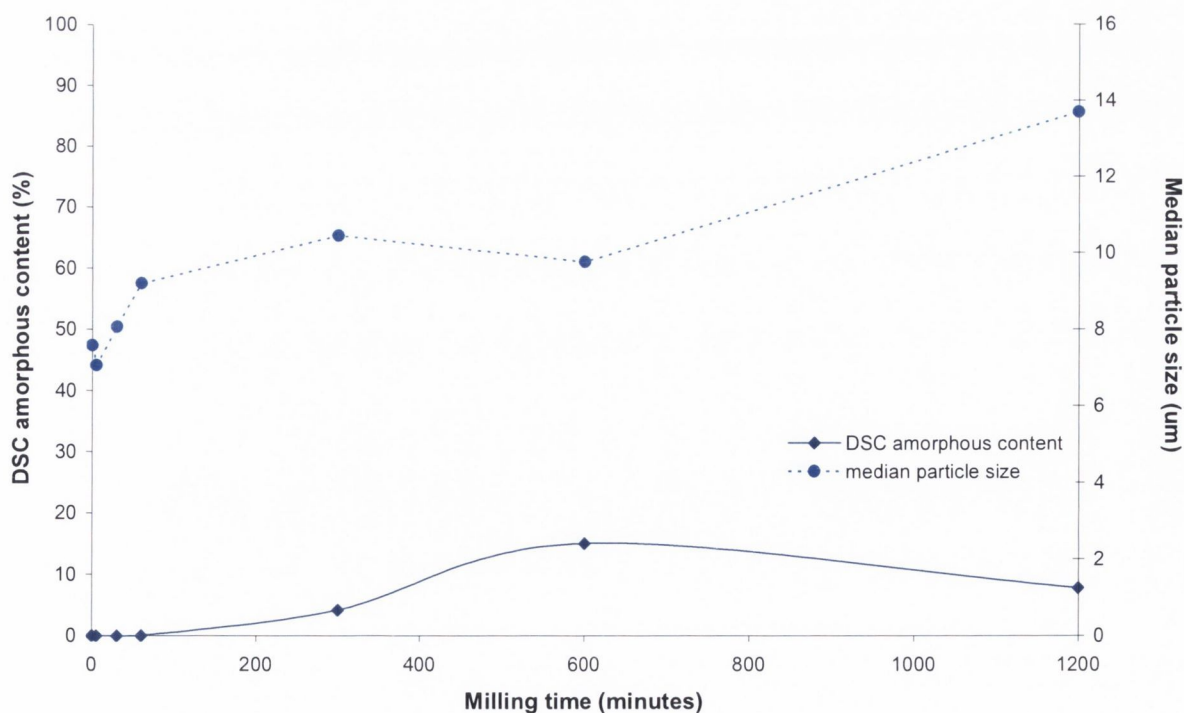


Figure 4: DSC amorphous content and the median particle size determined by Malvern particle size for the unmilled and ball milled STZ I powder. The ball milled SD powder was done at RT with a BTP powder weight ratio of 40:1 from 5 minutes to 20 hours. The Spearman correlation coefficient (r) was -0.78 obtained when these variables were compared.

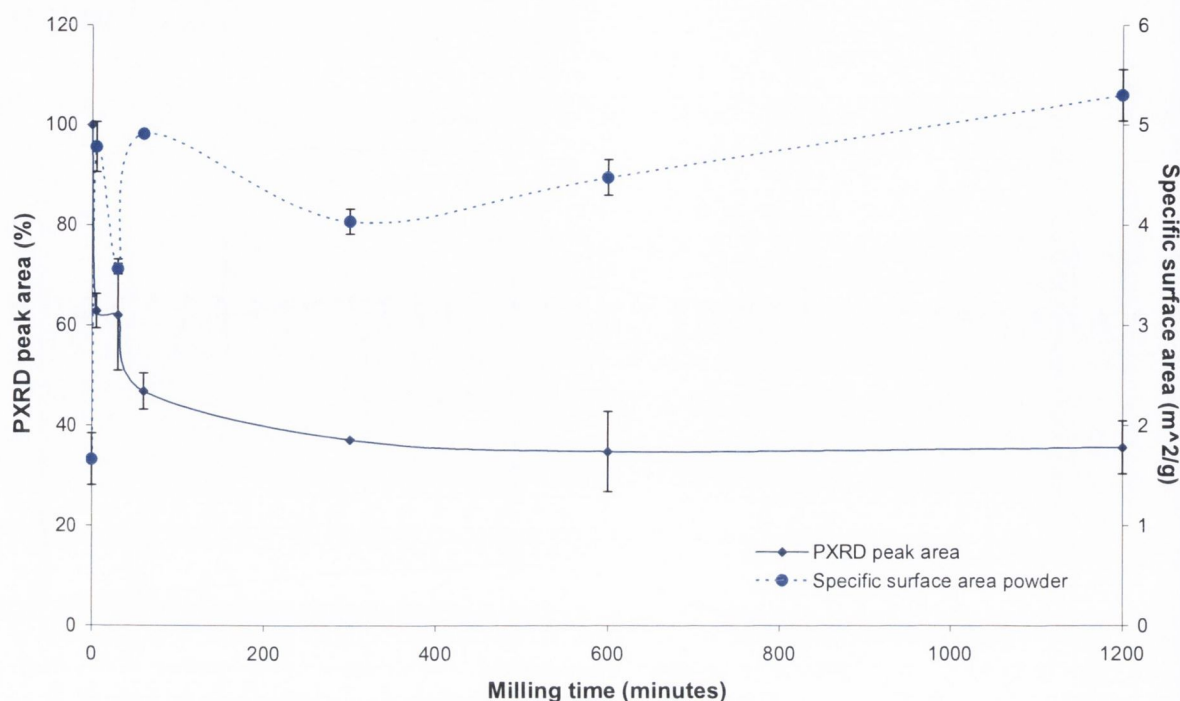


Figure 5: Specific surface area determined by BET and the PXRD peak area determined by Malvern particle size for the unmilled and ball milled STZ I powder. The ball milled SD powder was done at RT with a BTP powder weight ratio of 40:1 from 5 minutes to 20 hours. The Spearman correlation coefficient (r) was -0.61 obtained when these variables were compared.

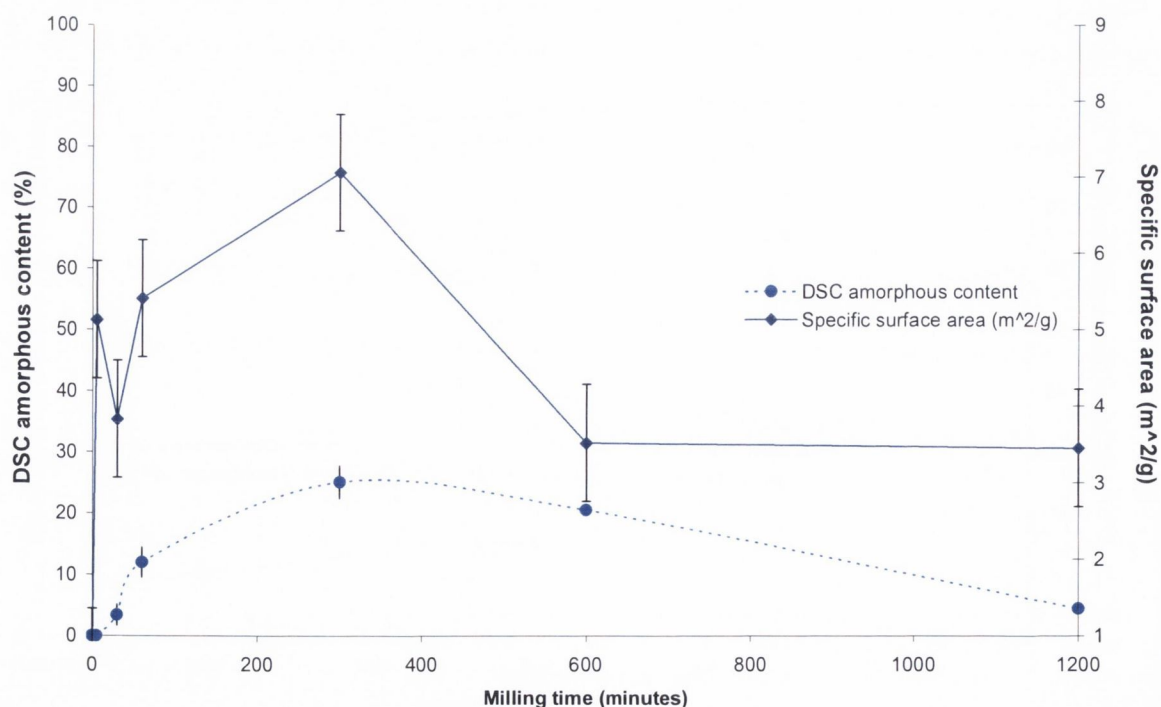


Figure 6: DSC amorphous content and the specific surface area of the powder determined by BET for the unmilled and ball milled STZ III-Y powder. The ball milled STZ III-Y powder was done at RT with a BTP powder weight ratio of 40:1 from 5 minutes to 20 hours. The Spearman correlation coefficient (r) was -0.61 obtained when these variables were compared.

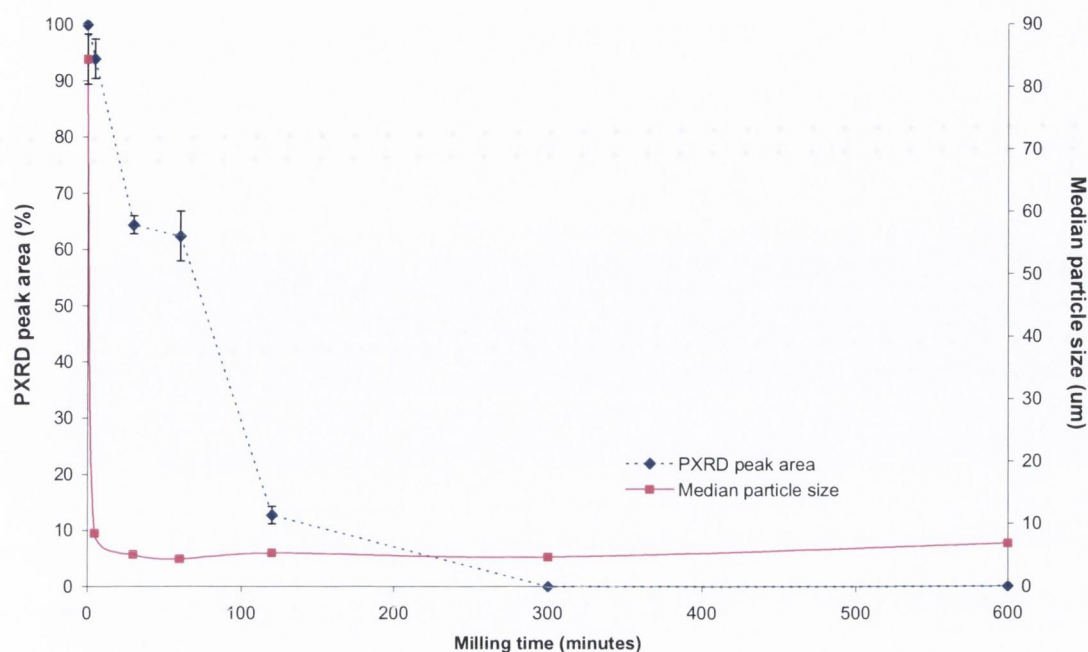


Figure 7: PXRD peak area and the median particle size of the powder determined by Malvern laser diffraction for the unmilled and ball milled STZNa powder. The ball milled STZNa powder was done at RT with a BTP powder weight ratio of 40:1 from 5 minutes to 10 hours. The Spearman correlation coefficient (r) was 0.67 obtained when these variables were compared.

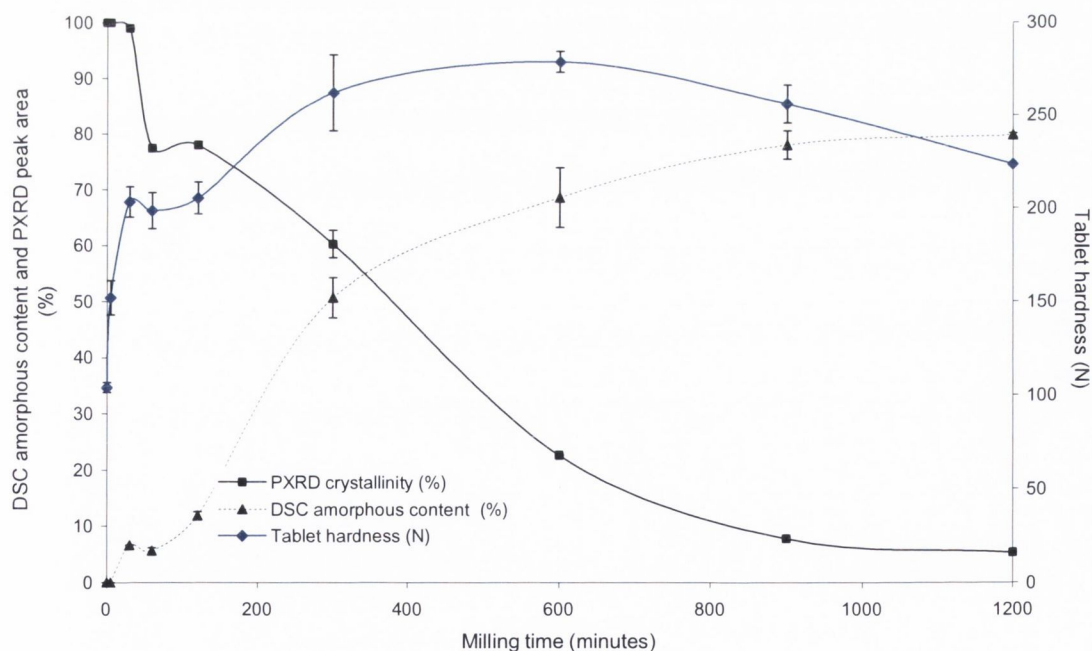


Figure 8: The DSC amorphous content, the PXRD peak area crystallinity of SD unmilled and milled at RT with a BTP weight ratio of 40:1 as milling time is increased from 5 minutes to 20 hours. These were compared to the tablet hardness obtained from tableting the unmilled and milled SD powder. The Spearman correlation coefficient (r) obtained when comparing DSC amorphous content with the tablet hardness was 0.79 and the r obtained when comparing PXRD peak area and tablet hardness was -0.78.

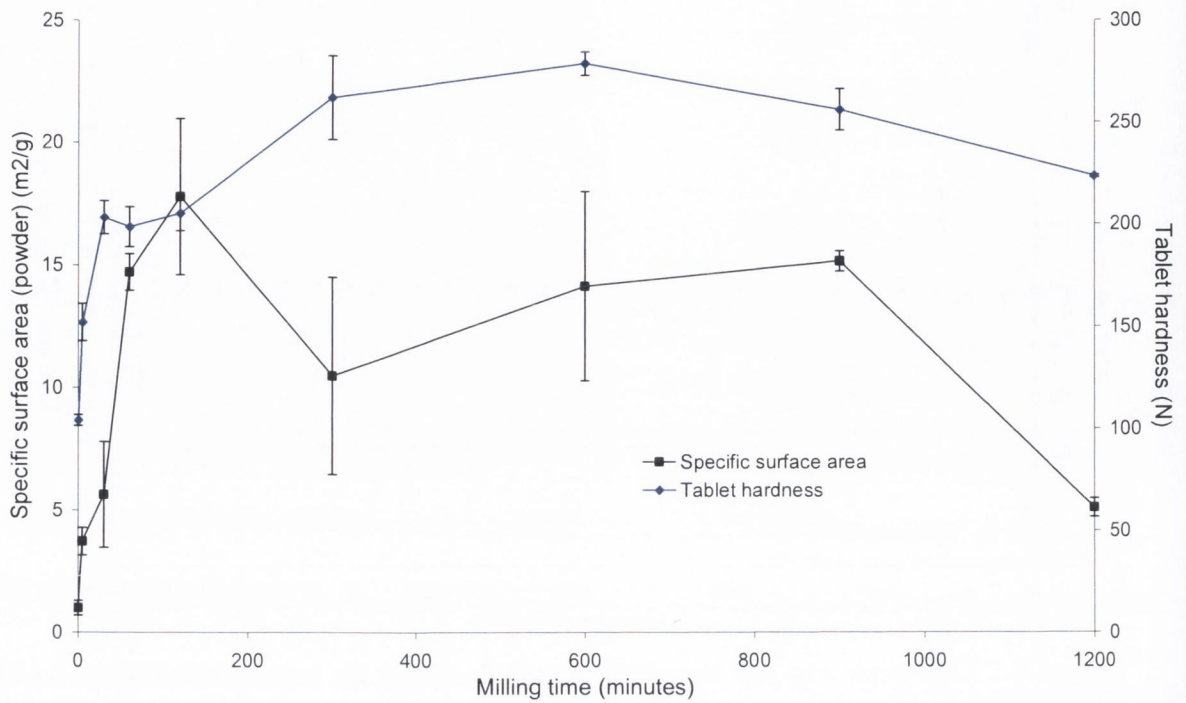


Figure 9: Specific surface area of the powder determined by BET and the tablet hardness for the unmilled and ball milled SD powder. These were compared to the tablet hardness obtained from tableting the unmilled and milled SD powder. The ball milled SD powder was done at RT with a BTP powder weight ratio of 40:1 from 5 minutes to 20 hours. The Spearman correlation coefficient (r) was 0.70 obtained when these variables were compared.

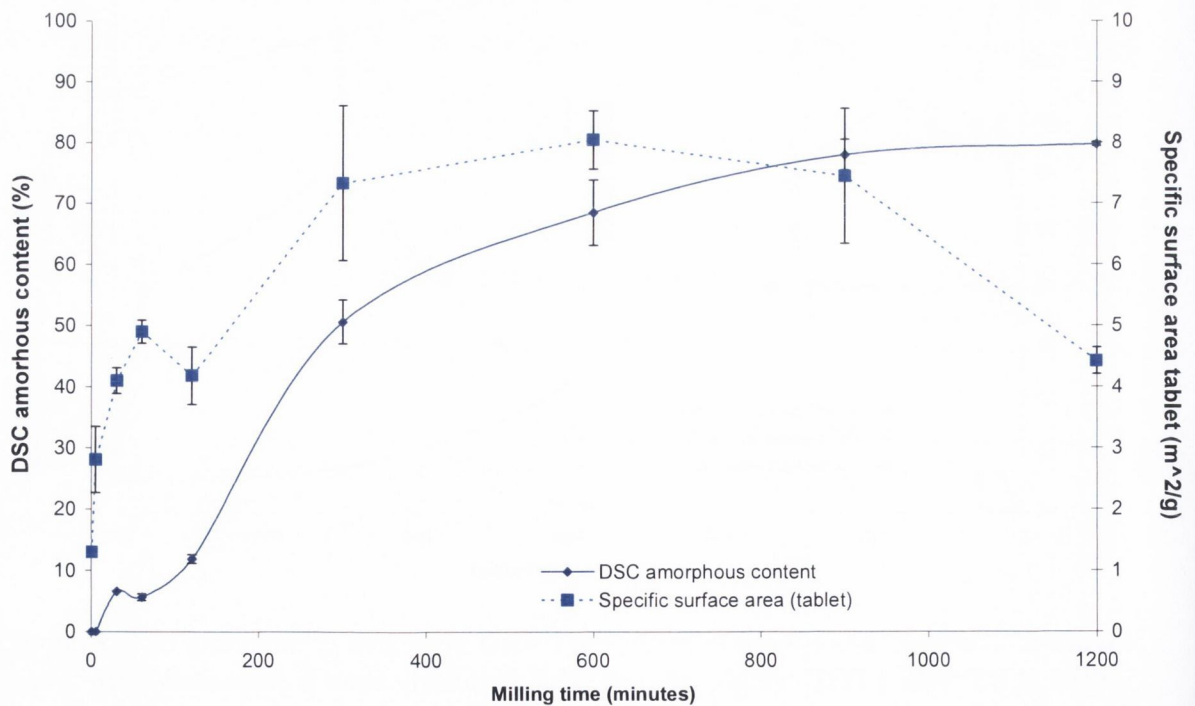


Figure 10: DSC amorphous content and the specific surface area of the tablet for the unmilled and ball milled SD powders and tablets. The ball milled SD powder was done at RT with a BTP powder weight ratio of 40:1 from 5 minutes to 20 hours. The Spearman correlation coefficient (r) was 0.73 obtained when these variables were compared.

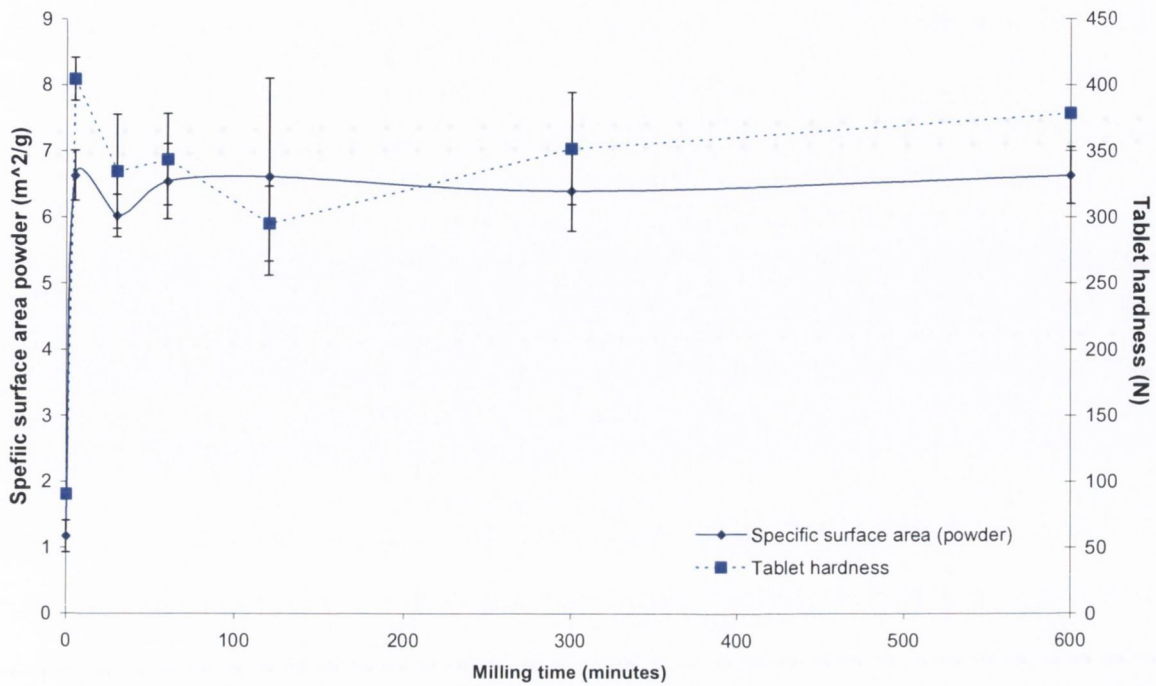


Figure 11: The specific surface area of the powder determined by BET for the unmilled and ball milled SDNa powders and the tablet hardness obtained from the tablets produced from the unmilled and milled powders. The ball milled SDNa powder was done at RT with a BTP powder weight ratio of 40:1 from 5 minutes to 10 hours. The Spearman correlation coefficient (r) was 0.74 obtained when these variables were compared.

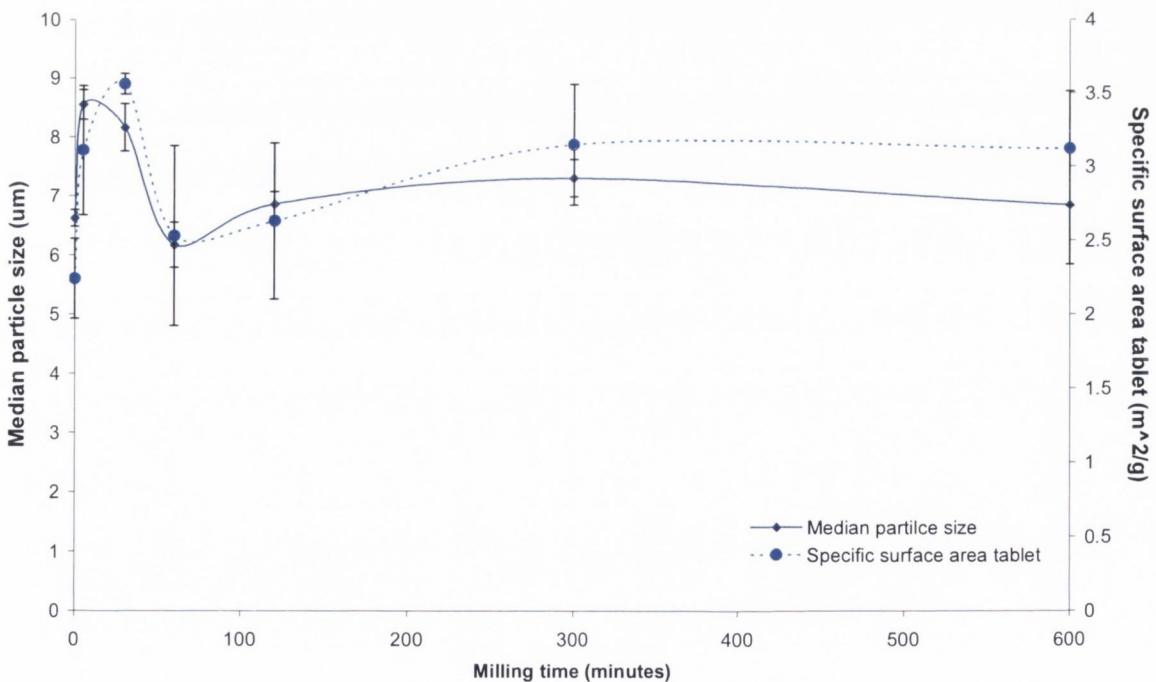


Figure 11: The median particle size determined by Malvern laser diffraction for the unmilled and ball milled SDNa powders and the tablet specific surface area determined by BET obtained from the tablets produced from the unmilled and milled powders. The ball milled SDNa powder was done at RT with a BTP powder weight ratio of 40:1 from 5 minutes to 10 hours. The Spearman correlation coefficient (r) was 0.68 obtained when these variables were compared.

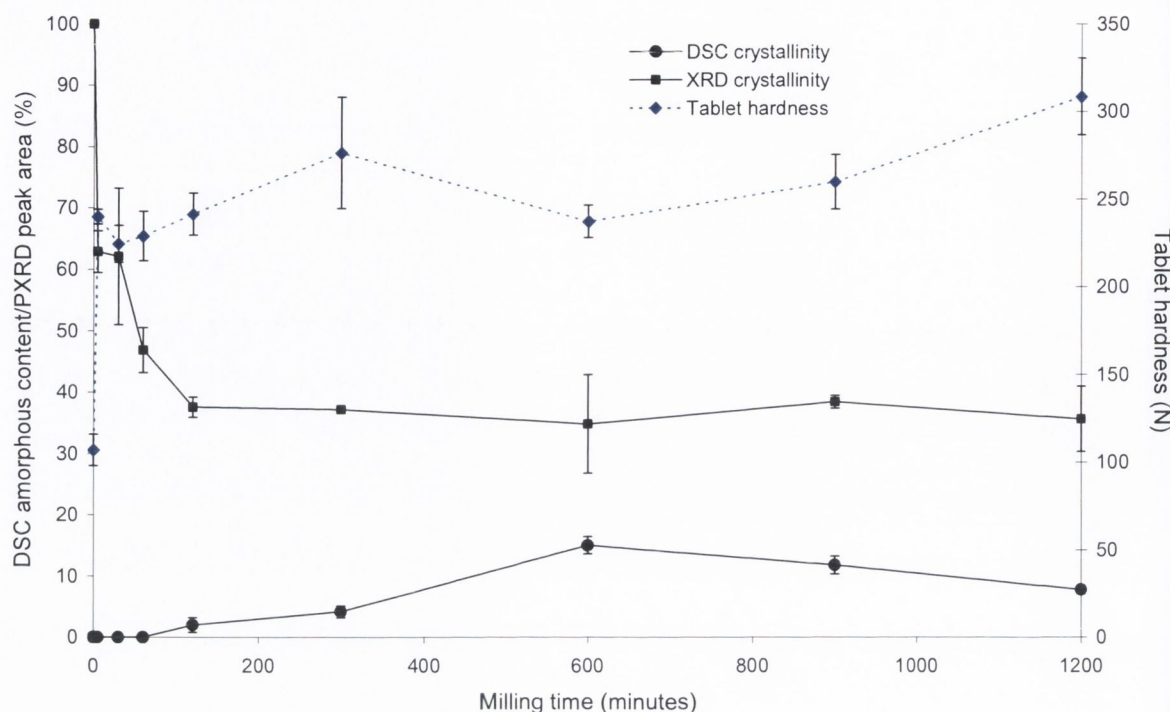


Figure 12: The DSC amorphous content, the PXRD peak area crystallinity of STZ I unmilled and milled at RT with a BTP weight ratio of 40:1 as milling time is increased from 5 minutes to 20 hours. These were compared to the tablet hardness obtained from tableting the unmilled and milled STZ I powder. The Spearman correlation coefficient (r) obtained when comparing DSC amorphous content with the tablet hardness was 0.62 and the r obtained when comparing PXRD peak area and tablet hardness was -0.65.

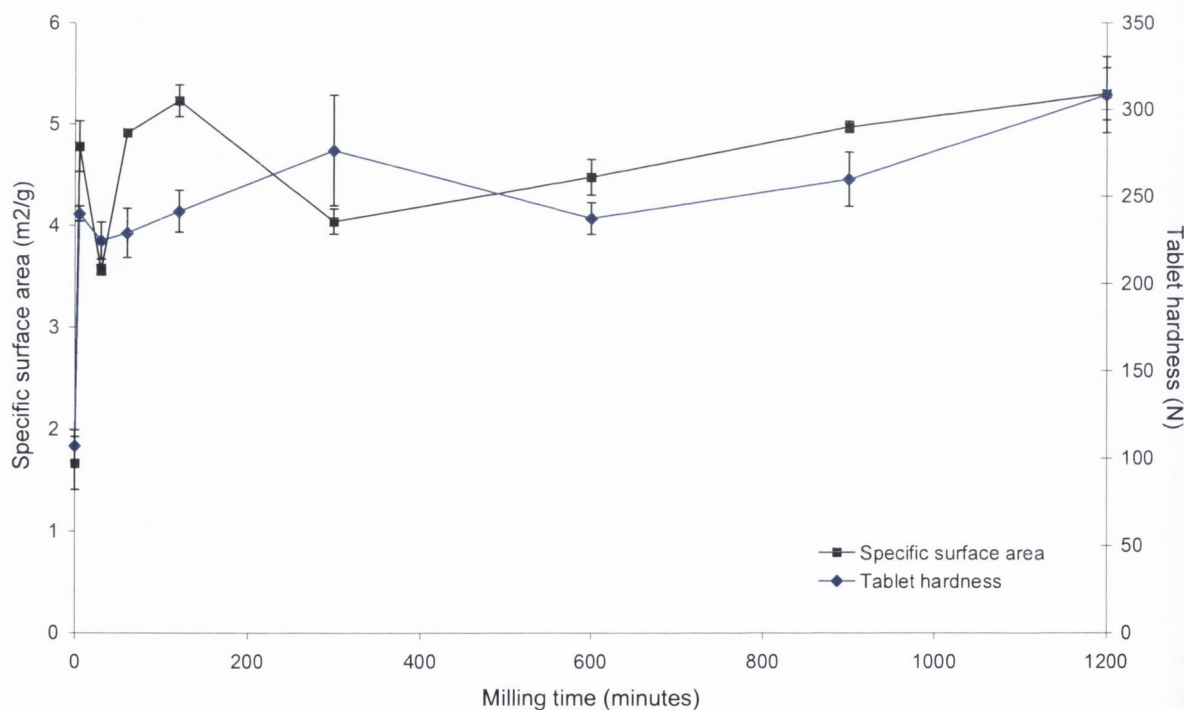


Figure 11: The specific surface area of the powder determined by BET for the unmilled and ball milled STZ I powders and the tablet hardness obtained from the tablets produced from the unmilled and milled powders. The ball milled STZ I powder was done at RT with a BTP

powder weight ratio of 40:1 from 5 minutes to 20 hours. The Spearman correlation coefficient (r) was 0.74 obtained when these variables were compared.

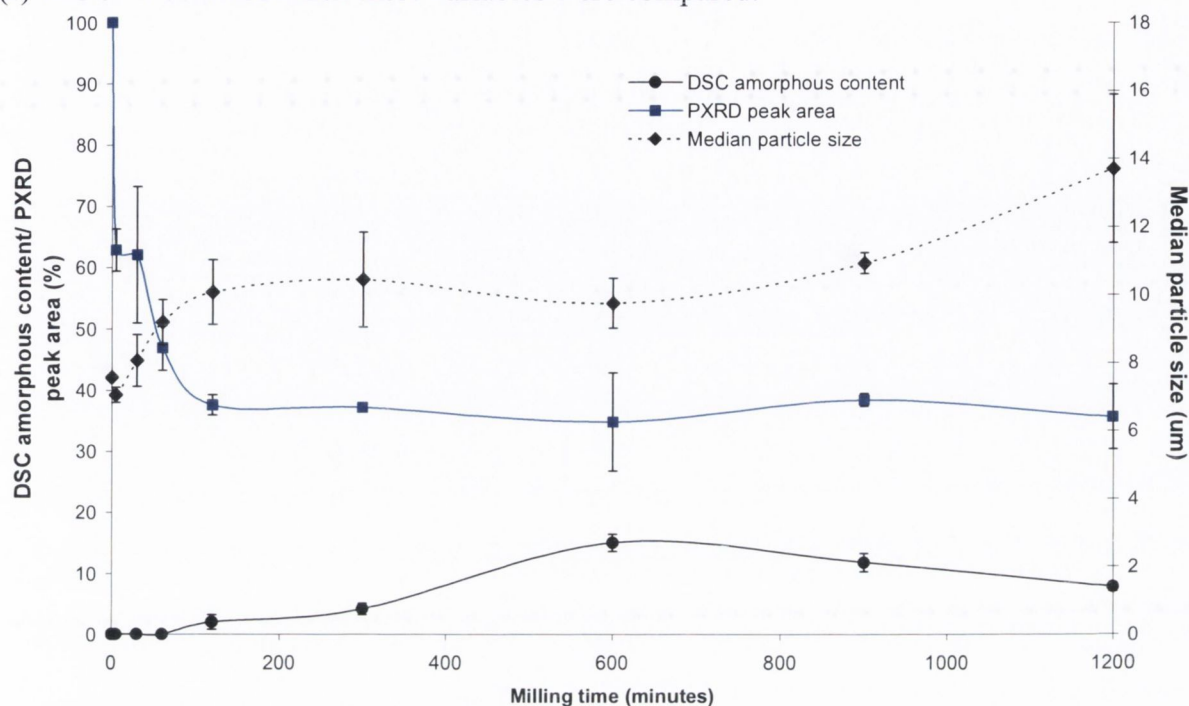


Figure 12: The DSC amorphous content, the PXR peak area crystallinity and the median particle size determined by Malvern laser diffraction of STZ I unmilled and milled at RT with a BTP weight ratio of 40:1 as milling time is increased from 5 minutes to 20 hours. The Spearman correlation coefficient (r) obtained when comparing DSC amorphous content with the median particle size was 0.77 and the r obtained when comparing PXR peak area and tablet hardness was -0.77.

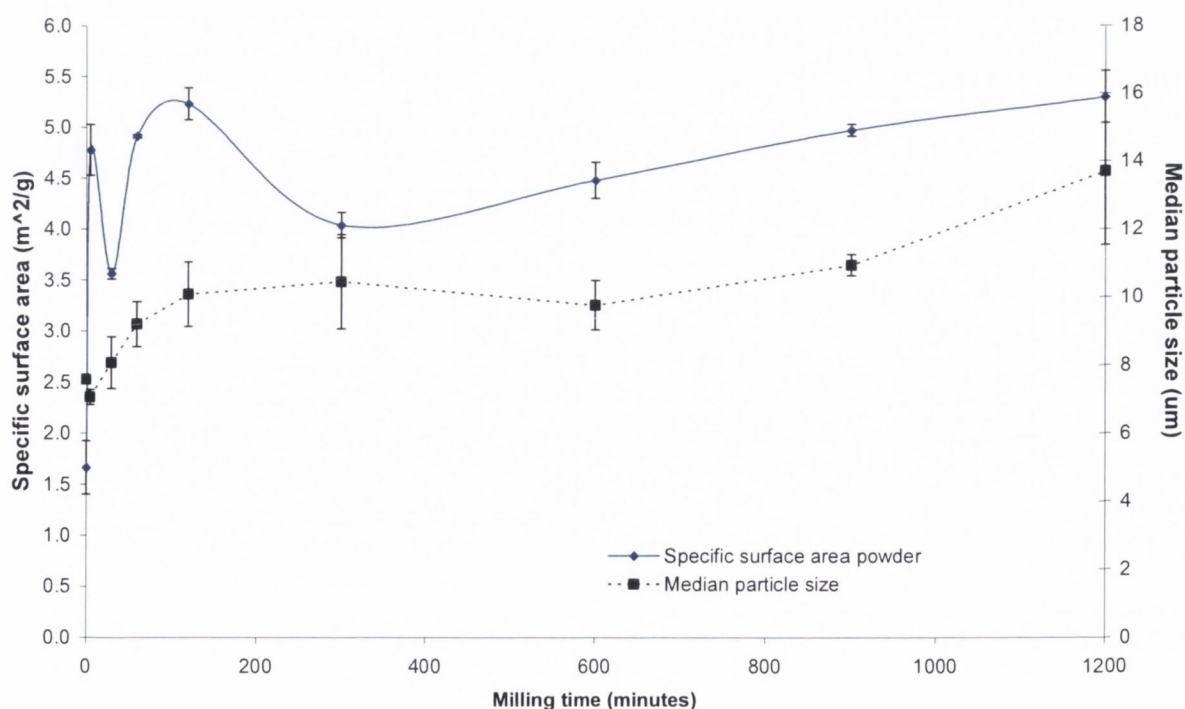


Figure 13: The specific surface area of the powder determined by BET and median particle size determined by Malvern laser diffraction for the unmilled and ball milled STZ I powders.

The ball milled STZ I powder was done at RT with a BTP powder weight ratio of 40:1 from 5 minutes to 20 hours. The Spearman correlation coefficient (r) was 0.63 obtained when these variables were compared.

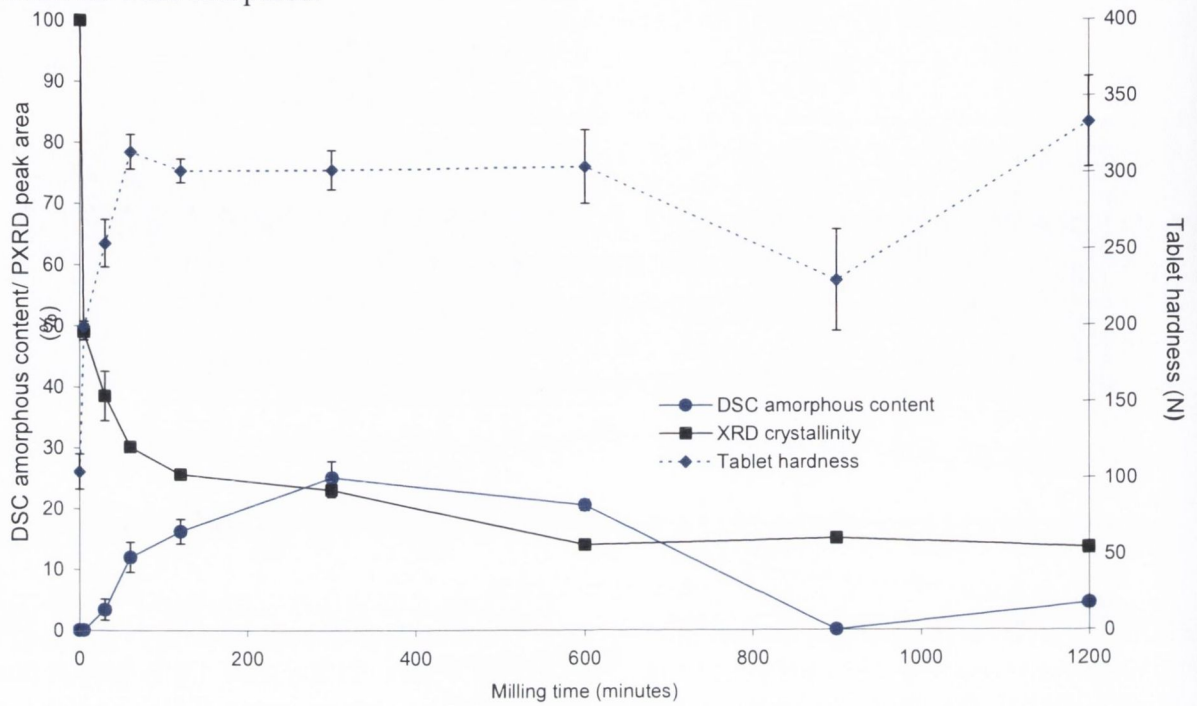


Figure 14: The DSC amorphous content, the PXRD peak area crystallinity of STZ III unmilled and milled at RT with a BTP weight ratio of 40:1 as milling time is increased from 5 minutes to 20 hours. These were compared to the tablet hardness obtained from tableting the unmilled and milled STZ III powder. The Spearman correlation coefficient (r) obtained when comparing DSC amorphous content with the tablet hardness was 0.70 and the r obtained when comparing PXRD peak area and tablet hardness was -0.72.

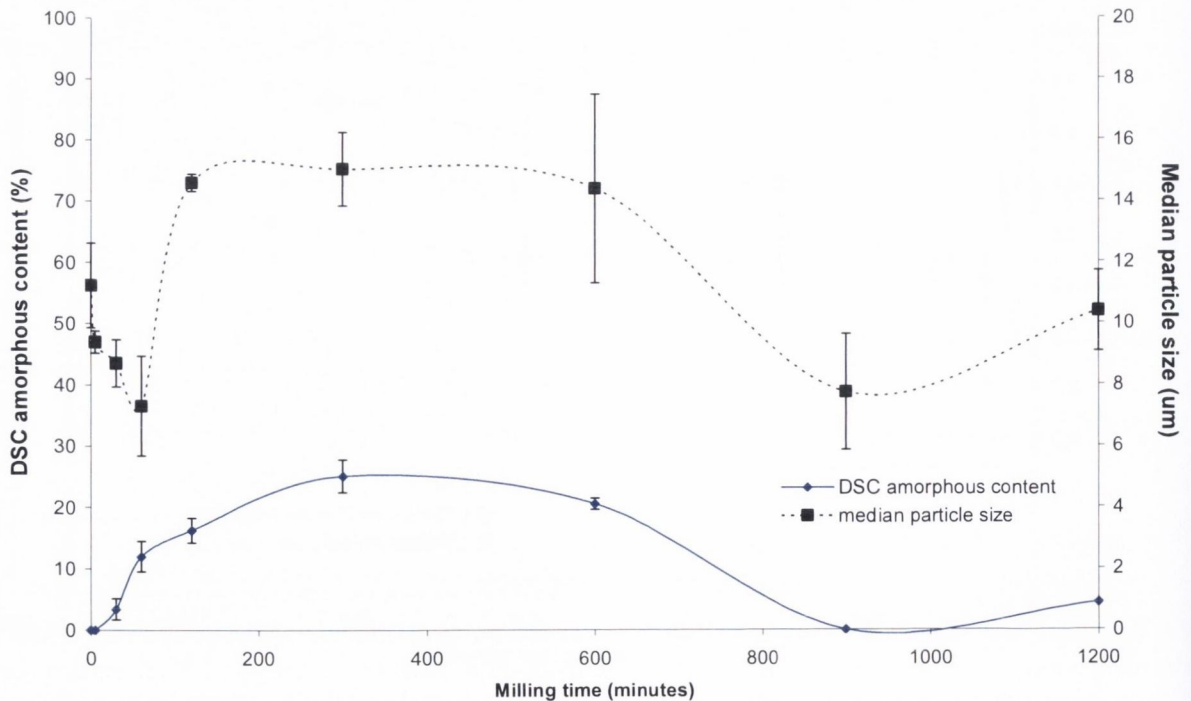


Figure 15: The median particle size determined by Malvern laser diffraction and the DSC amorphous content for the unmilled and ball milled STZ III powders. The ball milled STZ III powder was done at RT with a BTP powder weight ratio of 40:1 from 5 minutes to 20 hours. The Spearman correlation coefficient (r) was 0.59 obtained when these variables were compared.

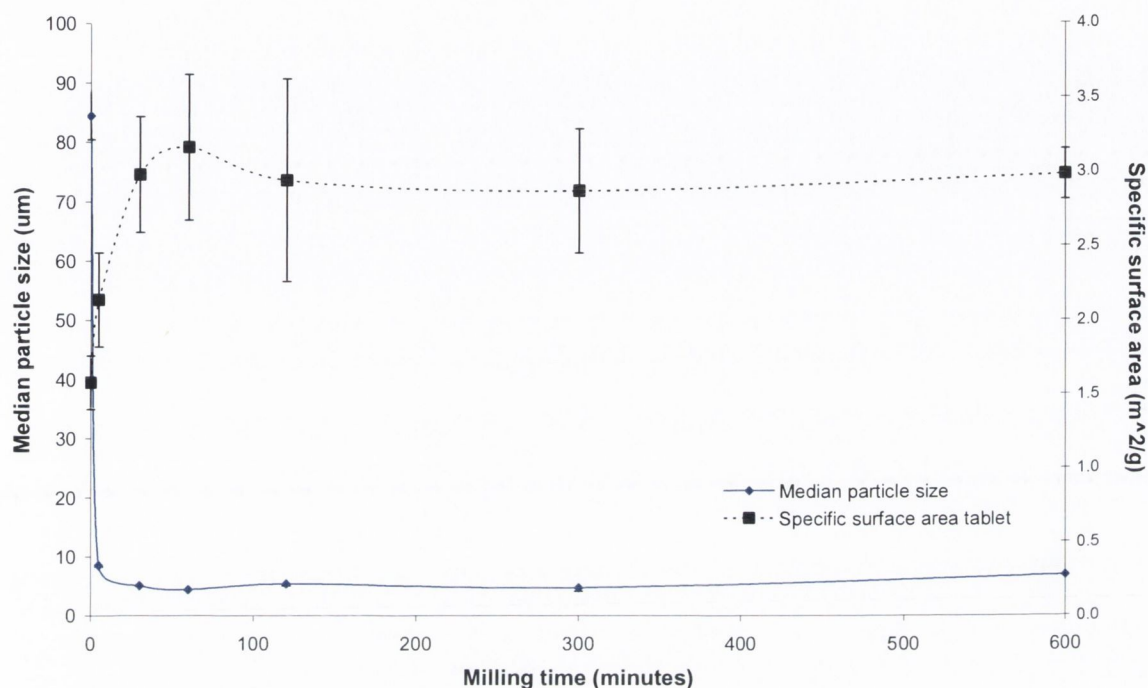


Figure 16: The median particle size determined by Malvern laser diffraction for the unmilled and ball milled STZNa powders and the tablet specific surface area determined by BET obtained from the tablets produced from the unmilled and milled powders. The ball milled STZNa powder was done at RT with a BTP powder weight ratio of 40:1 from 5 minutes to 10 hours. The Spearman correlation coefficient (r) was -0.72 obtained when these variables were compared.

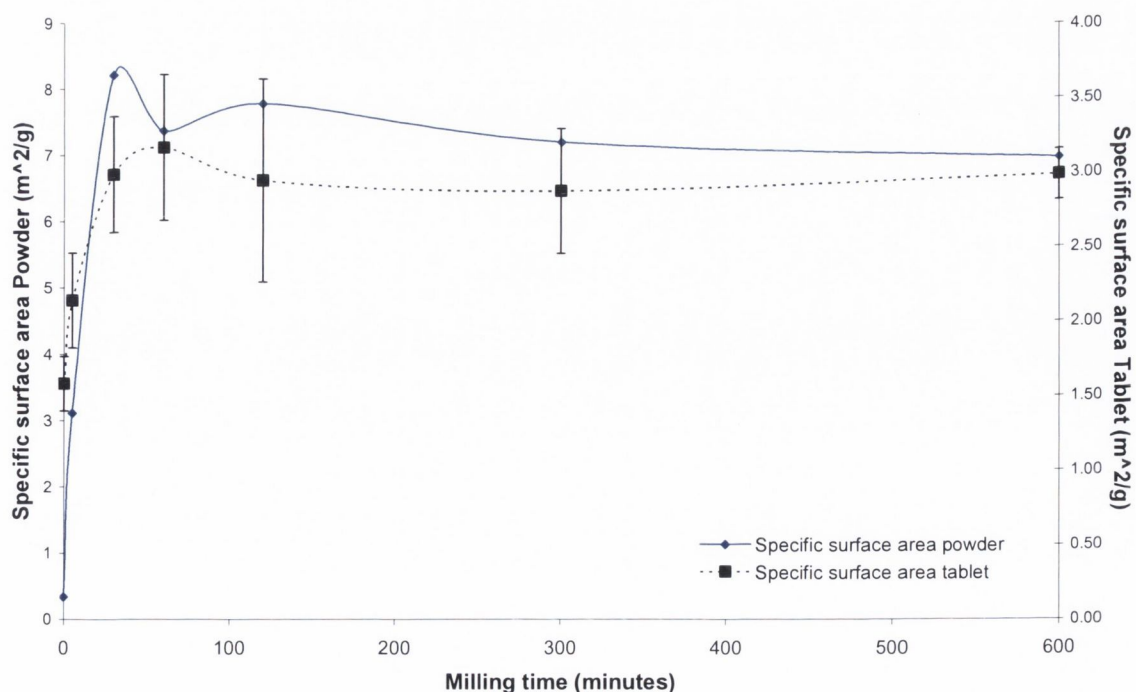


Figure 17: The specific surface area determined by BET of the STZNa unmilled and ball milled STZNa powder and the tablets produced from the unmilled and ball milled powders. The ball milled STZNa powder was done at RT with a BTP powder weight ratio of 40:1 from 5 minutes to 10 hours. The Spearman correlation coefficient (r) was 0.68 obtained when these variables were compared.

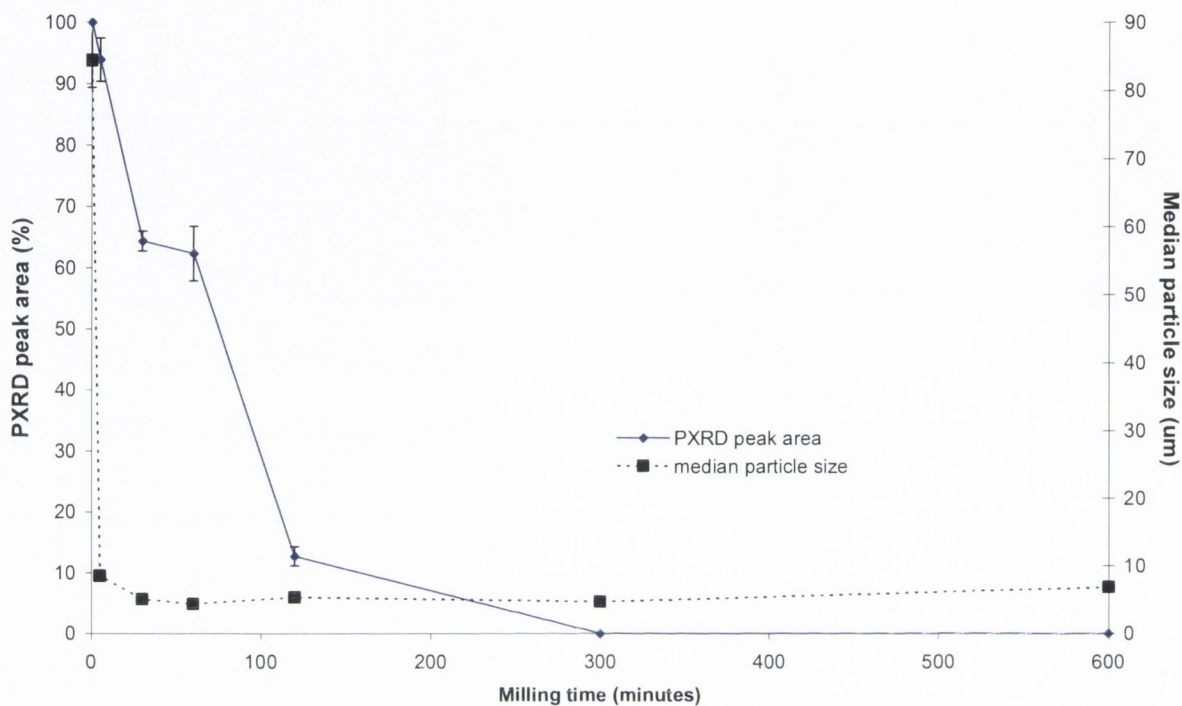


Figure 18: The median particle size determined by Malvern laser diffraction and the PXRD peak area for the unmilled and ball milled STZNa powders. The ball milled STZNa powder was done at RT with a BTP powder weight ratio of 40:1 from 5 minutes to 10 hours. The Spearman correlation coefficient (r) was 0.52 obtained when these variables were compared.

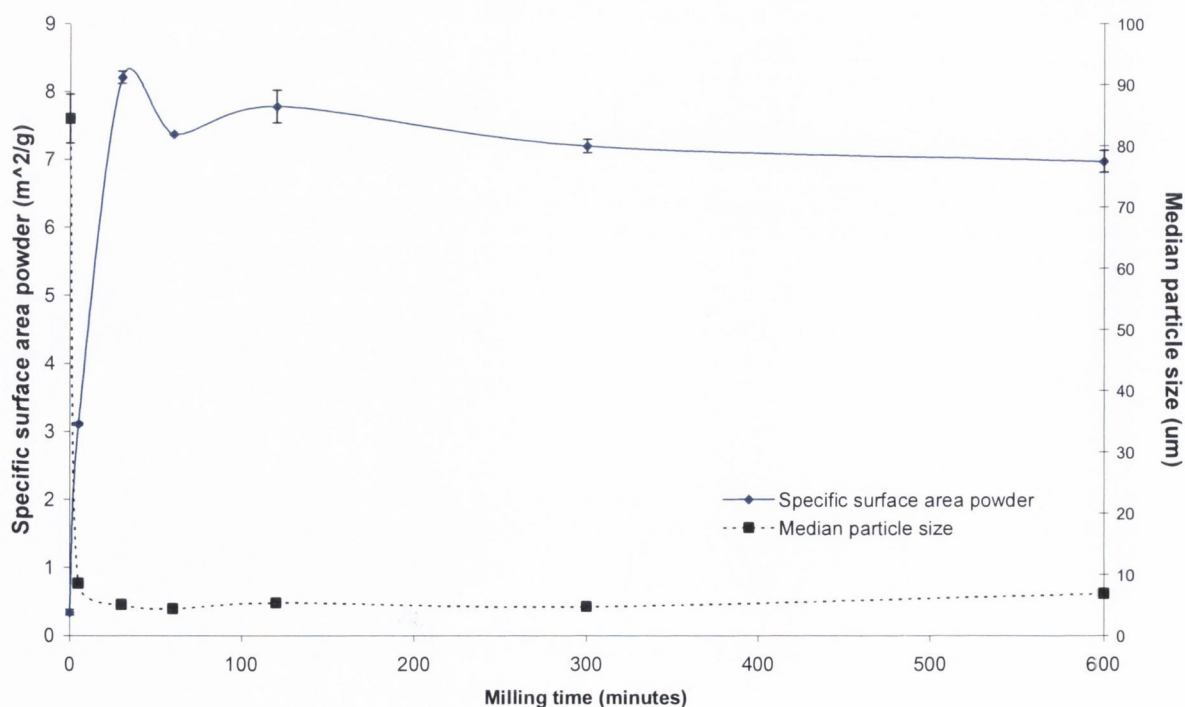


Figure 19: The specific surface area of the powder determined by BET and the median particle size determined by Malvern laser diffraction for the unmilled and ball milled STZNa powders. The ball milled STZNa powder was done at RT with a BTP powder weight ratio of 40:1 from 5 minutes to 10 hours. The Spearman correlation coefficient (r) was -0.71 obtained when these variables were compared.